



UNIVERSITY OF
LIVERPOOL

Department of Engineering

PhD Thesis

**Modelling and Experimental Investigation of
3D Laser Forming of Metallic Components**

Thesis submitted in accordance with the requirements
of The University of Liverpool for the Degree of
Doctor in Philosophy

By

Emile John Abed

November 2007

Emile Abed
Laser Group
Department of Engineering
University of Liverpool
Liverpool, UK
L69 3GH
Email: eabed@liv.ac.uk

Declaration

I hereby declare that all of the work contained within this dissertation has not been submitted for any other qualification.

Signed:



Date:

22 / 11 / 2007

Abstract

Laser forming is a non-contact thermal forming process that can shape metallic components as a means of rapid prototyping and as a method of distortion correction, adjusting and alignment. The process utilises a defocused laser beam to introduce thermal stresses, without melting, that cause plastic deformation resulting in controlled deformation.

To advance this process further for realistic forming applications in a manufacturing industry, it is necessary to consider controlled 3D laser forming. The work presented in this thesis uses a predictive and adaptive approach to control the 3D laser forming of mild steel and aluminium.

Key to the control of the process has been the development of predictive Matlab based models. These models calculate scan strategies derived from the required geometry

The first model uses lines of constant high to determine scan paths and the gradient at points along these lines to determine the scan speed. A second model uses lines of constant gradient magnitude to determine scan lines and the increment between these lines to determine the scan speed.

For both models, when the geometry is not formed within one pass, an incremental adaptive approach is used for subsequent passes, utilising the error between the current and desired geometry to give a new scan

strategy, by this means, any unwanted distortion due to material variability can be accounted for. Results are presented that demonstrate the controlled laser forming of a 3D semi-developable shape and for the correction of mechanically distorted struts in an accurate and repeatable technique on both large and small scale components. The data presented represents a significant step towards a realistic laser forming system for the manufacturing environment.

To increase the understanding of the laser forming process 2D laser forming experiments are also presented here. These investigations include factors influencing bending rate on multi-pass laser forming looking at known factors and an additional factor the influence of the change in beam profile area as a 2D bend increases. The change in energy fluence from the variation in beam profile area is shown to be a significant influence in laser forming.

To promote laser forming in the aerospace industry it is important to know the effects of heat treatment on a laser formed part. Because of this an investigation into the effects of post forming heat treatments on laser formed components is also presented in this thesis. Post forming heat treatments are often carried out in the aerospace industry to relieve any residual stresses that may have been induced into the part from the forming process. This investigation shows there is minimal change in the part geometry when a laser formed AA6061 part is heat treated. However some movement in the part is seen due to the relaxation of residual stresses from the laser forming process.

Acknowledgements

The author is extremely grateful and appreciative of all the contributions made and advice given that has made this work possible. In particular acknowledgements are given to the following people and organisations.

Firstly I would like to thank my supervisors/advisors Dr Geoff Dearden and Prof Ken Watkins for initially accepting my application for a PhD studentship and through their continuing support throughout my studies.

I would also like to thank the laser lab manager Mr Andy Snaylam for all his hard work in setting up of experiments and in the preparation of samples.

Thanks must also go to Dr Stuart Edwardson to whom the author is very much a pupil. Thanks for the teachings in the laser forming field and all the help and advice in experimental set-up and analysis throughout these studies.

A thank you must also go to Konrad Bartkowiak for help with analysing microstructure.

To all the members of the Liverpool Laser Group thank you for making the time spent studying in the group a pleasurable experience. Extra thanks must go to Mr Stephen Davis and Dr Paul Smith making the years

as a PhD student an enjoyable experience, especially lunchtimes with intelligent conversation, crosswords and cakes.

The author would like to also thank all the staff at the Lairside Laser Engineering Centre (LLEC) where he did his first laser forming research many years ago studying for my master degree.

Thanks go to the EPSRC for the funding of my PhD.

And finally a special thank you to the parents of the author Mr & Mrs John and Margaret Abed (Mum and Dad) for their constant support and unwavering faith throughout the authors PhD and all past studies.

Table of contents

Declaration	i
Abstract	ii
Acknowledgements	iv
Table of Contents	vi
List of Figures	xii
List of Tables	xxii
List of Symbols	xxiv
<i>1.0 Introduction</i>	<i>1</i>
<hr/>	
<i>2.0 Literature Review</i>	<i>4</i>
<hr/>	
2.1. Laser Forming	4
2.2. Laser Forming Mechanisms	7
2.2.1. The Temperature Gradient Mechanism (TGM)	8
2.2.2. The Buckling Mechanism (BM)	13
2.2.3. The Shortening or Upsetting Mechanism (UM)	15
2.3. Mathematical Models	18
2.3.1. Analytical Models	18
2.3.1.1. The Temperature Gradient Mechanism	18
2.3.1.1.1. The Trivial Model	19
2.3.1.1.2. Two Layer Model	21
2.3.1.1.3. Residual Stress Model	25
2.3.1.2. The Buckling Mechanism	29
2.3.1.3. The Upsetting Mechanism	32
2.3.2. Numerical Models	33

2.3.2.1. The Temperature Gradient Mechanism	34
2.3.2.2. The Buckling Mechanism	38
2.3.2.3. The Upsetting Mechanism	38
2.4. Previous Experimental Work	40
2.4.1. Fundamental Investigations	40
2.4.2. Previous Work within the Research Group	45
2.4.2.1. Magee 1998	45
2.4.2.1.1. Parametric Study	45
2.4.2.1.2. Two-Dimensional Laser Forming Demonstrator System	50
2.4.2.1.3. Three-Dimensional Laser Forming of a Dish Shape	51
2.4.2.2. Edwardson 2004	52
2.4.2.2.1. Metallurgical Study	53
2.4.2.2.2. Two-Dimensional Closed Loop Control	54
2.4.2.2.3. Three-Dimensional Laser Forming Empirical Study	55
2.4.2.2.4. Development of a Geometry Based Model for Three-Dimensional Laser Forming	57
2.4.3. Research in Macro Two-Dimensional Laser Forming	58
2.4.4. Research in Micro-Scale Two-Dimensional Laser Forming	61
2.4.5. Research in Three-Dimensional Laser Forming	63
2.4.6. Material and Metallurgy Studies	65
2.5. Potential Applications	70
2.5.1. Rapid Prototyping	71
2.5.2. Laser Assisted Bending	73
2.5.3. Distortion Correction	73
2.5.4. Micro Alignment	74
2.5.5. Manufacture of Parts using Laser Forming	74
2.6. State of the Art	76
2.7. Synopsis for Present Research	77
3.0 Experimental Procedure	78

3.1. General Set-up	78
3.1.1. Hardware	79
3.1.1.1. CO ₂ Laser	79
3.1.1.2. The Electrox 1.5kW CO ₂ Laser	81
3.1.1.3. Workstation	82
3.1.1.3.1. Beam Delivery	82
3.1.1.3.2. Part Manipulation	82
3.1.1.3.3. Measurement	84
3.1.1.3.4. Work-Piece Restraints	85
3.1.1.4. Characterisation of the Laser at the Work Surface	86
3.1.1.4.1. Laser Beam	86
3.1.1.4.2. Beam Diameter	87
3.1.1.4.3. Laser Power	87
3.1.2. Software	88
3.1.2.1. Visual Basic Based User Interface	89
3.1.2.1.1. Jog Controller User Interface	89
3.1.2.1.2. Two-Dimensional Laser Forming User Interface	91
3.1.2.1.2.1. Measurement and Calculation of 2D Sample	93
3.1.2.1.3. Co-ordinate Measuring Machine (CMM)	97
3.1.3. Absorptive Coating	99
3.1.4. Materials used in this Thesis	99
3.1.4.1. CR4 Mild Steel	102
3.1.4.2. Aluminium Alloy 6061	103
3.1.4.3. Aluminium Alloy 5251	104
3.2. Geometrical Influences	106
3.2.1. Edge Clamp Condition	107
3.2.1.1. Measurement	108
3.2.1.2. Predictive Model	108
3.2.2. V-block Condition	110
3.2.2.1. Measurement	110
3.3. The Effects of Post laser Forming Heat Treatment	111
3.3.1. Laser Forming	112

3.3.2. Measurement	113
3.3.3. Calculations	114
3.3.4. Heat Treatments	115
3.3.4.1. Annealing	115
3.3.4.2. Solution Heat Treatment and Quenching	116
3.3.4.3. Precipitation Heat Treatment	117
3.3.5. Micro Hardness Testing	117
3.4. Geometry Based Predictive/Adaptive Model for 3D Forming	119
3.4.1. Geometry Based Predictive/ Adaptive Model: Basic Procedure	120
3.4.1.1. Defining the Desired Shape	121
3.4.1.2. Defining the Actual Shape	122
3.4.1.3. Error Calculation	124
3.4.1.4. Irradiation Strategy	124
3.4.1.5. Galil CNC program	125
3.4.2. Irradiation Strategy for First Model	125
3.4.3. Irradiation Strategy for the Modified Model	128
4.0 2D Laser Forming Results and Discussion	132
4.1. Geometrical Influences on Multi-Pass Laser Forming	132
4.1.1. Summary of Known Influencing Factors	135
4.1.1.1. Strain Hardening	135
4.1.1.2. Section Thickening	136
4.1.1.3. Variation in Absorption	136
4.1.1.4. Thermal Effects	138
4.1.2. Edge Clamp Condition	140
4.1.2.1. Area Calculations	141
4.1.2.2. Calculated Effects	143
4.1.2.3. Empirical Confirmation	144
4.1.3. V-Block Condition	150
4.1.3.1. Area Calculations	151
4.1.3.2. Calculated Effects	152
4.1.3.3. Empirical Confirmation and Comparison	154
4.1.4. Possible Effects of the Influencing Factors on the Laser Forming of 3D Components	156

4.2. Effects of Post laser Forming Heat Treatment on Laser Formed Components	159
4.2.1. Laser Forming	161
4.2.2. Heat Treatments	170
4.2.2.1. Annealing	170
4.2.2.2. Solution Heat Treatment and Quenching	177
4.2.2.3. Precipitation Heat Treatment	181
4.2.3. Hardness Testing	183
4.2.4. Discussion: Effects of Post Forming Heat Treatments on Laser Formed Components	184
<i>5.0 3D Laser Forming Results and Discussion</i>	<i>187</i>
<hr/>	
5.1. Using Geometrical Properties for Creating Irradiation Strategies	188
5.1.1. Defining 3D Surfaces	188
5.1.1.1. Developable and Non-Developable Surfaces	189
5.1.1.2. Height	190
5.1.1.3. Gradient	191
5.1.1.4. Curvature	191
5.1.1.4.1. Mean Curvature	192
5.1.1.4.2. Gaussian Curvature	192
5.2. 3D Laser Forming of a Semi-Developable Shape using a Geometry Based Model	197
5.2.1. Irradiation Strategy	198
5.2.1.1. Error Between Desired and Actual Surface	198
5.2.1.2. Irradiation Pattern	199
5.2.1.3. Speed Selection	201
5.2.2. Experiments using the Geometry Based Model	205
5.2.2.1. Closed Loop 3D Laser Forming of a Mild Steel Semi-Developable Shape	205
5.2.3. Feasibility of High Magnitude 3D Laser Forming of Mild Steel	216
5.3. Modified Geometry Based Model	217
5.3.1. Irradiation Strategy	217
5.3.1.1. Decrease in Viewable Area	218
5.3.1.2. Irradiation Pattern	221
5.3.1.3. Speed Selection	225

5.3.2. Experiments using the Modified Geometry Based Model	226
5.3.2.1. 3D Laser Forming of a Semi-Developable Shape in 1mm Thick 80x200mm Aluminium at 400W	227
5.3.2.2. 3D Laser Forming of a Semi-Developable Shape in 1mm Thick 80x200mm Aluminium at 200W	239
5.3.2.3. 3D Laser Forming of a Semi-Developable Shape in 1mm Thick 400x200mm Aluminium at 200W	247
5.3.3. Laser Forming for the Correction of Distortion in Aluminium Struts	254
5.3.3.1. Laser Forming for the Correction of Aluminium 5251 Strut Mechanically Deformed to 15mm	257
5.3.3.2. Laser Forming for the Correction of Aluminium 5251 Strut Mechanically Deformed to 45mm	262
5.3.4. Discussion on the Geometry Based Model	271
<i>6.0 Conclusions and Future Work</i>	<i>274</i>
6.1. Geometrical Influences on Multi-Pass Laser Forming	274
6.2. Effects of Post Forming Heat Treatments on Laser Formed Components	276
6.3. 3D Laser Forming of a Semi-Developable Shape using the Original Geometry Based Model	278
6.4. 3D Laser Forming of Semi-Developable Shape and the Correction of Distortion using the Modified Geometry Based Model	279
6.5. Future Work	280
<i>References</i>	<i>283</i>
<i>List of Publications to Date by the Author</i>	<i>299</i>
<i>Appendix</i>	<i>302</i>

List of Figures

Figure 2.1:	Laser Forming Set-up & Process Variables	5
Figure 2.2:	The Laser Forming Mechanisms	8
Figure 2.3:	Energy conditions required for the TGM	9
Figure 2.4:	Stress-strain diagram of material as a parameter of temperature	10
Figure 2.5:	Principle of the Temperature Gradient Mechanism (TGM)	11
Figure 2.6:	Time run of the bend angle	12
Figure 2.7:	Stages in the Buckling Mechanism (BM)	14
Figure 2.8:	The Upsetting (Shortening) Mechanism (UM)	16
Figure 2.9:	The trivial model	20
Figure 2.10:	Forces and moments acting in the two layer model	21
Figure 2.11:	Layout for the residual stress model	22
Figure 2.12:	Model Geometry for the Buckling Mechanism	30
Figure 2.13:	Model for extrusion bending using the upsetting mechanism	33
Figure 2.14:	Decreasing bend rate with increasing scans over an identical track	44
Figure 2.15:	Bend angle with increasing traverse velocity for Ti6Al4V using a large beam diameter	46
Figure 2.16:	Bend angle with increasing traverse velocity for AA 2024 T3	48
Figure 2.17:	Bend angle with increasing number of scans over the same track	49
Figure 2.18:	Ideal bend angle and exaggerated view of edge effects	49
Figure 2.19:	Demonstrator Part	50
Figure 2.20:	Circle line system with square root radius increase (inside to out), and resulting contour plot of sample	52
Figure 2.21:	AA 6061 O 'As Received'	53
Figure 2.22:	AA 6061 O After 30 passes	54

Figure 2.23:	'Race track' strategy, Speed 20mm/s	56
Figure 2.24:	3D Contour Plot 'race track' strategy	56
Figure 3.1.1:	General construction of a FAF laser	81
Figure 3.1.2:	Electrox 1.5kW CO ₂ laser	81
Figure 3.1.3:	Workstation 2, CAD Drawing of layout	83
Figure 3.1.4:	Workstation 2 layout	84
Figure 3.1.5:	Nozzle arrangement and laser range finder	84
Figure 3.1.6:	Centre Clamp	85
Figure 3.1.7:	Edge clamp	85
Figure 3.1.8:	V- block	85
Figure 3.1.9:	Modified side clamp	86
Figure 3.1.10:	Electrox 1.5kW laser beam energy profile, PyroCam III image	86
Figure 3.1.11:	Burn prints in wood at 5mm steps, 127mm FL lens 130mm-220mm stand off	87
Figure 3.1.12:	Power offset calibration graph	88
Figure 3.1.13:	User interface for the jog controller	90
Figure 3.1.14:	User interface for the automated 2D laser forming of 80x80mm coupons	91
Figure 3.1.15:	User interface of the automated 2D laser forming of 40x80mm and 80x80mm coupons with full surface measurement	92
Figure 3.1.16:	Sample of a measurement taken using the surface scan	93
Figure 3.1.17:	Measured points on a flat 40x80mm coupon. The solid grey line shows the irradiation path and the two square grey points show z_1 and z_2 , the measurements used for calculating bend angle	93
Figure 3.1.18:	Values used for bend calculation before the first pass	94
Figure 3.1.19:	Values calculated and values used for bend calculation after the first pass.	95
Figure 3.1.20:	Values calculated and values used for bend calculation after the second pass	96
Figure 3.1.21:	User interface for the co-ordinate measuring machine (CMM)	97
Figure 3.1.22:	Example of a measure part using the co- ordinate measuring machine	98
Figure 3.1.23:	User interface of the Modified co-ordinate measuring machine (CMM)	99

Figure 3.1.24:	Absorptivity as a function of wavelength for normal incidence, smooth surfaces and room temperature. Metals 1 are those with full inner electron shells (Au, Ag, Cu,...) and Metals 2 are transition metals (Fe, Ni, Cr,...)	100
Figure 3.1.25:	Dependence of coupling rate of coated surfaces on interaction time and incident intensity	102
Figure 3.2.1:	Calculation of bend angle for the edge clamp	108
Figure 3.2.2:	Energy fluence with increasing bend angle and energy fluence with an increasing beam diameter equivalent to the same incident area increase	109
Figure 3.2.3:	Calculation of bend angle for the v-block	110
Figure 3.3.1:	The measured points on the sample. The bending line can be seen here as the middle vertical dashed line	114
Figure 3.3.2:	Schematic showing the calculation of the overall angle ' α_b '	115
Figure 3.3.3:	Picture of cut sections in resin.	118
Figure 3.3.4:	Locations for the hardness test	118
Figure 3.4.1:	Matlab output showing a Bezier surface patch for a pillow shape	119
Figure 3.4.2:	A Basic flow chart of the Geometry Based Predictive/Adaptive Model	121
Figure 3.4.3:	16 points used to define the desired surface	122
Figure 3.4.4:	Interpolated points for desired surface	122
Figure 3.4.5:	Measured points of the actual surface	123
Figure 3.4.6:	Interpolated points of actual surface	123
Figure 3.4.7:	Flow chart for first model	126
Figure 3.4.8:	Example of irradiation strategy for first model	127
Figure 3.4.9:	Example of speed range with calculated minimum speed (63.65mm/s) for first model	128
Figure 3.4.10:	Flow chart for modified model	129
Figure 3.4.11:	Example of irradiation strategy for modified model	130
Figure 3.4.12:	Example of the results of 2D forming used for speed calibration	130

Figure 4.1.1:	Example of the fall off in bend angle per pass during multi-pass TGM, laser forming over the same scan line using the same process parameters per pass. 1.5mm mild steel, 760W CW CO ₂ , 5.5mm beam diameter, 30mm/s, graphite coated.	133
Figure 4.1.2:	Thermocouple output, 8mm beam dia. 20mm/s, 760W, 10 passes, 40 second intervals	139
Figure 4.1.3:	Cantilever clamping/ Edge Clamp	140
Figure 4.1.4:	Illustration of the intersected incident beam area for an already bent sample	141
Figure 4.1.5:	Schematic of the incident beam geometry for the cantilever clamping condition	142
Figure 4.1.6:	Effect of bend angle on the incident beam area for a cantilever clamping condition. 5.5mm beam diameter	143
Figure 4.1.7:	Incident energy fluence with increasing bend angle for a cantilever clamping condition. 5.5mm beam diameter, 760W	144
Figure 4.1.8:	Bend angle development for a given beam diameter at a constant line energy, 1.5mm mild steel, 760W CW CO ₂ , 30mm/s	145
Figure 4.1.9:	Variation in bend angle per pass with increasing incident beam diameter. 1.5mm mild steel, 760W, 30mm/s.	146
Figure 4.1.10:	Energy fluence with increasing bend angle (from figure 4.1.7) and energy fluence with an increasing beam diameter equivalent to the same incident area increase	147
Figure 4.1.11:	Average variation in bend angle per pass with increasing incident beam diameter. 1.5mm mild steel, 760W, 30mm/s	148
Figure 4.1.12:	Bend angle per pass prediction with increasing existing bend angle. 1.5mm mild steel, 760W, 30mm/s, 5.5mm beam	148
Figure 4.1.13:	Predicted bend angle development due to increasing beam area with increasing bend angle and comparison with experimental results. 1.5mm mild steel, 760W, 30mm/s, 5.5mm beam diameter	149

Figure 4.1.14:	V-block or simply supported clamping arrangement	150
Figure 4.1.15:	Schematic of the incident beam geometry for a V block or simply supported clamping arrangement	151
Figure 4.1.16:	Effect of bend angle on the incident beam area for a V-block or simply supported clamping condition. 5.5mm beam diameter	153
Figure 4.1.17:	Incident energy fluence with increasing bend angle for a V-block or simply supported clamping condition. 5.5mm beam diameter, 760W, 30mm/s	154
Figure 4.1.18:	Comparison of the experimental bend angle development for the two clamping conditions, edge clamp and V block. 1.5mm mild steel, 760W CW CO ₂ , 30mm/s, 5.5mm beam diameter, graphite coated	155
Figure 4.2.1:	Sample 1, 2 and 3 after laser forming	162
Figure 4.2.2:	a) Irradiation line on sample 2, b) Irradiation line on sample 1	162
Figure 4.2.3a:	Sample 1 surface measurement	164
Figure 4.2.3b:	Sample 1 surface measurement, close-up of clamped side	164
Figure 4.2.4a:	Sample 2 surface measurement	165
Figure 4.2.4b:	Sample 2 surface measurement, close-up of clamped side	165
Figure 4.2.5a:	Sample 3 surface measurement	166
Figure 4.2.5b:	Sample 3 surface measurement, close-up of clamped side	166
Figure 4.2.6:	Position of the points measured on the surface. The dotted line at 50mm along the length is the bend/irradiation line and the lines at 5, 20 and 35mm are the lines along which the measurements are taken for the height along the length graphs.	167
Figure 4.2.7:	Height along length of sample 1 at 5, 20 and 35mm points across the width after laser forming and before heat treatment	168
Figure 4.2.8:	The height along length of sample 1 stopping at 55mm along the sample and at 5, 20 and 35mm points across width after laser forming and before heat treatment	168

Figure 4.2.9:	Height along length of sample 2 at 5, 20 and 35mm points across width after laser forming and before heat treatment	169
Figure 4.2.10:	Height along length of sample 3 at 5, 20 and 35mm points across the width after laser forming and before heat treatment	169
Figure 4.2.11a:	Sample 1 surface measurement after annealing	171
Figure 4.2.11b:	Sample 1 surface measurement after annealing, close-up of clamped side	171
Figure 4.2.12:	Sample 2 surface measurement after annealing, close-up of clamped end	173
Figure 4.2.13:	Sample 3 surface measurement after annealing, close-up of clamped end	174
Figure 4.2.14:	Height along length of sample 1 at 5, 20 and 35mm points across the width after annealing	174
Figure 4.2.15:	The height along length of sample 1 stopping at 55mm along the sample and at 5, 20 and 35mm points across width after laser forming and before heat treatment	175
Figure 4.2.16:	Height along length of sample 3 at 5, 20 and 35mm points across the width after annealing	175
Figure 4.2.17:	Height along length of sample 2 at 5, 20 and 35mm points across the width after annealing	176
Figure 4.2.18:	Sample 2 surface measurement after tempering to T4, close-up of clamped side	178
Figure 4.2.19:	Sample 3 surface measurement after tempering to T4, close-up of clamped side	179
Figure 4.2.20:	Height along length of sample 2 at 5, 20 and 35mm points across the width after tempering to T4	179
Figure 4.2.21:	Height along length of sample 3 at 5, 20 and 35mm points across the width after tempering to T4	180
Figure 4.2.22:	Sample 2 surface measurement, close-up of clamped side	182
Figure 4.2.23:	Height along length of sample 2 at 5, 20 and 35mm points across the width after tempering to T6	182
Figure 4.2.24:	Locations for the hardness test	183
Figure 4.2.26:	Results of micro hardness test on heat treated AA6061	184
Figure 5.1.1:	Developable and non-developable surfaces	190

Figure 5.1.2:	Gaussian curvature of a part-cylinder (a), bowl/pillow (b) and saddle shape (c)	193
Figure 5.1.3:	Saddle with colour map of Gaussian curvature	194
Figure 5.1.4:	Dome shape with a colour map of Gaussian curvature	195
Figure 5.1.5:	Part cylinder with a colour map of Gaussian curvature	195
Figure 5.1.6:	The desired semi-developable shape with a colour map of Gaussian curvature	196
Figure 5.2.1:	Contours of constant height and rotated resultant gradient vector	199
Figure 5.2.2:	Illustration of required forming direction for a given bend direction	200
Figure 5.2.3:	Height contour plot of pillow surface with an indication of the required gradient vector magnitude at points along the contour lines	201
Figure 5.2.4:	Laser forming of 1.5mm mild steel, 5.5 mm beam dia. 760W CO ₂ 10 – 70mm/s, graphite coating Calibration data	202
Figure 5.2.5:	Example of speed range with calculated minimum speed (63.65mm/s) for first model	204
Figure 5.2.6:	Desired shape, max forming 40mm	207
Figure 5.2.7:	Surface of error between flat sheet and desired shape	207
Figure 5.2.8:	Contour of error between flat sheet and desired shape	208
Figure 5.2.9:	Irradiation pattern for pass 1, 760W CW CO ₂ , 5.5mm beam diameter, speed range 30-85mm/s	208
Figure 5.2.10:	Result of first pass with normal scale and smaller scale of the z axis.	209
Figure 5.2.11:	Error between measured shape and desired shape	209
Figure 5.2.12:	Irradiation pattern generated for the pass 2. Traverse speed range 30-85mm/s	210
Figure 5.2.13:	Irradiation path for pass 3. Traverse speed 40-85mm/s	210
Figure 5.2.14:	Irradiation path for pass 5. Traverse speed 50-85mm/s	211

Figure 5.2.15:	Irradiation path for pass 7. Traverse speed 65-85mm/s	211
Figure 5.2.16:	Final formed surface showing all irradiation paths	212
Figure 5.2.17:	Final shape	212
Figure 5.2.18:	Error in the final shape	213
Figure 5.2.19:	Views of the final component	213
Figure 5.2.20:	Displacement and error of a single point at the edge of the work-piece throughout the experiment	215
Figure 5.2.21:	Highly formed component using the original irradiation pattern from pass 1	216
Figure 5.3.1:	Calculation of Δa to find Δx .	219
Figure 5.3.2:	the calculation of Δx from Δa	219
Figure 5.3.3:	The measured points before the decrease in viewable area is calculated	220
Figure 5.3.4:	The measured points after the decrease in viewable area is calculated.	220
Figure 5.3.5:	Illustration of required forming direction for a given bend direction	221
Figure 5.3.6:	Lines of constant height for a part-cylinder	222
Figure 5.3.7:	The lines of constant gradient magnitude for a part-cylinder	222
Figure 5.3.8:	Lines of constant height for a bowl(a) and a saddle(b) and lines of constant gradient magnitude for a bowl (c) and a saddle (d)	224
Figure 5.3.9:	Results from operating window for laser forming of 1mm and 2mm AA5251	226
Figure 5.3.10:	Desired shape for 80x200x1mm AA5251 being laser formed at a laser power of 400W	228
Figure 5.3.11:	Irradiation strategy for first pass at 400W and	228
Figure 5.3.12:	Height of measured points after pass 1 at 400W and 62mm/s	229
Figure 5.3.13:	Irradiation strategy for pass 2 at 400W and 62mm/s	229
Figure 5.3.14:	Height of measured points after pass 2 at 400W and 62mm/s	230
Figure 5.3.15:	Irradiation strategy for pass 3 at 400W and 62mm/s	231
Figure 5.3.16:	Height of measured points after pass 3 at 400W and 62mm/s	231
Figure 5.3.17:	Irradiation strategy for pass 4 at 400W and 62mm/s	232

Figure 5.3.18:	Measured points after pass 4 at 400W and 62mm/s	232
Figure 5.3.19:	Irradiation strategy for pass 5	233
Figure 5.3.20:	Final measured shape for 3D semi-developable forming of AA5251 at 400W	233
Figure 5.3.21:	Error between desired shape and final shape of 200x80x1mm AA5251 at 400W, beam diameter of 3mm and a speed of 62mm/s	234
Figure 5.3.22:	Heavily faceted component resulting from the initial strategy chosen	234
Figure 5.3.23:	The selected area for analysis of sample 1 and 2	235
Figure 5.3.24:	Magnified cross section of dwell point from sample 1.	236
Figure 5.3.25:	Magnified cross section of dwell point from sample 2.	236
Figure 5.3.26:	Desired shape for 200x80x1mm AA5251 being laser formed at a laser power of 200W	239
Figure 5.3.27:	Pass 1 irradiation path at 200W and 25mm/s	240
Figure 5.3.28:	Height of measured points after first pass at 200W and 25mm/s	241
Figure 5.3.29:	Pass 2 irradiation strategy at 200W and 28mm/s	241
Figure 5.3.30:	Height of measured points after pass 2 at 200W and 28mm/s	242
Figure 5.3.31:	Pass 3 irradiation pass at 200W and 31mm/s	243
Figure 5.3.32:	Height of measured points after pass 3 at 200W and 31mm/s	243
Figure 5.3.33:	Pass 4 irradiation strategy at 200W and 32mm/s	244
Figure 5.3.34:	Final geometry produced. 200x80x1mm AA5251, 200W, 3mm beam diameter, speed range 25-32mm/s.	244
Figure 5.3.35:	Error between desired and final shape in 200x80x1mm AA5251 at 200W 3mm beam diameter and speed range of 25-32mm/s	245
Figure 5.3.36:	Picture of final shape 200x80x1mm AA5251, 200W, 3mm beam diameter, speed range 25-32mm/s.	246
Figure 5.3.37:	Marks from the 3D forming of 200x80x1mm AA5251 at 200W and a speed range of 25-32mm/s	246

Figure 5.3.38:	Pass 1 irradiation strategy for forming of 400x200x1mm AA5251 at 200W	248
Figure 5.3.39:	Measured point after pass 1 for forming of 400x200x1mm AA5251 at 200W	248
Figure 5.3.40:	Pass 2 irradiation strategy for forming of 400x200x1mm AA5251 at 200W	249
Figure 5.3.41:	Final geometry produced after second pass. 400x200x1mm AA5251, 200W, 3mm beam diameter, speed 29mm/s.	250
Figure 5.3.42:	Error between the final and desired shape for 200x400x1mm component formed at 200W	250
Figure 5.3.43:	Marks from the 3D forming of 400x200x1mm AA5251 at 200W and a speed range of 31.4-35.9mm/s. The marks on the left are where the piece comes into the focus of the laser beam.	251
Figure 5.3.44:	Picture of final shape 400x200x1mm AA5251, 200W, 3mm beam diameter, speed 29mm/s.	251
Figure 5.3.45:	Reversal of process, laser formed and mechanically pre-bent samples (80x80x2mm AA5251; 900W; 45mm/s; 5mm beam diameter).	256
Figure 5.3.46:	Randomly mechanically distorted components (400x40x2mm AA5251).	257
Figure 5.3.47:	The starting shape to be flattened using the laser forming process	258
Figure 5.3.48:	The irradiation strategy for the first pass	258
Figure 5.3.49:	The measured shape after the first pass	259
Figure 5.3.50:	Irradiation strategy for second pass	259
Figure 5.3.51:	Final shape reached after second pass with approximately than +/-0.5mm error.	260
Figure 5.3.52:	Dwell marks and irradiation lines left by the laser forming process	260
Figure 5.3.53:	Flattened strut with an example of one of the pre laser formed struts with the same magnitude of mechanically forming	261
Figure 5.3.54:	Aluminium strut deformed mechanically to a maximum deformation of -45mm from the height at the centre.	263
Figure 5.3.55:	The irradiation strategy for the first pass.	263
Figure 5.3.56:	The result of the first pass	264

Figure 5.3.57:	Irradiation strategy for the second pass	264
Figure 5.3.58:	Resultant measurement from pass 2	265
Figure 5.3.59:	Irradiation strategy for pass 6	265
Figure 5.3.60:	The resultant measurement from the sixth pass.	266
Figure 5.3.61:	Irradiation strategy for pass 10	266
Figure 5.3.62:	Resultant measurement from pass 10	267
Figure 5.3.63:	The final irradiation strategy at pass 14	267
Figure 5.3.64:	The resultant measurement of the final pass.	268
Figure 5.3.65:	Strut with maximum 45mm mechanical deformation	268
Figure 5.3.66:	Strut after laser forming correction	269
Figure 5.3.67:	Increasing speed over 14 passes and resultant change in the increment between the lines of constant gradient for strut reversal experiment	270

List of Tables

Table 2.1:	Outline of the 3 main LF mechanisms	17
Table 2.2:	Degree of application potential for LF in various stages of a general product life-cycle (not specific to component scale, material or geometry)	71
Table 3.1.1:	Typical values of the reflectivity of various surfaces to 10.6 μ m radiation at normal angles of incidence	101
Table 3.1.2:	Mechanical properties of Mild Steel CR4	102
Table 3.1.3:	Thermal Properties of Mild Steel CR4	103
Table 3.1.4:	Typical mechanical properties of AA6061 in its various tempers	103
Table 3.1.5:	Thermal Properties of AA 6061 in three different tempers	104
Table 3.1.6:	Physical properties of AA5251	105
Table 3.1.7:	Mechanical properties of AA5251	105
Table 3.3.2:	Laser forming parameters of the individual samples	112
Table 4.2.1:	Laser forming parameters of the individual samples	161
Table 4.2.2:	Resultant angles after laser forming	163
Table 4.2.3:	Resultant angles after annealing of sample 1	172
Table 4.2.4:	Resultant angles after annealing of sample 2	172
Table 4.2.5:	Resultant angles after annealing of sample 3	172
Table 4.2.6:	Resultant angles after Tempering to T4 of sample 2	177
Table 4.2.7:	Resultant angles after tempering to T4 of sample 3	178
Table 4.2.8:	Resultant angles after Tempering to T6 of sample 2	181

List of Symbols

A	Absorption (constant)
A_l	Area
a	Heat conductivity
b	Breadth of plastic zone
C_p	Specific heat capacity
d_l	Laser beam diameter
D	Ratio of depth of plastic zone to sheet thickness
E	Elastic Modulus
F	Force
f	Lens focal length
I	Moment of Inertia
I_0	Intensity at centre of laser beam
k_f	Flow stress
k, λ	Thermal conductivity
l	Length
l_h	Length of heated zone
l_1	Length of plastically strained zone
l_2	Length of elastically strained zone
M	Bending moment
M^2	Beam Quality Factor
m	Mass

N	$\frac{8Ap_1\sqrt{at}}{\pi\lambda d_1^2}$	Parameter for normalising the temperature
P, p_1		Laser power
P_{c1}		Maximum principle curvature
P_{c2}		Minimum principle curvature
P_f	$\frac{d_1}{4\sqrt{at}}$	
G_c		Gaussian curvature
R_l, r_l		Laser beam radius
R_2		Distorted beam radius
s_0		Sheet thickness
s_1		Depth of plastic zone
T		Temperature
T_c		Critical temperature for plastic flow
t		time
v_l		Velocity
w		Displacement of a plate
x, y, z		Cartesian co-ordinates
Y		Yield Strength
α		Thermal diffusivity
α_b		Bend angle
α_{th}		Coefficient of thermal expansion
γ_{xy}		Shear Strain in the xy plane
ΔT		Time of heating
ΔT		Average temperature of heated zone
$\Delta T'$		Temperature increase
ε		Strain
ε_n		Strain in n direction (n = x, y, z etc.)

ε_{in}	Inherent strain (maximum plastic strain less elastic strain during heating)
κ	Thermal diffusivity
λ	Wavelength
ρ	Mass density

Chapter 1

Introduction

The work presented in this thesis centres around the controlled three dimensional laser forming of metallic components. This uses a predictive/adaptive geometry based model for closed loop control.

The laser forming process has become viable for the shaping of metallic components, as a means of rapid prototyping and for adjusting and aligning. Laser forming is of particular value to industries that rely on expensive stamping dies and presses for prototyping. In contrast with conventional forming techniques no mechanical contact is required for this process promoting the idea of 'virtual tooling'. As with other laser

applications, such as cutting and marking, laser forming offers process flexibility and the possibility of automation.

The origins of laser forming are in the ship building industry where flame bending is used to bend large metal sheets for ship construction. However, laser forming is a much more delicate and controllable process than its parent with the ability to form at a macro and micro scale with high accuracy.

With the use of a laser in thermal forming operations localised heating can be created. This minimises any potential effects from heating to other areas of the material therefore increasing the range of size and type of materials that can be formed.

Three main mechanisms of laser forming have been identified. These are the temperature gradient mechanism (TGM) the buckling mechanism (BM) and the upsetting or shortening mechanism (UM). For accuracy and consistency the TGM is the main mechanism used in this thesis. It produces a maximum bend angle of 3° per pass and always forms towards the laser. The BM however, can produce much larger bends. When forming with this mechanism it is more difficult to control accurately and the material can bend either way which is undesirable for control. If the material is prevented from bending by either external forces or the geometry of the material the UM can occur causing the material to shorten.

Since it was first conceived laser forming has been able to form 2D shapes. 2D laser forming is well established and it is possible to control this with high accuracy in applications that include micro scale

alignment. However laser forming hasn't managed to match the 3D capabilities of flame bending. In flame bending very large sheets of metal are heated using an oxyacetylene torch controlled by an experienced operator who learns from experience how to produce required shapes. This flame bending process can be envisaged to be a black art as the process can appear a little haphazard. To create a method for producing accurate 3D shapes using laser forming a full understanding is needed to control the process.

Presented in this thesis are 2D experiments investigating the influencing factors of multiple pass 2D laser forming and the effects of heat treatment on 2D laser formed parts. The results from these investigations are also related to 3D laser forming investigations. The main focus of this thesis is to investigate the potential of controlling the laser forming of 3D components using a geometry based model.

Chapter 2

Literature Review

2.1 Laser Forming

The inspiration behind Laser Forming (LF) originates in the flame bending or line-heating process. This uses an oxyacetylene torch to induce thermal stresses into a work-piece^{1, 2}. Flame bending has been used extensively for the profiling and straightening of heavy engineering components in both the construction and shipbuilding industries^{3, 4, 5}. This process is completely manual and relies heavily on operator skill to

successfully form these components. One of the main mechanisms used in flame bending requires a steep thermal gradient through the thickness of the work-piece. As the heat from a flame is not concentrated on a spot it can be difficult to create a steep thermal gradient. With a thinner cross section or higher thermal conductivity achieving a thermal gradient can become impossible.

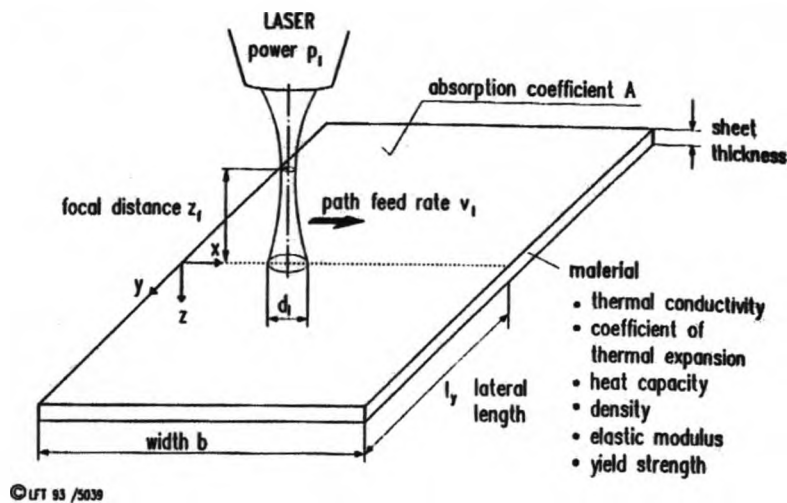


Figure 2.1: Laser Forming Set-up & Process Variables ⁶

This problem is vastly decreased with a laser as it produces a focused heated area on the surface of the work-piece, when compared to a flame. This not only makes it possible to thermally form components that previously would not have been possible to form but also introduces a heat source which has a very high degree of control.

The laser forming process is realised by introducing thermal stresses into the surface of a work-piece by heating the surface with a laser beam. These internal stresses induce plastic strains that result in local elastic-plastic buckling of the work-piece. The following sections describe the laser

forming mechanisms in detail with some practical applications discussed later in this chapter.

2.2 Laser Forming Mechanisms

Because of the control offered by the laser beam, different types of temperature fields can be generated, yielding different forming mechanisms and results. The mechanisms discussed here are the Temperature Gradient (TGM), Buckling (BM) and Shortening or Upsetting (UM) mechanisms (figure 2.2). There is a fourth mechanism, the point source mechanism, described by Vollertsen that isn't discussed here.

As its name suggests, the temperature gradient mechanism depends on maintaining a high temperature gradient across the sheet thickness. This is typically achieved with a heated area smaller or equal diameter to the thickness of the work-piece. This mechanism always results in a positive bend, towards the laser. The buckling mechanism is active if the temperature gradient across the sheet thickness is small and the diameter of the heated area is large. This mechanism can result in a bending towards or away from the laser beam. Which is a disadvantage as it is essential to control the direction of bending. The upsetting (or shortening) mechanism is based on nearly homogeneous heating of the material. Due to the geometrical restraints or other restraints buckling is avoided resulting in a shortening and thickening of the material. This shortening is used in two different ways for forming. Either plane sheets are treated with this mechanism resulting in spatially formed parts or extrusions are treated, giving specially bent extrusions⁶

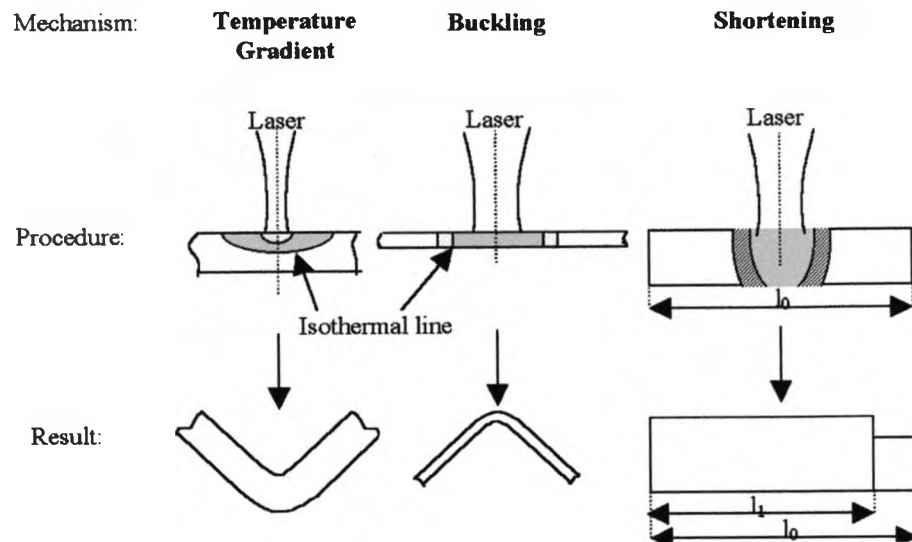


Figure 2.2: The Laser Forming Mechanisms ⁶

2.2.1 The Temperature Gradient Mechanism (TGM)

The conditions for the temperature gradient mechanism are energy parameters that lead to a steep temperature gradient through the sheet thickness (Figure 2.3). The path feed rate has to be chosen to be large enough that a steep temperature gradient can be maintained. It has to be increased if materials are used which have a high thermal conductivity. The laser path on the sheet surface is typically a straight line across the whole sheet. This straight line is incident with the bending edge.

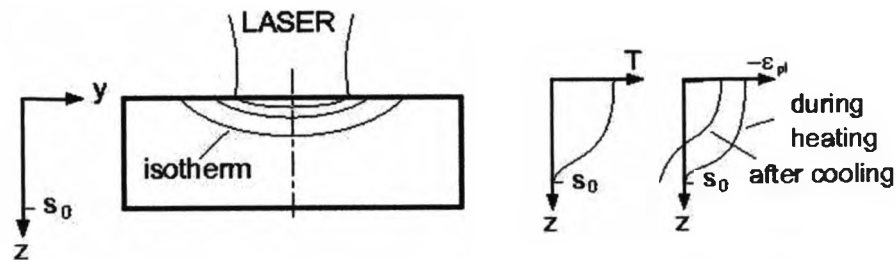
temperature-gradient

Figure 2.3: Energy conditions required for the TGM ⁶

The temperature gradient mechanism proceeds in the following steps:

1. Heating of the surface and thermal expansion against the cold bulk material
2. Development of counter bending
3. Further heating and plastic compression of the surface
4. Cooling of the surface and thermal contraction
5. Development of the bending angle

The first step of the temperature gradient mechanism is a heating of the surface which leads to purely elastic strains. Due to the thermal expansion of the surface layer there is a counter bending of the part, resulting in a bending away from the laser beam. The amount of the counter bending is minimal as it is the small heated area, which is approximately the size of the laser spot, generating forces to counteract the global stiffness of the whole sheet. Because the counter bend relaxes the stresses at the heated surface it is detrimental to the development of a bending angle towards the laser. This is because the relaxation of the surface stresses leads to a lower fraction of the thermal strain being converted into plastic strain.

Further heating leads to a decrease of the flow stress in the heated area and a further increase of the thermal expansion of the surface layer. At a certain

temperature which depends on the material and its geometry, the thermal strains reach the yield stress of the material. A further increase of the temperature results in a conversion of the thermal expansion into plastic compressive strains. As the yield stress is temperature dependent it is reduced here increasing the amount of plastic strain (figure 2.4). These plastic compressive strains are accumulated until the heating stops, after the laser has passed, or surface melting occurs.

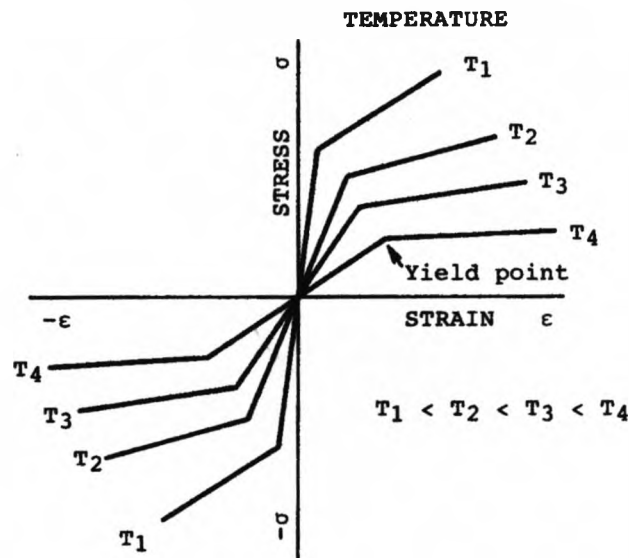


Figure 2.4: Stress-strain diagram of material as a parameter of temperature⁷

In contrast to the heating part of the cycle, where the heat flow is through the surface due to the coupling of the laser energy, cooling proceeds by heat conduction into the bulk material. This acts as a form of self quenching. Energy losses by radiation and heat conduction into the environment are of less importance and can be neglected at this stage. The heat flows into the surrounding sheet metal and gives cooling rates of typically 10-20 s. This is much slower than the heating times of about 0.5s. During cooling shrinkage of the heated material sets in. Due to the surface being plastically compressed during heating it is shorter after cooling to

room temperature compared to the non-heated lower layers of the sheet. Because of this a bending angle towards the laser beam develops. The magnitude of the bending angle depends on the coupled energy, the geometry of the part and the thermal and mechanical properties of the material. It lies typically between 0.1 degrees and 3 degrees after one laser pass.

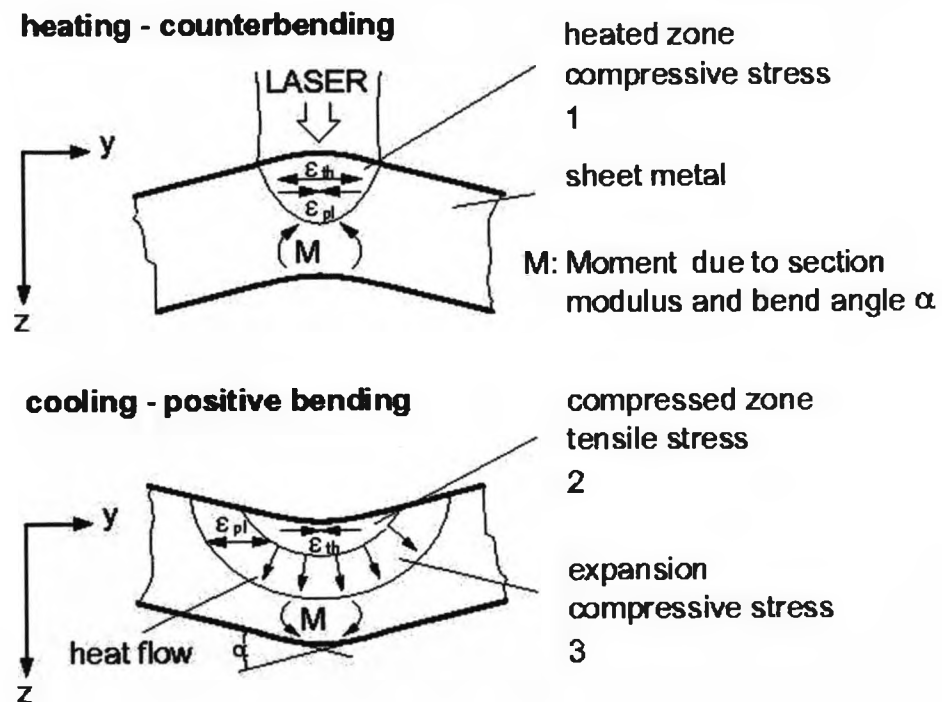
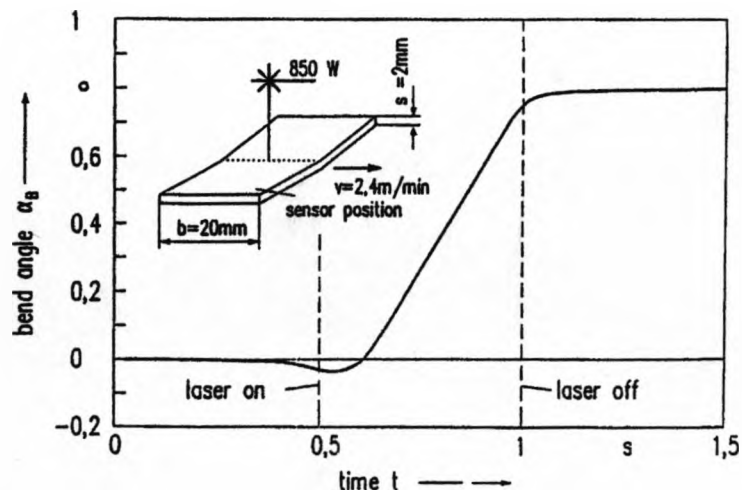


Figure 2.5: Principle of the Temperature Gradient Mechanism (TGM)⁶

The reason why the thermal expansion leads to plastic compression of the sheet and the thermal contraction doesn't lead to plastic tension of the material is due to the comparatively slow cooling of the material. During cooling of the irradiated area the temperature of the surrounding material sheet increases due to self quenching. This is much faster than the material can remove the heat to its surroundings. As this whole area, including the irradiated area is now cooling simultaneously the moments produced by

the cooling only have to counter-balance the local stiffness of the part, which is much smaller than the global stiffness the counter bend has to overcome during heating. So there is nearly no cancellation of the plastic compression, created during heating, allowing large bending angles to develop. This asymmetry of the heating is essential for the development of a bending angle for this mechanism⁶ (figure 2.5).

The asymmetry of the process can be seen in the temporal development of the bend angle. This was investigated experimentally by Vollertsen⁸. A steel sheet of 2mm thickness was bent with a laser power of 850W and a processing speed of 2.4m/min. A tactile sensor was placed at the beginning of the sheet which measured the relative motion. (It appears that the counter bend starts before the laser irradiates the sheet here figure 2.6 but this is due to the edge of the laser beam causing some initial heating effects.) Here a counter bend can be seen to be formed in the first few milliseconds, during heating, with the bend forming over a longer cooling phase.



© UFT 94/5972

Figure 2.6: Time run of the bend angle⁸

2.2.2 The Buckling Mechanism (BM)

The buckling mechanism operates if the laser beam diameter is large compared to the sheet thickness and the processing speed is slow resulting in a small temperature gradient across the sheet thickness. These conditions may be realised by different parameter combinations. One possibility is to irradiate a high alloyed steel foil (e.g. 100 μ m in thickness), using a low power laser and a low processing speed. Another possibility is to use material with a high thermal conductivity like copper. The buckling mechanism proceeds by the following steps:

1. Heating of a large area of the sheet metal and development of compressive stresses
2. Onset of buckling
3. Growth of the buckle
4. Shifting the buckle through the whole sheet
5. Relaxation of the elastic stresses.

The principle is shown in figure 2.7. Heating with the laser results in the thermal expansion of the material. This produces compressive stresses in the heated area. If the heated area is large enough a small natural deviation from perfect flatness in the sheet creates instability. The direction of the buckling is determined by different factors, these are for example the pre-bending of the sheet and the relaxation of residual stresses.

In the centre of the buckle the temperature is very high so that the flow stress is low in this region. Therefore the bending in this region is nearly totally plastic. In contrast the root of the buckle which is far away from the centre of the beam is heated to a much lesser extent. So the temperature is low and the flow stress in this region is high. Therefore the bending of the sheet in this region is fully elastic.

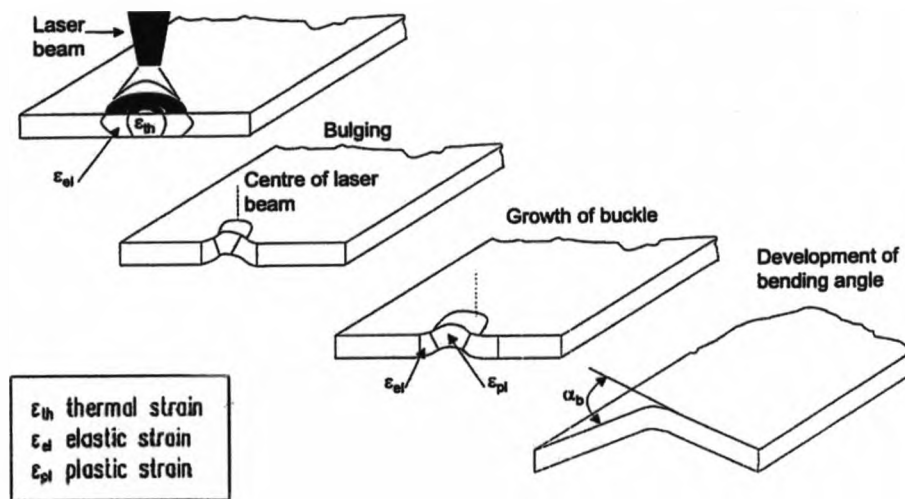


Figure 2.7: Stages in the Buckling Mechanism (BM)⁶

Due to further heating the thermal expansion of the material increases the magnitude of the buckle. As the laser beam traverses across the surface the buckle travels along the bending edge. Now the existing buckle predetermines the buckling direction of the remaining sheet. While the beam traverses across the surface the stiffness of the part is changed. At the beginning of the buckling process the bending arms were held in the original plane due to the stiff surrounding material. As an increasing amount of the sheet is formed by the buckle the forces that hold the bending arms straight, decrease. Therefore the elastic part of the buckle relaxes and only the plastic part remains in the sheet. This leads to the development of the bending angle which can be seen after irradiating the whole bending edge. After completion of the irradiation path the elastic

strains are fully relaxed so that an angular section remains. The buckling mechanism results typically in bending angles between 1 and 15 degrees.

This is significantly larger than observed for the temperature gradient mechanism. This is not a result of a higher degree of performance. With the buckling mechanism more energy can be coupled into the work-piece in one step. Trying the same for the temperature gradient mechanism would result in either surface melting or buckling. Therefore the energy which can be coupled into the work-piece is restricted for the temperature gradient mechanism.

2.2.3 The Shortening or Upsetting Mechanism (UM)

If the laser beam diameter is of the same order or greater than the sheet thickness, the path feed rate is low, the thermal conductivity of the material is relatively high and in addition the geometry of the part does not allow buckling of the material, the Upsetting (Shortening) Mechanism operates. This is true for thick sheets and for extrusions and other stiff structures. The upsetting mechanism proceeds by the following steps:

1. Heating of the cross section and thermal expansion.
2. Further thermal expansion that exceeds the elastic strain, resulting in a plastic compression of the cross section.
3. Cooling of the material without or with small tensile straining.

These steps are shown in figure 2.8. Using a low processing speed the sheet is heated nearly homogeneously through its thickness. Due to the temperature increase the flow stress decreases in the heated area and the thermal expansion approaches the elastic limit of the material. Further heating leads to plastic compression as the heated material is restricted in expansion by the surrounding material. Therefore a large amount of the thermal expansion is converted into a plastic compression. The plastic compression then remains during cooling causing the heated area to contract. Due to the low temperature gradient there is also a very small gradient in the plastic strain through the thickness.

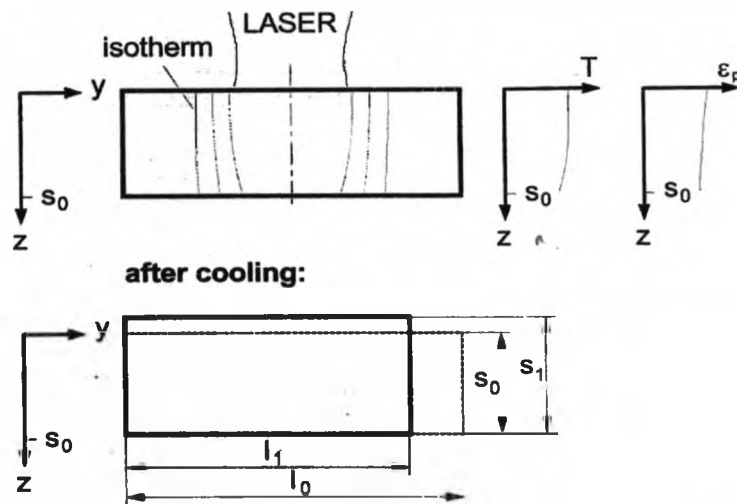


Figure 2.8: The Upsetting (Shortening) Mechanism (UM) ⁶

The plastic compressive strain remains in the sheet for the same reason which hinders plastic tension occurring in the case of the temperature gradient mechanism. During heating the expansion is only local and is hindered strongly by the surrounding material. So the thermal expansion is converted into a plastic compression. During cooling the cooling is active along the whole line which was heated. Therefore, the contraction is hindered less than the thermal expansion. Therefore nearly all the plastic

compression remains. This results in the shortening and thickening of the material.

Mechanism	Procedure	Forming efficiency	Results
Temperature Gradient (TGM)	Spot diameter ~ thickness Higher traverse speeds Applicable to thin sections	~1-2° bending per pass	High control Low efficiency
Buckling (BM)	Spot diameter > thickness Lower traverse speeds Applicable to thin sections	~15° bending per pass	High efficiency Reduced control
Shortening (Upsetting)	Spot diameter ~ thickness Applicable to stiff geometries (can't buckle)	Microns of shrinkage per pass	Shortening Thickening

Table 2.1: Outline of the 3 main LF mechanisms ⁹

2.3 Mathematical Models

The ability to investigate a complex process in a non-destructive manor in any situation is extremely useful, however as with any model assumptions are made and the quality of the output data is only as good as the quality of the input data. A number of the numerical models for each mechanism available in the literature are outlined in the next sections.

2.3.1 Analytical Models

A number of analytical models are available that have been developed to describe and expand on the three main LF mechanisms. Some of the key results and concepts are outlined here.

2.3.1.1 Temperature Gradient Mechanism

A number of models have been proposed for the temperature gradient mechanism^{6, 8, 10-15}. Here we look at Vollerstsen's trivial, two layer and residual stress model⁶.

A complete model should take into account every possible variation from observation taken during experimentation. In the case of the temperature gradient mechanism there are four parts to consider ⁶.

These are:

1. The temperature field
2. The plastic strains
3. The curvature during cooling
4. The bend angle

2.3.1.1.1 The Trivial Model

To fully account for all these factors analytically is almost impossible. To help with analytical modelling some assumptions are made. The trivial model is the simplest model discussed here. For ease of calculation there are many assumptions with a large number of experimental observations unaccounted for.

A two dimensional representation of the process is used for calculations. (figure 2.9) Some of the assumptions made are:

1. The material properties are independent of temperature
2. The heated layer is half the total thickness, $s_0/2$
3. The heated layer is heated homogenously with no heating in the lower layer

4. The thermal expansion is converted into plastic compression, with no counter bending or elastic strains
5. There is no straining of the compressed upper layer during cooling

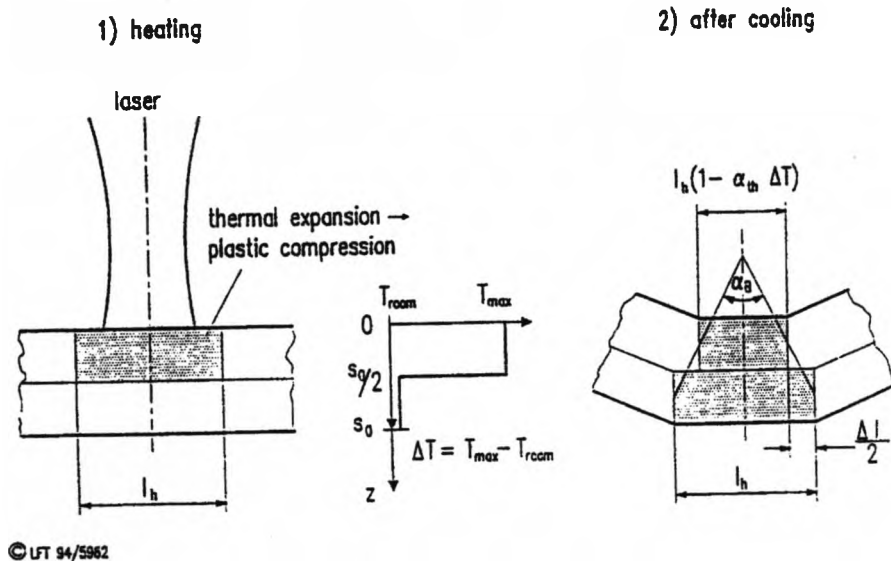


Figure 2.9: The trivial model ⁶

This results in the upper layer being shorter than the lower layer after processing producing a bend towards the laser. The bending angle can then be calculated from the temperature increase and the linear coefficient of thermal expansion. The temperature increase of the upper layer is calculated from the energy approach. A similar energy approach is used for calculating the bend angle in flame bending ¹⁶. The resulting calculation for the temperature increase is given by the coupled power divided by the mass and the heat capacity of the material. This gives a formula for the bend angle:

$$\alpha_B = \frac{4Ap_1\alpha_{th}}{v_1c_p\rho s_0^2} \quad (2.1)$$

2.3.1.1.2 Two Layer models for the TGM

Vollertsen two layer model continues from the trivial model, this model has been widely quoted and a number of comparative studies have been performed. The main difference between the two layer model and the trivial model is that in the trivial model the forces and moments while the sheet cools down are neglected. This is taken into account in the two layer model. The two layer model also has a variable thickness of the heated layer unlike the trivial model which assumes that the heated layer is half the thickness of the material.

A two dimensional representation of the process is used for calculations. (figure 2.10) Some of the assumptions made are:

1. The material properties are independent of temperature
2. The heated layer is heated homogenously with no heating in the lower layer
3. The thermal expansion is converted into plastic compression, with no counter bending or elastic strains
4. At the end of heating the two layers have the same lengths. This is because the thermal expansion is constrained by the bulk of the material.
5. Forces and moments are produced during cooling

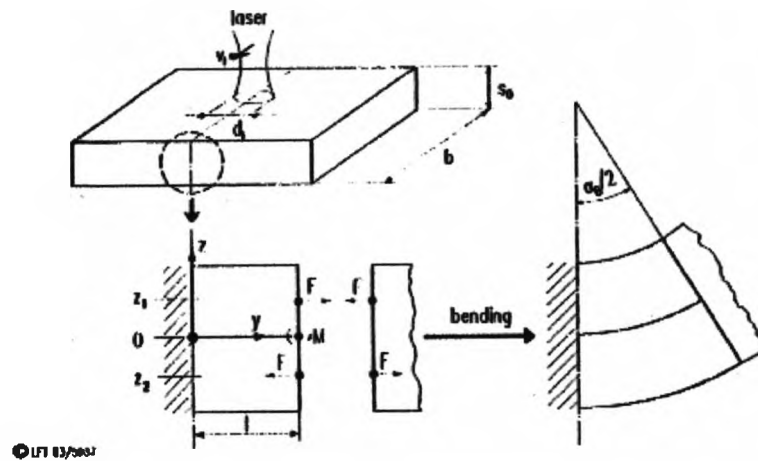


Figure 2.10: Forces and moments acting in the two layer model ¹¹

The bending angle is again calculated from geometrical considerations. Because the difference between the strain in the upper layer, ε_1 , and the strain in the lower layer, ε_2 , is proportional to the bend the following equation can be written.

$$\frac{\alpha_B}{2} = \frac{l(\varepsilon_1 - \varepsilon_2)}{s_0/2} \quad (2.2)$$

To use this equation, the strains need to be calculated. As the upper layer plastically compresses, it tends to shorten during cooling. As a tensile force acts on the upper layer, as the bulk material resist this shortening, this gives a strain which can be calculated from the force and the elastic modulus of the cross-section. The moment is negative and results in compression of the layer. After heating and before conversion of the thermal expansion into plastic compression, thermal expansion gives a positive strain. The resulting equation is shown below.

$$\varepsilon_1 = \frac{F}{E_1 A_1} - \frac{M_1}{(EI)_1} z_1 - \alpha_{th} \Delta T'' \quad (2.3)$$

There are two differences when it comes to calculating the strain in the lower layer. The first is that z_2 is negative which makes the strain due to moment positive. The second is that there is no thermal expansion as heating in the lower layer is neglected in this model. This gives the following equation for the strain in the lower layer.

$$\varepsilon_2 = \frac{F}{E_2 A_2} - \frac{M_2}{(EI)_2} z_2 \quad (2.4)$$

The expressions for ε_1 (equation 2.3), ε_2 (equation 2.4) and the expressions for the geometrical considerations (equation 2.5) are now combined to give:

$$\alpha_B = \frac{12\alpha_{th}\Delta T'' l s_1 (s_0 - s_1)}{s_0^3} \quad (2.5)$$

From this expression the temperature increase of the upper layer, the length of the heated layer and the thickness of the upper layer are unknown. It can be shown using the energy approach that:

$$\Delta T s_1 l (s_0 - s_1) = \frac{P_1 A s_0}{4c_p v_1 \rho} \quad (2.6)$$

Combining this with the previous equation (equation 2.5) gives an expression for bending angle which only has known parameters.

$$\alpha_B = 3 \frac{\alpha_{th}}{\rho C_p} \frac{A p_1}{v_1} \frac{1}{s_0^2} \quad (2.7)$$

In this work by Vollertsen ¹¹ experimental data from other authors was presented and compared with the analytical results, for the results presented there was a reasonable agreement. Although substantial improvement in the agreement between this model and experimental work was achieved (compared to previous analytical models for the flame forming process) some of the basic concepts were still omitted. The model assumed that all of the energy was used for plastic deformation and this ignored the energy used for the elastic straining.

In Yau's model ¹⁵ the two layer model approach was extended to include the counter-bending effect in order to account for some of the purely elastic straining. This modification resulted in two equations, one for the counter-bending angle and one for the bend angle at the end of the cooling cycle. The final equation for the bending angle (positive bend angle less counter-bend angle) including the temperature field equation in Yau's model is:

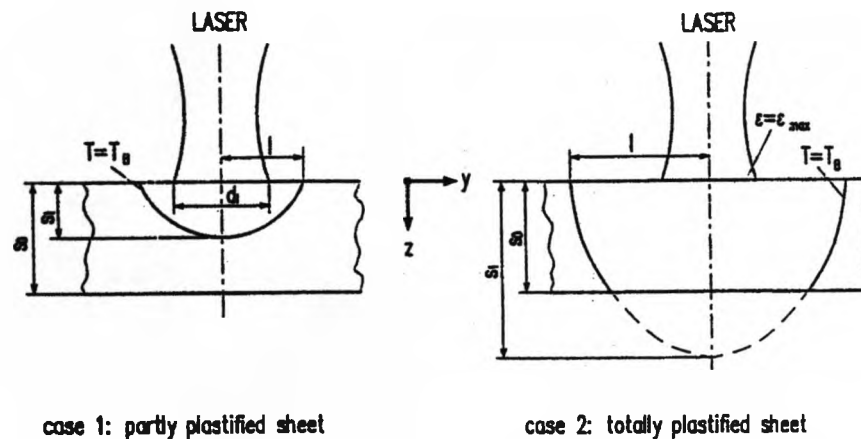
$$\alpha_b = 3 \frac{\alpha_{th}}{\rho C_p} \frac{A p_1}{v_1} \frac{1}{s_0^2} \left(\frac{7}{2} \right) - 36 \frac{l}{s_0} \frac{Y}{E} \quad (2.8)$$

Comparing equation 2.7 with equation 2.8, Yau's solution includes some material and geometrical parameters which reduce the calculated bend angle compared to Vollertsen's solution. Y is the Yield Strength and E the Young's Modulus of the material to be formed. Both solutions were implemented and they differ only slightly for a single pass¹⁷. This is because under the conditions of the temperature gradient mechanism the

counter-bending angle is very small and combined with the simplifying assumptions of the model the difference in the models is less than expected originally. Another factor in these models is that they predict a constant bend angle increase with increasing numbers of passes, it has been seen in a number of published studies that the bend angle rate falls off with increasing numbers of passes¹⁷, these equations do not take into account factors such as coating degradation (absorption dependent) and section thickening¹⁷.

2.3.1.1.3 The Residual Stress Model for the TGM

A critical assumption made in both the trivial model and the two layer model is that the temperature field jumps from room temperature to a high temperature where the upper and lower layers meet. Vollertsen extended this work to include the effects of a realistic temperature field¹². This model used the residual stress approach often used in welding analysis.



OUT 14/1138

Figure 2.11: Layout for the residual stress model⁶

Again this is based on a two dimensional representation (figure 2.11).

Some of the assumptions made are:

1. There is a boundary temperature; this is shown as the isotherm T_B .
2. There are two possible cases for the temperature field. The first is where the depth of T_B is the same or smaller than the sheet thickness and the second is where T_B is greater than the sheet thickness.
3. Below the boundary temperature no plastic deformation takes place
4. The thermal expansion is converted into plastic compression
5. There are elastic strains. These are accounted for by subtracting them from the thermal expansion.
6. Thermal expansion that occurs above the recrystallisation temperature does not produce added plastic strains.
7. The temperature field defines the plastic strain field
8. This field is an elliptical shape
9. Plastic strain is the source for the residual stresses which result in bending

As case 1 best represents the TGM case 2 will not be considered here.

The expression for the calculation of bend angle in case 1 is:

$$\alpha_b = \frac{\varepsilon l s_1}{s_0^3} (3\pi s_0 - 8s_1) \quad (2.8)$$

ε is the plastic strain due to thermal expansion minus the purely elastic strain during heating. If ΔT is greater than the recrystallisation temperature this is taken as the recrystallisation temperature.

$$\varepsilon = \alpha_{th} \Delta T - \frac{k_f(T)}{E(T)} \quad (2.9)$$

Plastic strain occurs if the strain due to the thermal expansion exceeds the purely elastic strain. The elastic strain is governed by temperature dependent properties, in that the flow or yield stress and Young's modulus fall as the temperature increases, thus making it easier to produce a plastic compression and hence bend a material.

To calculate the bend angle requires knowledge of the depth of the plastic zone, s , and the length of the plastic zone, l . An approximate solution in the range relevant to laser forming was used. Details of this approximation can be found in the reference¹².

The depth of the plastic zone was given by:

$$s_1 = -\ln \left(\frac{4T_c}{3N_f} P_f^{-2/3} \right) \frac{\sqrt{2P_f a t}}{2} \quad (2.10)$$

The length of the heated zone was given by:

$$l = P_f \sqrt{4at} \sqrt{\left[-\frac{1}{\sqrt{2p_f}} \ln \left(\frac{4T_c}{3N_f} P_f^{-3/2} \right) \right]} \quad (2.11)$$

This model showed the importance of the thermal conductivity on the process. A slight change in the thermal conductivity changes the thermal expansion and the position of the elastic-plastic interface, as the average temperature in the irradiated zone is sensitive to slight changes in the thermal conductivity. Consequently, it is possible that the bend angle itself is sensitive to small changes in the thermal conductivity. This is contrary to what was reported in the two layer model. In addition with this model the contribution of the thermal strain to the plastic bending was found by subtracting the fraction of the yield stress and the elastic modulus from the thermal expansion (equation 2.9). As mentioned, both the yield stress and the elastic modulus are temperature dependent, this required the function which related those parameters to temperature to be known in order to calculate this contribution accurately.

Provided with accurate information about the temperature dependent mechanical properties, the model can predict the bend angles with reasonable accuracy for an analytical route, comparison with experimental data showed this¹². However this analytical route calculates the bend angle at the end of the process and does not describe the transient stages. Knowledge of the transient stages is useful for successful process control¹⁷.

In analytical work by Magee¹⁷ it was argued that the above models for the TGM, although they have advanced the understanding of the process on a rudimentary level, are incomplete in terms of practical laser forming due to gross simplifications. It was shown in this work that there are other forces and moments acting in laser forming apart from the transverse bending moments. This indicates that there should in theory be two bend angles in laser forming under certain conditions, the angle transverse to the direction of scanning and the angle parallel to the direction of scanning. More recently, the bending parallel to the direction of scanning has been modelled analytically by S. Yongjun et al¹⁸. It is concluded that through investigation it can be found that under the TGM the plate bends about both the x and y axis. This work goes on to say that an analytical model to estimate the bend about the y axis (along the irradiation line) has also been created which approximately agrees with numerical simulation results.

2.3.1.3 The Buckling Mechanism

As described previously, the requirements for the initiation of the BM on sheet metal are that the laser beam diameter on the surface of the sheet is approximately an order of magnitude greater than the sheet thickness and that the material has a suitable thermal conductivity so that the laser processing parameters employed do not result in a temperature gradient in the depth direction of the sample. Using the large beam diameter results in a large amount of thermo-elastic strain which initiates the growth of an elastic-plastic buckle. The strain near the centre of the laser beam is plastic and the strain away from the centre of the beam is considered elastic in Vollertsen's model¹⁹. The elastic strain is released

when the laser beam traverses the exiting edge of the sample and the plastic strain results in a curvature and a bend angle. The model is derived from geometrical considerations (figure 2.12).

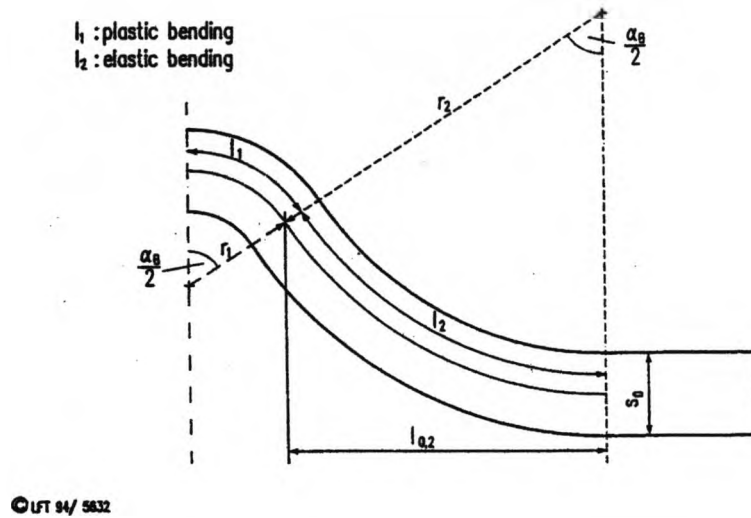


Figure 2.12: Model Geometry for the Buckling Mechanism¹⁹

The bend angle is given by:

$$\frac{\alpha_b}{2} = \frac{l_1}{r_1} = \frac{l_2}{r_2} \quad (2.12)$$

The radius r_2 in region 2 (elastic) is given by elastic bending theory.

$$M_{el} = \frac{Ebs_0^3}{12r_2} \quad (2.13)$$

For the plastic region 1, the moment is given by:

$$M_{pl} = \frac{1}{4} k_f(T_1)bs_0^2 \quad (2.14)$$

At the elastic plastic interface $M_{el} = M_{pl}$, such that r_2 can be now given by:

$$r_2 = \frac{Es_0}{3k_f(T_1)} \quad (2.15)$$

l_2 can be calculated from the new geometry (figure 2.4.5):

$$l_2 = l_{0,2} + \Delta L \quad (2.16)$$

where:

$$l_{0,2} = r_2 \sin\left(\frac{\alpha_b}{2}\right) \quad (2.17)$$

and:

$$\Delta l = \alpha_{th} \overline{\Delta T l_h} \quad (2.18)$$

Where ΔT is the average temperature of the heated zone of dimensions l_h , Δx and s_0 . ΔT is calculated from the absorbed laser power Ap_1 the processing velocity v_1 and the heat capacity and density, ρc_p of the material.

$$\overline{\Delta T} = \frac{Ap_1}{2c_p \rho s_0 v_1} \quad (2.19)$$

l_2 may be calculated from:

$$l_2 = r_2 \sin\left(\frac{\alpha_b}{2}\right) + \frac{f' \alpha_{th} Ap_1}{2c_p \rho s_0 v_1} \quad (2.20)$$

f' is the fraction of the thermal expansion that leads to an expansion of region two.

Using a value of 0.5 results in:

$$\frac{\alpha_b}{2} = \sin\left(\frac{\alpha_b}{2}\right) + \frac{3\alpha_{th}Ap_1k_f(T_1)}{4Es_0^2c_p\rho v_1} \quad (2.21)$$

Using the sine series expansion, the last expression for the bend angle was simplified. The final equation for the bending angle was:

$$\alpha_b = \left[36 \frac{\alpha_{th}k_f(T_1) Ap_1}{c_p\rho E} \frac{1}{v_1 s_0^2} \right]^{1/3} \quad (2.22)$$

Of note here is the much lower dependency of the bend angle on the temperature gradient, which is consistent with the buckling mechanism theory described earlier.

2.3.1.3 The Upsetting Mechanism

Kraus²⁰ modelled box section laser bending. Using the upsetting mechanism box sections or extrusions can be made to bend out of plane by careful selection of the sequence of irradiations. A similar approach to Vollertsen's models have been used where a geometry/strain relationship is drawn between the processing parameters and the bending angle. The final equation describing the bend angle in this case was found to be:

$$\alpha_b = \frac{1}{b} \left[\frac{2\alpha_{th}Ap_1b}{v_1c_p\rho(2d_1s_0 - s_0^2)} - \frac{k_f(T_1)d_1}{E(T_1)} \right] \quad (2.23)$$

The model assumed that three of the four sides of the box section were heated simultaneously to initiate the bending. In reality the sides are

usually irradiated sequentially. However, for the purposes of an analytical model this effect would be very difficult to include. Numerical studies into the sequence of irradiations in extrusion bending have also been carried out by Kraus using finite element methods.

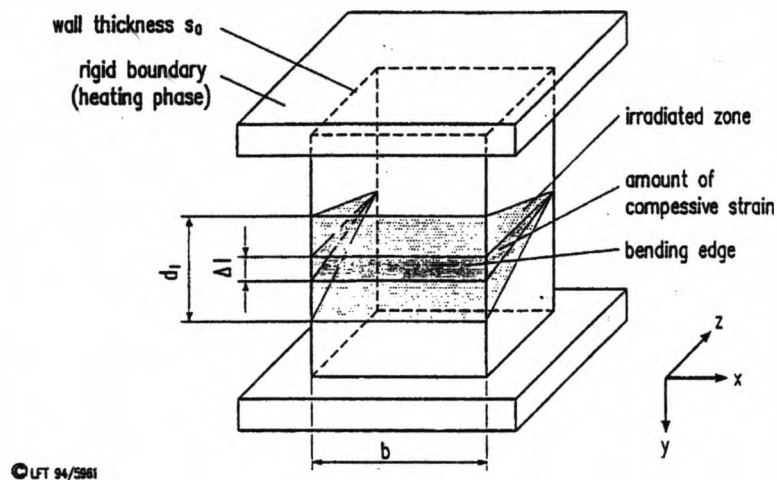


Figure 2.13: Model for extrusion bending using the upsetting mechanism⁸

2.3.2 Numerical Models

To increase the accuracy and versatility of mathematical modelling for the laser forming process, assumptions have to be replaced by considering a greater number of variables. However, this vastly increases the complexity of the analytical model. To achieve this a numerical method is used. The use of a numerical method in mathematical modelling has been possible with the increase of processor speeds in computers and the release of more user friendly software packages, such as ABAQUS. As computers continue to increase in processing speed and

software packages become more advanced numerical modelling is able to continue developing.

There have been a number of numerical models for the flame forming^{1, 21-24}. These are of use as flame bending was the process on which laser forming was originally inspired. Mathematical modelling is becoming more a part of the investigation process and is often presented in segments of papers. Because of this some investigations that use mathematical modelling are also presented in the previous experimental work section of this thesis. In the following sections early numerical models for the laser forming process are outlined along with investigations which are heavily based on numerical modelling.

2.3.2.1 Temperature Gradient Mechanism

Some of the earliest work into numerical modelling was work by Vollertsen in 1993²⁵. Here a finite difference model for a two dimensional analysis of the process was developed. The temperature-dependent material parameters were included in the model by taking values at particular temperatures of interest and linearly interpolating between them, and then those functions were used to relate the temperature to the material properties. A rectangular shaped source was used to represent the laser beam and the resultant two dimensional temperature field was used to calculate the thermal expansion, strains and stresses in the elements. A calculation was then made, taking into account the stiffness of the whole sheet, to work out the stress in each element. Where the stress exceeded the temperature-dependent yield stress, the elastic strains were converted to plastic strain. A loop was initiated which continued with this calculation until there was equilibrium of forces and moments.

After the thermal field had finished being computed, the bending angle was calculated from the length of the upper and lower layers of an element in conjunction with the sheet thickness. This model provided a very fast means of calculating the effects of various process parameters, but the simple boundary conditions that limited this approach led to the modelling with the finite element method (FEM)²⁶.

In 1997 Alberti *et al*²⁷ created a model using a finite element method. This modelled the TGM for the laser forming of sheet steel. It evaluated the temperature field and then the results of this analysis were introduced into a mechanical analysis. Illustrations for the temperature field and the deformation were provided at various stages of the process. Emphasis was placed on the importance of the temperature dependence of the yield stress of the material. A constant decay law was assumed for the relationship between increasing temperature and decreasing yield stress. This author also looked at a simulation combining thermal and mechanical bending for laser-assisted bending²⁸.

In 1997 Hsiao *et al* published work using the commercial package ABAQUS to model the laser forming process²⁹. They used the modelling in their work to emphasise the importance of the specimen size. Their results state that the angular distortion obtained on a short specimen is much smaller than for a long specimen. This agrees with experimental results by Vollertsen⁸. They also studied the effect of the fraction of the laser power and the square root of the velocity times the plate thickness as a parameter:

$$\frac{P_1}{s_0 \sqrt{v_1}} \quad (2.24)$$

In conjunction with this study Firth *et al* have used the code TOPAZ3D/NIKE3D for analysis. Results from this study were compared with experimental results and it was reported that the model predicted the trends correctly, but the absolute angles predicted were considerably smaller (about a factor of 3) in some cases.

In 1999 Yu *et al*³⁰ at MIT published numerical based research of laser forming. Presented was an ABAQUS based finite element model for thermomechanical analysis of the LF process. A re-zoning or re-meshing technique (redrawing the fine mesh around the beam as it moves) was employed to greatly reduce the simulation time yet preserve the required accuracy. A comparison of the numerical results and experimental data on 2.53cm thick mild steel using 2.6 kW of CO₂ laser power, obtained from Penn State University, showed the effectiveness of the model. However the observed errors between the model and experimental data were attributed to the inaccurate estimation of the heat absorption rate and the heat convection and radiation coefficients. It was concluded that a more accurate estimation of these parameters is essential for FEA modelling.

Li and Yao³¹ at Columbia University in 1999 presented numerical based work on the effects of strain rate in laser forming. An FEA model was created in ABAQUS of an 80 x 40 x 0.89mm mild steel coupon laser formed using a CO₂ laser source with a Gaussian distribution, only half the coupon was modelled as symmetry was assumed. It was found in this study that with strain rate increase, the thermal-induced distortion decreases and the bend angle reduces. The bend angle decreases by about 30% for nearly doubled strain rate under the conditions used. Residual stress in the Y direction (transverse) increases moderately with strain rate, with a doubled strain rate residual stress increases by about 15%. From

coupled experimental work it was found that with a strain rate increase the hardness of the formed sample decreases due to the reduced work hardening. This numerical/experimental approach was continued at Columbia with work on laser forming with constant line energy³² and analysis and prediction of edge effects in laser bending³³.

In 2001 Cosenza *et al*³⁴ presented an explicit fully coupled thermomechanical FE analysis of the LF process, again using ABAQUS. This study proposed a new FE modelling approach utilizing a dynamic explicit algorithm as opposed to the traditional implicit models. This permits the reduction of CPU times because of the linearity and the independence of the final set of equations. The FEA model of the LF of 140 x 20 x 3mm Fe360 sheet using a 6kW CO₂ laser source showed reasonable agreement with experimentally found data.

In 2002 Lee *et al*³⁵ in Taiwan published a study into the pulsed LF of thin 20x10x1mm 304 Stainless Steel using a single or multiple CO₂ laser pulse of an elliptical beam the width of the sample. An ABAQUS FE model was developed to simulate this unique set-up, and a good agreement was found with experimental data. The conclusions drawn from this study were that the bend angle increases with laser power and the laser radiation time. The bending angle decreases with the thickness of the specimen, provided the peak temperature of the specimen is below the melting point. It was found that if there is a high temperature gradient between the upper and lower surfaces a positive bend angle is produced, for a low thermal gradient a negative bend angle is produced. Finally it was concluded that the mechanisms of pulsed laser forming are dependent upon a number of operation parameters, the main influences are the laser power, the heating time (pulse length), the clamping

arrangement, the thermal properties and the residual stress state of the specimen.

2.3.2.2 The Buckling Mechanism

In work by Holzer *et al*³⁶, published in 1994, the buckling mechanism (BM) was modelled using the commercial finite element package ABAQUS. For this model it was assumed that the sheet was flat and free of residual stresses. The results of the model gave a convex bend away from the laser beam, as the resultant plastic strain in the non irradiated side of the sheet was greater.

2.3.2.3 The Upsetting Mechanism

In 1997 Kraus carried out a finite element analysis into extrusion forming²⁰. Important information about the temporal development of the process resulted from this work which could not be determined experimentally. For example during the cooling phase a contraction in the irradiated zone takes place, and tensile stresses build up if the thermal contraction is hindered by the surrounding material and the work-piece stiffness. These stresses can reach the yield stress depending on the process parameters employed and a plastic restraining may occur.

This effect is particularly noticeable in extrusion bending where the moment of inertia of the work-piece is high. From this analysis Kraus found that there is an upper limit to the plastic strain which should be

induced in order to minimise plastic restraining. The sequence of irradiations was also optimised using the finite element method (FEM).

A development on extrusion forming was work by Li & Yao in 2000³⁷. This work presented numerical (FEA) work on the use of laser forming to bend tubes. The mechanism was found to be a combination of thickening (shortening mechanism) of the laser scanned region due to thermally induced axial compressive stress, and a slightly outward displacement of the region caused by a component of the thermally induced circumferential stress. As a result bending is primarily achieved through the thickening of the scanned region instead of the thinning of the un-scanned region. The absence, when compared to conventional tube bending, of appreciable wall thinning is one of the major advantages of laser bent tubes. It was concluded from this study that the bending efficiency increases with the maximum scanning angle (distance scanned around the tube) up to a critical point. In addition the asymmetry of the LF process can be reduced by varying the scanning speed or employing a two segment scanning scheme.

2.4 Previous Experimental Work

2.4.1 Fundamental Investigations

One of the earliest investigations into laser forming was published in 1985 by Namba³⁸. Here experiments were carried out into the laser forming of titanium, aluminium, AISI 304 stainless steel and AISI 1045 carbon steel. A 1.5 kW CO₂ laser was used with a defocused beam at traverse speeds between 5 and 15m/min. It was proposed that a steep thermal gradient was produced resulting in thermal expansion, thermal stresses and plastic deformation. Namba described the following parameters as affecting the bend angle:

1. Incident laser beam power
2. Laser beam diameter
3. Power density distribution of the laser beam
4. Absorptivity of laser beam on a material surface
5. Scanning speed of laser beam
6. Number of repetitions of laser beam scans
7. Density of the material, specific heat capacity of the material
8. Thermal expansion coefficient
9. Yield strength

10. Young's modulus
11. Poisson's ratio
12. Strain hardening coefficient
13. The dimensions of the work-piece
14. The melting temperature of the material and the fracture strength of the material.

In 1987 Scully determined that the positive bend angle can be calculated using the following equation³⁹:

$$\alpha_b = \frac{P_1}{s_0 \sqrt{v_1}} \quad (2.25)$$

This relationship was taken from earlier work by Masubuchi *et al*⁴⁰ on flame forming. In later work Vollertsen also shows that there is a strong linear dependence of the bend angle on the laser power and processing speed.

Vollertsen is credited with producing a considerable amount of the early fundamental research on laser forming. Some of the key results and conclusions drawn from this research⁸ are discussed here. In the experiments carried out relating to processing speed dependence, a power law was assumed between the bend angle and the processing speed. A linear dependence was obtained for 3.5mm sheet with scanning speeds in the range 7 -70 mm/s, the gradient was found to be -0.63. A negative slope was to be expected as this is derived from the notion that the increase in processing speed decreases the coupled energy which is

proportional to the bend angle. However at lower speeds it was found that this is not the case. Here the bend angle continues to increase up to a point with increasing traverse speed. This behaviour may be attributed to the fact that the possibility of a steep temperature gradient is reduced with a decrease in speed. Ultimately an increase in speed results in a greater difference of the plastic strains between the upper and the lower layer of the sheet and a larger bend angle per unit time may be achieved. However, if the velocity is increased to a very high value then the temperature increase will be small and only an elastically reversible bending may occur. Also of note from this work is the concept of a threshold energy for the process. It was shown that no plastic deformation occurs below a given energy input.

The thermal conductivity of a material in laser bending is also discussed. This is an important parameter because it determines the temperature field and hence the development of the thermal strain. Therefore if a material has a high thermal conductivity it is going to be difficult to produce the temperature gradient which is essential for this laser forming mechanism. In general it is better that the material should be a relatively poor conductor in order for the temperature gradient mechanism to occur.

A number of geometrical influences have also been investigated. It has been shown that the thickness of the sheet is one of the major variables in the development of the bend angle. The bend angle is related linearly to the inverse of the square of the sheet thickness for the temperature gradient mechanism⁸.

The length of the bending edge is also of significance for the development of the bend angle. If the length of the bending edge is increased from 5 to 13 mm then the bend angle is increased by a factor of

3²³. This is due to the changing section modulus with changing length and the difference in the temperature field due to the change of length in the lateral direction. Another factor influencing the bend angle is the length of the bending leg. If the bending leg is short then the cooling of the work-piece is restricted to one side⁸ and the temperature gradient decreases and hence the bending decreases. If the bending leg is long then the gravitational forces acting on the length will affect the bend angle. The weight of the leg results in tensile stresses in the surface of the sheet thus reducing the compressive stresses from heating and diminishing the bend angle.

Secondary geometrical effects were reported by Scully *et al*³⁹. In this work less distortion occurs near the edges of the plates. This is because the heat flow pattern is altered in comparison to the innermost part of the plate where the heat flow is to surrounding material. This results in less distortion near the edge of the work-piece. This was also attributed to the rigidity of the plate becoming non symmetric near the plate edge.

For multiple passes both Scully³⁹ and Masubuchi⁴⁰ reported a linear relationship between the number of passes over an identical track and the resultant bend angle. In later work this linear relationship of the bend angle on the number of passes was not found to be true for a range of materials. Sprenger⁴¹ showed that there is a decreasing bend angle rate with increasing scans due to the strain hardening of the material (figure 2.14).

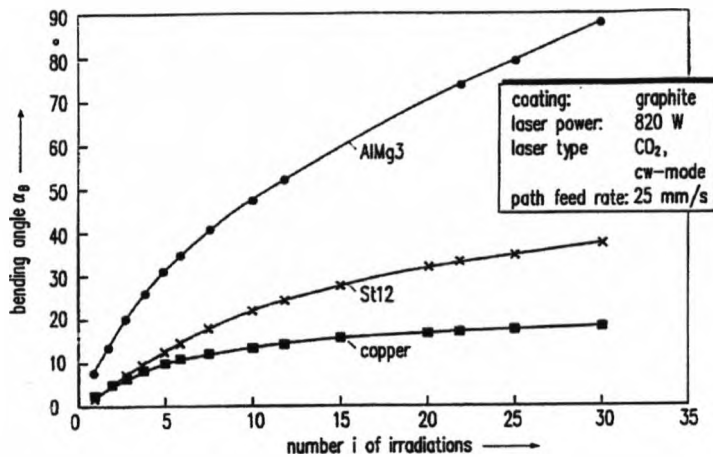


Figure 2.14: Decreasing bend rate with increasing scans over an identical track⁴⁰

Two main reasons for this were discussed:

1. Effect of the change in thickness along the bend edge

The thermal expansion which is converted into plastic deformation is not cancelled during cooling and a bend angle results. Because the material has thickened due to the plastic compression altering the modulus of the section and the same laser parameters are used for subsequent scans the angle achievable decreases each time.

2. Effect of strain hardening of the material

In materials with a large strain hardening coefficient and which are relatively thick it has been shown that the cold working of the underside of the sheet contributes significantly to the decreasing bending rate.

2.4.2 Previous Experimental Work within the Research Group

Work by Magee in 1998 and then Edwardson in 2004, whilst they were PhD students studying at the University of Liverpool, is the forerunner to some of the investigations described within this thesis. Because of this a more detailed account of these previous investigations is discussed in the following sections.

2.4.2.1 Magee 1998¹⁷

The experimental work summarised in this section consisted of empirical work carried out on AA 2024 T3 aluminium alloy and Ti6Al4V titanium alloy. Parametric investigations were carried out into the single and multi-pass, large and small beam diameter 2D laser forming of these materials, which led to the development of a 2D laser forming demonstrator system for a part cylinder shape. Development of scan strategies for the 3D laser forming of dish shapes was also carried out.

This work was part of a joint research programme between the University of Liverpool and BAE systems.

2.4.2.1.1 Parametric Study

This work investigated the factors influencing the angular dimensions of laser formed 80x80mm 0.8-1mm gauge plates of Ti6Al4V and AA 2024 T3, commonly used aerospace alloys. The plates were clamped at one

end, graphite coated and irradiated with a CO² laser. Altering the power density and the interaction time of the laser beam incident on the samples varied the energy input to the plate surface. The experimental results revealed that the bend angle development is critically dependent on the energy supplied to the plate surface. A large and small beam diameter was used in the forming of titanium and aluminium alloy. In the case of the titanium alloy it was found that the temperature gradient mechanism was active for both studies, both for the large and small laser beam diameter to sheet thickness ratios. This was attributed to the low thermal conductivity of the titanium alloy. An optimum traverse velocity in terms of maximising the bend angle achieved per scan was identified for this material when the beam diameter was in the order of 12 times the sheet thickness (figure 2.15).

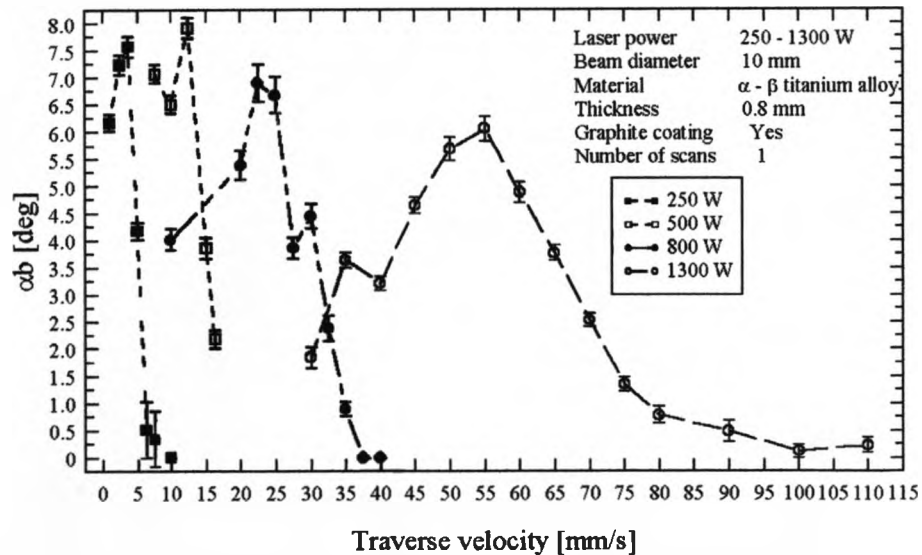


Figure 2.15: Bend angle with increasing traverse velocity for Ti6Al4V using a large beam diameter^{17,42}

Below the optimum velocity the bend angle dropped due to the loss of a high temperature gradient and hence a smaller amount of differential straining through the thickness direction. These results support the idea

that the temperature gradient, and the efficiency of the process, increase as the processing speed increases. This efficiency increase is offset by a reduction in the bend angle after the optimum point. This is because the increasing velocity results in less coupled energy, less thermal expansion, and a smaller reduction of the flow stress in the heated zone. Since all of these factors contribute to overcoming the elastic share of the bending, the bend angle begins to drop off again.

For the aluminium alloy it was found that for one laser scan using a large beam diameter the bend angle is decreasing with increasing traverse velocity (figure 2.16), this is in contrast with the titanium alloy where a peak occurs. Since the thermal conductivity of the aluminium alloy is high, the temperature gradient in the depth direction of samples was small for the lower traverse speeds. Under these conditions the buckling mechanism (BM) was thought to be active. In the higher velocity range, for the small beam diameter to sheet thickness ratio the TGM was active, the bend angle continued to drop sharply. This is attributed as before to the reduction in coupled energy and the elastic effects becoming more pronounced.

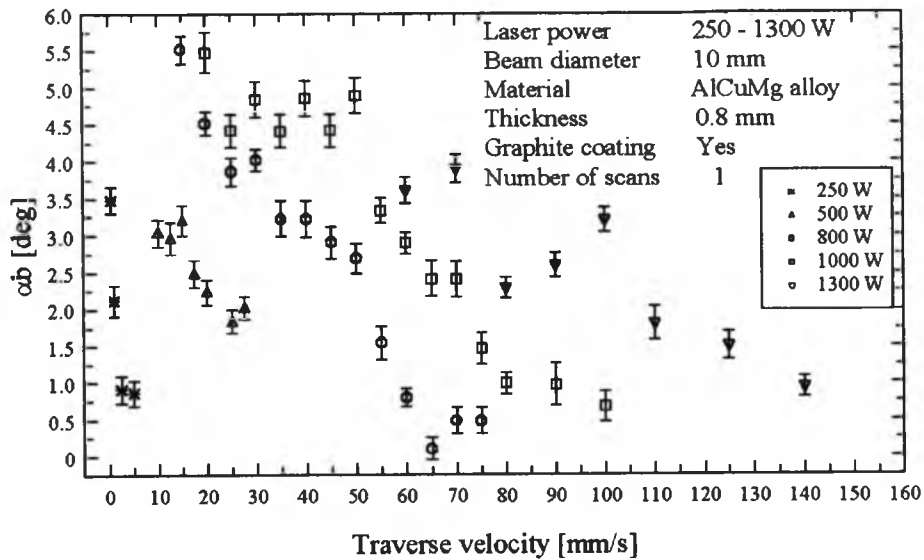


Figure 2.16: Bend angle with increasing traverse velocity for AA 2024 T3^{17, 42}

The decrease in bend angle with number of scans was also investigated (figure 2.17). The cause of this reduction has been reported as being due to the strain hardening of the material⁴¹ and a change in absorption as the number of scans increase. This study concluded that for the materials studied the effect of sheet thickness increase in the irradiated area per scan is of greater significance than strain hardening.

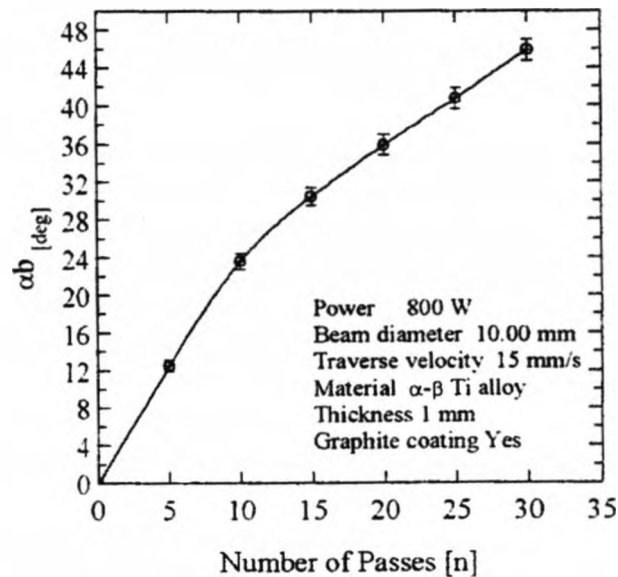


Figure 2.17: Bend angle with increasing number of scans over the same track¹⁷

This study also looked at edge effects or the changing bend angle along the length of the bending edge in laser forming. The laser forming process is asymmetric about the laser beam; as a result the bend angle cannot be constant along the entire bending edge until the laser beam has completely scanned the sample. Ideally, after the process, the bend angle would be constant along the bending edge, however normally the bend angle varies with plate location (figure 2.18).

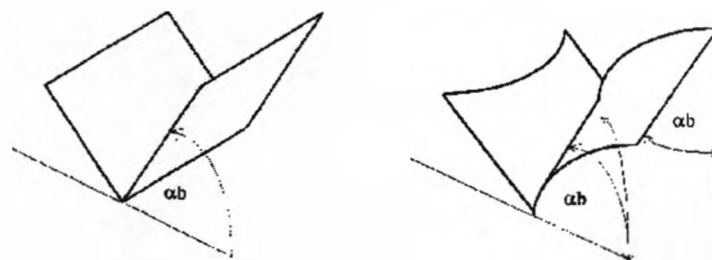


Figure 2.18: Ideal bend angle and exaggerated view of edge effects^{17, 43}

2.4.2.1.2 Two-Dimensional Laser Forming Demonstrator System

A laser forming demonstrator system was developed to demonstrate the process on a large primitive 2D shape. Data from the parametric and metallurgical study on the smaller tokens discussed earlier was used to develop the processing parameters for the system. The demonstrator part after some initial trials with larger parts was chosen as a flat rectangular AA2024 T3 sheet of dimensions 450x225 x0.8mm that was to be formed into a part-cylinder of radius 900mm (figure 2.19). The part was large in terms of laser forming operations to date, and the shallow radius of curvature is almost at the spring-back limit of conventional forming operations. The system was set up using a CO₂ CW laser, CNC tables, a pneumatic clamping system and a 3D CAM laser stripe measurement system.

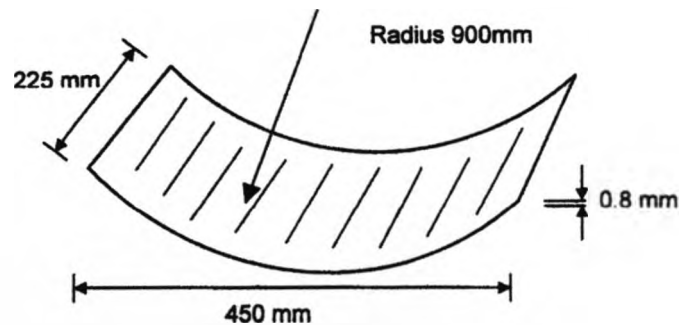


Figure 2.19: Demonstrator Part^{17, 44}

The demonstrator system then relied on user intervention in order to determine what the next processing steps were. These steps included:

1. Next scan pattern
2. Next Starting point and direction for scan pattern
3. Next clamping location
4. Next energy input

This adaptive approach was taken because the part produced by a constant scan pattern, direction and clamping arrangement was twisted and distorted. The part produced by altering these parameters and the energy input at different stages of the process had increased accuracy, surface smoothness and reproducibility^{17, 42, 45}.

2.4.2.1.3 Three-Dimensional Laser Forming of Dish Shapes

A case study was also made by J. Magee *et al*^{17, 46} into the 3D laser forming of a dish shape from flat circular 2mm gauge mild steel CR4 sheet. The objective of the investigation was to establish rules about the positioning and sequencing of the laser irradiation lines for the symmetrical laser forming of such a dish shape. The scan patterns investigated employed radial or circular scan lines, or a combination of both to form the part. The samples were verified using a co-ordinate measuring machine.

It was found that in order to achieve a smooth and symmetrical dish shape:

1. Geometrical symmetry should be reached as soon as possible after the initial irradiations.
2. A symmetrical temperature distribution over the plate surface should be realised.
3. Any pre-orientation bend should be avoided
4. The laser beam parameters, particularly the irradiation angle of incidence and the irradiation spot diameter, should be held constant.

The circle line system with square root radius increase, irradiating from inside too out, was found to be one of the best strategies (figure 2.20).

This strategy employed the upsetting mechanism along the concentric circular scan lines to achieve the forming result.

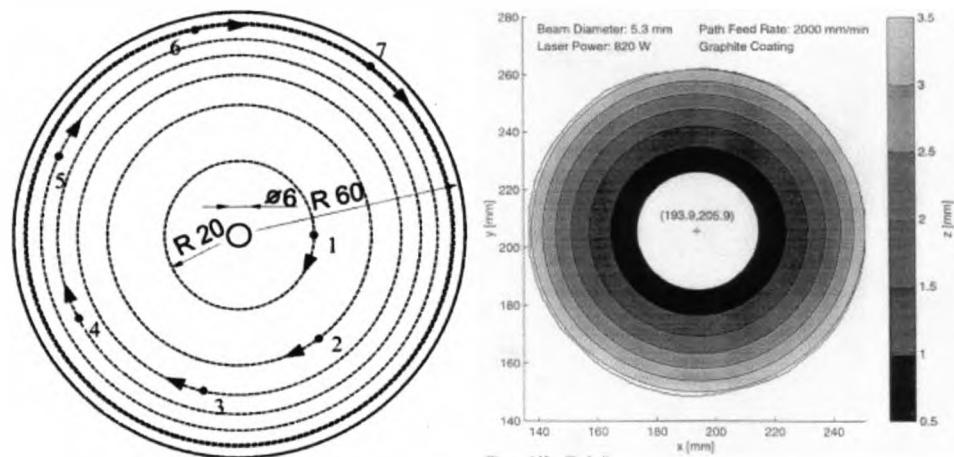


Figure 2.20: Circle line system with square root radius increase (inside to out), and resulting contour plot of sample^{17, 46}.

2.4.2.2 Edwardson 2004⁴⁷

Work summarised in the following section consists of a metallurgical study into the effects of two dimensional laser forming on mild steel and aluminium alloy. Also investigated was the closed loop control for two dimensional forming of Aluminium alloy. Under the title of three dimensional forming an empirical study is looked at into the forming of non-developable shapes in mild steel and titanium. Also the investigation into the development of a geometry based three dimensional model is summarised here.

This work contributed to a larger EPSRC funded research programme entitled 'Laser Forming of Aerospace Alloys – A Direct Fabrication Technique'. The research programme involved a consortium of three universities; The University of Liverpool, Heriot Watt University and

Cambridge University; and 2 industrial partners; BAE SYSTEMS and Rolls-Royce plc.

2.4.2.2.1 Metallurgical Study

In work by Edwardson a metallurgical investigation was conducted on laser formed 1.5mm mild steel CR4 and 1.6mm AA6061 in three different tempers, O, T4 and T6, to ascertain some of the effects of LF on the structure and mechanical properties of the materials

This found that the optical microscopy of laser formed mild steel at various energy parameters and numbers of passes revealed that the effects if any of LF on the microstructure of mild steel are subtle when there is no obvious melting. Hardness values do increase with increasing numbers of passes and the largest increases were observed near the mid and lower sections of the plate thickness consistent with a cold working or strain hardening effect.

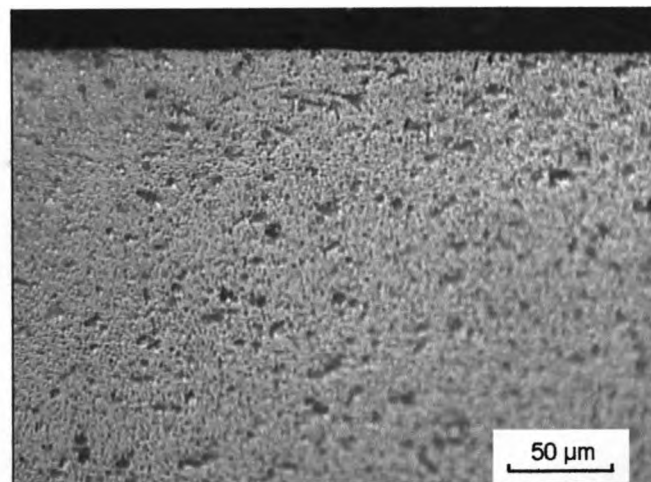


Figure 2.21: AA 6061 O 'As Received'⁴⁷

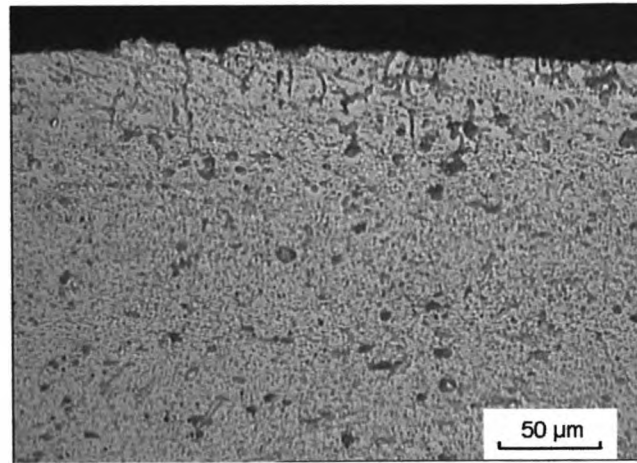


Figure 2.22: AA 6061 O After 30 passes⁴⁷

Similarly to the mild steel data, the optical microscopy of the laser formed AA 6061 in three different tempers revealed only subtle changes to microstructure. A possible precipitate coarsening was observed in the upper surface area after 5 passes in all of the heat treatments. Which were found to revert back to the original microstructure after 30 passes. This was attributed to the fact that, due to coating loss, the amount of energy coupled into the surface reduced significantly after 10 passes. Hardness tests on the laser formed AA 6061 samples revealed additional effects on the metallurgy. For the O condition little effects on the hardness were observed for increasing numbers of passes. For the T4 and T6 tempers it was observed that up to 10 passes there was a decrease in the average hardness within the heated area. From 10 passes up to 30 passes there was a recovery somewhat in the hardness values.

2.4.2.2.2 Two-Dimensional Closed Loop Control

In other work a system was presented that could produce accurate bends using closed loop control for 2D laser forming of 80x80mm coupons of two materials, 1.5mm mild steel and 0.9mm AA1050 - H14.

The factors considered essential for control of the process were:

1. The current bend angle.
2. The difference between current and desired bend angle.
3. The current bend angle rate or bend angle increase per pass.
4. Selection of a bend angle rate per pass so as to avoid overshoot (when the bend angle difference between current and desired angle is small, i.e. bend angle rate should be less than or equal to the required deformation).

2.4.2.2.3 Three-Dimensional Laser Forming Empirical Study

An investigation was conducted into the 3D laser forming of the primitive shapes, the saddle, the pillow and the twisted shape using an empirical approach to determine the scan strategies. Also investigated was the use of 3D laser forming on thick sections, specifically for the ship building industry.

The results of these investigations showed that the problem of 3D laser forming is extremely complicated. For the study on the saddle shape it was found that it was possible to produce a saddle shape from rectangular sheet Mild Steel CR4 using a concentric 'race track' strategy. This strategy was also found to work in 1.6mm Ti64 and in square length to width ratio sheets. Another successful strategy was presented based on a cross-hatch pattern and an incremental route. The 'race track' strategy for the saddle shape was found to scale up to larger thicker materials to some

degree, however, it was concluded that more forming lines were required to account for the increased surface area.

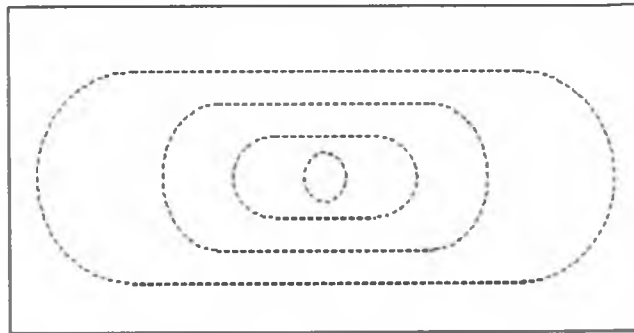


Figure 2.23: 'Race track' strategy, Speed 20mm/s⁴⁷

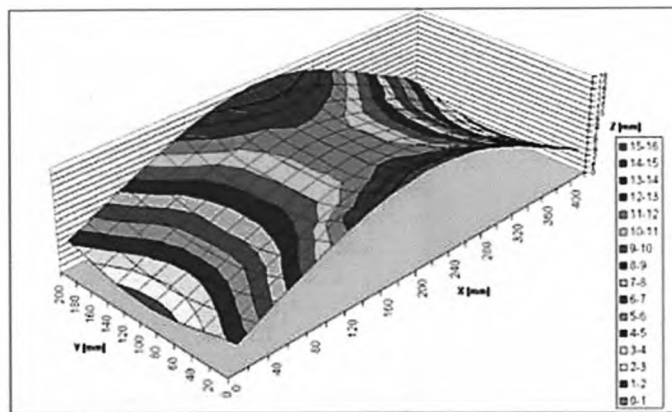


Figure 2.24: 3D Contour Plot 'race track' strategy⁴⁷

For the pillow shape a concentric rectangular forming strategy was developed for TGM conditions using rectangles of the same length to width ratio as the sheet to be formed. A limitation to the amount of symmetrical forming possible with this strategy was found.

For the Twisted shape a strategy of the production of a combination of a twisted shape and a part-cylinder was developed. The part-cylinder was

then un-formed out of the shape by processing the reverse side of the plate to leave the desired twisted shape in the sheet.

Any pre-stressing of a work piece was considered a large factor in the magnitude of forming and any distortion of the final part. Symmetrical laser forming is hindered due to the asymmetric nature of the laser forming process itself, in that it is not possible to form the whole plate at once.

2.4.2.2.4 Development of a Geometry based Model for Three-Dimensional Laser Forming

Edwardson realised from the empirical study that in order to develop control of the process of 3D laser forming it was necessary to have the ability to define the surface to be formed. In addition by defining the surface and analysing properties such as gradient and curvature, it was thought this may lead to a method of scan strategy prediction. To this aim, a method of surface creation and analysis was devised using Matlab.

It was discovered for the pillow shape that by forming along the contour lines of constant height of the desired surface a successful scan strategy was produced. By considering the concept of developable and non-developable surfaces another method of energy distribution over a surface was proposed. For a singly curved developable surface the TGM should be the dominant mechanism used to produce plastic bending strains and out of plane deformation. For a doubly curved non-developable surface, material needs to be removed (in-plane) in order to allow the deformation to take place. This suggests that the shortening mechanism should be the dominant mechanism when forming this type of surface, the in-plane plastic shrinkage accounting for the limiting material near the edges.

2.4.3 Research in Macro-Scale Two-Dimensional Laser Forming⁴⁸

There have been a number of 2D laser forming experimental investigations recently published that are of note⁴⁹⁻⁶⁴. The experiments and conclusions of a number of them are outlined here.

Chan *et al*⁶⁶ in Hong Kong published work in 2000 on the laser forming by a low power Nd:YAG laser (90W max) of thin stainless steel (0.25-1mm thick). Although some of the results had been observed before in other studies there were a few interesting findings: A threshold heat input was observed in the process, below which no bending occurs. In addition when the energy input was above critical value the bend angle stops increasing with any further increase in heat input, possibly due to the loss of thermal gradient through the thickness. This concurs with earlier work by Vollertsen⁸.

In 2001 Mucha *et al*⁵⁰ from Poland presented a paper on a comparative study of the laser forming of plates using circular and rectangular beam cross-sections. It was shown that the shape of the incident laser beam has a large effect on the LF process, for the same energy parameters the bend angle generated by the rectangular beam is 1.3 to 2.5 times greater than the one generated by the circular beam. In addition it was argued that a greater control of the process could be achieved using a rectangular beam. Also in the work was an extensive analytical model, it was argued that the dimensionless form of the derived dependencies from this model

would be a useful method of selecting appropriate processing parameters for any material.

Liqun *et al*^{52, 53} from the Harbin Institute of Technology, China, have published a number of interesting studies on LF. There has been an increase in recent years of the number of papers to come out of China in the laser materials processing field in general. Research on using different cooling methods in LF and an update on the factors involved in multi-pass LF have been presented. It was found that the use of an effective cooling method can significantly increase the process efficiency of LF. A number of cooling methods were employed including water jet and high pressure CO₂ gas cooling from the underside of the plate. It was found that cooling can increase the temperature gradient through the thickness, however the peak temperature in the sample is decreased and so the benefits of having cooling during processing are lessened. In addition the high temperature difference between the top and bottom of the plate can cause unwanted metallurgical effects such as an increase in hardness. In another study work was presented on multi-pass laser forming and the factors influencing the bend angle fall off at higher numbers of passes, although many of the results had been observed in previous work a number of key results were of interest. The work was conducted on 2mm thick aluminium using a 2kW Nd:YAG laser and a 10mm beam diameter, thus no coating was required. It was observed that there was a significant thickening of the sample in the irradiated area and that the thickening became more pronounced after 20 irradiations (0.5mm thickness increase). It was argued that this thickening effect was a large factor in the bend angle rate fall off after 20 or more irradiations. It was also found that the tensile strength of the sample decreased with increasing irradiations, thus ruling out this factor as a possible reason for bend angle fall off.

The industrial viability of LF depends on the process efficiency and speed compared to other competitive techniques, in combination with repeatable accuracy. Mechanical forming of thin sheet material is relatively fast and can produce large deformations in a single process step, but it is inaccurate (due to variable 'springback' and tool wear). In contrast, LF is comparatively slow, but offers a high degree of control and remote application. To exploit the combined attributes of LF and mechanical forming, a hybrid forming process has been proposed and demonstrated by Magee and De Vin, in which LF is applied as a secondary process to adjust mechanically formed parts^{56,57}.

A high degree of control is required for LF to be an industrially viable process, especially for 3-D LF. To address this for 2-D LF, Thompson and Pridham at Dundee investigated a closed-loop control system, for the case of laser bending to a pre-defined bend angle with some success⁵⁸⁻⁶⁰. Other approaches to this problem have been taken, Cheng and Lin in Taiwan have published work on using a neural network to predict and hence control the bend angle during the laser forming of 304 stainless steel⁶¹. This intelligent approach could be a useful method accounting for the many variables and unknowns in the process. Peck and Jones⁶² are developing this approach into a commercial system for the manufacture of single unit windshield wiper blades for Trico Products Corp. The system employs a high power diode laser to laser form and heat treat a continuous metal strip fed underneath it, this metal strip when cut to length forms the curved backbone of the windshield wiper. A trained neural network provided by NA Technologies monitors the process and can make adjustments on the fly to the power output of the diode laser

and hence the bend angle, this type of laser is well suited to this dynamic power requirement.

The use of pulsed laser energy for LF has also been under investigation by some researchers^{63, 64}, and this has led to possibilities for new LF mechanisms. Laser Peen Forming (an extension of Laser Peening⁶³) or Laser Shock Forming⁶⁴, in which the application of a negative residual stress to one side of a component results in a bending effect, is a key example that is now being realised through the emergence of high pulse energy Nd:Glass lasers.

2.4.4 Research in Micro-Scale Two-Dimensional Laser Forming⁴⁸

Many of the investigations into micro forming are for potential applications in the electronics industry. A great deal of work has been carried out into the use of micro forming for high resolution adjustments of electronic components in post production. Here a laser would be used to finely adjust actuators. These adjustments can be made on mounting frames, reed switches or magnetic head sliders in disk drives⁶⁵⁻⁶⁹. Another application is the forming of complex shapes which can potentially be used as mountings or housings for electronic components⁷⁰⁻⁷³.

Pioneering studies on micro-scale LF by Hoving and co-workers at Philips⁶⁵ helped establish some important results for precise adjustment of components by the shortening or Upsetting Mechanism. Following on from this, the Philips research team have developed a number of micro-adjustment applications for LF^{65, 66}, with the first concept being the laser

adjustment of digital audio head mounting frames. A second application under development is the laser adjustment of reed switches. Here, out-of-plane LF (laser bending) is used for adjustment of the 10-50 micron gap between the two nickel-iron reed elements, which then determines the value of the magnetic field above which the reed switch closes in operation. Widlaszewski⁶⁸ investigated various modelling techniques of thermal deformations induced into a small metal frame which could be used as an actuator. This frame was designed in such a way that when heated by a laser spot the area irradiated would be upset resulting in very small angular movement in the frame. It was found that analytical modelling gave the best understanding of this particular process.

In 1997, Tam and co-workers at IBM Almaden developed and implemented in manufacture a Laser Curvature Adjust Technique (LCAT) system for adjusting the curvature of magnetic head sliders in disk drives using a novel laser microbending technique⁶⁷. This development addressed a need for precise and highly controlled adjustment of the positive camber curvature of a slider, to improve its tribological properties and allow reduced flying heights (below 25nm) above the disk surface to provide increased disk storage density. In work by Zhang *et al*⁶⁹ the micro adjustment of hard disk suspensions was investigated numerically. A three dimensional model was employed which showed that a bend resolution of 0.1° could be achieved with 20W of laser power and scan lengths from 50 to 200 µm.

The laser forming of plastic using an Nd:YAG laser has been experimentally investigated by Uno and co-workers at the West Japan Railway Co. in Osaka⁷⁴, with the aim of changing the design shape of plastic components produced by injection and compression moulding. The bending direction is controlled by selective painting of the plastic

surface with a black resin, on the side whose surface is to undergo shrinkage in the LF process. A cw Nd:YAG laser of a few watts average power is applied from one side only, since the plastic is transparent to the laser wavelength, with the resin then transferring its absorbed heat to the material from the surface to which it is adhered.

A number of other studies fall into the micro scale LF area⁷⁰⁻⁷⁴, these involve the laser forming of thin metallic foils using low power lasers. Complex structures can be formed in these thin materials with very little power, thus applications can be found in the electronics industry for alignment (mentioned earlier) and for the manufacture of mounts and housings for components. In work by Yoshioka *et al*⁷¹⁻⁷³ at the Chiba institute in Japan a method of sample holding was developed to reduce unwanted distortion when forming thin foils. A sample was held in place using a glass plate over it, the sample was then irradiated through the glass and not allowed to deform. Once the plate was lifted after processing, the part sprung into the desired shape, thus eliminating any asymmetric or temporal effects. For more complex shapes a mask was used to hold the sample down during processing. Bartowiak *et al*⁷⁵ also created complex shapes. This was accomplished with the use of high speed scanning optics.

2.4.5 Research in Three-Dimensional Laser Forming⁴⁸

A considerable amount of research recently in LF has been aimed at prototyping of 3-D components and structures for applications in ship building, aerospace, automotive and artistic design^{46, 76, 77-92}.

It has been shown that laser forming shows great potential for the manufacturing of metallic components, using a 2D straight line or 3D spatial forming approach. However in order to advance the process further for realistic forming applications and for straightening and aligning operations in a manufacturing industry it is necessary to develop systems for accurate and repeatable part production.

Intelligent predictive systems, perhaps based on Knowledge-Based Systems (KBS), neural networks or thermo-mechanical models can achieve predictability through a knowledge of the material (including its stress history) combined with a developed, highly tuned process model/control algorithm. Systems of this type have been reported by a number of groups⁸²⁻⁸⁴.

In an adaptive system the use of sensors to provide accurate controlled feedback coupled with the development of intelligent control software, provides an incremental or even real time closed loop method of accurate 3D laser forming, based on the current part characteristics independent of material variability⁸⁶⁻⁹². It is likely that future three dimensional laser forming systems would include elements of both these approaches, in that an initial prediction for a scan strategy would be made based on a knowledge base of known data, the part's geometry would be monitored, and the scan strategy would be adapted either in process or for subsequent passes so as to achieve the desired result.

Work by Kim *et al*⁸⁶ suggests an adaptive approach with the use of feedback control. When forming a free curve shape feedback control is used for each single bending angle by incorporating a statistical method. This created an accurate shape with small errors. As a consequence of

these small errors feedback control algorithms were proposed resulting in better accuracy.

A great deal of investigation has been carried out at ARL in Penn state University by E. Reutzel et al into three dimensional laser forming⁷⁷⁻⁹¹. A strong influence in this work is the ship building industry where flame forming is used. In work presented in 2003 a simple linear bending relationship is used for an initial scan prediction⁹⁰. An adaptive approach is then used to complete the process. A differential geometry approach to simulation of laser forming has also been investigated in this research group⁹¹. The advantage of this technique is computational efficiency in comparison to FEA simulation. However there is a decrease in accuracy when simulating large deformations.

Cheng et al use FEM analysis to predict scan paths which are decided on the concept of in-plane strain, bending strain, principal minimal strain and the temperature gradient mechanism of laser forming⁹³. In this work both a saddle and a pillow shape were successfully formed.

2.4.6 Material and Metallurgical Studies

As has been mentioned LF has great potential as a tool for prototyping, aligning and removal of distortion or as a direct manufacturing tool. Key to the future success of LF is what effects if any the process has on a material's integrity and properties. In order to prove the process a number of material and metallurgical studies have been conducted on a variety of materials^{39, 94-106}. In particular the effect of the rapid and repeated heating

and cooling cycles below melting points associated with LF. Initial work in the field was mainly carried out on steel^{39, 97}, but has since been extended to other materials including titanium and its alloys^{94, 95, 97, 98}, aluminium and its alloys^{45, 95, 99, 100}, aluminium-matrix composites¹⁰¹ and chromium¹⁰³. Other fundamental investigations have also been reported, including investigations into material anisotropy¹⁰⁴⁻¹⁰⁷. A summary of the more relevant publications to this study are presented here.

In work by Thompson and Pridham⁹⁶ at the University of Dundee on laser formed mild steel, it was shown from mechanical and metallurgical tests that LF parts (in mild steel) are likely to perform at least as well as conventionally formed equivalents. It was reported that in general laser forming increases the yield strength of the material locally to the irradiated area. This increase in strength may not be utilised fully, since the bulk of the material will not have been altered by the process, but most significantly LF does not weaken structures. The slight loss of ductility reported would mean that a laser formed part may not be suitable for large amounts of subsequent manual forming. This was not felt to be a problem, since LF is likely to be used as the sole forming operation or a fine adjustment after conventional bending.

In work by Shackle *et al*⁹⁵ from UMIST on 2mm gauge Ti-6Al-4V (Ti64) sheet, an investigation on the metallurgical implications of LF on this aerospace alloy was reported. The effect of a post-forming heat treatment was also investigated. The LF samples were processed in air and in argon. O₂ readily diffuses into the surface of Ti64 at temperatures exceeding 550°C and produces a brittle α -case, this can weaken the material as crack propagation points can form in the surface region. Due

to this factor LF on this material has to be carried out in an inert atmosphere, the α -case was not present in the samples processed in argon.

Ti64 is a dual phase, $\alpha+\beta$ alloy, where the β -transus temperature is at 982°C. It was found by optical microscopy, FEGSEM and TEM methods that after LF a HAZ is produced that consists of a fully martensitic region, where the temperature has exceeded the β -transus, surrounded by a partially transformed zone where the temperature has risen above the M_s (martensitic) temperature ($\sim 800^\circ\text{C}$) into the $\alpha+\beta$ phase field. No microstructural changes were found at lower temperatures. Within the HAZ a complex, refined, martensitic structure was produced due to the very high heating and cooling rates into and from the β and $\alpha+\beta$ phase fields (reported as a maximum of 9100Ks^{-1} as derived from a finite volume model). However, because of the very rapid nature of the thermal cycle the original solute distribution in the parent material was little altered and could still be seen within the fully transformed region. An increase in hardness was reported in the irradiated region reducing into the thickness, however the application of a post-forming heat treatment (PFHT 700°C for 4 hours in Ar) resulted in an overall reduction in hardness of the HAZ due to a re-precipitation of Vanadium rich β at the martensitic plate boundaries and the disappearance of the majority of the martensitic plates in most regions within the HAZ.

A tensile test on the LF samples was also reported, it was found that during tensile deformation the higher hardness of the HAZ acted as a local constraint on plastic deformation and failure always occurred in the parent material away from the irradiated area. The bulk tensile properties of the Ti64 sheet consequently remained relatively unaffected by the LF process. Studies in other alloys of Titanium^{94, 97, 98} also confirmed the viability of LF with these materials.

Work on aluminium and aluminium alloys by Merklein *et al*^{99, 100} at the University of Erlangen revealed the microstructural development and mechanical properties in laser formed Al1050 and an Al6082 in two heat treatment conditions T41 and T61. The work was conducted on 80mm wide 1mm thick samples using a 1kW cw Nd:YAG laser, a graphite coating was still used however. SEM and TEM methods were used for analysis. Changes in the mechanical behaviour as well as in the microstructure were observed. The soft and annealed AA-1050 showed hardening due to the LF process. This was proved by hardness tests and by SEM/TEM images showing the dislocation motion and changes in microstructure. For the two heat treatments of the Al6082 there were little or no differences in forming characteristics over a number of irradiations found between them. For the artificially aged T61 alloy, the hardness produced by ageing is lost in the HAZ and immediate area after LF and is comparable to the naturally aged T41 values. For the T41 alloy only a slight decrease in hardness is observed in the HAZ.

In 2003 Yao *et al*¹⁰⁶ from Columbia University presented research on the effect of material anisotropy on the laser forming process, both numerical and experimental results. Cold rolled sheet metal exhibit anisotropic properties which are mostly caused by preferred orientations of grains developed during rolling reductions. The anisotropic index or R value of a material in a particular orientation was determined using an ASTM standard tensile test. The grain textures in the formed samples were determined using an electron back-scatter diffraction method (EBSD). It was found that there was a significant difference in the laser forming characteristics of the cold rolled AISI 1010 mild steel depending on the orientation of the scan line to the rolling direction in the sample. It was found that the anisotropic effects increased with increased rolling

reductions i.e. thinner materials. It was also concluded that the higher the temperature achieved in the sample the less the materials' anisotropy has an effect.

2.5 Potential Applications

Laser forming has potential for prototyping, aligning and removal of distortion or as a direct manufacturing tool in the industry sectors aerospace, automotive, shipbuilding and microelectronics. A number of possible applications in these sectors have already been discussed in the previous sections.

The full potential of LF will only be realised through improved process knowledge and associated system developments. With many of the currently identified limitations already being addressed in ongoing research, the process has significant potential for use in a broad range of industrial applications and sectors, including shipbuilding. Table 2.2 is a summary of the short-term degree of application potential in various stages of a (component non-specific) product life cycle. Compared to other forming processes, LF has the advantage of process flexibility, in that it could be carried out alongside other laser processes (cutting, welding & others) by multi-purpose laser systems. For large scale LF of metals e.g. in shipbuilding, the high equipment costs and safety requirements are currently key concerns, but these should be alleviated by the continuing development of cheaper, more compact and more efficient sources (diode and fibre lasers) and automated LF systems.

Degree of application potential	Stage of industrial application (Product Life Cycle)				
	<i>Design & Development</i>	<i>Manufacture (Processing)</i>	<i>Product Assembly</i>	<i>In-service Operation</i>	<i>Repair & Maintenance</i>
<i>High</i>	Rapid Prototyping	Forming (Hybrid LF)	Precision Alignment & Adjustment		
<i>Medium</i>		Distortion & Shape Correction		On-board Automatic Correction	Damage and Distortion Correction
<i>Low</i>		Forming (LF)			

Table 2.2: Degree of application potential for LF in various stages of a general product life-cycle (not specific to component scale, material or geometry)⁹

Laser forming at a macro level is developing from a knowledge base of basic 2D mechanisms to a practical realisation of 3D laser forming of complex structures routes to practical 3D laser forming may encompass elements of both predictive and adaptive systems. Promising applications for LF are in rapid prototyping, net shape production and distortion correction.

2.5.1 Rapid Prototyping ⁴⁷

Laser forming can compete with die forming in terms of process flexibility and cost in low volume parts. It can also compete with hot creep forming. This process involves the forming of material, usually titanium alloy, using a heated die and press tool. A plate (sprayed with Boron Nitride to aid thermal diffusivity) is placed in the press tool and die, the plate is then heated to 800°C and formed over the die using much less force and inducing much less stress in the component when compared to cold forming. If Ti64 is used, the plate is then sand and

vapour blasted prior to chemical etching to remove the α -case (mentioned earlier) due to the process taking place in air. The disadvantages of this process specific to LF are:

- Long tool change-over times (1/2 day)
- Long warm up/cool down times of the die (16 Hours)
- Removal of α -case
- Cost of effluent disposal
- Cost of tooling
- Storage of tooling
- Inflexibility
- Cooling of dies between components
- High energy consumption (20Kw/H)

LF has a number of advantages over hot creep forming in these areas:

- Increased flexibility
- Reduced tooling costs
- Possible Single piece forming of components
- Reduced need for etching (Argon atmosphere or local shrouding)
- Faster changeover times (batches of 1 possible)
- Simple product changes

2.5.2 Laser Assisted Bending

Laser forming has emerged as a viable means of assisting conventional forming processes. As laser forming can produce small accurate bends it can be used to finely form components after they undergo the initial conventional forming technique⁵⁶. Another technique is for deep drawing where the laser is used to heat up sections of the unformed material on the drawing edge. This is where the most deformation occurs. This assists mechanical forming by reducing the amount of force required¹⁰⁸.

2.5.3 Distortion Correction

Structures produced using the vacuum or blown technique in superplastic forming of titanium alloys in the aerospace industry are complicated and currently out of reach for the laser forming process. However, there is a great deal of post forming distortion with this technique that is currently manually corrected, at great time and expense. It is possible to correct this distortion in an automated process using laser forming⁴⁷. Also in the aerospace industry it is often necessary to chemically etch parts to reduce wait. Again this produces distortion which is corrected manually¹⁰⁸. This can also be corrected using laser forming. This particular problem resulted in the strut reversal investigation in this thesis. This shows the feasibility of correcting this distortion using laser forming.

In the shipping industry welding of panels produces distorted panels. A number of advancements have been made in reduced distortion welding techniques. These include laser-based or hybrid techniques¹¹⁰. There is

however still distortion that can potentially be corrected using laser forming⁹.

2.5.4 Micro Alignment

A large amount of work into micro alignment has been completed by Hoving *et al*⁶⁶. Here the ability to accurately form very small angles in thin materials is taken advantage of. The main application of micro adjustment is in the electronic industry. Work included an actuator for CD lens adjustment that could be adjusted in using the laser forming process. Another application used a laser to adjust the 10-50 μ m gap between reed switches. Here the reed switch would be adjusted post processing with the laser being able to penetrate the glass housing of the reed switch.

2.5.5 Manufacture of Parts using Laser Forming

A likely application for 2D and 3D laser forming would be the ship building industry in the fabrication of hulls. (This seems fitting as this is the home of the flame forming technique, which is the original source of laser forming.) Currently mechanical methods of steel plate bending, for a material thickness range of up to 20-25mm (1inch) are used. The most straightforward case is the 2-D laser forming of part cylinder shapes for hull skin panels to be subsequently welded together. However, as the capabilities of 3D laser forming begin to evolve, it will be possible to consider using the process to produce primitive 3D shapes involving

various double curvatures, which would then be patched together as elements of a larger, more complex structure⁹.

2.6 State of the Art Review

Currently the state of the art of laser forming is based strongly in the micro adjustment of electronic actuators. This process is on the verge of breaking through into industry, particularly in the adjustment of hard disk suspension. This is fuelled, in part, by the rapid advancement of the computer industry requiring data to be stored on hard disks more densely.

At the macro level of laser forming there have been large advancements in 3D forming. This is, in part, due to the increase in accuracy and versatility in mathematical modelling of the process. An area of note is the in the manufacture of ship hull components⁸⁷⁻⁹¹.

2.7 Synopsis for Present Research

Two-dimensional (2D) forming has been investigated numerous times over the years and a great deal is known about the process. However there are number of variables in the process and some of the subtleties still need to be investigated. The work on 2D laser forming in this thesis looks at the effect of heat treatment on 2D laser formed AA6061 parts and the influence of the change in geometry of the work-piece during the laser forming process.

A less well investigated area of laser forming into which a great deal of research is currently being carried out is the investigation into controlled three-dimensional (3D) laser forming. There is a great deal of potential for this process to be applied in industry. However, first it must be competitive with well established processes such as die forming. For laser forming to be competitive it must show that it is a reliable, repeatable, flexible and cost effective. Many current processes cannot compete with the laser forming process for flexibility, though even this is not enough if the process doesn't fulfil, at least in part, all of these requirements. The geometry based predictive/adaptive model for 3D forming in this thesis is a step towards fulfilling these requirements. In this thesis a model using a purely geometric technique is used to form 3D semi-developable shapes, in mild steel and aluminium, and also in the correction of various distortions in aluminium struts.

Chapter 3

Experimental Procedure

3.1 General Set-up

This section describes the general experimental set-up used. This contains a brief description of the laser, the laser forming system, which includes work-piece movement and measurement, and the use of absorptive coatings. More specific experimental set-up for separate investigations is detailed later on in this chapter.

3.1.1 Hardware

3.1.1.1 The CO₂ Laser¹¹⁰

For a better understanding of the laser used for the investigations in this thesis a brief description of how a CO₂ laser works is given here.

A laser works by taking advantage of the stimulated emission phenomenon. This phenomenon is the release of energy, as a photon, of an excited species through stimulation caused by the strike of a photon. The photon created is in phase and travelling in the same direction as the stimulating photon. This causes a change in energy from the excited energy state to the lower energy state and is the source of the laser beam. This makes the laser spectrally pure.

Many materials can display the stimulated emission phenomenon, but few have significant power capability. For this population inversion is necessary. This is where there are more atoms or molecules in the excited state than in the lower energy state, this allows amplification rather than absorption. To achieve a population inversion the lifetime of the excited species has to be longer than the lifetime of the lower energy state. This is possible with carbon dioxide (CO₂).

To initiate the stimulated emission phenomenon the gas mixture in the laser cavity is kept at a low pressure with a high voltage electrical discharge placed across it. This results in a plasma containing CO₂ distributed at its various energy states. This distribution is determined by the Boltzmann distribution. CO₂ molecules at the upper energy state will

lose their energy by either colliding with the cavity wall or by spontaneous emission. Spontaneous emission releases a photon of light with a wavelength of $10.6\mu\text{m}$ which can be travelling in any direction. Some will travel along the length of the cavity and will begin to oscillate between the cavity mirrors. As the photons strike molecules of CO_2 in the upper energy state the molecule will release a photon with the same phase and direction, as described in the stimulated emission phenomenon. There are then two photons oscillating between the mirrors of the cavity. These, in turn will strike two more CO_2 molecules in the upper energy state. This process continues releasing more and more photons with the same phase travelling in the same direction. As the upper energy state is now depleting more of the electrical energy is transferred to the upper energy level to satisfy the Boltzmann distribution.

To maintain this situation the upper energy state should be slower to drop to the lower energy state, through spontaneous emission, than the lower state is excited to the upper energy state. This allows the population inversion to occur resulting in more amplification rather than absorption of the photons. To help maintain the population inversion nitrogen (N_2) is used. N_2 has an energy gap between the different quanta of oscillation which is within a few hertz of what is required to take cold CO_2 and excite it to upper energy state. Because of this a requirement of CO_2 laser design is the ability to keep CO_2 cool.

The gas mixture in the laser cavity is around 78% helium (He), this is for good conduction and stabilisation of the plasma, 13% N_2 , for the exciting of cold CO_2 to the upper energy state, and 10% CO_2 as the active medium. In this case the gas is cooled by convection as it's a fast axial flow (FAF) laser.

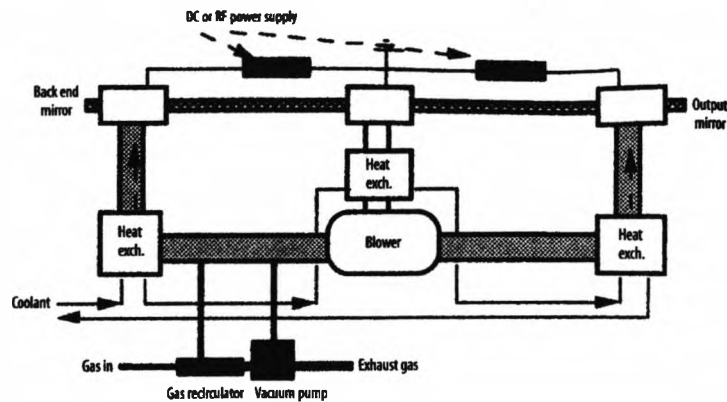


Figure 3.1.1: General construction of a FAF laser¹¹⁰

3.1.1.2 The Electroxx 1.5kW CO₂ Laser

The laser used for all the laser forming processes performed in this thesis was an Electroxx 1.5kW CO₂ fast axial flow (FAF) continuous wave (CW) laser. This laser has a folded cavity to conserve space and increase the cavity length. A general rule with the cavity is that the longer the cavity is the more power output it can produce. The cavity is housed in the lasers casing (figure 3.1.2) along with the vacuum pump, blower, heat exchanger and power supply (figure 3.1.1).



Figure 3.1.2: Electroxx 1.5kW CO₂ laser

The three constituent gases are fed into the laser from three large gas bottles, each with its own regulator to ensure an accurate gas mixture, a high voltage (HV) power supply and cooled water from a chiller unit (Coolmation) to cool the heat exchangers and optics.

3.1.1.3 Workstation

The laser is shared between two workstations. Only workstation 2 is described here as it is specifically designed for laser forming operations.

3.1.1.3.1 Beam Delivery

A gold coated copper turning mirror is pneumatically powered to rotate through 90° allowing the beam to be shared between both workstations. This mirror is water cooled along with all of the optics in the beam delivery. Two additional turning mirrors are used and the beam is enclosed in flight tubes as it travels approximately 3.5m to the processing head. The processing head contains the focussing optic, a zinc selenide (ZnSe) lens, and the co-axial nozzle arrangement (figure 3.1.4).

3.1.1.3.2 Part Manipulation

The workstation consists of a 3 axis CNC table. The z axis controls the focusing optics and nozzle arrangement and the x and y axis controls the movement of the work-piece under the laser (figure 3.1.4). The z axis has 300mm of movement and provides focus control and beam size selection, this axis has a built in brake to avoid any unwanted movement. The x and y axes each have 435mm of travel. All axes are driven by DC servo motors.

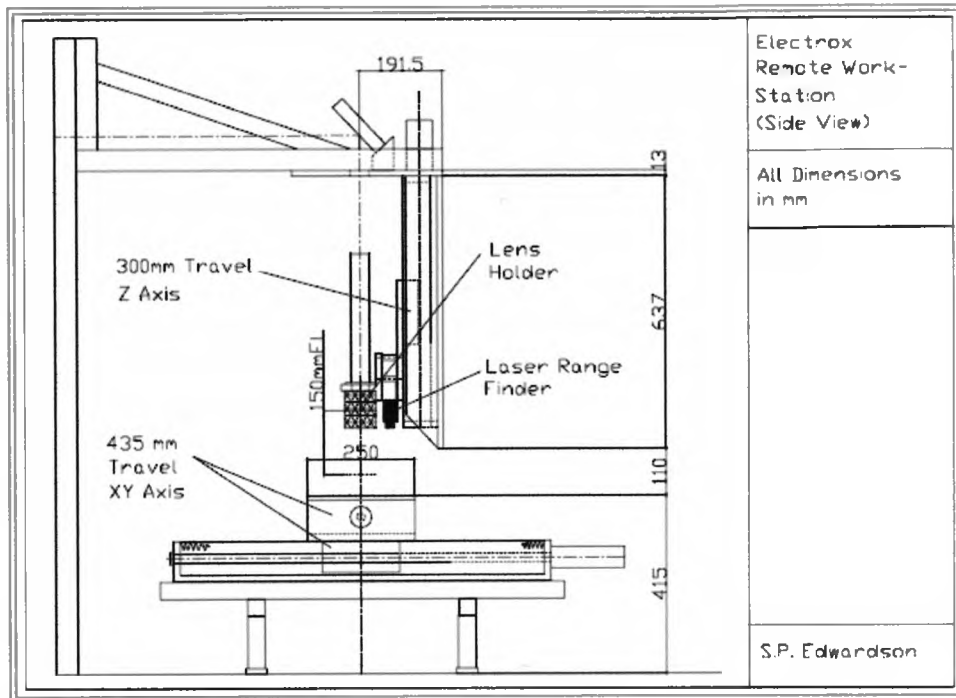


Figure 3.1.3: Workstation 2, CAD Drawing of layout⁴⁷

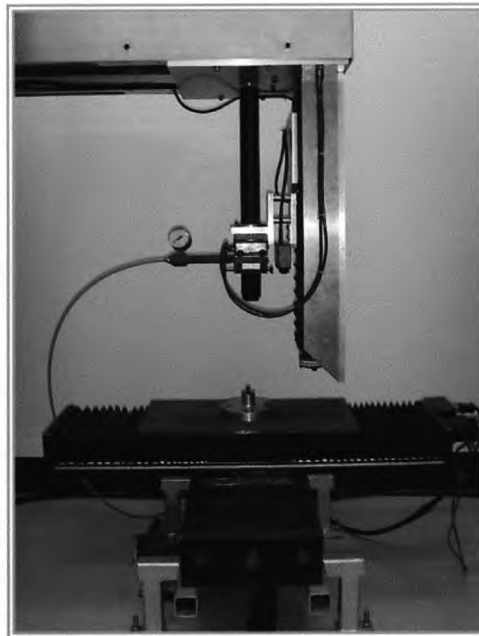


Figure 3.1.4: Workstation 2 layout

The tables and control system are based around the Naples Coombe Ltd, Servostep 1700 system. This uses a Galil DMC1730 PC based controller (ISA card) interfaced with the tables via servo amplifiers housed in a Servostep chassis. As the controller is PC based this allows for custom software to be written, this software is discussed later in this chapter. The control card has full digital I/O plus analog input capabilities. Along with focus and movement control the laser shutter can also be controlled using this system. This control is in series with the manual control, therefore both have to be 'on' to open the shutter.

3.1.1.3.3 Measurement

Integrated into this system is an MEL M5 laser range finder. This gives the system an online single point non-contact method of high accuracy measurement of the height of a work-piece. The laser range finder has a range of 100mm, a resolution of 30 μ m (on a white surface) and produces a +/- 10V analog signal corresponding to +/- 500mm from a reference point 220mm from the sensor, this signal is then fed into the controller. In figure 3.5 the laser range finder can be seen mounted behind the lens holder. It operates on the principle of triangulation between a red diode spot and a photo-sensitive diode. Fixed to the top of the x , y tables is a steel work bed which has a number of drilled and tapped holes allowing the clamps to be attached.

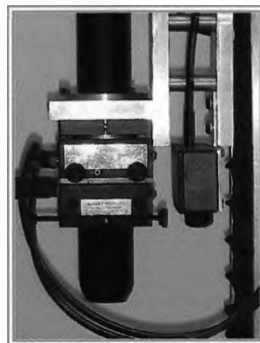


Figure 3.1.5: Nozzle arrangement and laser range finder

3.1.1.3.4 Work-Piece Restraints

There are four methods of holding the work-piece in the investigations carried out in this thesis. A centre clamp is used for 3D forming (figure 3.1.6); this allows freedom of movement of the work-piece as it is clamped at a single point, decreasing the possibility of additional stresses to the work-piece. However, this does require a hole to be drilled into the centre of the work-piece.



Figure 3.1.6: Centre Clamp

For the 2D forming an edge clamp (figure 3.1.7) and a V-block (figure 3.1.8) is used. These are the simplest method of restraining and don't require a hole to be drilled. For the strut reversal investigations a modification to the edge clamp is used (figure 3.1.9). This clamps the centre of the strut on either side to allow forming across its whole length.

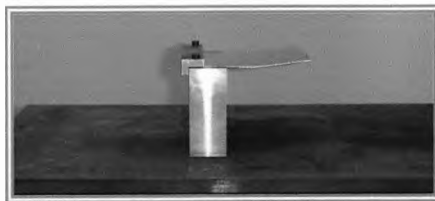


Figure 3.1.7: Edge clamp



Figure 3.1.8: V- block

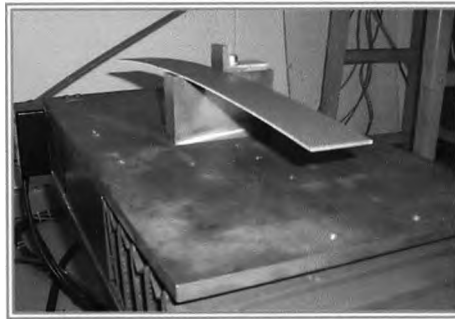


Figure 3.1.9: Modified side clamp

3.1.1.4 Characterisation of the Laser at the Work Surface

3.1.1.4.1 Laser Beam

The laser beam produced has an M^2 of, approximately, 2.5. M^2 is a value of beam quality, 1 being a perfect Gaussian distribution. This laser has a ‘top hat’ energy distribution which is advantageous in laser forming as a larger area of the surface can be heated equally minimising the melting on the centre of the irradiation track, which is an issue with a Gaussian energy distribution. An image of the beam was taken with a Spiricon Pyrocam III laser beam analyser; this image can be seen in figure 3.1.10.

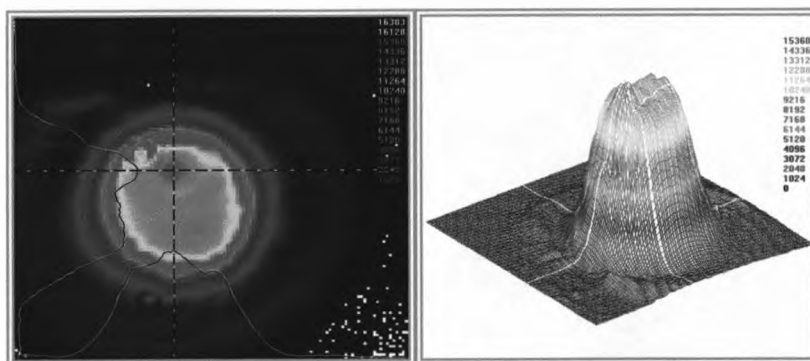


Figure 3.1.10: Electrox 1.5kW laser beam energy profile, PyroCam III image⁴⁷

3.1.1.4.2 Beam Diameter

As the beam diameter is a factor in laser forming it is important to know the beam diameter at varying distances away from the work piece. This is achieved by creating a burn print onto a piece of wood (figure 3.1.11). The z axis is moved up 5mm after a burn print has been created. This allows a measurement of the beam diameter to be taken at 5mm intervals. The actual effective beam diameter is taken as the inner ring of higher intensity and not the overall diameter. This corresponds to the 'top hat' profile with a slight halo of lower intensity as seen in figure 3.1.10. A large diameter nozzle (figure 3.1.5) and a small amount of compressed air is delivered co-axially to cool the lens and protect against debris for this test and throughout the laser forming studies.

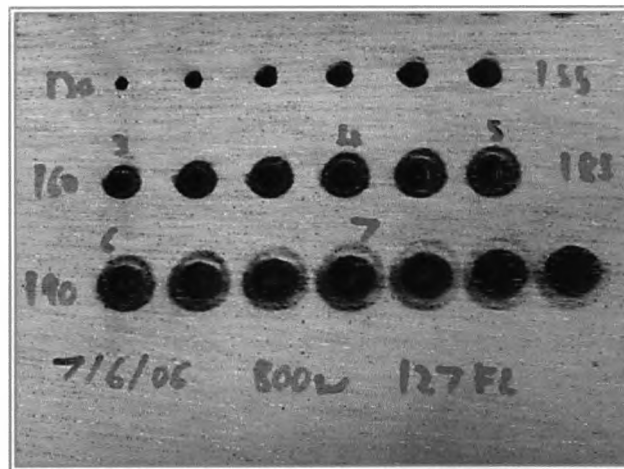


Figure 3.1.11: Burn prints in wood at 5mm steps, 127mm FL lens
130mm-220mm stand off

3.1.1.4.3 Laser Power

The power of the laser is selected manually on a hand held control box. The reading of the power is based on a calibrated thermocouple measurement from the back mirror of the cavity. This is an accurate reading for the laser power when leaving the laser but not for the power at

the working surface. This is because energy is lost as optics absorbs some of the power. Because of this a power reading is taken at the surface for varying powers at the laser. This reading is taken using a power puck. A power puck is a calibrated device whereby the temperature rise, in a coated black metal block exposed to a laser beam, is directly proportional to the incident laser power. A graph to correlate the relationship is then plotted (figure 3.1.12). This graph is then used to determine the power required on the laser to achieve the desired power at the surface.

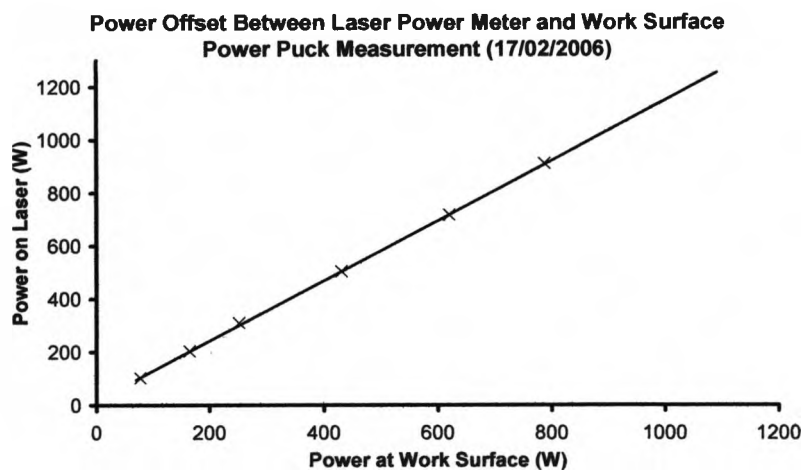


Figure 3.1.12: Power offset calibration graph

3.1.2 Software

The CNC tables are controlled by a Galil DMC 1730 ISA PC based controller. This control card comes with some basic software for terminal based line control and part program creation and downloading, using the Galil CNC language. Using this language it is possible to control the position of the CNC tables with absolute co-ordinates (with respect to the table origin) and relative co-ordinates (with respect to current position).

Traverse speed of each axis and vector speed in a co-ordinated movement, acceleration and deceleration in each axis can also be controlled. The Galil CNC language measures movements in encoder counts rather than distance. To adjust distance into encoder counts the conversion factor is $1\text{mm} = 1000$ counts for the z stage and $1\text{mm} = 400$ counts for the x and y stages.

The control also has dynamic link libraries (.dll) and ActiveX driver for custom software authoring in Microsoft Visual Studio applications, such as Visual Basic. This allows for a user interface to be created that can hide CNC commands, such as jogging the tables or returning the tables to the origin, behind buttons. These operations may otherwise take several lines of typing.

3.1.2.1 Visual Basic Based User Interfaces

3.1.2.1.1 Jog Controller User Interface

The jog controller contains the following features.

Controls:

- Jogging of individual axes at selected speeds
- Homing of the axes
- Resetting of the origin
- Start positioning
- Terminal

Displays:

- Real-time position report of each axes
- Real-time output from the laser range finder
- I/O status

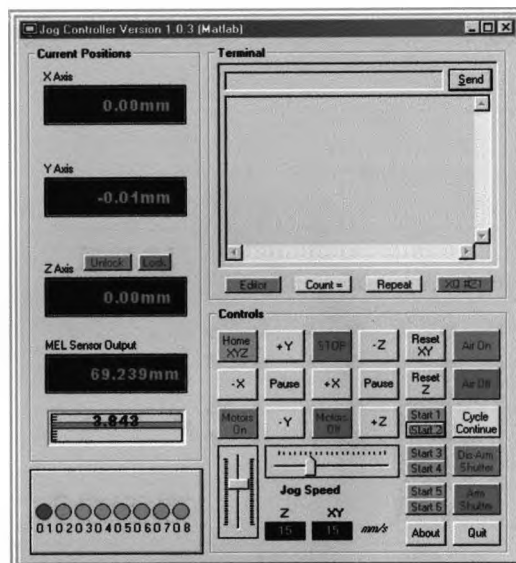


Figure 3.1.13: User interface for the jog controller

The jog controller contains start position controls to place the tables at a set start position and reset the origin. Each start button has a different start position which relates to an individual clamp and/or work-piece size. This allows the tables to be aligned before the start of any processing. The terminal has the ability for command line control for part program control and also access to the Galil editor for the creation and downloading of part-programs. The Galil editor is crucial in some of the investigations allowing programs created in computer modelling to control the tables.

3.1.2.1.2 Two-Dimensional Laser forming User Interface

This controller is specifically design for single line multiple pass 2D forming. This controller contains the following features:

Controls:

- Processing parameter selection
 - Speed
 - Time delay between each pass
 - Number of passes
 - Focal position
 - Material Thickness
- Homing of the axes
- A button to start 2D laser forming

Display

- Bend angle after each pass
- Current pass number

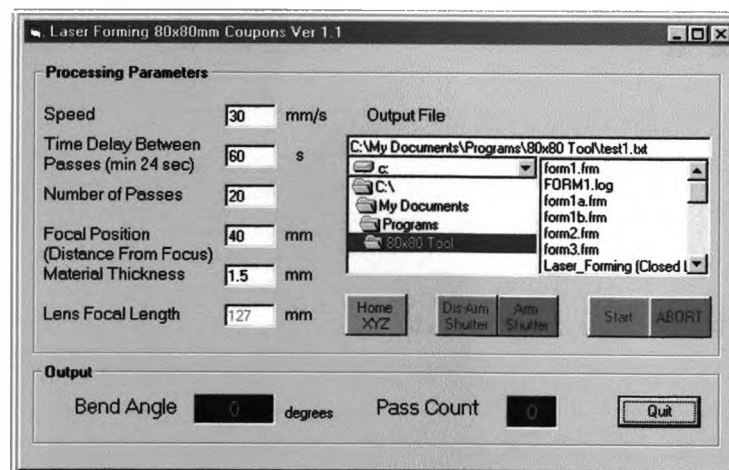


Figure 3.1.14: User interface for the automated 2D laser forming of 80x80mm coupons

The controller also has the ability to generate an output file, in a comma delimited text file (.csv), containing the pass number and corresponding bend angle. There were minor alterations on the method of calculating the bend angle in each investigation so this is not discussed here but will be discussed in the relevant section.

In later investigations the user interface was modified to include full surface scans (figure 3.1.15). This took into consideration the area seen by the laser range finder decreasing. Because of this height measurements were able to be taken closer to the edge of the work-piece, increasing the accuracy of the angle measurement.

There are a number of start buttons in this version these give an option of whether only the pre-forming and post-forming scan is needed, saving time, or a scan after every pass. Also a choice of work-piece size for the scan size to adjust and in one case it takes into consideration a change of clamping.

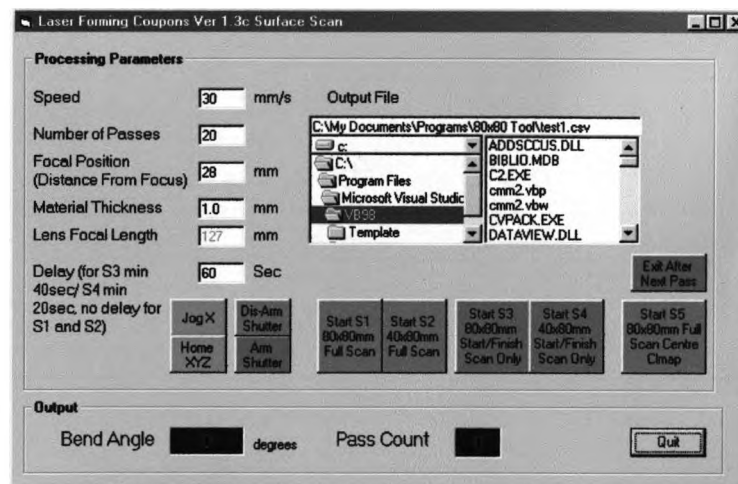


Figure 3.1.15: User interface of the automated 2D laser forming of 40x80mm and 80x80mm coupons with full surface measurement

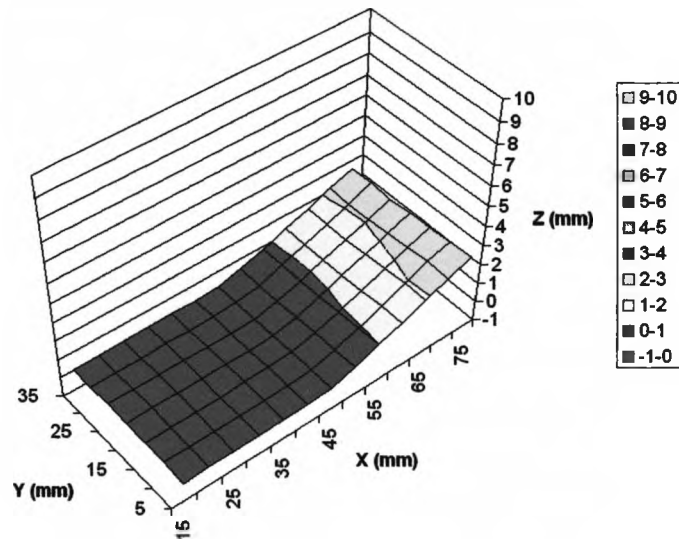


Figure 3.1.16: Sample of a measurement taken using the surface scan

3.1.2.1.2.1 Measurement and Calculation of 2D Sample

The measurement of bend angle and the calculation of the distribution of the measured points during forming are explained here. For each pass the laser range finder scans the surface of the work-piece taking measurements at 5mm increments. Two of these measurements are used to calculate the bend angle, shown as grey on figure 3.1.17.

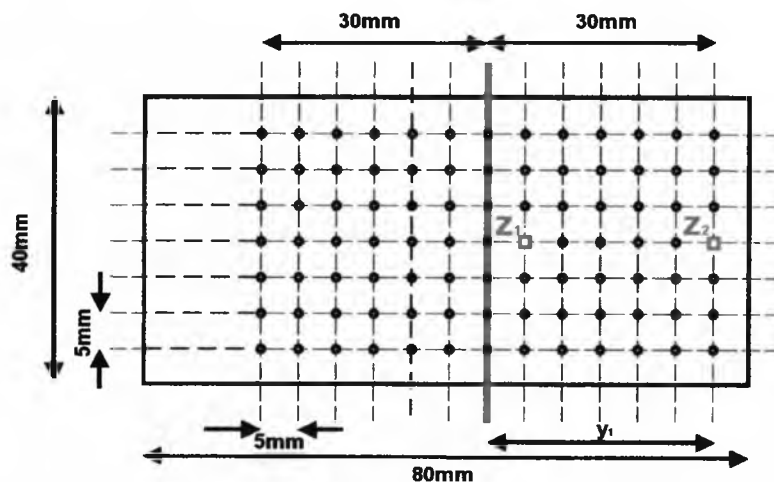


Figure 3.1.17: Measured points on a flat 40x80mm coupon. The solid grey line shows the irradiation path and the two square grey points show z_1 and z_2 , the measurements used for calculating bend angle.

This bend angle is then used to adjust the increment in the y direction, y_{inc} , of the measurement points for the next measuring pass. By doing this it is possible to measure the whole surface after each pass and a more accurate bend angle can be calculated as it is possible to measure points further apart. This can be done here because the measurement points can be close to the edge without the risk of the laser range finder missing the work-piece as it forms.

The method of calculating the bend angle and altering the measuring increment is as follows. Before any processing a surface measurement is taken. It is assumed that the work-piece starts flat so the increments are evenly spaced (figure 3.1.17). (There is an area that is not measured as the edge clamp obstructs this area.) The points in grey in figure 3.1.17 correspond to measurements for distance away from the laser range finder z_1 and z_2 .

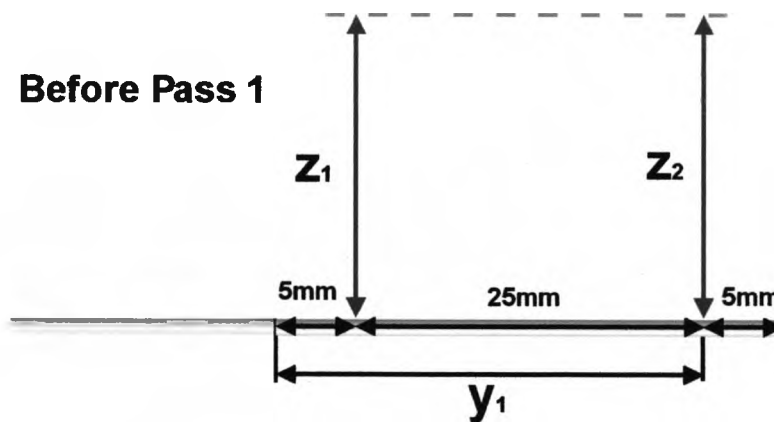


Figure 3.1.18: Values used for bend calculation before the first pass

As the work-piece is flat before the first pass $z_1 = z_2$.

To work out the angle the difference in distance from the laser range finder, z , is needed.

$$z = z_1 - z_2 \quad (3.1)$$

For this case $z = 0$

For the flat case we know the distance from the bend, the irradiation line, to the measurement points at the bending edge is 30mm, y_1 and we know that the increment, y_{inc} , is 5mm.

Therefore:

$$y_{inc} = \frac{y_1}{6} \quad (3.2)$$

This increment, y_{inc} , will decrease throughout the experiment allowing the measurement points to remain on the work-piece. The bend angle, θ , is then calculated:

$$\theta = \arctan \frac{z}{5y_{inc}} \quad (3.3)$$

For this case $\theta = 0$.

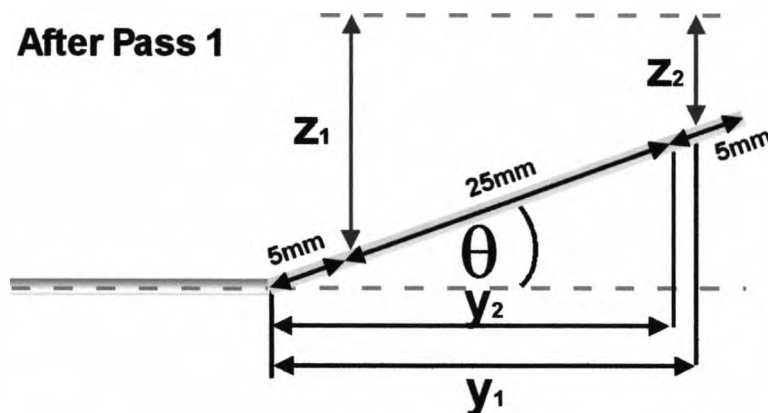


Figure 3.1.19: Values calculated and values used for bend calculation after the first pass.

After pass 1 the same measurement points as before are used (figure 3.1.18). These points are sufficiently placed from the edge so they don't miss the work-piece due to the bending in the first pass.

The method here is the same as before with the addition of working out the new distance from the bending line to 5mm from the edge, y_2 (figure 3.1.19).

$$y_2 = 25 \cos \theta \quad (3.4)$$

This now give us a new increment between measuring points, y_{inc} .

$$y_{inc} = \frac{y_2}{6} \quad (3.5)$$

This increment, y_{inc} , is now used positioning the measured points after the second pass (figure 3.1.20).

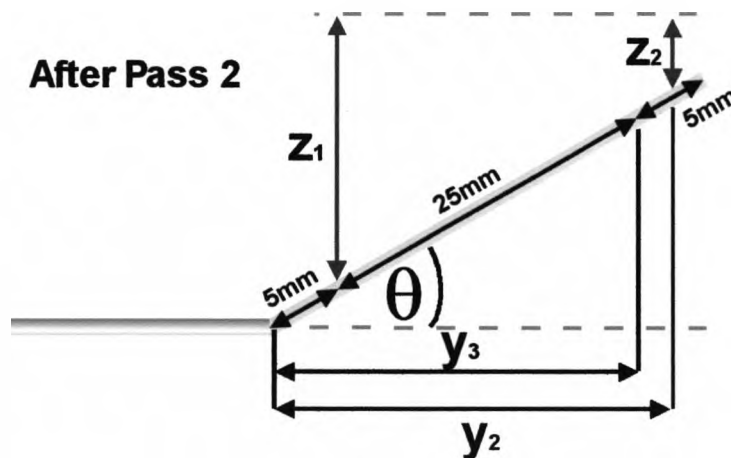


Figure 3.1.20: Values calculated and values used for bend calculation after the second pass.

The same process is then continued after every pass. This system works a step behind the laser forming passes with the corrected increment being used on the future measurement rather than the current one. This saves time as only one surface measurement is required. This also requires the distance of each measuring point along the y axis to be recorded as this will vary with each pass.

3.1.2.1.3 Co-ordinate Measuring Machine (CMM)

The CMM utilises the laser range finder and the CNC tables to plot the height of the work-piece surface. This is done by the CNC tables moving the work-piece stopping at specified intervals where the laser range finder takes a height measurement. These measurements can then be used to map the work-piece surface.

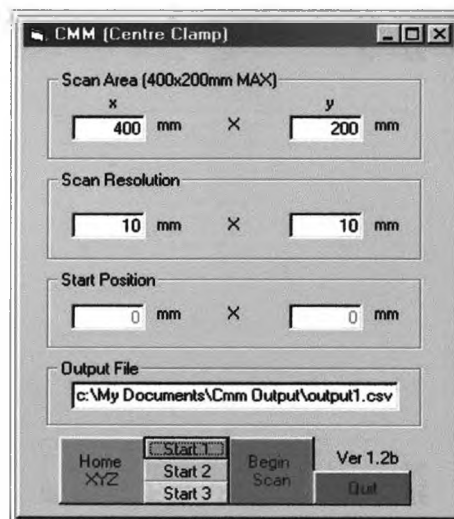


Figure 3.1.21: User interface for the co-ordinate measuring machine (CMM)

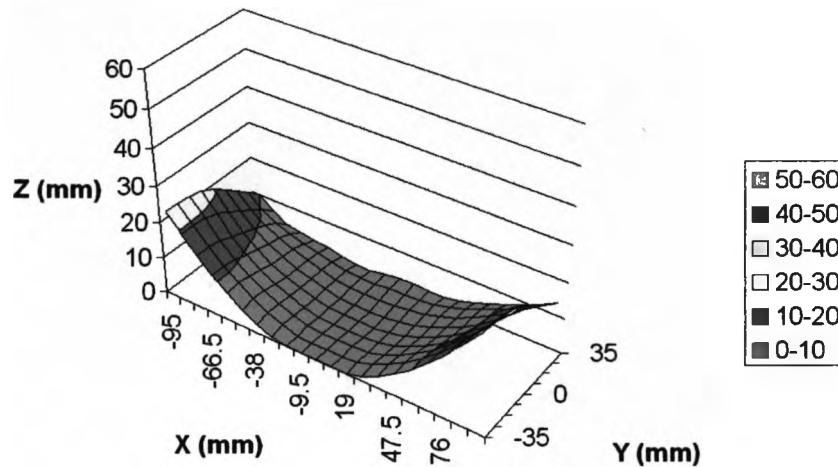


Figure 3.1.22: Example of a measure part using the co-ordinate measuring machine

In the first version of the CMM user interface used in this study, the size of the scan area can be specified along with the scan resolution (figure 3.1.21). As with the 2D laser forming control interface a corner delimited text file (.csv) is generated where the height information is stored.

A problem found in the measurement of the work-piece surface is that, after a certain amount of forming, the laser range finder will begin to miss the work-piece. This is because as the work-piece forms the area viewable from directly above the work-piece decreases. This is a similar problem as in the 2D laser forming. However this is far more complicated because in the case of 3D forming the work-piece forms in a continuous curve and can also form along any axis. To continue forming a modification to the CMM interface was created (figure 3.1.23). This does not require the specification of the scan area or the scan resolution. This is already decided within the Matlab program, decrease in viewable area (discussed later on in this thesis). The Matlab program calculates the amount the viewable area has decreased in the previous pass and distributes the measurement points

respectively. This program writes a visual basic program which is then placed behind the 'Begin Scan' button on the interface.

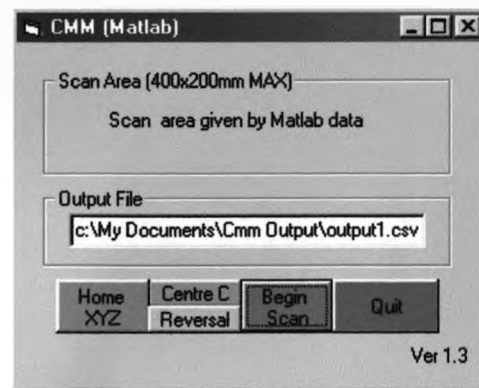


Figure 3.1.23: User interface of the Modified co-ordinate measuring machine (CMM)

Here the start buttons points are replaced with descriptive buttons for ease of use and still perform the same function as in previous user interfaces. Again a file is generated where the heights are stored.

3.1.3 Absorptive Coating

It is essential for the laser radiation to couple with the work-piece in the laser forming process. When using a CO₂ laser in the laser forming process if no method of increasing absorption is used sufficient coupling is very difficult to achieve. This is because most metals absorb almost no light at 10.6 μ m wavelength of a CO₂ laser (figure 3.1.24). Additional to this the

amount of absorption decreases again because of the decrease in laser intensity of defocused beam in the laser forming process.

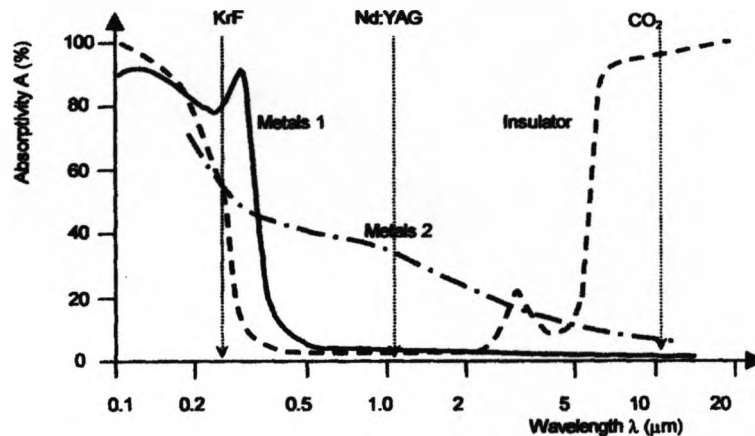


Figure 3.1.24: Absorptivity as a function of wavelength for normal incidence, smooth surfaces and room temperature. Metals 1 are those with full inner electron shells (Au, Ag, Cu,...) and Metals 2 are transition metals (Fe, Ni, Cr,...) ¹¹¹

Because of the high reflectivity it is necessary to consider methods to increase the absorption of the laser into the work-piece. There are many methods of accomplishing this.

- Roughening of the surface
- Oxidising the surface
- Coating the surface

The reflectivities of various methods of increasing absorption are shown in table 3.1.1.

Surface Type	Reflectivity (%)		
	Direct	Diffuse	Total
<i>Sand paper roughened (1μm)</i>	90	2.7	92.7
<i>Sandblasted (19μm)</i>	17.3	14.5	31.8
<i>Sandblasted (50 μm)</i>	1.8	20	21.8
<i>Oxidised</i>	1.4	9.1	10.5
<i>Graphite</i>	19.1	3.6	22.7
<i>Molybdenum Sulphide</i>	5.5	4.5	10

Table 3.1.1: Typical values of the reflectivity of various surfaces to 10.6 μ m radiation at normal angles of incidence¹¹⁰

Absorptive coatings are the most common means of increasing the absorption of CO₂ laser radiation and are widely used in industry. The laser power is absorbed in these thin layers and transferred to the work-piece. As the coating has to transport the released heat to the metal surface the thermal conductivity of the work-piece will influence the overall absorption coefficient.

In this study graphite spray is used throughout. This is applied manually to a work-piece, which has been cleaned with acetone to remove contaminants. This can have an influence on the absorption as the thickness, usually 6 μ m⁴⁷, of the coating can vary. On small substrates maintaining an even layer of graphite is not a problem. On the larger substrates however there can be small areas where the thickness alters. Another influence is the degradation of the coating during the process. This is minimised in laser forming due to the relatively low intensity and high traverse speed required for the process (figure 3.1.25). However with multiple passes over the same irradiation line a re-coating of the substrate

can be necessary. The graphite coating is quoted to have an absorptivity of 77.3% (table 3.1.1) this can vary depending on the substrate.

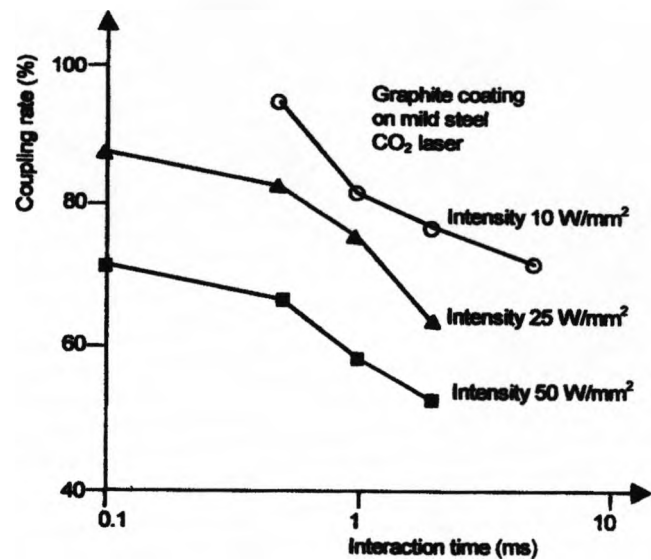


Figure 3.1.25: Dependence of coupling rate of coated surfaces on interaction time and incident intensity¹¹¹

3.1.4 Materials used in this Thesis

3.1.4.1 CR4 Mild Steel

Technical data on this material is given in the following tables:

Density	Young's Modulus	Strength	Yield Strength	Tensile Shear Modulus	Bulk Modulus	Hardness
[kg/m ³]	[GPa]	[MPa]	[MPa]	[GPa]	[GPa]	[Vickers]
7870	205	365	305	80	140	108

Table 3.1.2: Mechanical properties of Mild Steel CR4¹¹²

Melting Point [°C]	1515
Thermal Conductivity [W/m K]	49.8
Coefficient of Thermal Expansion [10 ⁻⁶ /K] 20°C	12.2
Coefficient of Thermal Expansion [10 ⁻⁶ /K] 250°C	13.5
Coefficient of Thermal Expansion [10 ⁻⁶ /K] 500°C	14.2
Specific Heat Capacity [J/kg K] 50-100°C	448
Specific Heat Capacity [J/kg K] 250-300°C	536
Specific Heat Capacity [J/kg K] 400-450°C	649
Specific Heat Capacity [J/kg K] 650-700°C	825

Table 3.1.3: Thermal Properties of Mild Steel CR4¹¹²

3.1.4.2 Aluminium Alloy 6061 (AA6061)

Temper	Tensile strength	Yield strength	Hardness	
	(MPa)	(MPa)	(HB)	(HV, converted from HB) ¹¹³
O	124	55	30	32
T4	241	145	65	71
T6	310	276	95	102

Table 3.1.4: Typical mechanical properties of AA6061 in its various tempers¹¹⁴

	O	T4	T6
Melting Range[°C]	582-652	582-652	582-652
Thermal Conductivity [W/mK]	180	154	166.9
Coefficient of Thermal Expansion [10 ⁻⁶ /K] 20°C	23.6	23.6	23.6
Coefficient of Thermal Expansion [10 ⁻⁶ /K] 250° C	25.2	25.2	25.2
Specific Heat Capacity [J/kg K]	896	896	896

Table 3.1.5: Thermal Properties of AA 6061 in three different tempers.¹¹⁴

Listed in table 3.1.4 are typical mechanical properties of AA 6061 in its most common tempers. These tempers are the ones used in this investigation. Included are the hardness values used to verify that these tempers have been achieved. As the original values are in Brinell hardness (HB) they have been converted using conversion tables to Vickers hardness (HV), which are the units used by the micro hardness tester.

3.1.4.3 Aluminium Alloy 5251

Some of the properties of AA5251 are listed in table 3.1.6 and 3.1.7. The temper used in these experiments is H22.

Density [g/cm ³]	2.69
Melting Point [°C]	625
Modulus of Elasticity [GPa]	70
Thermal Conductivity[W/m.K]	134
Thermal Expansion [10 ⁻⁶ /K]	25

Table 3.1.6: Physical properties of AA5251¹¹⁵

Temper	H22	H24	H26	0
Vickers hardness [HV]	65	70	75	46
Proof Stress 0.2%[MPa]	165	190	215	80
Tensile Strength[MPa]	210	230	255	180
Shear Strength [MPa]	125	135	145	115
Elongation A5 [%]	14	13	9	26

Table 3.1.7: Mechanical properties of AA5251¹¹⁵

3.2 Geometrical influences

To date there has been a considerable amount of work carried out on two-dimensional laser forming, using multi-pass straight line scan strategies to produce a reasonably controlled bend angle in a number of materials, including aerospace alloys. A key area, however, where there is a limited understanding, is the variation in bend angle achieved per pass (or bend angle rate) during multi-pass laser forming along a single irradiation track (producing a positive bend), in particular the decrease in bend angle per pass after many irradiations for a given set of process parameters consistent with the TGM⁶.

Understanding of this variation in bend angle per pass is essential if the LF process is to be fully controlled for a manufacturing environment. There are many influencing factors for this. Here an additional cause for this is proposed based on the geometrical effects of the component deformation, which in turn influences the process parameters per pass. This theory is confirmed through empirical analysis of the 2D laser forming process.

This fall off in bend angle can be seen in the results from the initial experiment. This used the edge clamp with multiple scan lines at the same position. These results are compared with results for forming with the same line energy and various beam diameters which simulates the decrease in energy fluence of the geometrical effect. For further comparison the same

parameters as the initial experiment are used with a v-block, this changing the geometrical effect.

3.2.1 Edge Clamp Condition

The material formed is 1.5mm CR4 mild steel at power of 760W, beam diameter of 5.5mm and a traverse speed of 30mm/s. A graphite absorptive coating is used without re-coating and 60 passes are completed. The piece is formed using the previously described general set-up using the 1.5kW CO₂ laser.

Equations to calculate the beam area are determined. These are used to work out the influences of the geometry effect on the beam area, and therefore energy fluence as a function of the current angle.

To simulate the effects of a decrease in energy fluence experiments are performed with 5.5, 6, 6.5, 7 and 8mm beam diameters. To be able to make a comparison to the original experiment the same parameters are used which keeps the line energy constant. From the results of this experiment it is possible to calculate a predictive model of the effects of the change in geometry as the work-piece forms.

3.2.1.1 Measurement

The user interface for the automated 2D laser forming of 80x80mm coupons is used with the following method of calculating angle used.

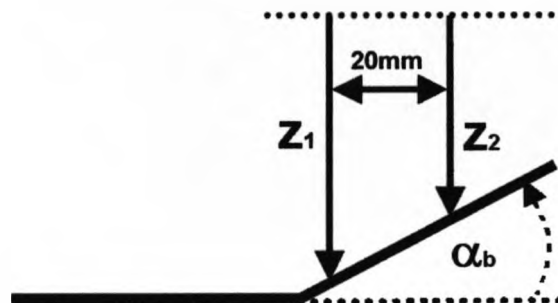


Figure 3.2.1: Calculation of bend angle for the edge clamp

$$\alpha_b = \arctan\left(\frac{z_1 - z_2}{20}\right) \quad (3.2.1)$$

3.2.1.2 Predictive Model

Using the results of the effects of various beam diameters of bend angle per pass it is possible to find an equation for the relationship between bend angles per pass and beam area. An average bend angle per pass for each of the beam diameters for the first 30 passes is taken. By only using the first 30 passes the bend angle in the experiment doesn't exceed 35°. This is before any significant change in beam area occurs due to the geometrical

effect. This average is used to find an equation for the relationship between the bend angles per pass as a factor of beam area.

It is noted that the change in beam diameter does not simulate the geometrical effect exactly as the traverse length of the beam changes with the diameter and with the elliptical beam created by the geometrical effect this is constant. This gives a variation in the energy fluence (figure 3.2.2). However there is a close relationship which is sufficient for a predictive model which will be used as a comparison for the experimental results.

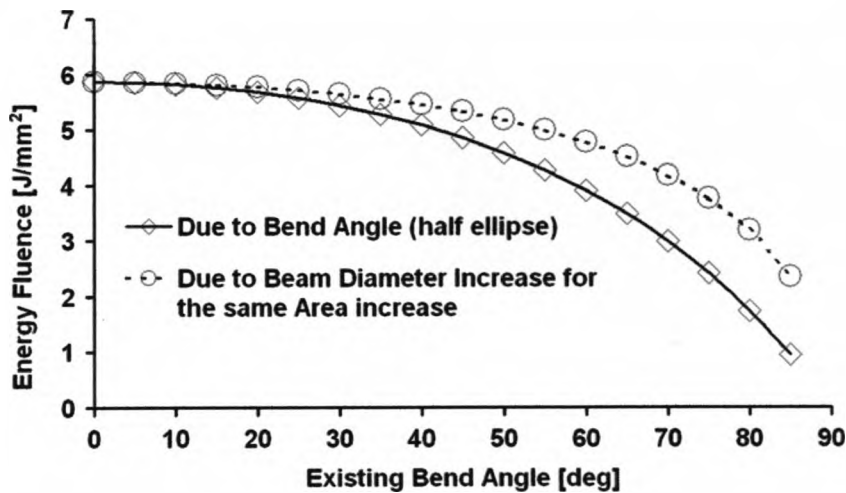


Figure 3.2.2: Energy fluence with increasing bend angle and energy fluence with an increasing beam diameter equivalent to the same incident area increase.

As the bend angle per pass for an area of the elliptical beam is now known the relation between the bend angles per pass with increasing existing bend angle can be determined.

3.2.2 V-block condition

The equations for the change in beam area as the bend angle increases are determined and the relation in beam area and energy fluence with beam angle is shown graphically. The experiment is repeated with the same parameters as the initial experiment in a v-block. These results can then be compared.

3.2.2.1 Measurement

The same user interface is used for the v-block as with the edge clamp with a change in the angle calculation.

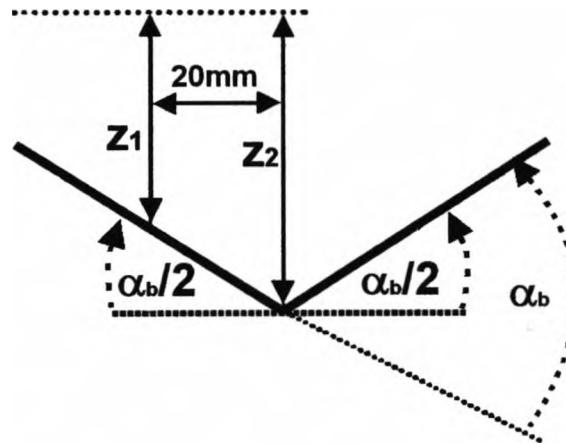


Figure 3.2.3: Calculation of bend angle for the v-block

$$\alpha_b = 2 \arctan\left(\frac{z_2 - z_1}{20}\right) \quad (3.2.2)$$

3.3 Effects of Post Forming Heat Treatments on Laser Formed Components

This investigation is carried out on AA6061 as it is heat treatable and has 3 temper settings which will allow the alloy to go through various differing heat treatments. Aluminium alloy AA6061 is a commonly used heat treatable alloy and has many applications due to its high strength, corrosion resistance and ability to be welded. This investigation takes three 2D laser formed samples, measures the heights across the surface and then heat treats them.

The first heat treatment, which all the samples undergo, is full annealing. This will relax any residual stresses in the samples and give them a 0 temper which is the softest most ductile form of AA6061 possible. The samples heights are then measured again.

The next heat treatment is solution heat treatment and quenching. This is performed on two of the samples. The sample is heated to a high temperature and then cooled rapidly in a cold water bath. Again the samples are measured after this process. This strengthens the samples achieving a T4 temper.

The final heat treatment is precipitation hardening, which will only be performed on one of the samples. This is a long heating process at a much

lower temperature than the previous treatments and artificially ages the sample. This strengthens the sample further achieving a T6 temper.

The next step is to perform a micro hardness tests on each sample to ensure that the Temper states have been attained. For this investigation a 0 temper 1.6mm thick AA6061 is used which had been mechanically cut into 40 x 80mm coupons. The 0 temper is used as it is the base temper that all other tempers are derived from. Forming at the 0 temper has the added advantage of that it is the softest most ductile temper and any residual stresses have been removed.

3.3.1 Laser Forming

The basic set up is the same as described in the general set up. A 1.5kW CO₂ laser is used and the work piece is clamped using the edge clamp. The three samples were laser formed using different parameters shown in table 3.3.2. All of the samples were formed with the direction of the pass alternating each time; this is to help prevent the build up of stresses on one side of the sample. The choice of parameters used is taken from previous work within the group⁴⁷

	Sample 1	Sample 2	Sample 3
Power at surface (W)	500	500	500
Beam diameter (mm)	3	3	3
Beam velocity (mm/s)	55	55	45
Number of passes	20	5	5
Number of passes before re-coating of graphite spray.	10	n/a	n/a

Table 3.3.2: Laser forming parameters of the individual samples

The user interface used is the automated 2D laser forming of 40x80mm and 80x80mm coupons with full surface measurement shown in figure 3.3.1. No dwell time is selected as the piece has its surface measured after each pass. Including the time it takes for the measurement the dwell is approximately 5 minutes and 15 seconds. In previous work it is noted that a re-coating of the graphite would be required after 10 passes. Because of this the selected number of passes for sample 3 is 10 with the sample being re-coated with graphite and then another 10 passes completed at with the same parameters. No re-coating is required for sample 2 and 3.

3.3.2 Measurement

The samples were measured using the same system as described in the earlier section. The work-piece is moved under a laser range finder and measured at intervals across the surface, this giving an accurate surface layout (figure 3.3.1). For these measurements the clamp is used to provide an accurate reference point. To prevent stresses to the sample that would affect the surface measurement the jaws of the clamp are not used. To keep the sample in position it is placed on the clamp with some double sided adhesive tape. Measurements are taken before the first heat treatment and then after each heat treatment.

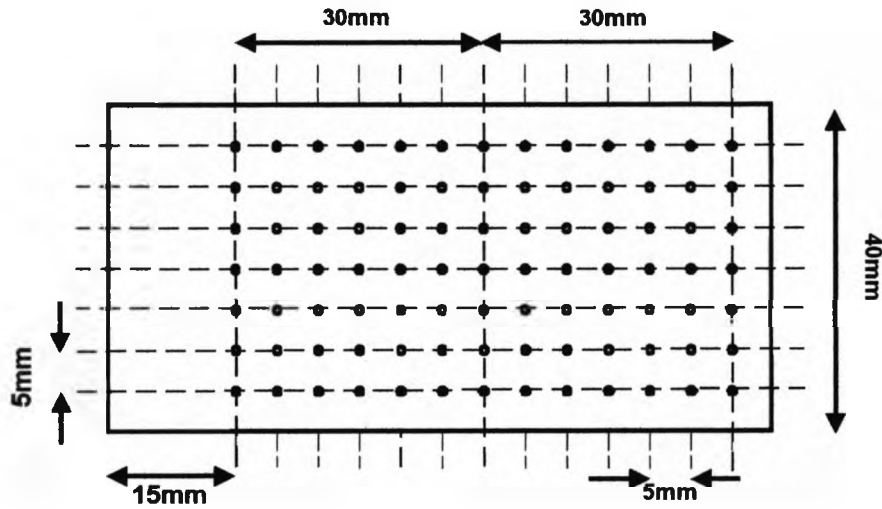


Figure 3.3.1: The measured points on the sample. The bending line can be seen here as the middle vertical dashed line.

3.3.3 Calculations

The average angle is taken from the average of the 7 total angles which are positioned at 5 mm intervals across the sample (figure 3.3.1).

To calculate the total angle, α_b , at each position first the angle of the clamped side, σ , and the angle of the free side, ϕ , are calculated. These are shown in the following equations:

$$\sigma = \tan^{-1}\left(\frac{(z_2 - z_1)}{30}\right) \quad (3.3.1)$$

$$\phi = \tan^{-1}\left(\frac{(z_3 - z_2)}{30}\right) \quad (3.3.2)$$

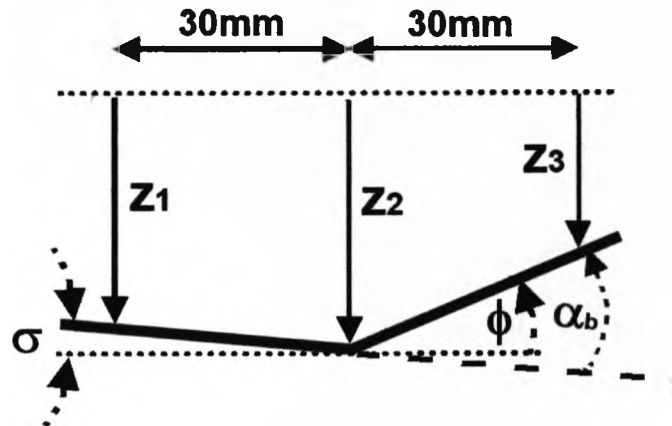


Figure 3.3.2: Schematic showing the calculation of the overall angle ' α_b '

The total angle, α_b , can then be calculated:

$$\alpha_b = \phi + \sigma \quad (3.3.3)$$

3.3.4 Heat Treatments

3.3.4.1 Annealing¹¹⁶

The softest, most ductile, and most workable condition of both non-heat treatable and heat treatable wrought aluminium alloys is produced by annealing to the temper designation 0. In the case of heat-treatable alloys, the solutes are sufficiently precipitated to prevent any natural age hardening from occurring.

For this investigation all three samples are fully annealed. They are placed in a furnace and then heated to 415°C for three hours. To ensure the cooling rate doesn't exceed 30°C/h the furnace is turned off and the samples remain inside allowing them to cool with the oven. In annealing, it is important to ensure that the proper temperature is reached in the full volume of the load; therefore it is common for the soak period to be at least one hour. The maximum annealing temperature isn't as crucial, though it is undesirable to exceed 415°C because of the possibility of oxidation. The cooling rate is vitally important to produce the maximum grain size in the samples and achieve full annealing, therefore slow cooling is used. This also has the added advantage of minimising distortion. All three samples are then measured, using the same method as before, with the CMM using double sided adhesive tape to keep the sample in place on the clamp.

3.3.4.2 Solution Heat Treatment and Quenching¹¹⁶

To achieve precipitation hardening it is necessary to go through solution heat treatment of the samples. The objective of this is to take the soluble hardening elements in the alloy into the solid solution. This process consists of soaking the alloy at a sufficiently high temperature for a long enough to achieve nearly homogeneous solid solution. To do this the samples are placed in a pre heated furnace at 530°C for 1 hour.

To achieve the T4 temper designation it then necessary for the sample to be quenched. This is an important stage in the precipitation hardening process as by rapidly cooling to a lower temperature, approximately room temperature, the solid solution is preserved. This is achieved by quenching the samples in a cold water bath. This process increases the hardness and the strength of the material.

3.3.4.3 Precipitation Heat Treatment¹¹⁶

After solution treatment and quenching, hardening is achieved either at room temperature (natural aging) or with precipitation heat treatment (artificial aging). The precipitation heat treatment can be used to improve many properties but often at the risk of reducing another property. For example, if you raise the strength of the material, the corrosion resistance may decrease. For this reason it is very important to consider the temperature and duration of the precipitation heat treatment of the sample. Sample 2 is going to be heated in the furnace at 160°C for 18 hours. This will achieve a T6 temper which is a commonly used temper designation for engineering applications.

3.3.5 Micro Hardness Testing

As the hardness of AA6061 varies with temper it is possible to use this to test if the heat treatments are carried out correctly.

After processing all the samples are mounted in resin. The cutting direction was perpendicular to the bent line. The laser processed area of the samples was kept in the centre of the strips with the lateral sides approximately 10 mm in length each. The hot mounting process took about 15 minutes for each sample and the operation temperature was approximately 150°C.

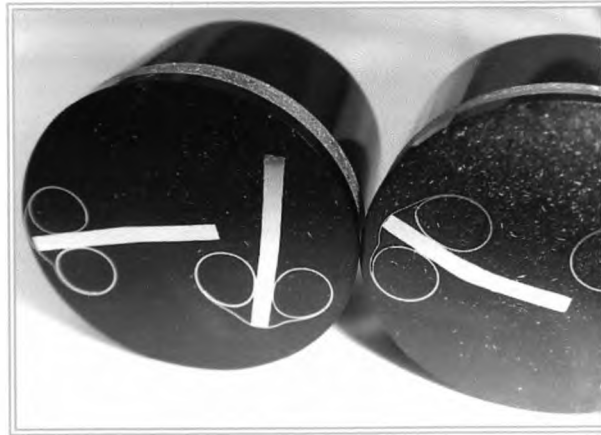


Figure 3.3.3: Picture of cut sections in resin.

The samples are cut through a cross section of the bend and mounted in resin (figure 3.3.3). This allows the hardness to be taken within the sample and across the bend. The hardness is measured at the top and the bottom of the bend along the whole sample (figure 3.3.4).



Figure 3.3.4: Locations for the hardness test

The micro hardness tester measures hardness in Vickers hardness. A mass of 100g is used for a time of 15 seconds. The indentations were measured using the microscope, to an accuracy of $0.1\mu\text{m}$.

3.4 Geometry Based Predictive/Adaptive Model for 3D Forming

2D laser forming has been around for many years. Because of this the advancements in 2D forming have been considerable and it is currently possible to control bend angle in various materials, including aerospace alloys, with reasonably accurate results. The next step is to investigate 3D laser forming. To advance this process, it is necessary to develop a method to predict irradiation strategies for various 3D surfaces. This also gives rise to a means of distortion correction.

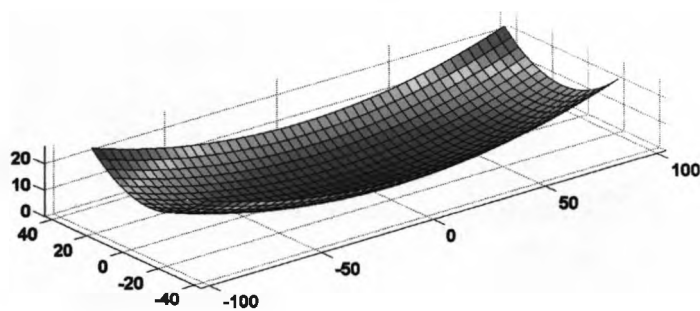


Figure 3.4.1: Matlab output showing a Bezier surface patch for a pillow shape

It was concluded from earlier empirical studies⁷⁶ that, in order to develop control of the process of 3D laser forming, it was necessary to have the ability to define the surface to be formed. In addition, by defining the surface and analysing properties such as gradient and curvature, it was thought this may lead to a method of scan strategy prediction. A related study to this investigation¹¹⁷, based of the controlled 3D laser forming of a pillow or dome shape, concluded that scan strategies based on contours of constant height of a surface using the temperature gradient mechanism (TGM)¹⁰ can produce successful results. The desired shape, the pillow shape in this case, was defined by a Bezier surface patch (figure 3.4.1) in Matlab. This mathematical function allows the definition of a continuous 3D surface from only a limited number of supplied coordinates for the surface, the rest of the data then being interpolated over a given range.

3.4.1 Geometry Based Predictive/ Adaptive Model:

Basic Procedure

There are two geometry-based models discussed in this thesis. The following procedure is the same for both the original and modified models (figure 3.4.2). Additional procedure relating to individual models is outlined in sections 3.4.2 and 3.4.3.

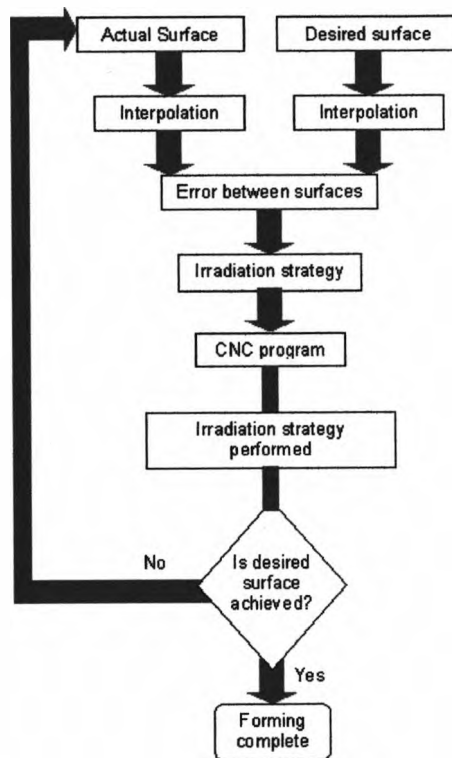


Figure 3.4.2: A Basic flow chart of the Geometry Based Predictive/ Adaptive Model

3.4.1.1 Defining the Desired Surface

The first step is to define the surface which is desired. This is done in Matlab using a minimal number of points. In this case 9 points for a part-cylinder, saddle or pillow and 16 points for the more complex cowling shape (figure 3.4.3), the values at these points correspond to the height of the desired surface with a maximum value of 1. The maximum value is 1, so the desired height can be adjusted easily. These points are interpolated in Matlab to gain a full smooth surface of the necessary number of points; these are chosen manually, across the required surface area (figure 3.4.4).

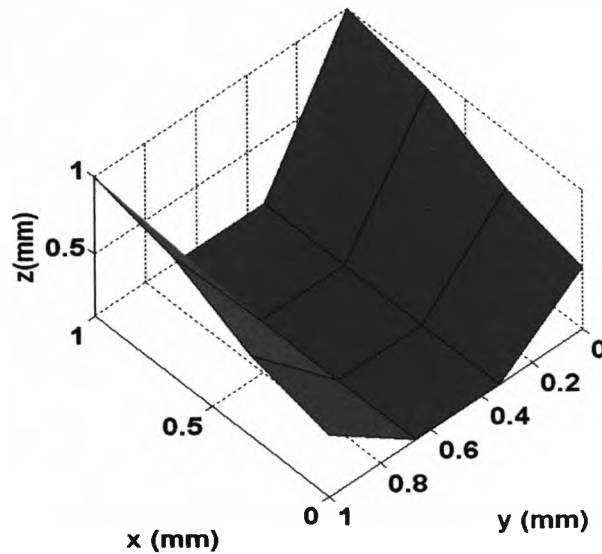


Figure 3.4.3: 16 points used to define the desired surface

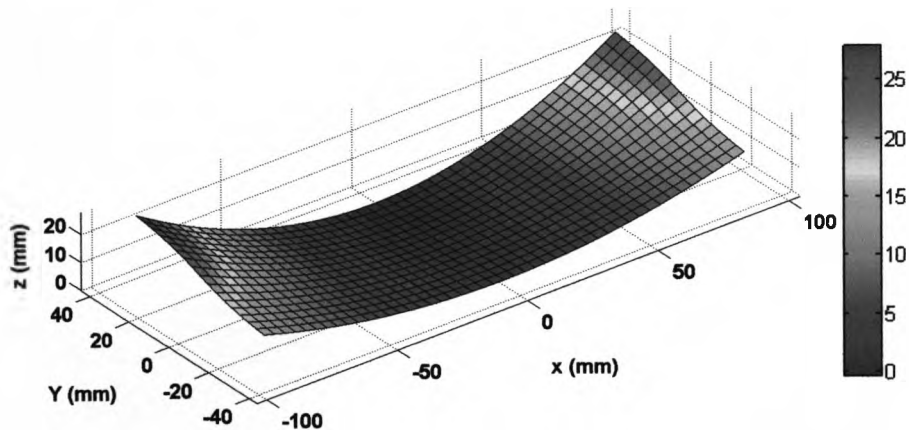


Figure 3.4.4: Interpolated points for desired surface

3.4.1.2 Defining the Actual Surface

The actual surface is measured using the CMM, described earlier. The measurements from the CMM are placed in an excel file so they can be normalised. This involves finding a value for the point at the centre of the clamp where there is a bolt. This is done by finding the average of the

surrounding points. All the points are then subtracted by this value, zeroing the value at the centre and measuring all points in height from the centre (figure 3.4.5). As with the desired surface these points are interpolated to gain a full smooth surface of required points, this is the same number of points as for the desired surface (figure 3.4.6).

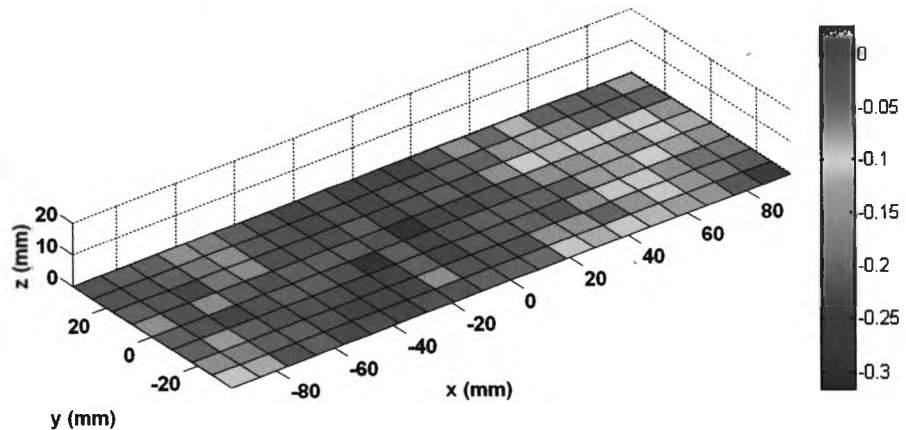


Figure 3.4.5: Measured points of the actual surface

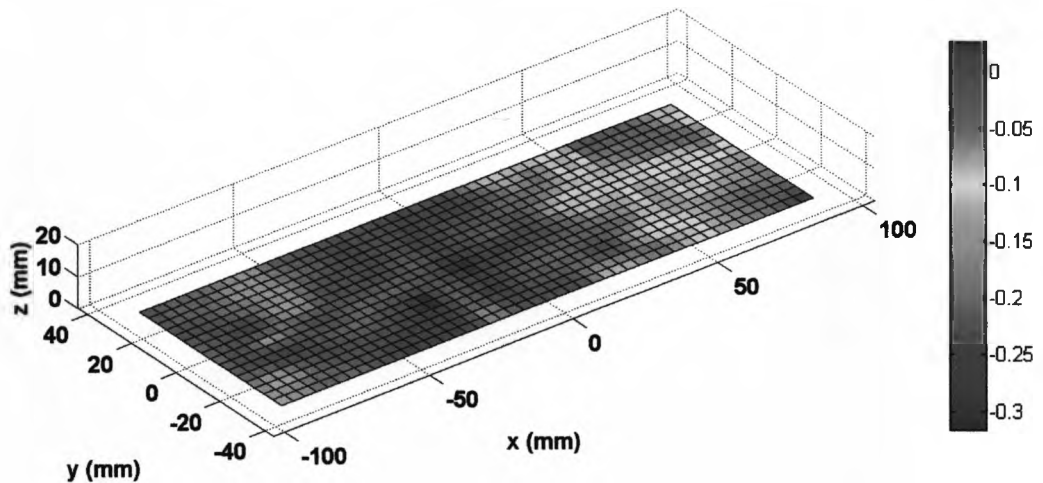


Figure 3.4.6: Interpolated points of actual surface

3.4.1.3 Error Calculation

All of the irradiation strategies are based on the error between the actual surface and the desired surface. This is a simple calculation where the interpolated measured heights of the actual surface are subtracted from the interpolated required heights of the desired surface. To do this, the matrix of the interpolated points from both surfaces are made to be equal in size.

3.4.1.4 Irradiation Strategy

The resulting matrix form of the error is then used to determine the irradiation strategy. The irradiation strategy is the path/pattern of the laser and the speed of the laser. The speed is used to control the amount of energy used in processing, this is in place of laser power which is difficult to control. Therefore in every case when using the model the laser power is constant throughout. The path is determined using two methods in this thesis, the lines of constant height method and the lines of constant gradient magnitude method. The laser speed is also determined differently in both these cases. This is explained further in the related sections. An example of the Matlab program which calculates the irradiation strategy is shown in appendix I.

3.4.1.5 Galil CNC Program

The Matlab program then writes two Galil CNC programs based on the irradiation strategy, a program for the front side path and the reverse side path. An example of this can be seen in Appendix II. This program controls the CNC tables and the laser shutter. The power is pre-determined and is constant throughout. These programs are uploaded to the Galil card using the Galil editor in the Jog controller user interface. The irradiation strategy can then be carried out. The work-piece is then measured and if the desired surface isn't achieved the whole process begins again. If the desired shape is achieved the process is finished.

3.4.2 Irradiation Strategy for the Original Model

Here the procedure is the same as the basic procedure with some added detail in determining the irradiation strategy. For this model the lines of constant height are used as an irradiation pattern and the minimum speed is calculated by the amount of strain required to produce the desired shape (figure 3.4.7).

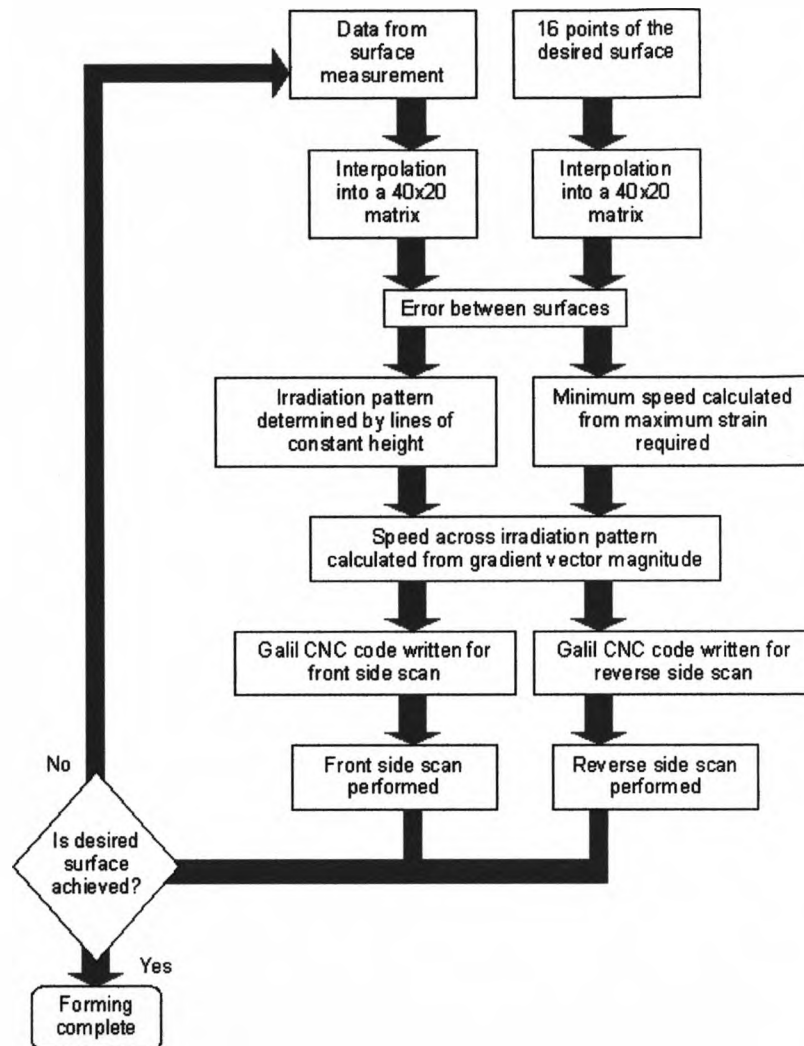


Figure 3.4.7: Flow chart for the original model

Figure 3.4.8 is an example of an irradiation strategy created by this method. The lines are relatively simple as they are the line of constant height. The dot colour refers to the side of the work-piece the irradiation lines should be placed on. The red dots indicate the reverse side scans and blue the front side scans. This is determined by the height, if the height is above the required height, the dot is red and if it is below the dot is blue. The size of the dots indicates the magnitude of the gradient and therefore the amount of forming required. This is used to distribute the laser speed

between the maximum speed, at the smallest dots and the calculated minimum speed for the largest dots. This is because the minimum speed produces the maximum amount of forming.

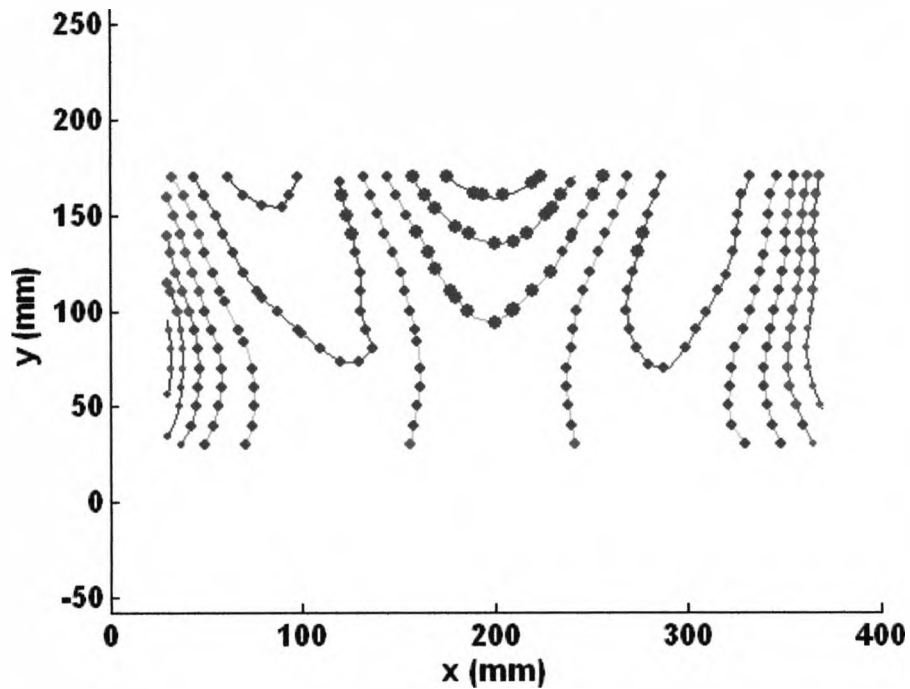


Figure 3.4.8: Example of irradiation strategy for first model

For calculating the speed, the first step is to select a speed range. The maximum speed is chosen to be just under the forming threshold to allow for fine adjusting. A minimum speed is selected just above the point where damage will be done to the surface. This allows for maximum amount of possible forming with no damage to the work-piece. A minimum speed is then calculated before each pass, using strain equations. If this is less than the pre-selected minimum speed, it is not used. An example of the speed range can be seen in figure 3.4.9. This calculation is discussed in more detail in the results and discussion chapter of this thesis.

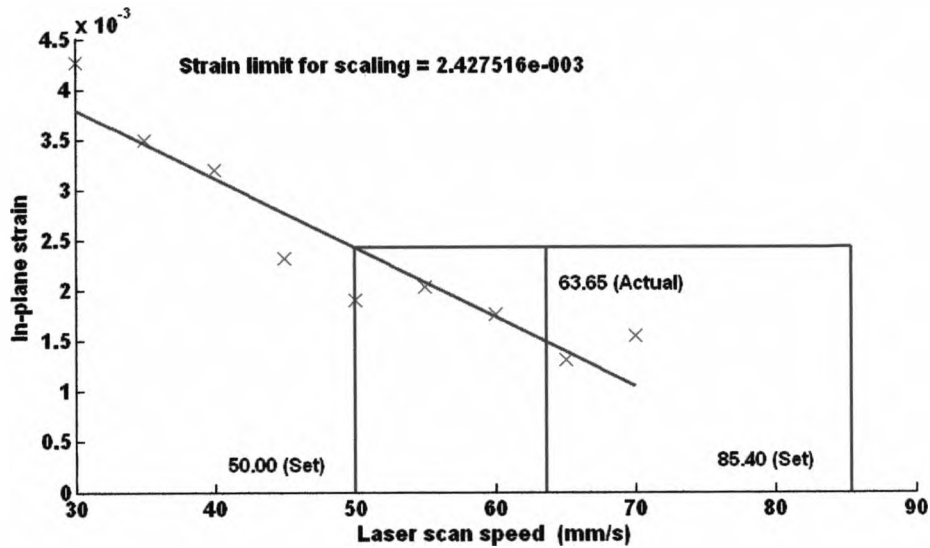


Figure 3.4.9: Example of speed range with calculated minimum speed (63.65mm/s) for first model

3.4.3 Irradiation Strategy for Modified Model

Again the procedure is the same as the basic procedure with some added detail in determining the irradiation strategy. For this model, the lines of constant gradient vector magnitude are used as an irradiation pattern and the speed is determined by the increment of the gradient between irradiation lines. Also included in this model is a subroutine which takes into account the decrease in the area viewable from above as the work-piece forms (figure 3.4.10).

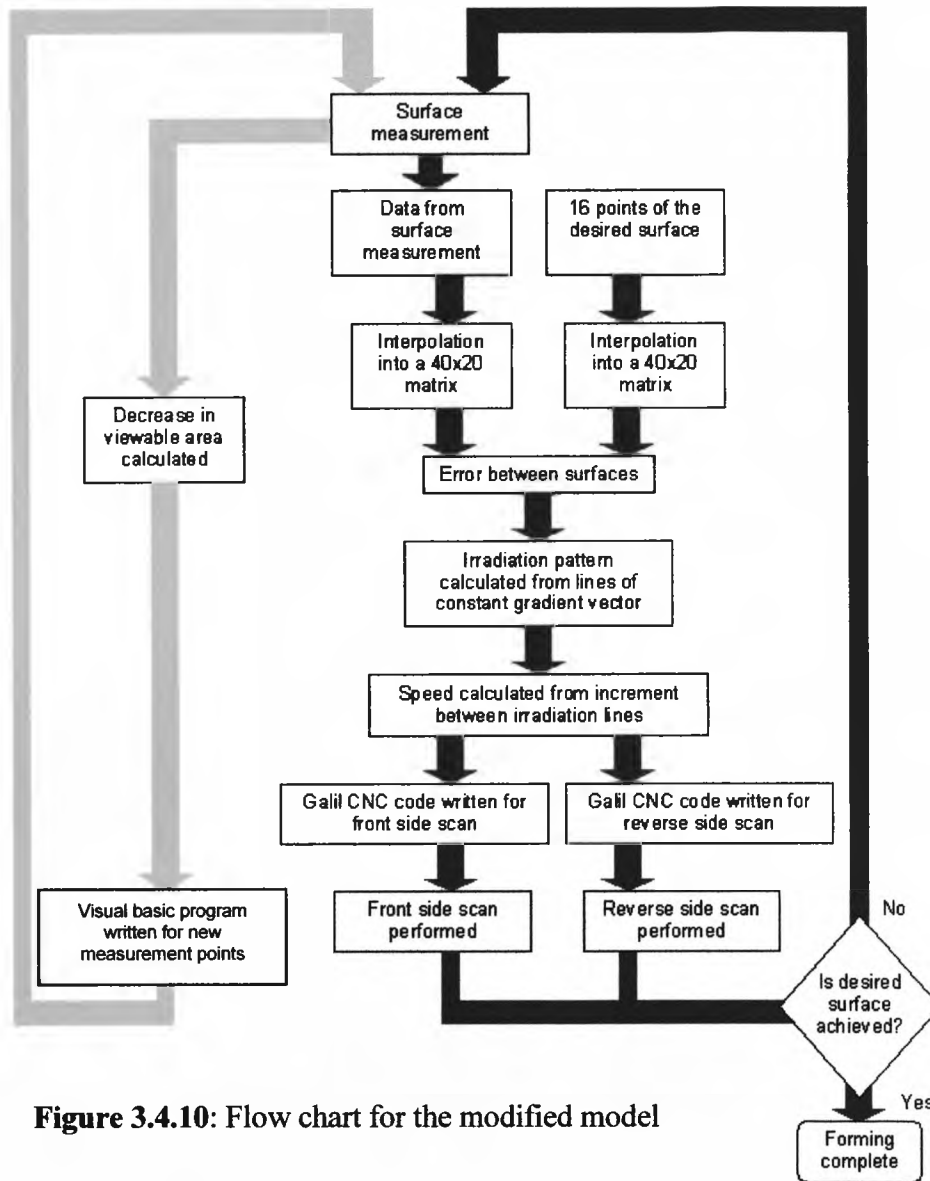


Figure 3.4.10: Flow chart for the modified model

Here the irradiation lines are based on the lines of constant gradient vector (figure 3.4.11). Again the colour of the dots indicates the scanned side, which is determined by the direction of the gradient. As in the original model the size of the dots indicates the speed required. However, this is determined in a different way to the original model. Here the speed is determined by the increment of the gradient between the irradiation lines. As the gradient is directly related to the angle the speed can be selected

from the results of 2D laser forming (figure 3.4.12). As the lines are a contour of the gradient, these are distributed evenly and therefore the speed is constant throughout the pass.

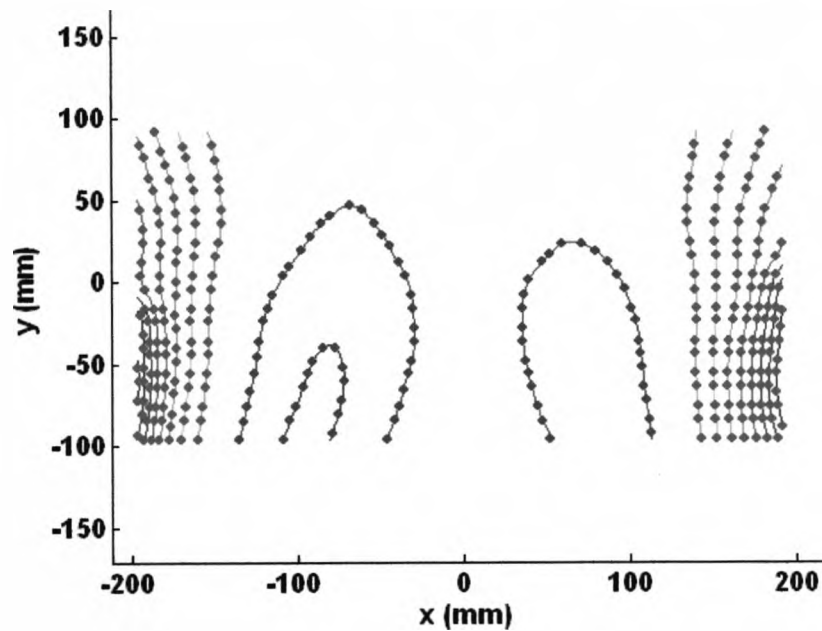


Figure 3.4.11: Example of irradiation strategy for modified model

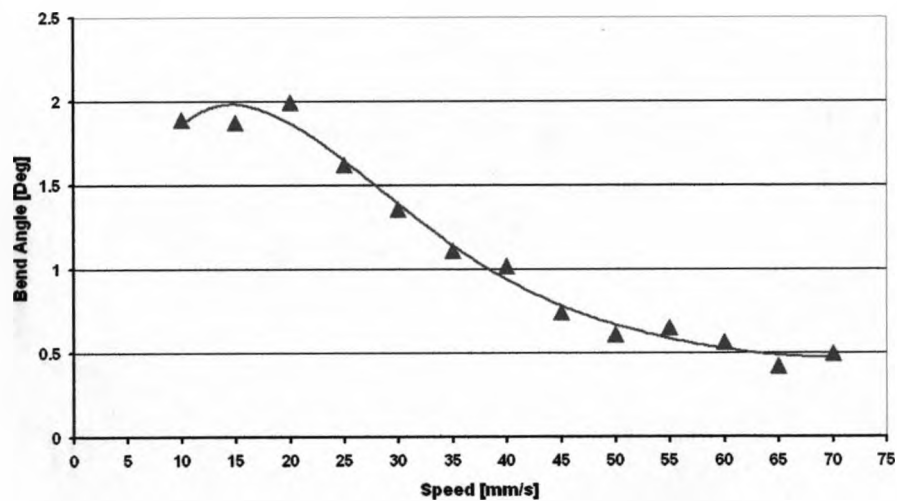


Figure 3.4.12: Example of the results of 2D forming used for speed calibration

Also included in this model is the method for taking into account the decrease in measured area which writes a Visual Basic program that is placed behind the 'Begin Scan' button on the modified CMM user interface to adjust the co-ordinates of the measured points accordingly. An example of this Visual Basic program is shown in appendix III. This calculates the decrease in the x and y direction of each element from the height data. Ideally this would be done after the laser pass and the calculated decrease in area would then be used to measure the surface again. This is not done as a measurement pass takes approximately 10 min, to save time the calculated decrease in viewable area is taken from the previous laser pass. This still has the advantage of allowing the measuring points to be placed close to the edge preventing the measuring points from missing the work-piece.

Chapter 4

2D Laser forming Results and Discussion

2D laser forming studies are looked at here as investigations in their own right and also as tools to help in the investigation of 3D forming.

In this chapter the influence of the change in beam geometry as a part forms is investigated. Here previously-investigated potential factors of multi-pass forming are discussed.

The effects of post laser forming heat treatments are also investigated in this chapter. As post-forming heat treatments are often carried out in the aerospace industry to relieve any residual stresses that may have been induced into the part from the forming process this may effect the possible application for the laser forming process.

4.1 Geometrical Influences on Multi-Pass Laser Forming

To date there has been a considerable amount of work carried out on two-dimensional laser forming, using multi-pass straight line scan strategies to produce a reasonably controlled bend angle in a number of materials, including aerospace alloys. A key area, however, where there is a limited understanding, is the variation in bend angle achieved per pass (or bend angle rate) during multi-pass laser forming along a single irradiation track (producing a positive bend), in particular the decrease in bend angle per pass after many irradiations for a given set of process parameters consistent with the TGM⁶. An example of this can be seen in figure 4.1.1, where data from the multi-pass 2D laser forming of a 1.5mm mild steel CR4 coupon is presented (CW CO₂ laser).

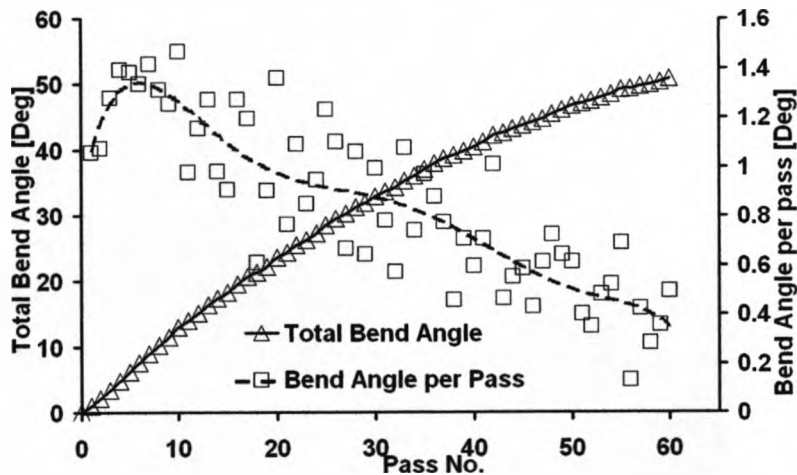


Figure 4.1.1: Example of the fall off in bend angle per pass during multi-pass TGM, laser forming over the same scan line using the same process parameters per pass. 1.5mm mild steel, 760W CW CO₂, 5.5mm beam diameter, 30mm/s, graphite coated.

It can be seen in figure 4.1.1 that as the number of passes increases over the same irradiation line the bend angle achieved per pass varies. The overall bend angle is shown on the left hand primary Y axis and the bend angle per pass is shown on the right hand secondary Y axis. It can be seen that after the first five passes the bend angle per pass falls consistently for subsequent passes.

Understanding of this variation in bend angle per pass is essential if the LF process is to be fully controlled for a manufacturing environment. The research presented here summarises the current theories as to why this occurs and proposes a further hypothesis based on the geometrical effects of the component deformation, which in turn influences the process parameters per pass. This hypothesis is confirmed through empirical analysis of the 2D laser forming process.

The material used here is 80x80 x1.5mm CR4 mild steel. This material is used due to its cost, availability and the fact that it is a common material found in virtually every manufacturing sector. This material was purchased with a bright surface finish and laser cut to the required dimensions from a local laser cutting job-shop. Having the material laser cut meant that any additional residual stresses due to cutting would be minimal as large residual stresses could influence the geometry of a formed part.

4.1.1 Summary of Known Influencing Factors

There are a number of theories identified in the literature to explain the variation in bend angle per pass during multi-pass LF using the TGM, these are:

- Strain hardening.
- Section thickening.
- Variation in absorption.
- Thermal effects.

4.1.1.1 Strain Hardening

Strain hardening has been cited by a number of researchers^{47, 97, 101} as a significant factor in the fall off of the bend angle per pass with increasing numbers of passes. The strain hardening phenomenon is attributed to the entanglement of dislocations. Plastic deformation in metals proceeds atomic step by atomic step by the generation and movement (by external force) of dislocations within the crystal lattice. During plastic deformation multiple dislocations created within the lattice interact during movement, as deformation continues the dislocation density increases and entanglement occurs. Further deformation is rendered more difficult by this entanglement and this manifests itself as an increase in hardness. Significant increases in hardness have been observed within the laser scanned region in a number of materials^{41, 97, 101}. Although surface

hardness does not give a direct measurement of the strain hardening phenomenon an indication of its value can be determined. If significant strain hardening occurs through the cross-section of the heated region over increasing number of passes, the bending strength of the section would increase, and hence the bend angle per pass would decrease.

4.1.1.2 Section Thickening

An increase in the section thickness of the heated scan line after laser forming has been reported in a number of studies^{6, 17, 45, 47, 95, 97, 98, 123}. This thickening effect has been observed to increase pass by pass when irradiating over the same scan line in multi-pass 2D LF. The effect is attributed to a conservation of volume, in that the lateral plastic compression in the upper surface consistent with the TGM during LF forces material upwards to some degree in order to conserve the volume. It is akin to pinching the upper surface along a line in order to create the bend. If the section is thicker then the material will be harder to bend due to the increase in the section modulus, or alternatively the moment generated about the section for a given set of energy parameters is less effective. This phenomenon has been shown to be confined to approximately the first 20 passes (dependent on process parameters)¹¹⁹.

4.1.1.3 Variation in Absorption

Key to the laser forming process is the coupling of a defocused low intensity (invariably infra red) laser beam into a (usually metallic)

surface. (Further discussion into absorption and absorptive coatings is given in chapter 3 of this thesis). A considerable amount of the research to date on LF has employed the use of CO₂ (10.6 μ m) and Nd:YAG (1.06 μ m) lasers with some high power diode laser work. At these wavelengths, especially 10.6 μ m, metals are highly reflective (~2% absorptance), for this reason absorptive coatings are usually used. Coatings such as graphite provide an interface for the incident laser radiation to be absorbed and then transferred to the metallic substrate, producing an overall efficiency of 60-80% depending on the substrate. As would be expected, variations in the absorptivity of the surface of a workpiece to be formed will affect the bend angle per pass as the coupled energy will vary also. Coatings such as graphite will be damaged and burnt off by repeated irradiations, thus pass by pass the coupled energy will decrease and hence the bend angle achieved after each pass will also decrease.

For laser wavelengths and material combinations (e.g. Nd:YAG and mild steel or Ti64) where coatings are not required, variations in absorption can still be present. Surface darkening effects (akin to laser marking) caused by multiple irradiations have been reported¹²⁰. These effects can lead to increased absorption which in turn can lead to excessive heating and surface damage for subsequent passes. For highly reactive surfaces the use of an inert shrouding gas has been shown to eliminate this effect¹²¹.

4.1.1.4 Thermal Effects

Thermal effects refer to the heat build up within a component after each pass influencing the subsequent passes. The heat retained in the part can have one of two effects:

1. Aid the process by reducing the temperature dependent properties of the material i.e. flow stress. The analogy being that a hot component is easier to form than a cold one.
2. Increase the bulk material temperature of the component such that the thermal gradient generated by each subsequent pass is reduced (when employing TGM conditions) and hence the bend angle realised is reduced.

These points have been illustrated by thermocouple and numerical analysis of the multi-pass laser forming process^{119, 122-124}. It has been shown that the peak temperature achieved within the scan line increases pass by pass if there is insufficient dwell time between passes to allow complete re-cooling of the component. This is consistent with the first point that the heat retained in the part is aiding the process. It was also shown that that the temperature increase for each pass is approximately the same but this is built on the increased bulk material temperature. This additional temperature increase for subsequent passes is akin to forming with higher power and hence more forming should be possible. Reducing the inter-pass delay can enhance this effect and has been proven to be

useful for the forming of thick section materials, a so called ‘double pass’ technique⁴⁷.

The bulk material temperature increase with increasing number of passes observed in previous work^{47, 119, 122-124} (figure 4.1.2) may potentially have a detrimental effect on the thermal gradient generated which is balanced against the potential benefit outlined above. This would be the case if the bulk material temperature continued to rise indefinitely; however by acquiring thermocouple data for several more passes it was possible to eliminate this effect¹¹⁹. It was observed that although the bulk temperature increased for the first few passes, for the subsequent passes, up to approximately 10, equilibrium was reached. This means that the potential beneficial and detrimental thermal effects on the bend angle per pass are confined to the first few passes or so. The beneficial effects may be responsible for the initial increase in bend angle per pass observed in figure 4.1.1 over the first few passes, where the steadily increasing peak temperature realised along the scan line produces an increased bend angle.

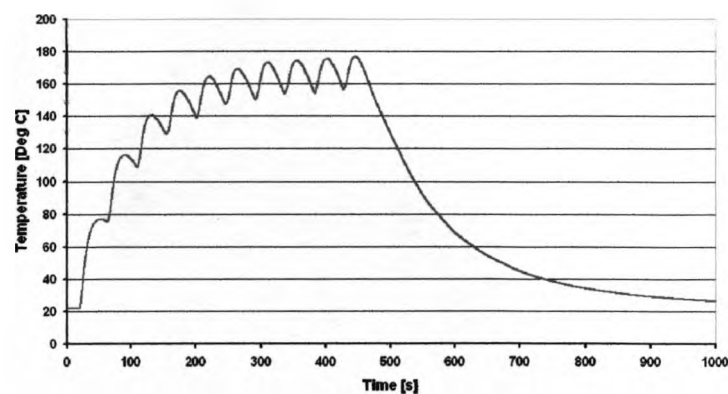


Figure 4.1.2: Thermocouple output, 8mm beam dia. 20mm/s, 760W, 10 passes, 40 second intervals⁴⁷

4.1.2 Edge Clamp Condition

The previous sections have outlined a number of factors that influence variations in bend angle development during multi-pass 2D LF using the TGM. An additional factor is proposed here based on the geometrical effects of the component deformation influencing the process parameters. It was observed that when laser forming a component using an edge or cantilever clamping arrangement (figure 4.1.3) the incident beam geometry is influenced by the existing bend in the sample. More accurately only half of the beam geometry is influenced. As the sample bends pass by pass the portion of the beam incident on the bending leg of the sample becomes increasingly elliptical. This can be illustrated by the intersection of a cylinder with an inclined plane as shown in the CAD drawing in figure 4.1.4.

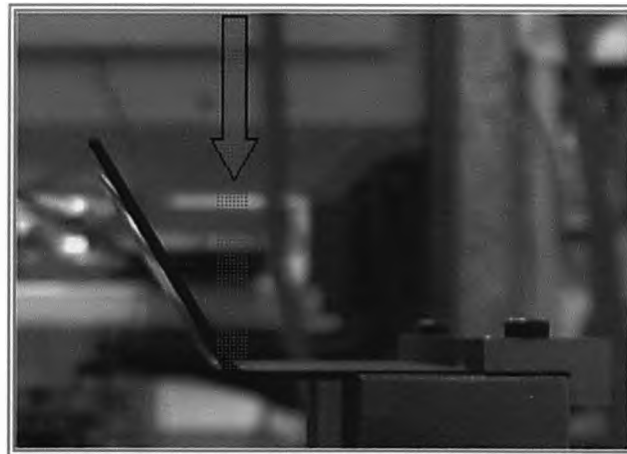


Figure 4.1.3: Cantilever clamping/ Edge Clamp

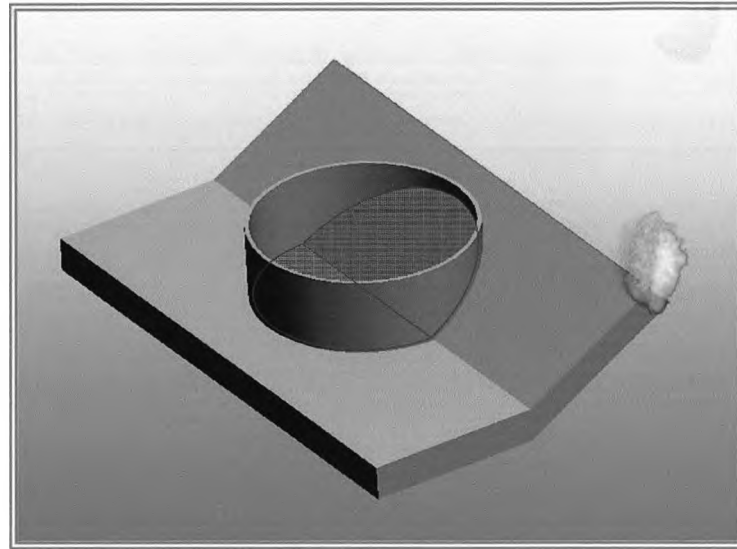


Figure 4.1.4: Illustration of the intersected incident beam area for an already bent sample

4.1.2.1 Area Calculations

It can be seen in figure 4.1.4 that the incident beam area on the sample as the sample bends becomes a combination of a half circle and a half ellipse, with the ellipse becoming more distorted pass by pass. It was thought that this would constitute an effective increase in the incident beam area on the sample and hence a reduction in the power density and energy fluence (power density times the interaction time), this may in turn influence the bend angle achieved per pass. In order to confirm this, the bend angle dependent incident beam area had to be found. A schematic of the incident beam geometry is given in figure 4.1.5; where D_I is the beam diameter, R_I is the beam radius, R_2 is the distorted beam radius (elliptical) and α_b is the bend angle.

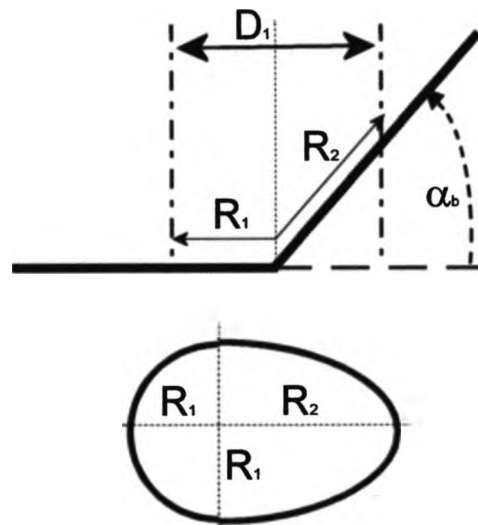


Figure 4.1.5: Schematic of the incident beam geometry for the cantilever clamping condition

The distorted beam radius R_2 is given by:

$$R_2 = \frac{R_1}{\cos \alpha_b} \quad (4.1.1)$$

The total incident beam area, A , is given by:

$$A_1 = \frac{\pi R_1^2}{2} + \frac{\pi R_1 R_2}{2} \quad (4.1.2)$$

Substituting for R_2 and rearranging gives:

$$A_1 = \frac{\pi R_1^2}{2} \left(1 + \frac{1}{\cos \alpha_b} \right) \quad (4.1.3)$$

4.1.2.2 Calculated Effects

Calculating the incident beam area for a range of bend angles from 0-90° for a tested set of parameters yields the effect of a pre-existing bend angle on the process parameters (figure 4.1.6).

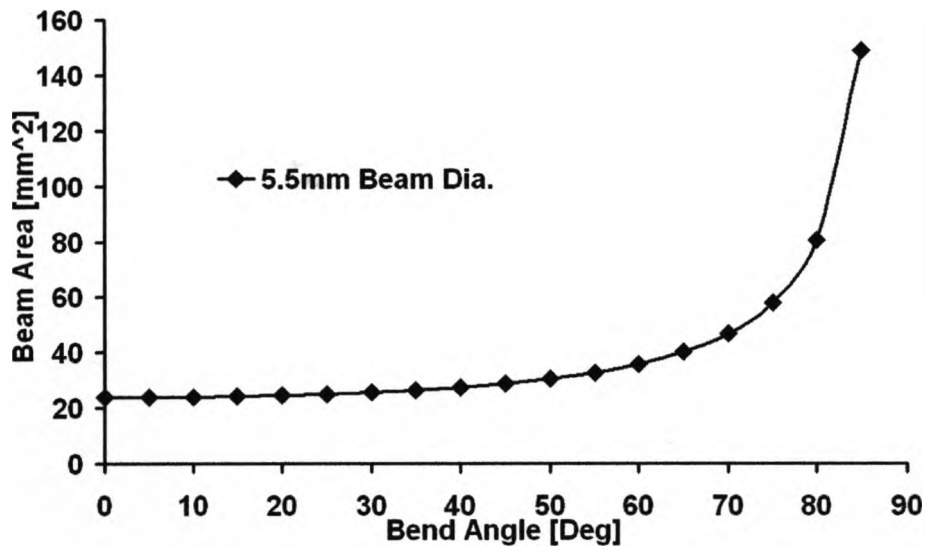


Figure 4.1.6: Effect of bend angle on the incident beam area for a cantilever clamping condition. 5.5mm beam diameter

It can be seen in figure 4.1.6 that as the bend angle increases the total incident beam area also increases as half of the beam is distorted up the bending leg of the component. The beam area increases significantly at higher bend angles, increasing exponentially approaching 90°. It is possible to determine the effect of the increasing beam area on the energy fluence (figure 4.1.7).

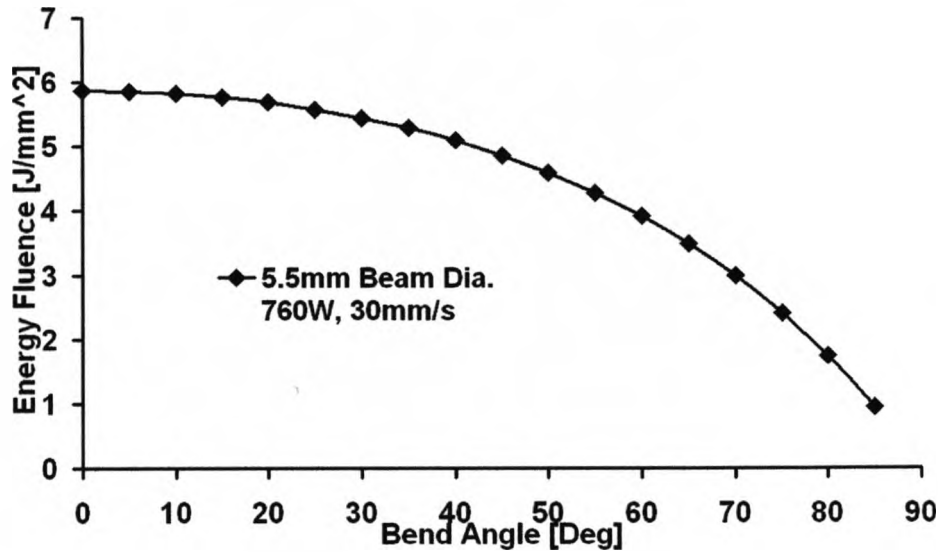


Figure 4.1.7: Incident energy fluence with increasing bend angle for a cantilever clamping condition. 5.5mm beam diameter, 760W,

4.1.2.3 Empirical Confirmation

It can be seen in figure 4.1.7 that the incident energy fluence falls consistently as the bend angle increases for this clamping condition. This significant fall in energy fluence will have an effect on the bend angle per pass, specifically at higher number of passes. An empirical method of confirming this theory was devised. A series of experiments was performed using the same processing conditions as above but with various beam diameters. This was to demonstrate the effect of an increasing beam area, with constant line energy, on the multi-pass LF process. For the same power and process speed (760W and 30mm/s) beam diameters in the range 5.5–8mm were employed to laser form 1.5mm mild steel CR4 samples up to 30 passes. Only a single constant beam diameter for each sample was used and the total bend angle per pass was recorded. This data is presented in figure 4.1.8.

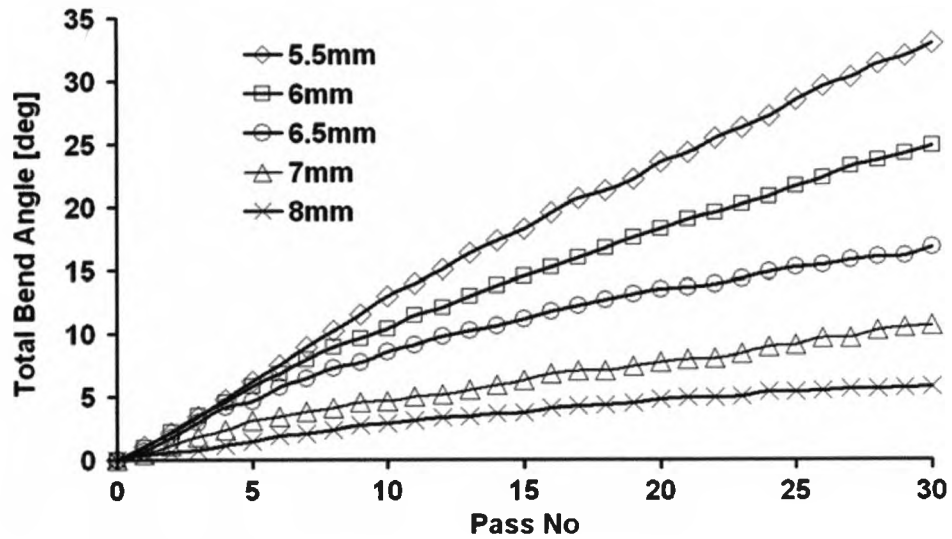


Figure 4.1.8: Bend angle development for a given beam diameter at a constant line energy, 1.5mm mild steel, 760W CW CO₂, 30mm/s

It can be seen in figure 4.1.8 that as the beam diameter is increased the total bend angle achieved after 30 passes falls considerably; this is consistent with other work in this area¹²⁵. This can be further illustrated by analysing the bend angle achieved per pass for a given beam diameter; this is shown in figure 4.1.9. It can be seen that the bend angle achieved per pass falls with an increasing beam diameter and hence beam area, thus demonstrating that the bend angle per pass is influenced by the beam area. It can also be seen that the bend angle per pass varies according to the pass number, the data being sampled at figure 4.1.9. This is consistent with the previously discussed bend angle fall-off phenomenon observed earlier with the increasing number of passes (figure 4.1.1). It is likely that the fall-off recorded here is not significantly due to the proposed geometrical factor as a potentially detrimental increase in incident beam area does not occur until higher bend angles (figure 4.1.6).

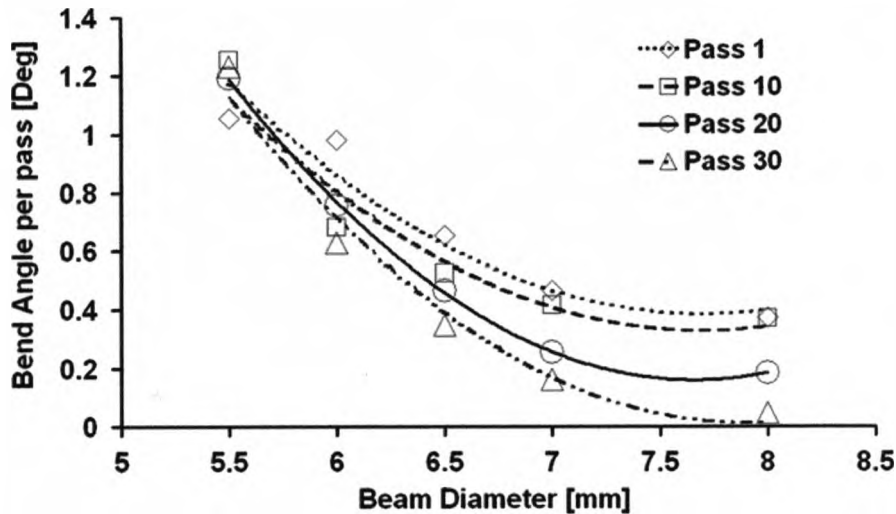


Figure 4.1.9: Variation in bend angle per pass with increasing incident beam diameter. 1.5mm mild steel, 760W, 30mm/s.

Unfortunately the conditions of these verification experiments are not the same as in the original experiment. Although the processing parameters, line energy, beam area etc are the same, the geometry of the incident beam is not. In the original experiment the beam is distorted and becomes more elliptical on one half only with an increasing bend angle; the other side remains semi-circular. Thus the beam diameter does not vary in the traverse direction but only perpendicular to it and only on the bending leg side. In the experiment in figures 4.1.8 and 4.1.9 the beam diameter is increased uniformly for each run giving an increase in incident beam area; however, as the beam diameter increases in the traverse direction as well, the interaction time is therefore different from the original experiment and thus the energy fluence realised is different. This can be illustrated by calculating the effective beam diameter (assuming a circular beam) for a given beam area (from equation 4.1.3) and thus calculating the energy fluence for this condition; this is shown in figure 4.1.10. It can

be seen that the fall-off due to the proposed geometrical factor (part-elliptical beam) with increasing bend angle is slightly greater than the effect of an increasing beam diameter. It was thought, however, that as a similar decreasing trend was produced and only an indication of the influence of the geometrical factor was required, a model could be developed based on this data to predict the bend angle development for a given existing bend angle.

By taking the average of the data in figure 4.1.9 it is possible to obtain a relationship between the bend angle per pass and the beam diameter. Because the maximum bend angle in these experiments is below 35° the geometrical influence is minimal.

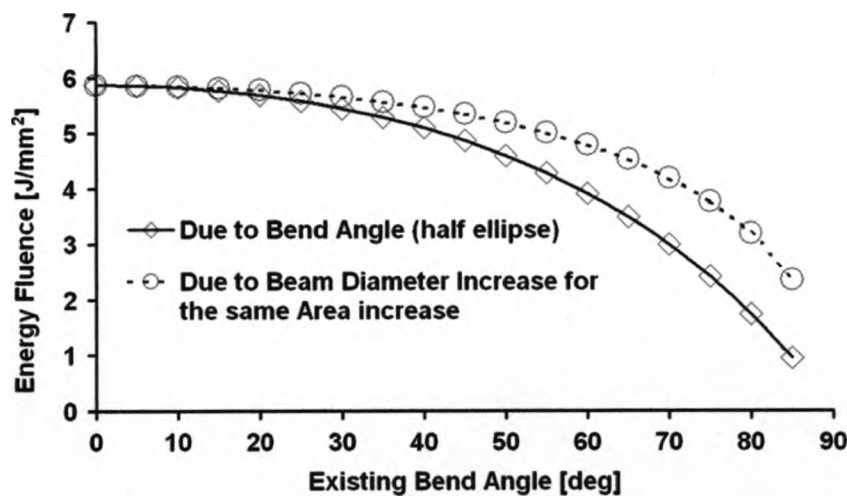


Figure 4.1.10: Energy fluence with increasing bend angle (from figure 4.1.7) and energy fluence with an increasing beam diameter equivalent to the same incident area increase.

This relationship can be converted into variation of bend angle per pass with increasing area of the beam ($A = \pi r^2$) (figure 4.1.11). As we know the area of the elliptical beam with the increase in bend angle (equation

4.1.3) the relation between the bend angle per pass with increasing existing angle can be determined (figure 4.1.12).

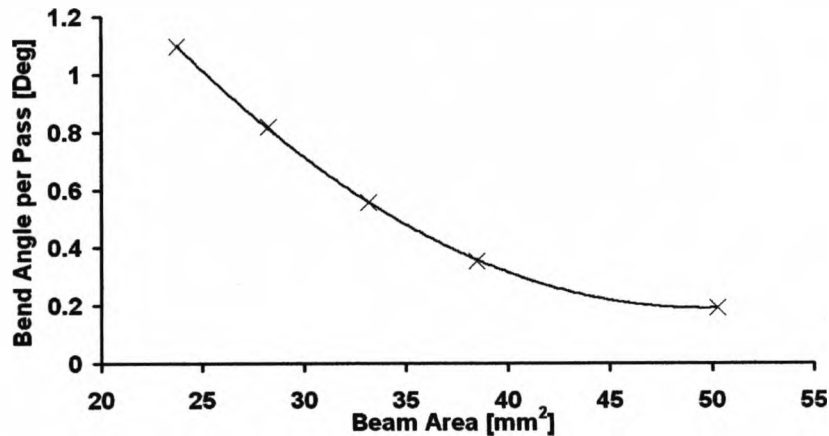


Figure 4.1.11: Average variation in bend angle per pass with increasing incident beam diameter. 1.5mm mild steel, 760W, 30mm/s

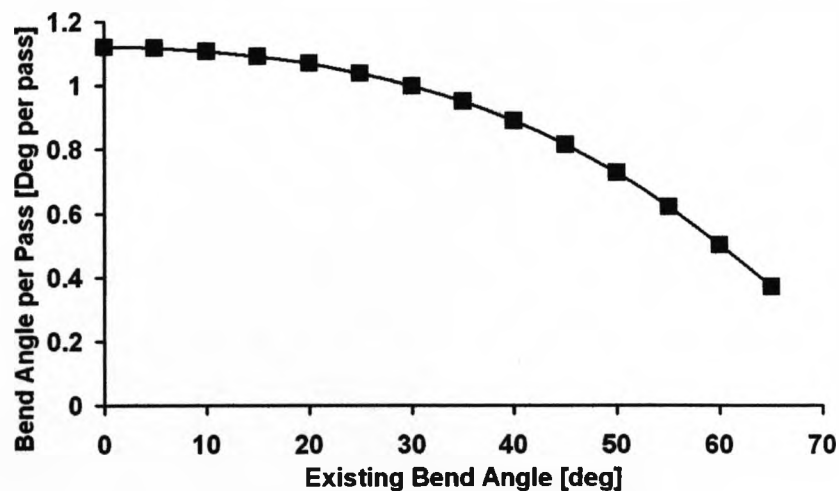


Figure 4.1.12: Bend angle per pass prediction with increasing existing bend angle. 1.5mm mild steel, 760W, 30mm/s, 5.5mm beam



The prediction based on this relationship is given in figure 4.1.13; the data was only calculated up to 60° as the experimental data was only available up to this angle (due to measurement limitations). Using this

relationship it is possible to generate a prediction of the total bend angle development with increasing number of passes taking into account the existing bend angle. This prediction is shown along with the experimental data from figure 4.1.1. It can be seen that there is a good agreement between the predicted and experimental trends demonstrating the significance of the geometrical factor. At higher bend angles, however, the predicted data diverges slightly and appears not to show as significant a fall-off as the experimental data; this could be attributed to the difference in energy fluence fall-off of the verification data mentioned earlier or the influence of other factors such as strain hardening that are unaccounted for in the model.

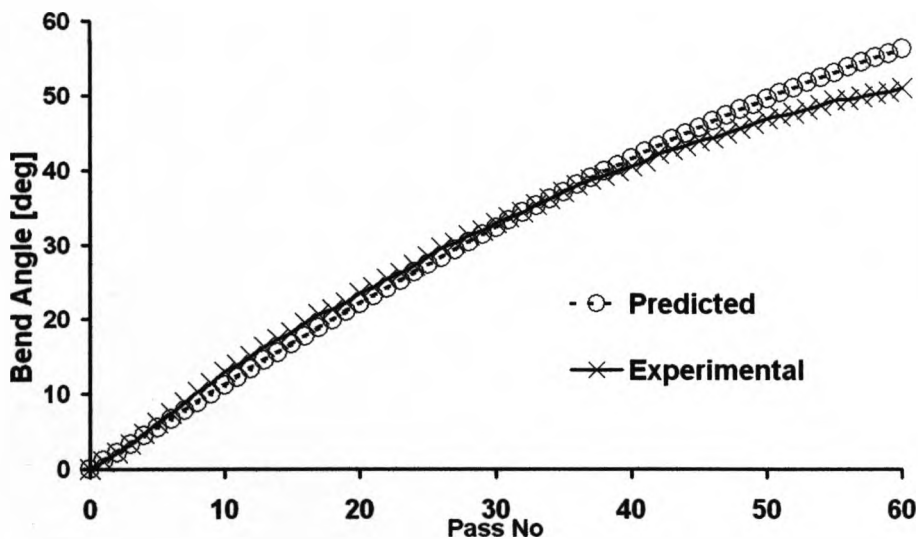


Figure 4.1.13: Predicted bend angle development due to increasing beam area with increasing bend angle and comparison with experimental results. 1.5mm mild steel, 760W, 30mm/s, 5.5mm beam diameter.

From the analytical and empirical data presented in this section it has been shown that the bend angle per pass, when LF employing a cantilever or edge clamp, is influenced by the formed bend angle. It has been shown that as the bend angle increases the incident laser beam geometry is distorted, resulting in an effective increase in the beam area and a reduction in the incident energy fluence. A prediction of the bend angle development based on this phenomenon has been shown to be close to experimental data in terms of the prediction of bend angle per pass fall-off. Thus this effect must be considered to be an influential factor in the bend angle per pass fall-off phenomenon

4.1.3 V-Block Condition

As the geometrical factor described in the previous section relies on the clamping arrangements employed, an alternative clamping arrangement was devised. By using a V block or simply supported arrangement, as seen in figure 4.1.14, it was thought that an even forming may be possible, eliminating the oblique angle of incidence of part of the laser beam at higher bend angles.



Figure 4.1.14: V-block or simply supported clamping arrangement.

For this arrangement the coupon is supported by four bolts and kept in place by sticky pads on top of the bolt heads and by the partial locating fence around the outside of the coupon. The bend angle can be verified using a laser range finder, taking height readings on the scan line and either side of it. This also allows for the implementation of automatic focus control, maintaining the same focal position per pass as the coupon deforms away from the laser. (These calculations and further detail on clamping arrangement is discussed in chapter 3.)

4.1.3.1 Area Calculations

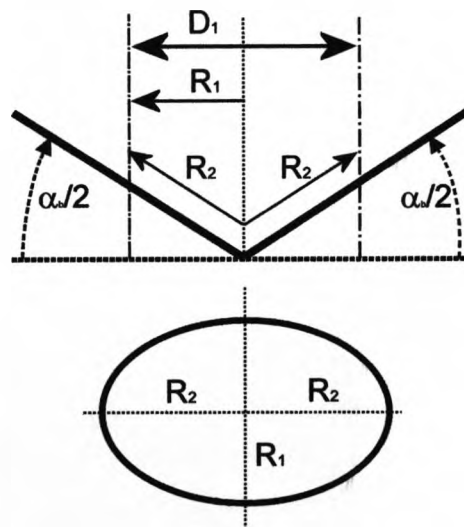


Figure 4.1.15: Schematic of the incident beam geometry for a V block or simply supported clamping arrangement.

As with the cantilever clamping condition it is possible to determine the effect of an increasing bend angle on the total incident beam area. Instead of half of the beam being distorted, both sides of the beam in this case become more elliptical as the bend angle (α_b) increases (figure 4.1.15).

The distorted beam radius R_2 is given by:

$$R_2 = \frac{R_1}{\cos(\alpha_b/2)} \quad (4.1.4)$$

The total bend angle dependent incident beam area, A , for the V block clamping condition is given by:

$$A_1 = \frac{\pi R_1 R_2}{2} + \frac{\pi R_1 R_2}{2} \quad (4.1.5)$$

Substituting for R_2 and rearranging gives:

$$A_1 = \frac{\pi R_1^2}{\cos(\alpha_b/2)} \quad (4.1.6)$$

4.1.3.2 Calculated Effects

Calculating the incident beam area for a range of bend angles from 0-90° for the same set of parameters used for the cantilever clamping condition yields the effect of a pre-existing bend angle on the process parameters for this boundary condition. This is shown in figure 4.1.16 (using the same scale as figure 4.1.6).

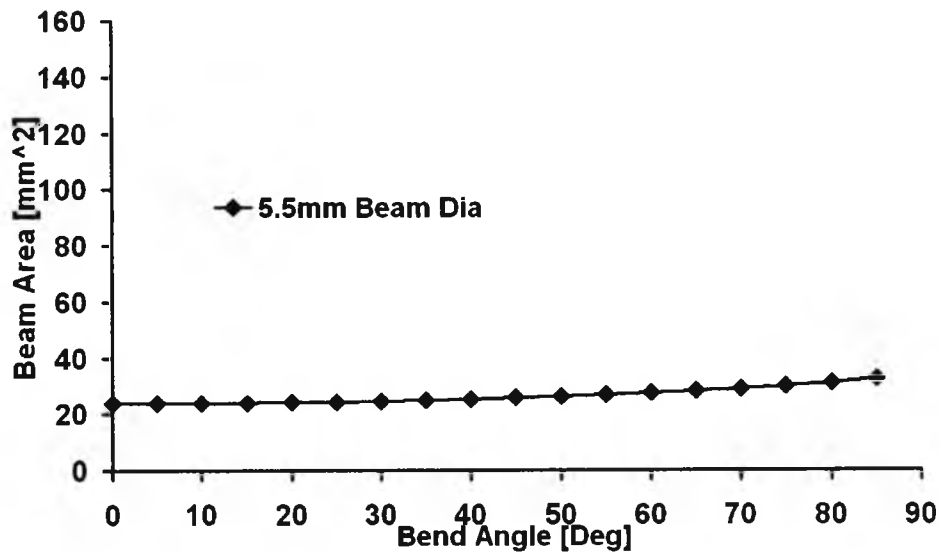


Figure 4.1.16: Effect of bend angle on the incident beam area for a V-block or simply supported clamping condition. 5.5mm beam diameter.

It can be seen in figure 4.1.16 that the incident beam area is not as significantly affected by the increasing bend angle when compared to the cantilever clamping condition (figure 4.1.6). This is due to the dependence on only the half bend angle ($\alpha_b/2$); the effective incidence angle does not become as oblique in this clamping condition. This can be further emphasised by the incident energy fluence for an increasing bend angle (figure 4.1.17).

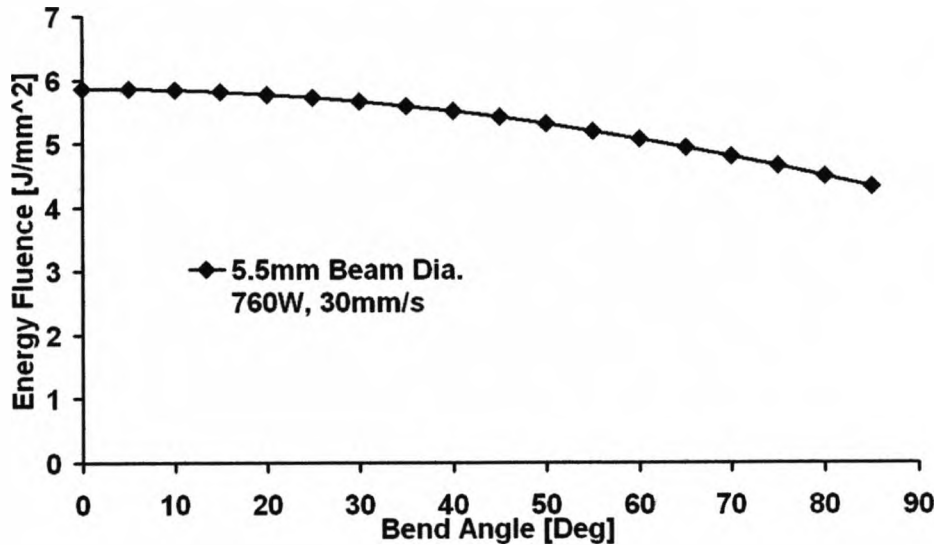


Figure 4.1.17: Incident energy fluence with increasing bend angle for a V-block or simply supported clamping condition. 5.5mm beam diameter, 760W, 30mm/s.

It can be seen in figure 4.1.17 that while there is some fall off in energy fluence with increasing bend angle, this is not as significant as the cantilever condition (figure 4.1.7) for higher bend angles. This presents an opportunity to test this bend angle dependence phenomenon by comparing experimental data for the two clamping conditions. Bend angle output for 60 passes for each of the two clamping conditions using the same energy parameters is given in figure 4.1.18.

4.1.3.3 Empirical Confirmation and Comparison

It can be seen in figure 4.1.18 that there are differences between the two clamping conditions in the bend angle development over the 60 passes recorded. It can be seen that the bend angle development per pass is virtually identical for 15 passes with some fall off in the bend angle per

pass for both clamping conditions (due to the factors discussed earlier); as the process parameters are the same this can perhaps be expected. After this point there is more forming produced by the V block clamping condition. From 25 passes onwards, in figure 4.1.18, an interesting effect can be noted. The edge clamp or cantilever data shows a consistent fall off in the bend angle per pass; this is illustrated by the straight dotted line from the 25 pass point. The V block data after an initial fall off up to 25 passes exhibits little or no fall off in the bend angle per pass for the remaining 35 passes, illustrated again by the straight dotted line. This appears to confirm the significance of the geometrical effect of the component distortion influencing the process parameters i.e. energy fluence. By eliminating or reducing this effect by changing the clamping conditions it has been possible to reduce the bend angle fall off per pass significantly.

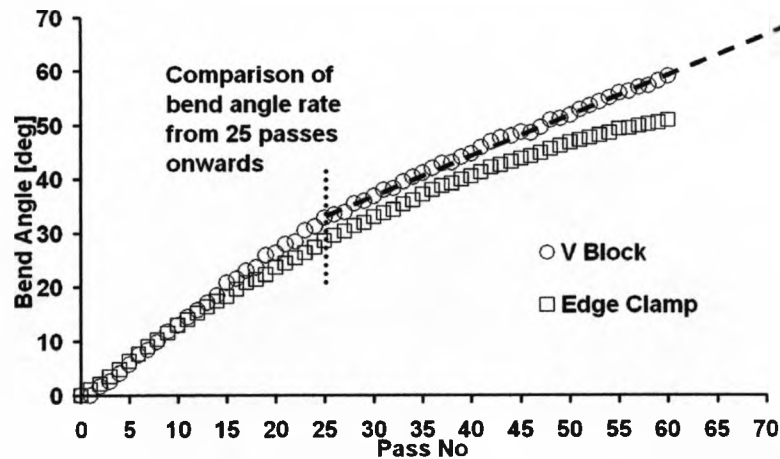


Figure 4.1.18: Comparison of the experimental bend angle development for the two clamping conditions, edge clamp and V block. 1.5mm mild steel, 760W CW CO₂, 30mm/s, 5.5mm beam diameter, graphite coated.

This has occurred to such an extent that it calls into question just how influential the other factors described earlier are on the bend angle per pass, in particular for higher bend angles. It is certain that the bend angle dependent geometrical effects described in this work are not the only influencing factors on the bend angle per pass. As described earlier there are a number of factors identified that are influencing the bend angle development at any one time, each of these factors are likely to be more dominant than the others at different stages in the multi-pass process. Further work in this area is required to confirm the significance of each of the factors and at which point in a bend angle development during multi-pass 2D laser forming each factor is dominant.

4.1.4 Possible Effects of the Influencing Factors on the Laser Forming of 3D Components

An incremental approach is used in this thesis for the laser forming of 3D components. This requires an irradiation pattern to be produced for each pass which consist of many lines. The surface is then measured and another irradiation pattern is determined. Because of the multiple pass nature of this process the influencing factors applicable to 2D multi-pass laser forming can also be applied to 3D forming, though with a variation in the effect.

For strain hardening, section thickening and variation in absorption there is likely to be an effect on 3D laser forming but with a decreased effect initially. Because these factors are limited to localised areas they will

have a larger effect on multi-pass 2D laser forming than on 3D laser forming. This is because the irradiation pattern rarely follows the same path in the 3D case, as the process here is adaptive. However the irradiation lines can interact with irradiation lines from previous passes, this could result in non-uniformity in the amount of forming experienced from a pass. With an increase number of passes this interaction is more likely to occur and therefore these effects become less localised and may begin to affect the piece as a whole, resulting in a decrease in forming throughout and possibly becoming a major factor.

Thermal effects are applicable for the 3D case here, although with a subtle distinction. For the case of 2D laser forming the base temperature of the part increases per pass until equilibrium is reached and the base temperature is stable throughout the process no longer changing the effects it has on the amount of forming. This is dependent on the time allowed between passes for the part to cool. For the case of 3D forming this dwell is a few minutes allowing the part to cool completely. However with a number of irradiation lines across the work-piece for this case the thermal effects can occur during a pass. As each line of the irradiation pattern is passed the temperature of the part will increase. As there is very little time between each line being passed the build up of heat in the whole piece will be much more than for the 2D case, though the localised heating will be reduced as the lines do not pass over each other. This could affect the amount of forming throughout a single pass. This will affect every pass, unlike 2D laser forming where the temperature reaches equilibrium, because for this case the part cools completely after each pass. Another effect of this could be that an increase in temperature of the whole piece may increase the amount of absorptive coating that is burnt off.

The effects of geometrical influences on the work-piece are increased for the 3D laser forming case. For the first pass this is not an affect, which is the same for the 2D case. However with 3D laser forming the greater the distance away from where the piece is clamped the greater the incident angle of the laser beam. For this case the whole beam profile is increased, decreasing the energy fluence. This is a larger effect than the 2D case for the edge clamp where half the beam is affected. This can result in a decrease in forming at the edges in 3D forming.

Because of the cumulative effect of all the influencing factors, apart from the thermal effect, it would be advantageous to the 3D laser forming process to form the work-piece in as few passes as possible. However the method for doing this would be to increase the energy into the system increasing the possibility of thermal effects. Further investigation is needed to find if there is a limit the amount of 3D laser forming possible in a single pass due to this effect.

4.2 Effects of Post Forming Heat Treatments on Laser Formed Components

A great deal of work has been carried out in laser forming although little investigation has been carried out into the effects of post forming heat treatments on laser formed parts. Post forming heat treatments are often carried out in the aerospace industry to relieve any residual stresses that may have been induced into the part from the forming process. Another possibility is that post forming heat treatments can strengthen the part after forming has been performed in the 'soft' annealed state. Due to the mechanism of laser forming it is important to know if it is susceptible to unwanted deformation after experiencing these heat treatments.

This investigation is carried out on AA6061 as it is heat treatable and has 3 temper settings which will allow the alloy to go through various differing heat treatments. Aluminium alloy AA6061 is a commonly used heat treatable alloy and has many applications due to its high strength, corrosion resistance and ability to be welded.

This investigation takes three 2D laser formed samples, measures the heights across the surface and then heat treats them.

The first heat treatment, which all the samples undergo, is full annealing. This will relax any residual stresses in the samples and give them a '0'

temper which is the softest most ductile form of AA6061 possible. The samples heights are then measured again.

The next heat treatment is solution heat treatment and quenching. This is performed on two of the samples. The sample is heated to a high temperature and then cooled rapidly in a cold water bath. Again the samples are measured after this process. This strengthens the samples achieving a T4 temper.

The final heat treatment is precipitation hardening, which will only be performed on one of the samples. This is a long heating process at a much lower temperature than the previous treatments and artificially ages the sample. This strengthens the sample further achieving a T6 temper.

The next step is to perform micro hardness tests on each sample to ensure that the Temper states have been attained.

Aluminium alloy 6061 is one of the most widely used heat treatable alloys and also one of the most versatile. It's easily welded and is often used for medium to high strength applications. With excellent resistance to atmospheric conditions and good resistance to sea water AA 6061 can be found in applications from bicycle frames to aircraft components.

Listed in table 3.3.1 are the typical mechanical properties of AA 6061 in its most common tempers. These tempers are the ones used in this investigation. Included are the hardness values used to verify that these tempers have been achieved. As the original values are in Brinell hardness (HB) they have been converted using conversion tables to Vickers hardness (HV), which are the units used by the micro hardness tester.

4.2.1 Laser Forming

Three samples were laser formed using different parameters shown in table 4.2.1. All of the samples were formed with the direction of the pass alternating each time; this is to help prevent the build up of stresses on one side of the sample. The choice of parameters used is taken from previous work within the group⁴⁷. The part is then positioned on the clamp using double sided adhesive tape to keep it in place; this is to align the part to allow it to be measured.

As sample 2 has the least energy input out of the 3 samples it is considered the most susceptible to the effects of heat treatment and is therefore the main focus of this investigation. The lower heat input into sample 2 can be seen with an only just visible witness line in comparison with sample 1 (figure 4.2.2). Because of this sample 2 will experience all three heat treatment stages.

	Sample 1	Sample 2	Sample 3
Power at surface (W)	500	500	500
Beam diameter (mm)	3	3	3
Beam velocity (mm/s)	55	55	45
Number of passes	20	5	5
Number of passes before re-coating of graphite spray.	10	n/a	n/a

Table 4.2.1: Laser forming parameters of the individual samples

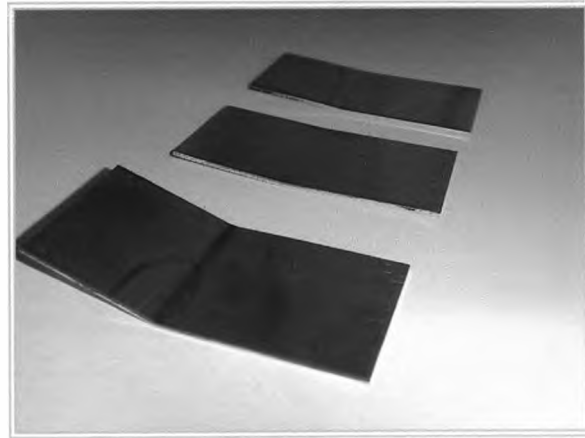


Figure 4.2.1: Samples 1, 2 and 3 after laser forming

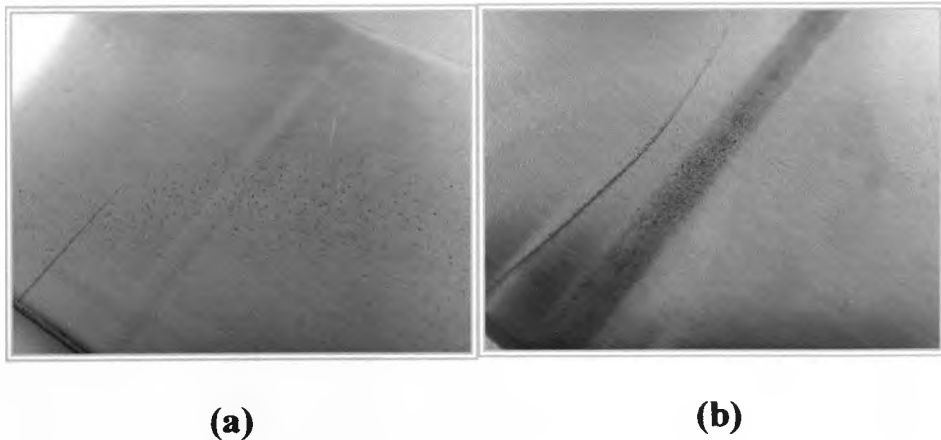


Figure 4.2.2: a) Irradiation line on sample 2, b) Irradiation line on sample 1

Here the 2D laser forming is not perfectly two dimensional. This is not apparent initially as the distortion and the edges effects are tenths of a

millimetre or tenths of a degree in magnitude. Table 4.2.2, shows the variation in angles across the samples.

In figures 4.2.3a, 4.2.4a and 4.2.5a it is possible to see some of the distortion, with figures 4.2.3b, 4.2.4b and 4.2.5b showing the full extent of the distortion with the use of a much smaller scale. The edge effect here can be attributed to the heat build up at the end of the irradiation line and shrinkage along the irradiation line⁴³.

<i>Sample</i>	<i>Angle at Position (°)</i>							<i>Average Angle (°)</i>
	5 mm	10 mm	15 mm	20 mm	25 mm	30 mm	35 mm	
1	17.66	17.61	17.38	17.46	17.47	17.74	17.95	17.61
2	4.75	4.62	4.49	4.36	4.42	4.64	4.71	4.57
3	4.77	4.76	4.58	4.43	4.5	4.64	4.87	4.65

Table 4.2.2: Resultant angles after laser forming

The greatest amount of distortion in all the pieces is on the side they are clamped. This is significantly more distortion than in the unclamped side. An explanation for this is the edge clamp arrangement contributing additional stresses by restricting any movement in the traverse direction of the sample at one end.

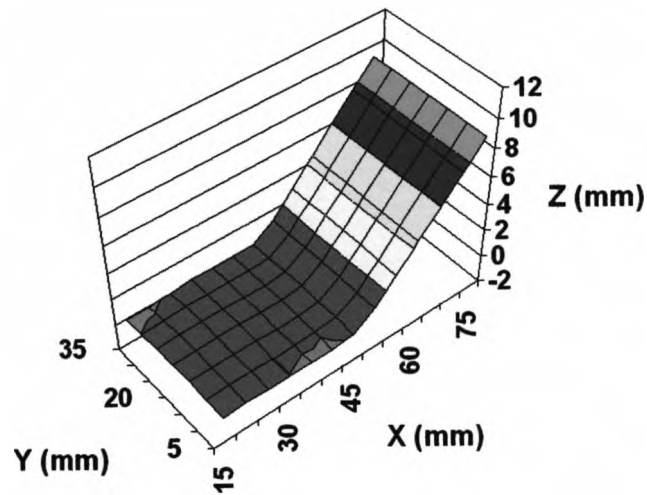


Figure 4.2.3a: Sample 1 surface measurement

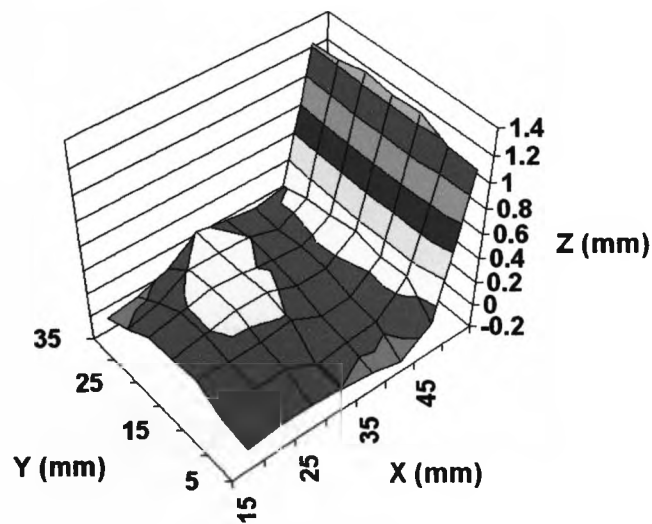


Figure 4.2.3b: Sample 1 surface measurement, Close-up of clamped side

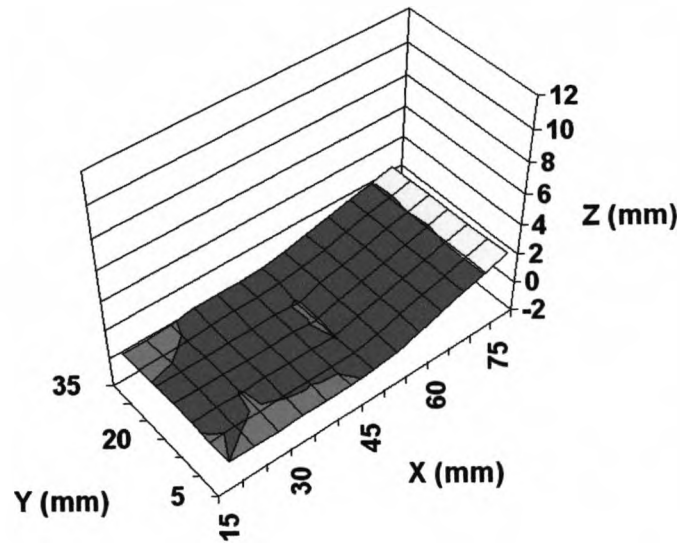


Figure 4.2.4a: Sample 2 surface measurement

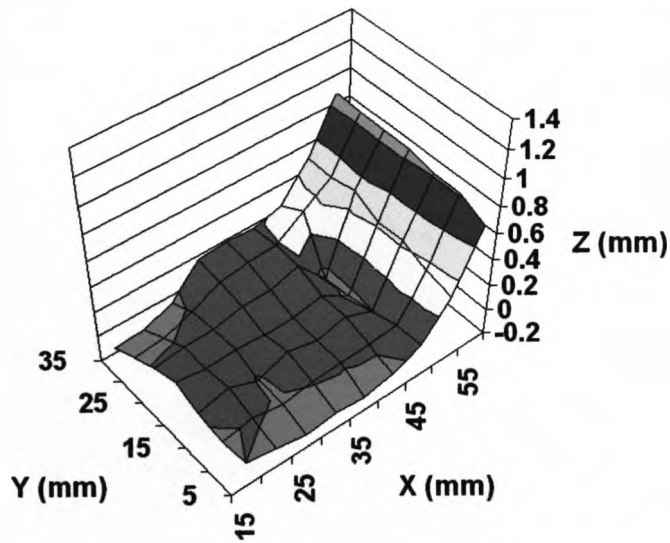


Figure 4.2.4b: Sample 2 surface measurement, close-up of clamped side

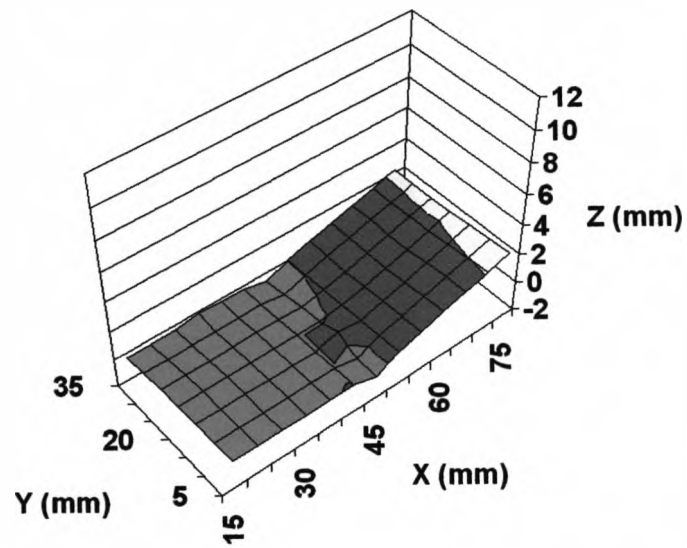


Figure 4.2.5a: Sample 3 surface measurement

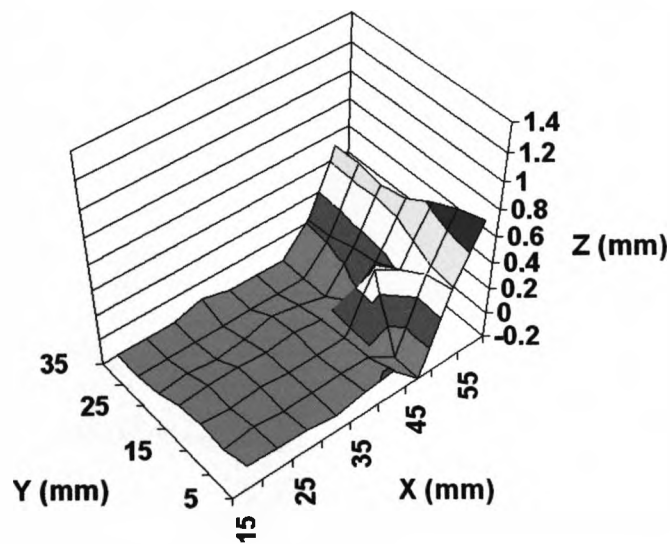


Figure 4.2.5b: Sample 3 surface measurement, close-up of clamped side

The bend angle is a quick way to see the results of laser forming and/or the effects of heat treatment in a sample. However, because of the distortion the bend angle does not give a full account as to what is happening in the sample. This is because to calculate the bend angle it only takes three points along the length of the sample. To have a better account of what is happening the height along the sample at 5mm, 20mm and 35mm across is used to create three lines on a graph (figure 4.2.6). To aid in the interpretation of the graphs each line has been normalised so the measured point closest to the clamp and the measured point at the irradiation line are zero. From these graphs (figures 4.2.7 - 4.2.10) it can be seen that there is distortion in the whole piece in every case. It should be noted that the clamped side has a much larger proportion of the distortion.

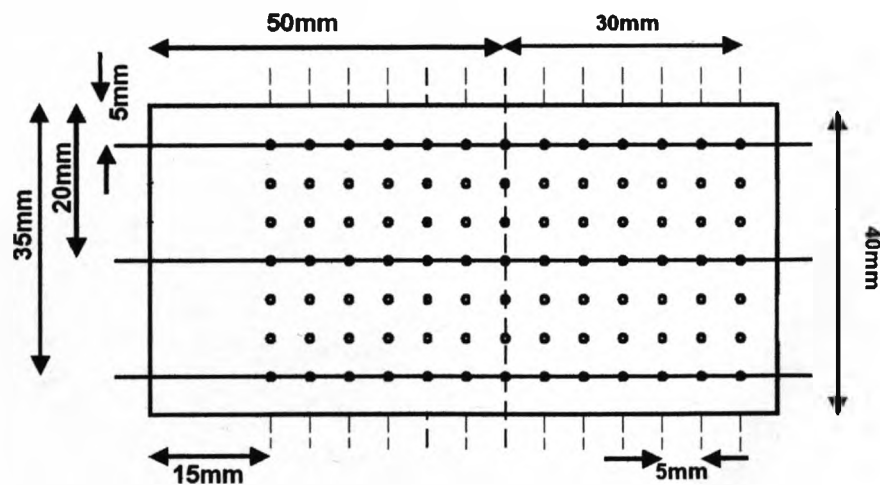


Figure 4.2.6: Position of the points measured on the surface. The dotted line at 50mm along the length is the bend/irradiation line and the lines at 5, 20 and 35mm are the lines along which the measurements are taken for the height along the length graphs.

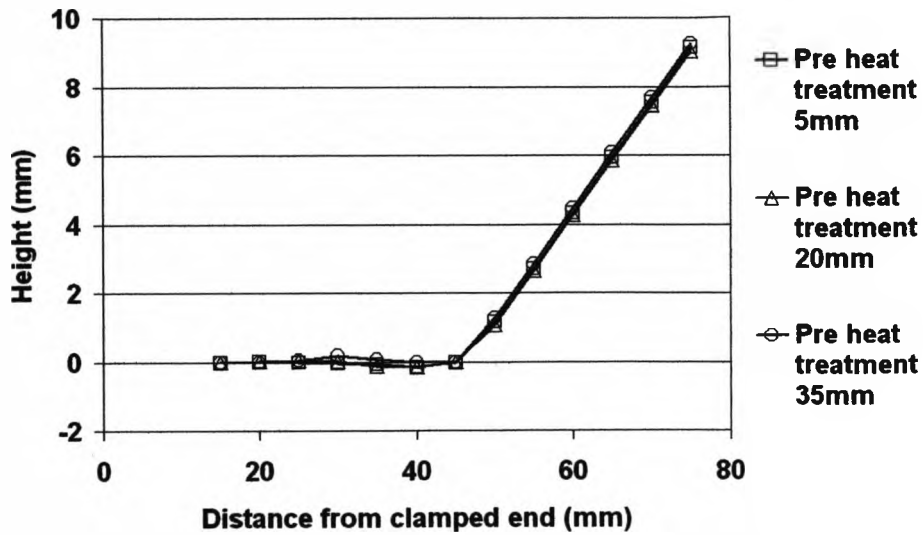


Figure 4.2.7: Height along length of sample 1 at 5, 20 and 35mm points across the width after laser forming and before heat treatment

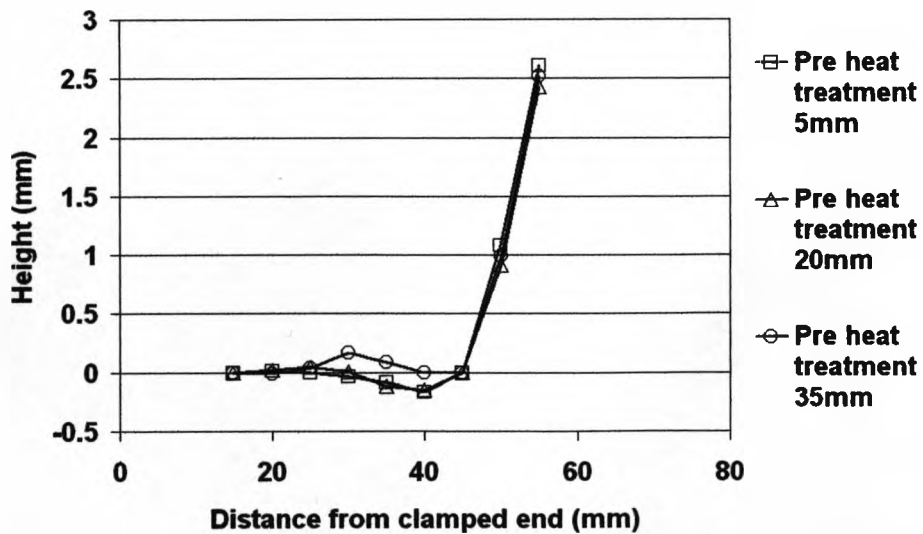


Figure 4.2.8: The height along length of sample 1 stopping at 55mm along the sample and at 5, 20 and 35mm points across width after laser forming and before heat treatment

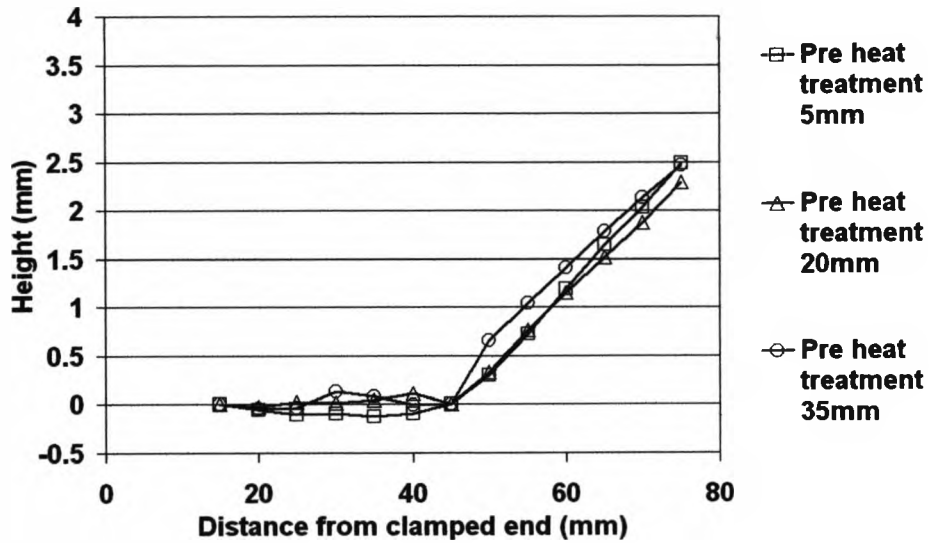


Figure 4.2.9: Height along length of sample 2 at 5, 20 and 35mm points across width after laser forming and before heat treatment

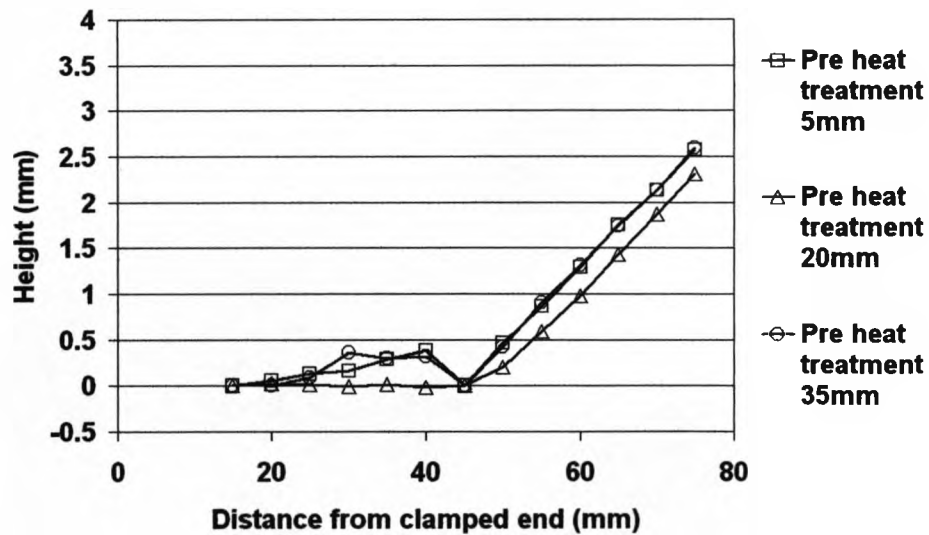


Figure 4.2.10: Height along length of sample 3 at 5, 20 and 35mm points across the width after laser forming and before heat treatment

It can be seen from these results that 2D laser forming isn't an exclusively 2D process. There is a small camber effect, which is expected in 2D forming as it is known that the irradiated area shrinks along its length as well as across it⁴³. A greater effect, which is less well documented, is the distortion in the clamped side caused by the restriction of the clamp.

Here the asymmetric nature of forming causes the side of the sample which is irradiated first to start bending before the rest of the piece, as seen in work on Ti-6Al-4V by M. Reeves *et al*¹²⁶. This causes the sample to exert forces onto the clamp resulting in stresses in the work piece, giving us the distortion seen here. This distortion doesn't appear to build up with the number of passes as sample 1, which had 20 passes on it, has a similar amount of distortion as sample 2, which had 5 passes. In sample 3 however, the distortion at the clamped side is larger which can be attributed to the added heat input per pass with the slower traverse speed experienced by this part.

4.2.2 Heat Treatments

4.2.2.1 Annealing

The softest and most workable condition is produced by annealing to the temper designation '0'. For this investigation all three samples are fully annealed. They are placed in a furnace and then heated to 415°C for three hours. To ensure the cooling rate doesn't exceed 30°C/h the furnace is turned off and the samples remain inside allowing them to cool with the oven. The cooling rate is vitally important to produce the maximum grain

size in the samples and achieve full annealing, therefore slow cooling is used. This also has the added advantage of minimising distortion. All three samples are then measured, using the same method as before, with the CMM using double sided adhesive tape to keep the sample in place on the clamp.

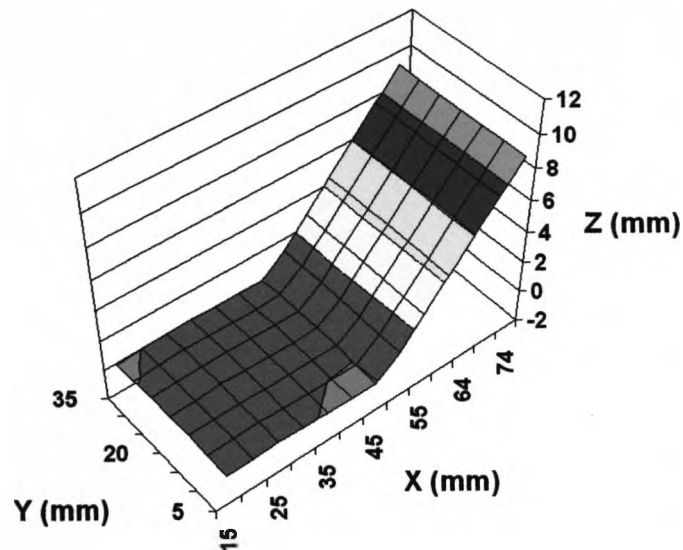


Figure 4.2.11a: Sample 1 surface measurement after annealing,

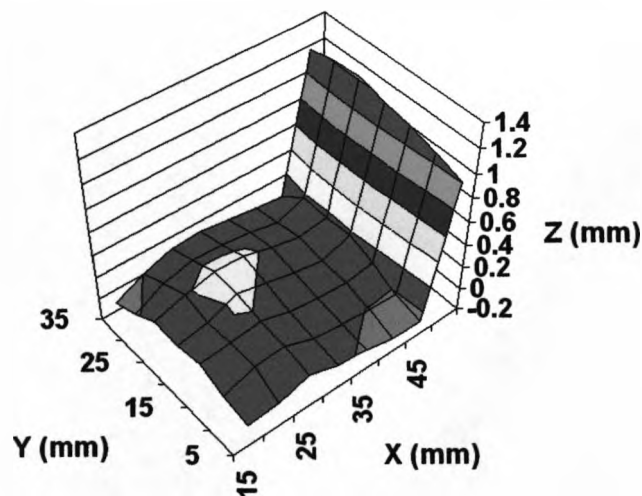


Figure 4.2.11b: Sample 1 surface measurement after annealing, close-up of clamped side

Position	5 mm	10 mm	15 mm	20 mm	25 mm	30 mm	35 mm	Average
Angle after annealing (°)	17.37	17.33	17.19	17.3	17.29	17.56	17.77	17.4
Difference between annealing and laser forming angle (°)	0.29	-0.27	-0.2	-0.16	-0.19	-0.18	-0.18	-0.21

Table 4.2.3: Resultant angles after annealing of sample 1

Position	5 mm	10 mm	15 mm	20 mm	25 mm	30 mm	35 mm	Average
Angle after annealing (°)	5.05	4.43	4.27	4.21	4.15	4.27	4.32	4.39
Difference between annealing and laser forming angle (°)	0.29	-0.19	-0.22	-0.15	-0.27	-0.37	-0.39	-0.19

Table 4.2.4: Resultant angles after annealing of sample 2

Position	5 mm	10 mm	15 mm	20 mm	25 mm	30 mm	35 mm	Average
Angle after annealing (°)	5.27	4.94	4.92	4.74	4.46	4.74	4.83	4.84
Difference between annealing and laser forming angle (°)	0.49	0.18	0.34	0.31	-0.05	0.1	-0.04	0.19

Table 4.2.5: Resultant angles after annealing of sample 3

The changes in the samples after annealing are at the same scale as the original distortion. The results from the bend angles across the samples show this change (tables 4.2.3 – 4.2.5). These changes in bend angle vary in magnitude and direction and never exceed 0.5° . The average change in bend angle for sample 1, 2 and 3 are -0.21° , -0.19° and 0.19° respectively. This suggests that the effects of annealing on the laser formed bend are minimal at worst, as there is no definitive change in bend angle.

A reason for the change in bend angle can be seen in figures 4.2.11 – 4.2.13. By taking a closer look at the surface measurements of the clamped end it can be seen that the distortion from the effects of laser forming are reduced. This is confirmed in figures 4.2.14 – 4.2.17 where this reduction in distortion can be seen more clearly

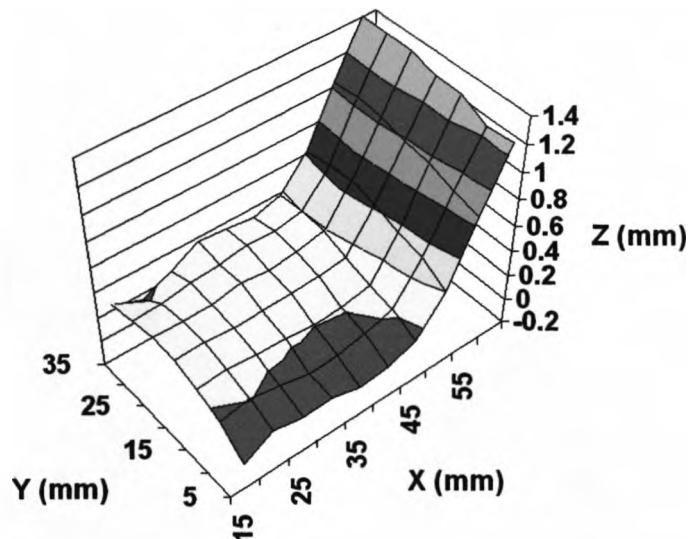


Figure 4.2.12: Sample 2 surface measurement after annealing, close-up of clamped end

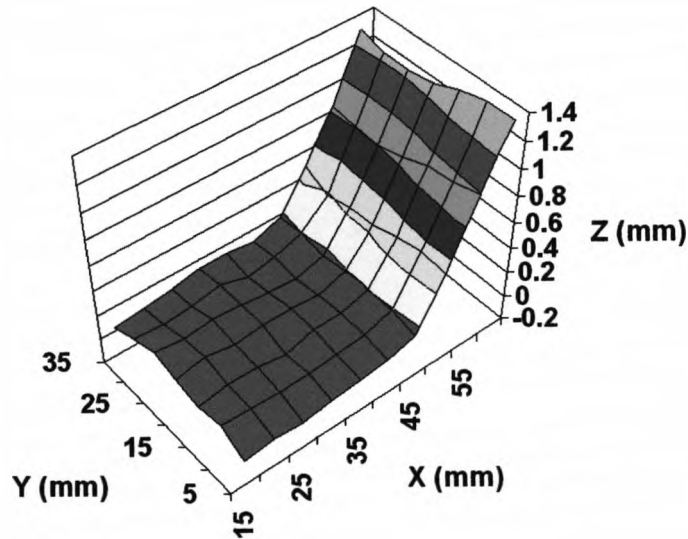


Figure 4.2.13: Sample 3 surface measurement after annealing, close-up of clamped end

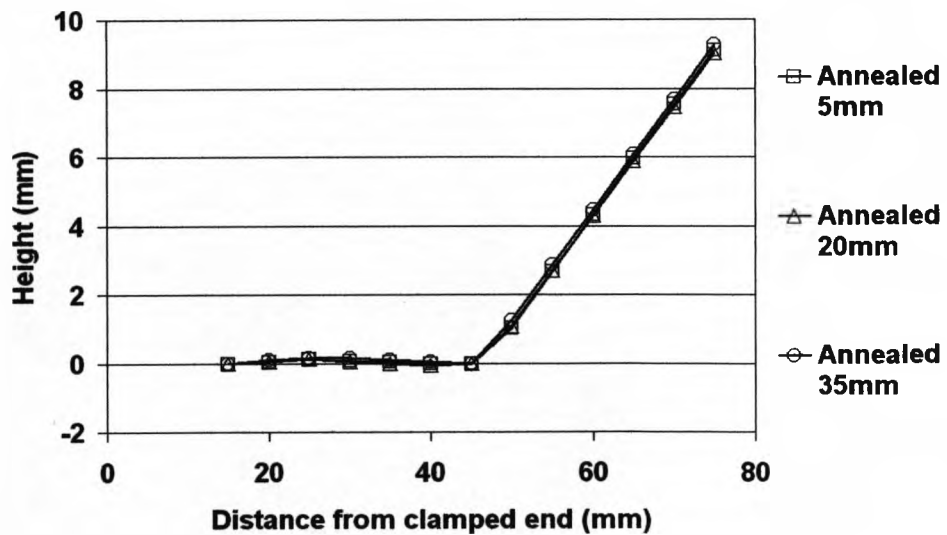


Figure 4.2.14: Height along length of sample 1 at 5, 20 and 35mm points across the width after annealing

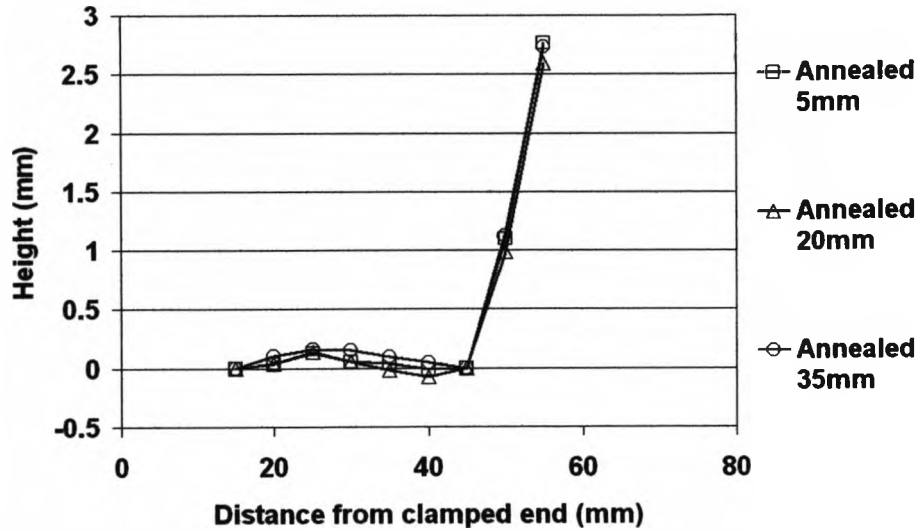


Figure 4.2.15: The height along length of sample 1 stopping at 55mm along the sample and at 5, 20 and 35mm points across width after laser forming and before heat treatment

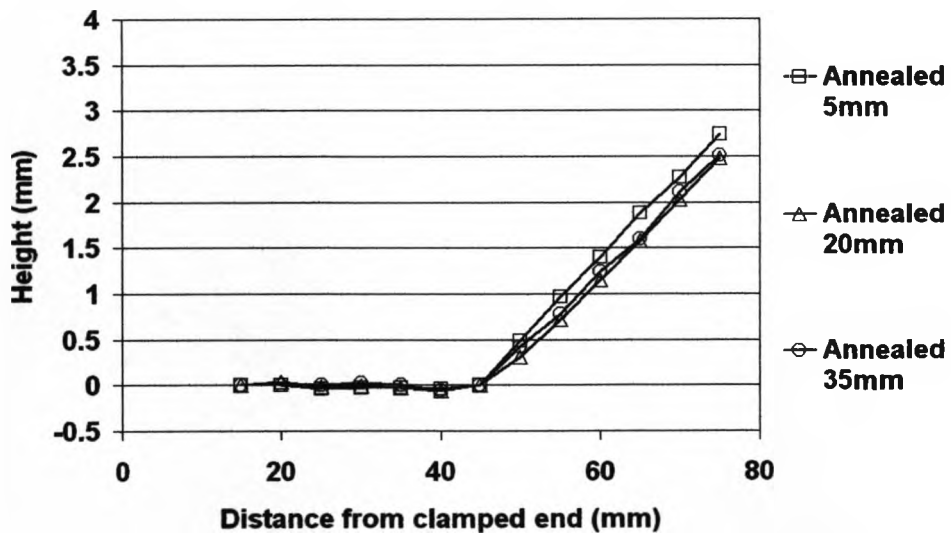


Figure 4.2.16: Height along length of sample 3 at 5, 20 and 35mm points across the width after annealing

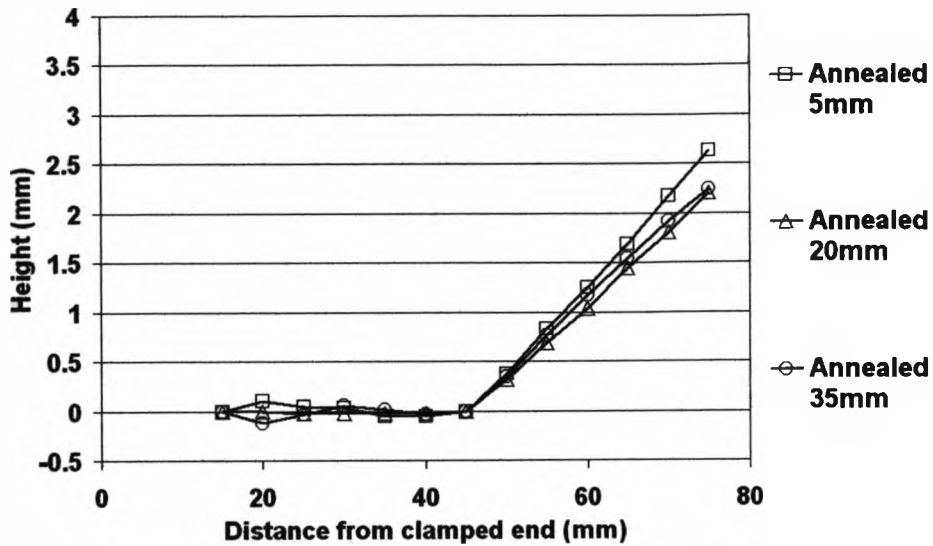


Figure 4.2.17: Height along length of sample 2 at 5, 20 and 35mm points across the width after annealing

The removal of distortion is due to the relaxation of residual elastic strains caused by stresses in the work-piece during the laser forming process. As the work-piece cools after each pass some elastic strains, especially at the clamped side of the piece, are retained only to be released when heated. It can be seen that the elastic strains in the clamped side are relaxed in the annealing process. In sample 2 at 35mm across and sample 3 at 5mm and 35mm across a decrease in distortion can also be seen at either side of the bend. This removal has little effect on the bend angle and overall geometry of the sample when compared to the removal of the distortion in the clamped side. However this does show that there are some elastic strains in this region that may not be able to be explained by the clamping arrangement. Though this effect is minimal here it could become problematic in 3D forming where a series of irradiation lines are used.

4.2.2.2 Solution Heat Treatment and Quenching

To achieve precipitation hardening it is necessary to go through solution heat treatment of the samples. To do this the samples are placed in a pre heated furnace at 530°C for 1 hour.

To achieve the T4 temper designation the sample is then quenched. This is achieved by placing the samples in a cold water bath. This process increases the hardness and the strength of the material.

It can be seen here that tempering to T4 has had a much greater effect on sample 3 with an average angle increase of 1.4° from annealing stage with a maximum of 1.92° compared to an average increase in bend angle from the annealing stage in sample 2 of 0.13° with a maximum of 0.34° (tables 4.2.6 and 4.2.7).

Position	5 mm	10 mm	20 mm	20 mm	25 mm	30 mm	35 mm	Average
Angle after T4 tempering (°)	4.85	4.71	4.61	4.49	4.4	4.23	4.28	4.51
Difference between T4 and annealing angle (°)	-0.2	0.28	0.34	0.28	0.25	-0.04	-0.04	0.13
Difference between T4 and laser forming angle (°)	0.1	0.09	0.12	0.13	-0.02	-0.41	-0.43	0.1

Table 4.2.6: Resultant angles after Tempering to T4 of sample 2

Position	5 mm	10 mm	20 mm	20 mm	25 mm	30 mm	35 mm	Average
Angle after T4 tempering (°)	6.29	6.19	6.21	6.19	6.38	6.05	6.48	6.26
Difference between T4 and annealing angle (°)	1.03	1.25	1.29	1.45	1.92	1.31	1.65	1.4
Difference between T4 and laser forming angle (°)	1.52	1.43	1.63	1.76	1.88	1.41	1.61	1.52

Table 4.2.7 Resultant angles after tempering to T4 of sample 3

This increase amount of distortion in sample 3 can be seen again in the surface measurement (figures 4.2.18 and 4.2.19) and the height along the length of the sample (figure 4.2.20 and 4.2.21).

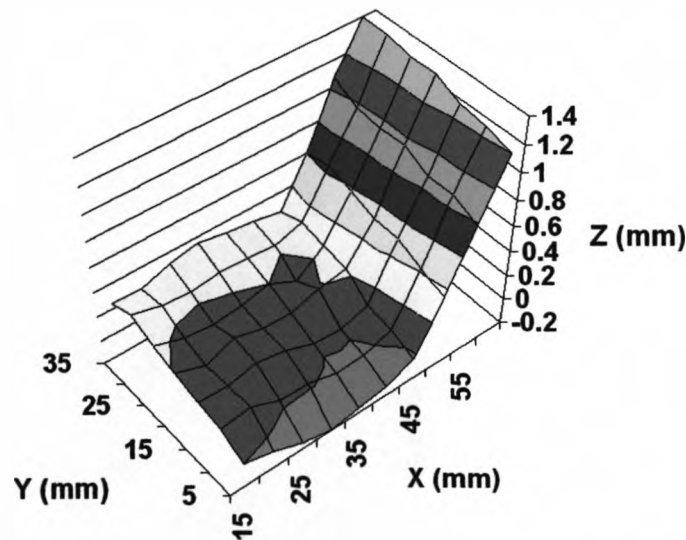


Figure 4.2.18: Sample 2 surface measurement after tempering to T4, close-up of clamped side

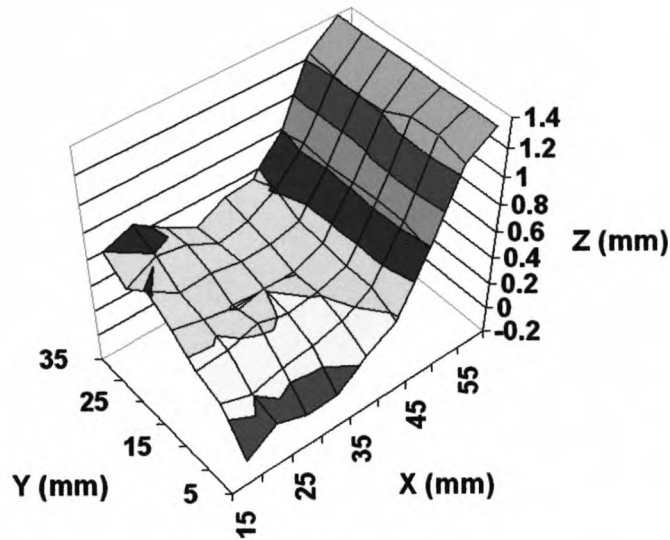


Figure 4.2.19: Sample 3 surface measurement after tempering to T4, close-up of clamped side

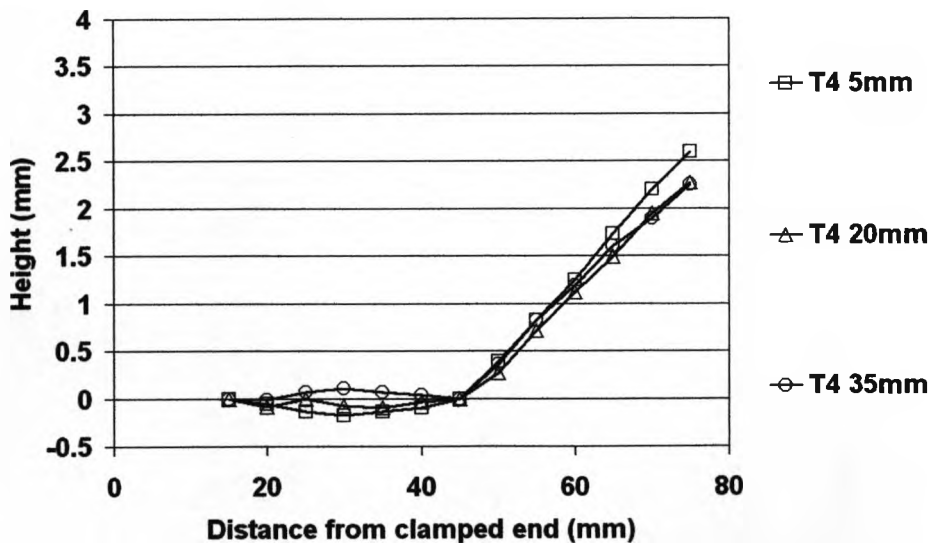


Figure 4.2.20: Height along length of sample 2 at 5, 20 and 35mm points across the width after tempering to T4

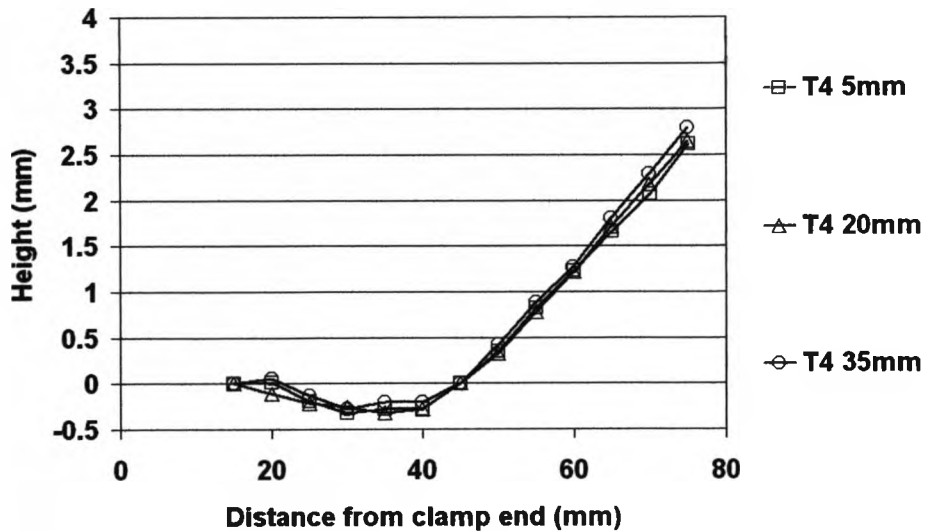


Figure 4.2.21: Height along length of sample 3 at 5, 20 and 35mm points across the width after tempering to T4

The reason for the difference in the amount of distortion in the sample is due to quenching. Although cold water immersion is the most common method for quenching it presents problems involving residual stress and warping. The ASM handbook explains that this inconsistency is common place due to a significant variability in the symmetry of cooling among identical thin section parts¹¹⁶. This explains the difference in the reaction of the samples to this heat treatment and also explains the added distortion which has influenced the bend angle.

In figures 4.2.20 and 4.2.21 it can be seen that for tempering to T4 the whole piece distorts. This is a much more evenly distributed distortion

than in the samples after the laser forming process suggesting that the distortion is no longer due to the effects of the restraints of clamping.

With tempering to T4 the distortion in the whole sample is the most significant effect on bend angle.

4.2.2.3 Precipitation Heat Treatment

After solution treatment and quenching, hardening is achieved either at room temperature (natural aging) or with precipitation heat treatment (artificial aging) Sample 2 is going to be heated in the furnace at 160°C for 18 hours. This will achieve a T6 temper which is a commonly used temper designation for engineering applications.

Position	5 mm	10 mm	20 mm	20 mm	25 mm	30 mm	35 mm	Average
Angle after T6 tempering (°)	5.36	4.87	4.71	4.54	4.61	4.57	4.52	4.74
Difference between T6 and T4 angle (°)	0.51	0.15	0.1	0.05	0.2	0.34	0.25	0.23
Difference between T6 and annealing angle (°)	0.31	0.44	0.44	0.33	0.45	0.3	0.2	0.31
Difference between T6 and laser forming angle (°)	0.61	0.24	0.22	0.18	0.18	-0.07	-0.18	0.61

Table 4.2.8: Resultant angles after Tempering to T6 of sample 2

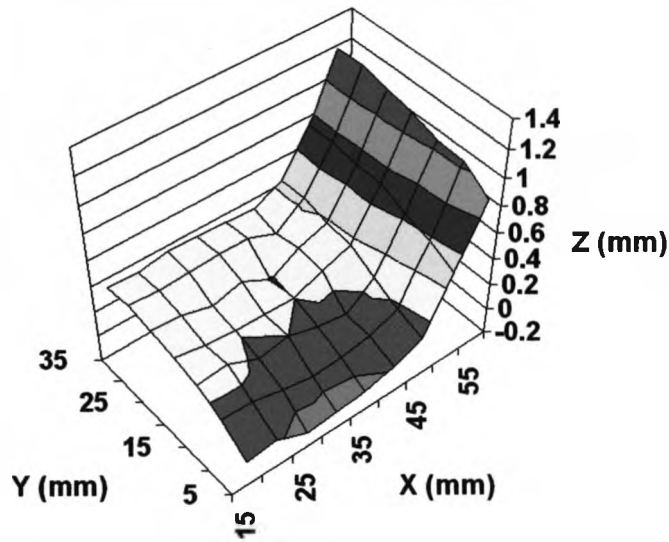


Figure 4.2.22: Sample 2 surface measurement, close-up of clamped side

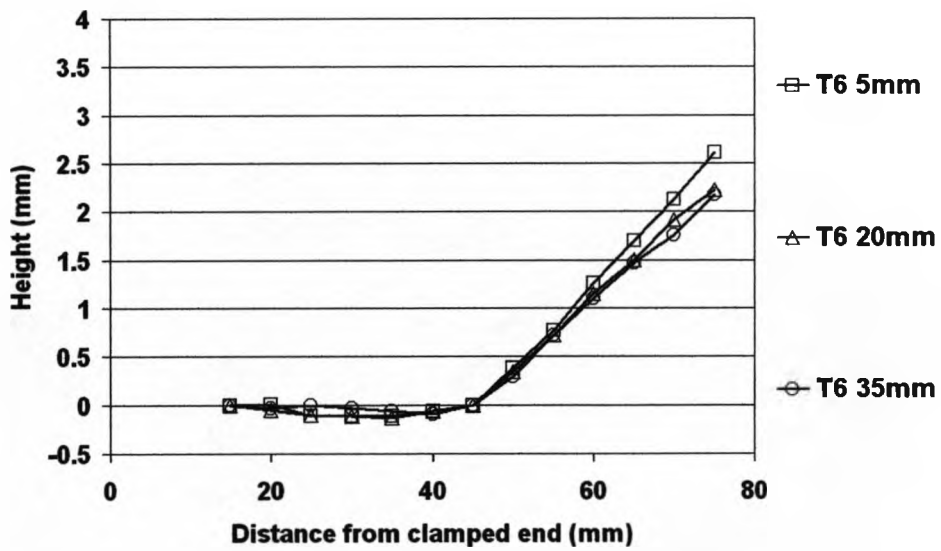


Figure 4.2.23: Height along length of sample 2 at 5, 20 and 35mm points across the width after tempering to T6

Tempering to T6 is a much more delicate process than tempering to T4 as it involves a slow heating to a lower temperature with no need for rapid cooling. It can be seen that this has a similar effect to the annealing process, figures 4.2.22 and 4.2.23, with the relaxation of residual stresses obtained in quenching.

4.2.3 Hardness testing

As the hardness of AA6061 varies with temper it is possible to use this to test if the heat treatments are carried out correctly.

The samples are cut through a cross section of the bend and mounted in resin. This allows the hardness to be taken within the sample and across the bend. The hardness is measured at the top and the bottom of the bend along the whole sample (figure 4.2.24).



Figure 4.2.24: Locations for the hardness test

It can be seen in figure 4.2.26 that the expected hardness¹¹⁴ corresponds to the actual hardness. Though not precise this is close enough to show that the samples have been heat treated successfully.

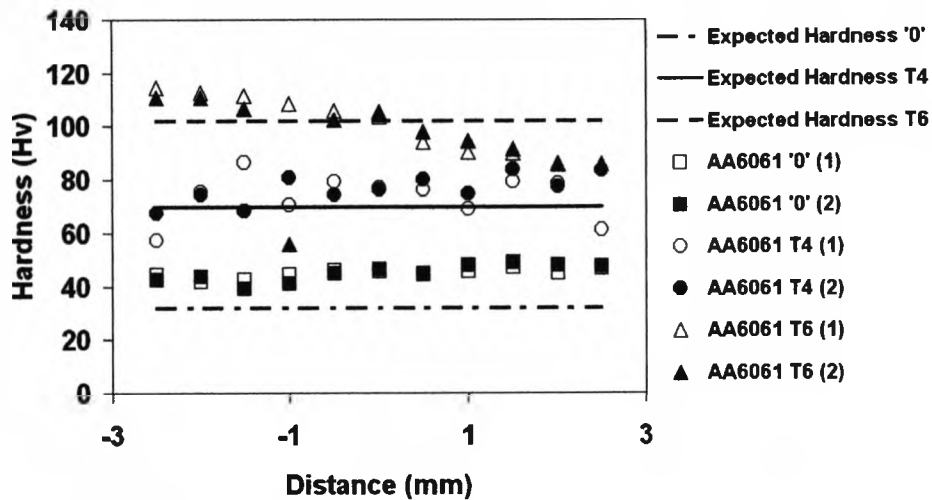


Figure 4.2.26: Results of micro hardness test on heat treated AA6061¹¹⁴

4.2.4 Discussion: Effects of Post Forming Heat Treatment of a Laser Formed Component

No major changes in the geometry of the samples were observed in any of the heat treatments. The bend angle was maintained throughout with small changes in magnitude. In every case this is attributed to the change in distortion in the samples.

This distortion is caused by residual stresses in the samples initially from the laser forming process and in later measurement by the quenching process. After the effects of annealing no further effects of post forming

heat treatments were observed that are linked to the laser forming process.

In the annealing process it is observed that the residual stresses are relaxed and a removal of the distortion is observed. This is the reason for any changes in the geometry, and therefore bend angle, after the first heat treatment. Also observed here is the removal of distortion around the bend region in certain cases. This suggests that there are residual stresses in this region after the laser forming process that may not have been caused by the clamping arrangement. Further investigation with a less restrictive clamp is needed to confirm this.

Another factor here could be the dwell time. In this investigation the dwell time was much longer than normal, approximately 5 minutes 15 seconds. This allows the piece to cool fully. As the whole work-piece is cold the speed of cooling in the irradiated region is increased. Because of this the possibility of containing residual stresses and distortion, which can be relaxed during heat treatment, are increased.

Though the effects of post forming heat treatments on 2D laser formed parts are minimal this could be a cumulative effect in 3D laser forming. This is because for 3D laser forming a series of irradiation lines are used. It is therefore possible for residual stresses to build up in a 3D part increasing the amount of relaxation of residual stresses which deforms the part in annealing. However, this may be reduced because in 3D laser forming, due to the number of irradiation lines the part increases in temperature throughout a pass. This decreases the cooling rate as the pass is carried out minimising the build up of residual stresses in later irradiated lines. For the first lines that are irradiated the cooling rate will be fast due to self-quenching increasing the possibility of residual stress,

however the same heating effect that reduces the cooling rate later in the pass may also help relax some of the residual stresses that occur earlier in the pass, thus minimising any effect of post forming annealing. Further investigation is required into the post forming effects of annealing on a 3D laser formed part to determine these effects.

Chapter 5

3D Laser Forming Results and Discussion

2D laser forming has been around for many years and consequently a large number of investigations have been carried out in this field. Because of this the advancements in 2D forming have been considerable and it is currently possible to control bend angle in various materials, including aerospace alloys, with reasonably accurate results. The next step is to investigate 3D laser forming.

In order to advance the LF process for realistic forming applications and for straightening and aligning operations in a manufacturing environment, it is then necessary to consider 3D LF. Less work has been completed in this field compared to 2D LF; however, the process has been shown to have a great deal of potential. In order to compete directly

with conventional forming techniques, such as die forming, the process must be proven to be reliable, repeatable, cost effective and flexible. It is the potential flexibility of 3D laser forming that offers the greatest benefit. A change to required part geometry could be implemented easily through the CAD driven process, which can be compared to the expensive and in-flexible hard tooling requirements of the die forming process. The work presented here aims to prove the viability of this technique as a direct manufacturing tool and as a means of correcting unwanted distortion (e.g. distortion resulting from processes such as chemical etching). To this aim, progress towards repeatable closed loop controlled 3D LF is presented.

5.1 Using Geometrical Properties for Creating Irradiation Strategies

An irradiation strategy consists of two main parts, an irradiation pattern, which is the path the laser takes, and the energy distribution across the pattern; this is controlled by the traverse speed of the laser. In these investigations the irradiation strategy is determined by geometrical properties.

5.1.1 Defining 3D Surfaces

It was concluded from earlier empirical studies⁷⁶ that, in order to develop control of the process of 3D laser forming, it was necessary to have the ability to define the surface to be formed. In addition, by defining the

surface and analysing its properties it was thought this may lead to a method of scan strategy prediction. The considered geometrical properties of 3D surfaces that can be used for creating an irradiation strategy are listed below.

- Height
- Gradient
- Curvature
 - Principal Curvatures
 - Mean Curvature
 - Gaussian Curvature

5.1.1.1 Developable and Non-developable surfaces

There are two types of 3D surfaces, developable and non-developable. A developable surface is defined as one that can be unfolded or developed into a plane surface without stretching or tearing. Because of this property, they are of considerable importance to sheet-metal and plate-metal based industries. Applications include windshield design, binder surfaces for sheet metal forming processes, aircraft skins, ship hulls and others¹²⁷. The concept of these surfaces is shown schematically in figure 5.1.1.

The examples shown are of a developable surface, a part-cylinder, and a non-developable surface, a dome or pillow shape. An analogy can be drawn to how these surfaces have been formed and what laser forming mechanism would be required to form a flat sheet into the two shapes.

For a singly curved developable surface the TGM should be the dominant mechanism used so as to produce plastic bending strains and out of plane deformation (simulated by V grooves). For a doubly curved non-developable surface, material needs to be removed (in-plane) in order to allow the deformation to take place. This suggests that the shortening mechanism should be the dominant mechanism when forming this type of surface, the in-plane plastic shrinkage accounting for the limiting material near the edges (at the expense of the section thickening).

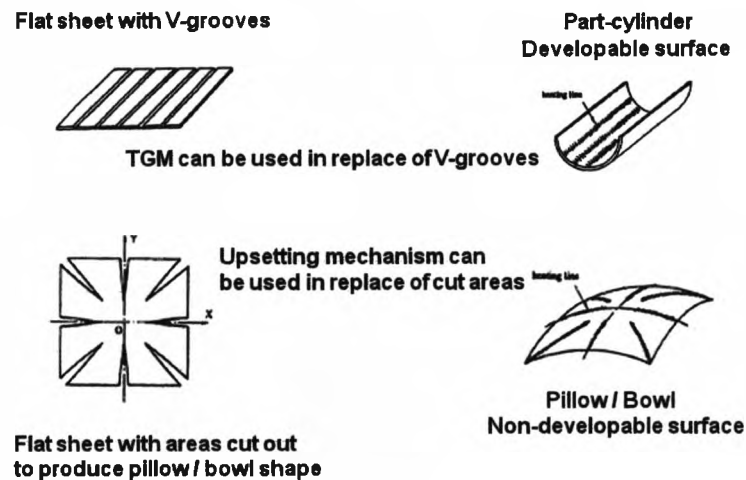


Figure 5.1.1: Developable and non-developable surfaces¹²⁸.

5.1.1.2 Height

The height, at various points, is the simplest way of defining a 3D surface and is probably the most likely property of a surface to be used in day-to-day life. For the possibility of using height as a method of determining irradiation strategies in laser forming it is necessary to consider the contours of height. These are a common method of defining a 3D surface in a 2D medium, e.g. on a map. The rate of change of height is defined in the contours of height by the distance between these lines. Because in laser

forming to increase the gradient of a surface more energy is needed the closer lines at steeper gradients here suggests a possible correlation. This method is used to create the irradiation pattern in the original geometry based model.

5.1.1.3 Gradient

The gradient is a relatively basic measurement in flat surfaces as the gradient is the same value for the whole surface. In the case of a singly curved surface the gradient will change along the length of the surface and will always have the same direction. For a 3D surface the gradient can change in magnitude and direction. Because the gradient is a vector using it to create a potential irradiation pattern requires lines of constant gradient magnitude to be considered. However, this does not take into account the direction of the gradient. The gradient magnitude is used in the original model to determine the energy distribution and in the modified model to determine the irradiation pattern and the energy distribution.

5.1.1.4 Curvature

By simply having a curvature a surface can be described as being three dimensional. To have a curvature the surface has to deform out of plane as this is the rate of change of gradient. It is a more complicated method to convert the values of curvature into a potential irradiation pattern. The method for doing this in a singly curve surface is not possible because the curvature for this case can be equal throughout. For a doubly curved surface there is an added complication as there are two curvatures to be

accounted for. These are the principal curvatures which are the maximum and minimum curvature at each point. It is possible to gain an irradiation pattern by considering these separately creating two irradiation patterns. There is no chance of the principal curvatures being equal across the whole surface, as in the case for a singly curved surface, because for two curves to interact on a continuous surface the curvature has to change. Another possibility is to use the principle curvatures to calculate the mean and Gaussian curvature.

5.1.1.4.1 Mean Curvature

The mean curvature, as the name suggests, is the average of both the principle curvatures¹²⁹. It is possible to use this to create a single irradiation strategy. However this value can be equal across a 3D surface, for example in a saddle shape it is possible for the maximum and minimum principle curvatures at all the points to have the same magnitude but in opposite directions. This would give a mean curvature of zero across a doubly curved 3D surface which is obviously incorrect.

5.1.1.4.2 Gaussian Curvature

Another possibility is the Gaussian curvature; this is the product of the principle curvatures¹²⁹. This produces an equal value across a singly curved surface. However it is a useful tool in defining the developability of surfaces. All 3D surfaces can be described as three main types, the non-developable saddle and bowl surfaces and the developable part-cylinder surface.

By having a straight edge a developable surface, such as a part-cylinder, has one principal curvature equal to zero (figure 5.1.2a). A shape that does not have a straight edge at any point is non-developable and has a non-zero

Gaussian curvature. To be more accurate, a surface that has positive maximum and minimum principle curvatures, like a pillow or bowl shape, has a positive Gaussian curvature (figure 5.1.2b) and a surface that has principal curvatures that are both positive and negative, like a saddle shape, has a negative Gaussian curvature (figure 5.1.2c).

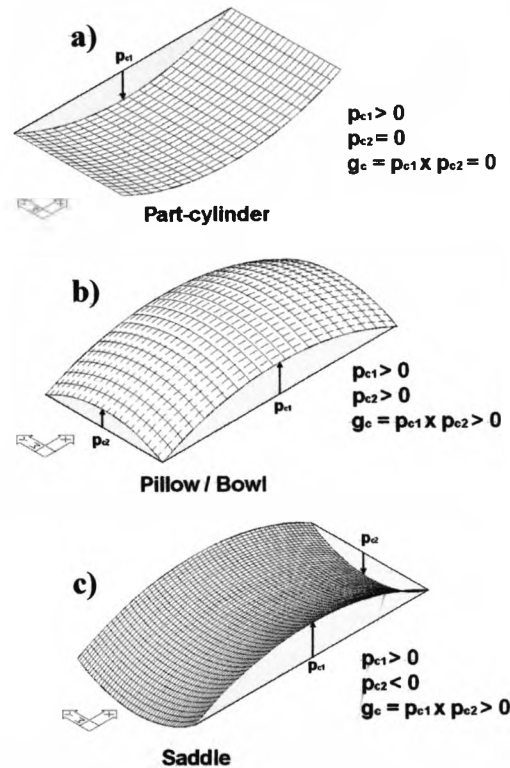


Figure 5.1.2: (a) Gaussian curvature of a part-cylinder, (b) bowl/pillow and (c) saddle shape.

Because in the forming of non-developable surfaces a large amount of in-plane strain is required for a small magnitude of out of plane movement this immediately limits the amount of forming possible. This means that it is only possible to form shallow non-developable shapes. This is different in the case of developable shapes which can be formed to a high degree due to the use of the small amount of bending strain required for out of plane movement in comparison. The Gaussian curvature can be

considered a measure of the developability of a surface and can therefore also be used as a guide to the laser formability of a shape. This is because the more non-developable a surface is, the greater the amount of material that needs to be removed. There is also the possibility that the forming process has a limit which can be defined numerically through Gaussian curvature, giving an operating window to the laser forming process. Another method can then be used to form these shapes. A possible method may be by removing material in the most non-developable areas, prior to laser forming, creating a type of net shape. Another possibility is to use the Gaussian curvature as either a method of determining energy distribution in an irradiation pattern or determining the pattern itself in non-developable surfaces.

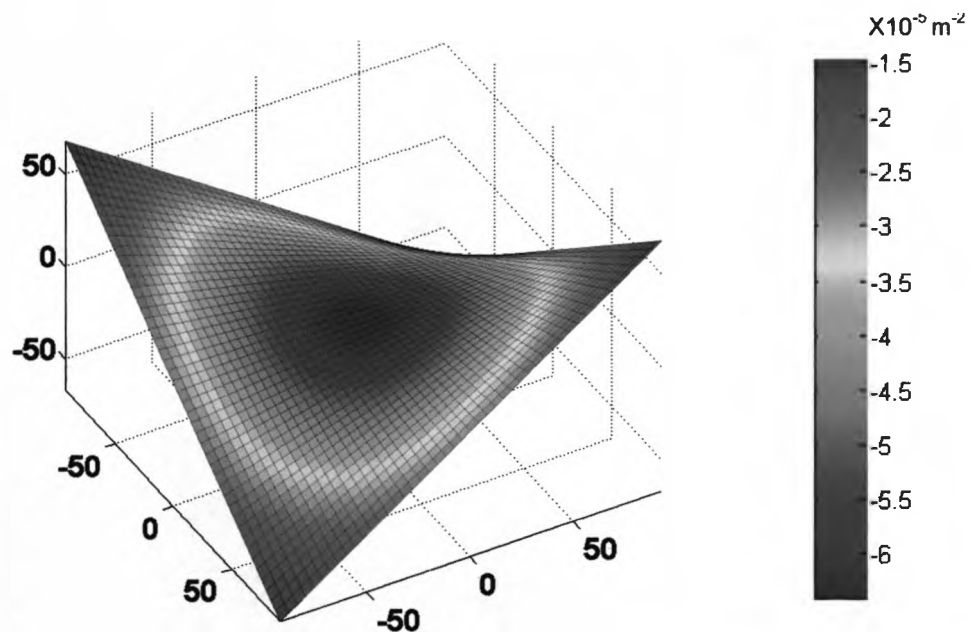


Figure 5.1.3: Saddle with colour map of Gaussian curvature

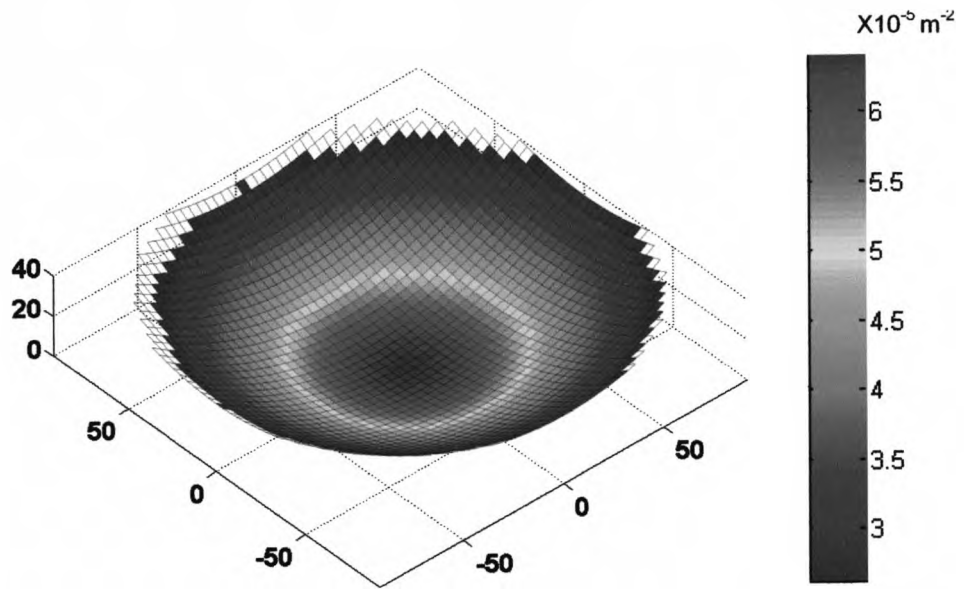


Figure 5.1.4: Dome shape with a colour map of Gaussian curvature

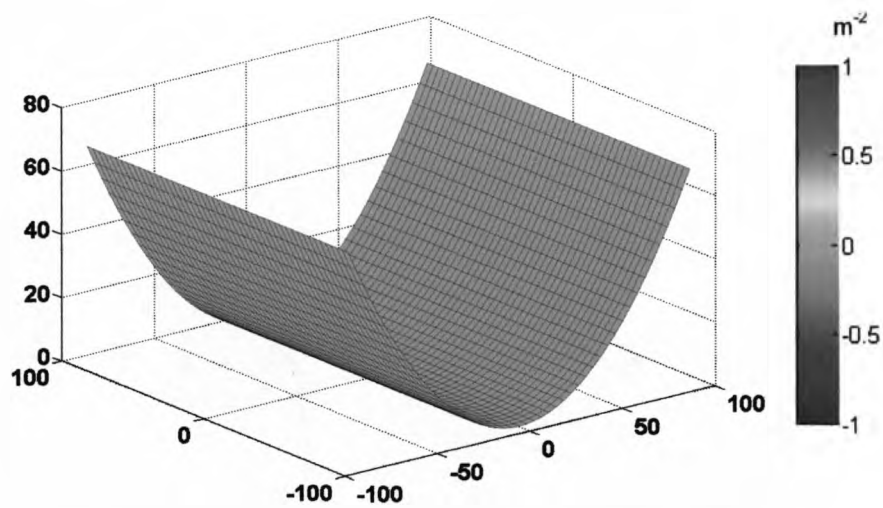


Figure 5.1.5: Part cylinder with a colour map of Gaussian curvature

The shape that was chosen for investigation for this paper is what we've classed as a semi-developable shape that resembles a possible part that may be used in industry (figure 5.1.6). There are areas on this surface that are non-developable; however these are of a small magnitude and can be formed using the laser forming process. This utilises the possibility of some non-developable forming along with a high magnitude of developable forming, taking advantage of the versatility of the process.

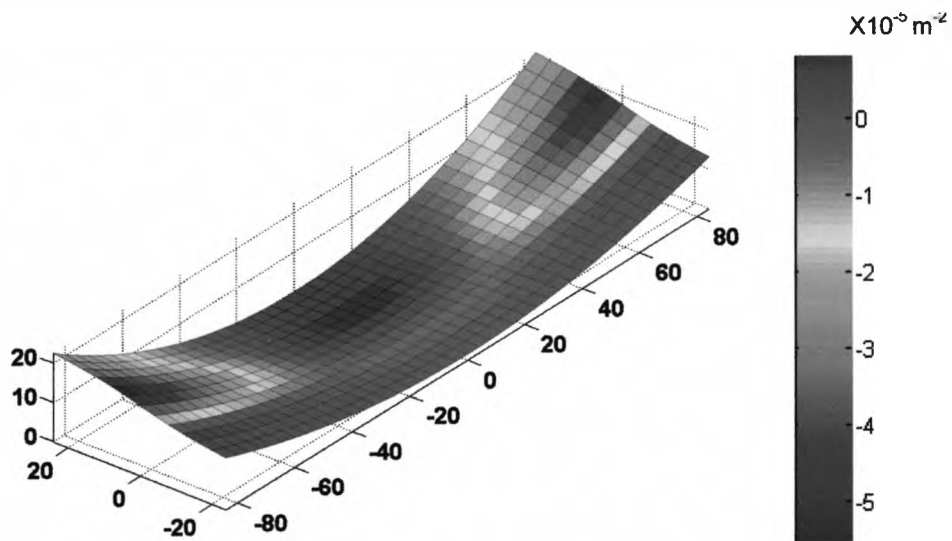


Figure 5.1.6: The desired semi-developable shape with a colour map of Gaussian curvature

5.2 3D Laser Forming of Semi-Developable Shape using a Geometry Based Model

Initial 3D LF investigations⁷⁶ were based around a purely empirical approach to establish rules for the positioning and sequencing of the irradiation lines required for the controlled 3D laser forming of symmetrical/uniform saddle and pillow ('dome') shapes from rectangular 400x200x1.5mm mild steel CR4 sheet. It was concluded from this work that the development of an on-line monitoring system with predictive distortion correction abilities is a requirement if any 3D laser forming operation is to be used in a manufacturing environment. This is due to the unknowns that can be present when forming in an open-loop set-up, such as residual stresses and variability in the absorption of the incident laser radiation. A foreseeable problem with a system which makes online distortion correction during processing is that the final geometry of the part is not reached until sometime after processing has stopped, when the plate has cooled somewhat and the elastic stresses have been released leaving a plastically formed part¹¹⁶. This suggests that a strategy of a one off single pass to produce a required geometry would be extremely difficult to predict and control. A more sensible method of producing a required geometry would be to increment towards it over a number of passes, taking surface measurements after each pass so as to have the ability to take account of any unwanted distortion.

The development of a closed loop demonstrator system for 3D laser forming is presented here, based on the recommendations and knowledge gained from empirical 2D and 3D laser forming studies and through the development of a predictive model.

5.2.1 Irradiation Strategy

5.2.1.1 Error between Desired and Actual Surfaces

The first step is to define the desired surface. This is done in Matlab using a minimal number of points. These points are interpolated in Matlab to gain a full smooth surface of the necessary number of points. The actual surface is measured using the CMM. As with the desired surface these points are interpolated to gain a full smooth surface of required points, this is the same number of points as for the desired surface.

All of the irradiation strategies are based on the error between the actual surface and the desired surface. This is a simple calculation where the interpolated measured heights of the actual surface are subtracted from the interpolated required heights of the desired surface creating a third surface. To do this the matrix of the interpolated points from both surfaces must have matrices of equal dimensions.

Because the scan strategy prediction is geometry based the error between a given shape and a desired shape could form the basis for a further scan

strategy. Lines of constant error between two surfaces are akin to the error between a flat sheet and a desired shape that give the lines of constant height (the principle of which has been demonstrated previously¹¹⁷). This can allow for the correction of a formed shape if the desired shape is not formed by the initial prediction. Thus an iterative method can be used to increment towards a desired shape. This method may also allow for the correction of unwanted distortion in a pre-formed shape, potentially by forming on both sides of a component.

5.2.1.2 Irradiation Pattern

A related study to this investigation¹¹⁷, based on the controlled 3D laser forming of a pillow or dome shape, concluded that scan strategies based on contours of constant height of a surface using the temperature gradient mechanism (TGM)¹⁰ can produce successful results.

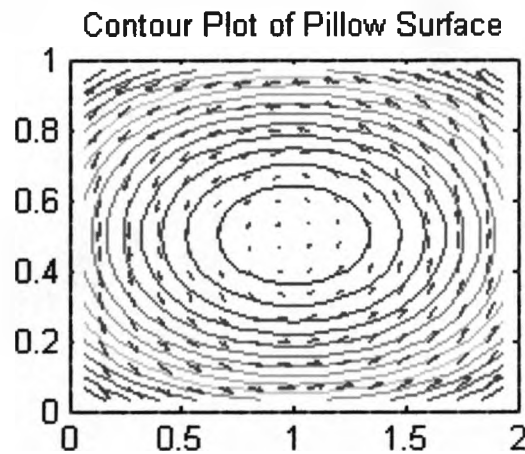


Figure 5.2.1: Contours of constant height and rotated resultant gradient vector

Scan lines based on contours of constant height were further confirmed by considering the gradients in X and Y of the surface and the resultant gradient vector (figure 5.2.1). If a required resultant gradient vector is in a given direction then laser forming at right angles to it using the TGM¹⁰ should produce the desired result, this is illustrated in figure 5.2.2 for a simple bend.

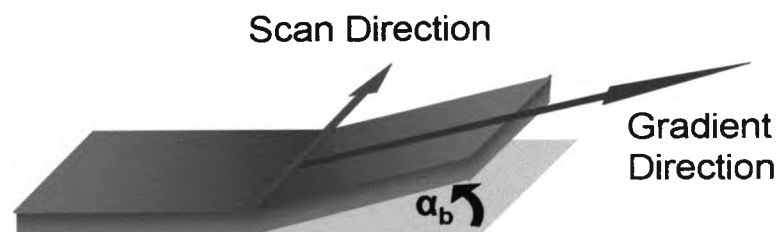


Figure 5.2.2: Illustration of required forming direction for a given bend direction

By overlaying the rotated resultant gradient vector on the contour plot of constant height for the given shape (figure 5.2.1), represented by the quiver arrows) it can be seen that there is a similarity between the two, thus providing confirmation of the contour plot strategy.

5.2.1.3 Speed Selection

Now that a usable method of scan line prediction had been discovered it was realised that a more subtle approach to the energy input per scan line was necessary. Observations of the quiver data presented in figure 5.2.1 indicated that a higher gradient magnitude is required near the edges of the plate as opposed to the centre. Hence increasingly more forming or energy input is required nearer to the edges. This is illustrated further in figure 5.2.3, where the resultant gradient vector magnitude has been calculated for points along the contour lines of constant height for the pillow shape. The vector magnitude is represented by the size of the red dot at locations on the lines.

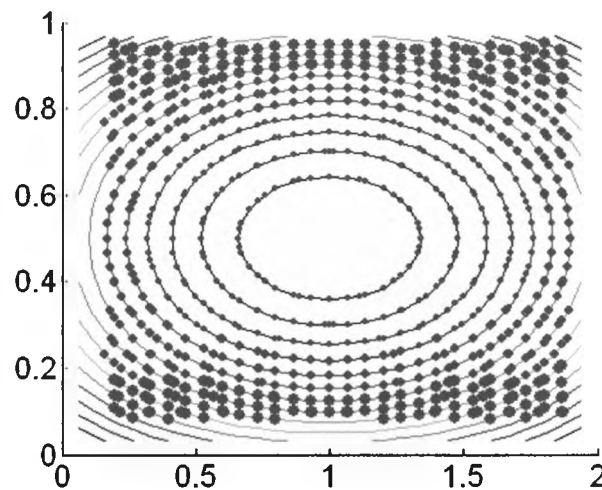


Figure 5.2.3: Height contour plot of pillow surface with an indication of the required gradient vector magnitude at points along the contour lines

It can be noted in figure 5.2.3 that the gradient vector magnitude not only varies between each contour line but there is also a subtle variation along the same contour line as well. These variations in required gradient vector magnitude should correspond to variations in required energy input and in practice, bend angle or forming requirement to produce the geometry. The most straightforward method of varying the energy input is through the process speed.

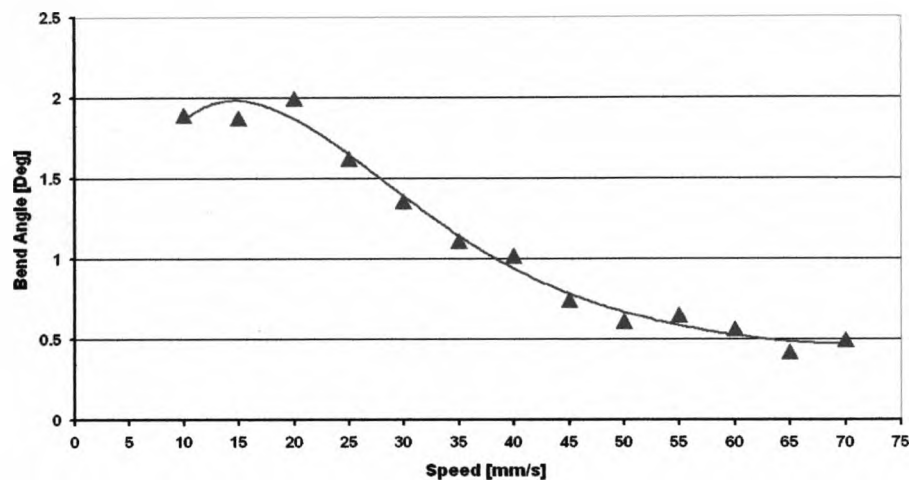


Figure 5.2.4: Laser forming of 1.5mm mild steel, 5.5 mm beam dia. 760W CO₂ 10 – 70mm/s, graphite coating Calibration data

A method of determining the distribution of the energy fluence is to use the magnitude of the resultant gradient vector as a scaling factor for known energy parameters selected by the traverse speed (figure 5.2.4). The parameters to give a required deformation or gradient magnitude can be determined from simple analysis of 2D laser forming. The results

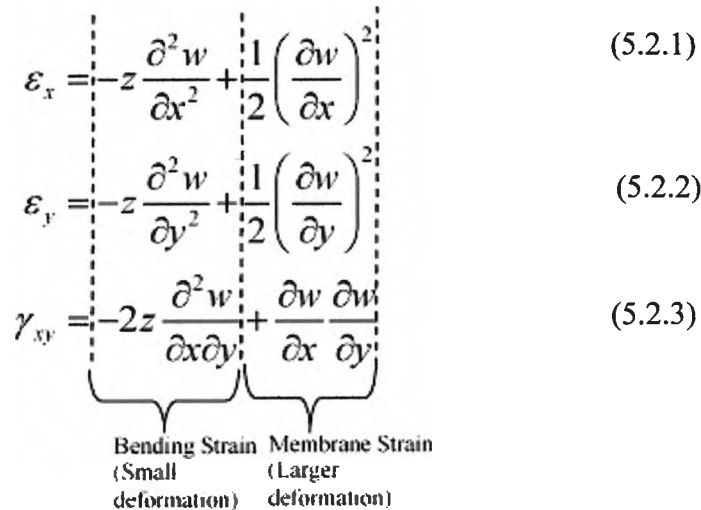
showing the bend angle produced for a given speed on 80x80x1.5mm mild steel coupons are shown in figure 5.2.4.

These results are then used to calibrate the speed for required strain. From the analysis of thin plates with small deflections¹³⁰ (of the order of the plate thickness) the strain components within a sheet can be expressed in terms of the deflection of a plate, w . The strain components at a given location in x and y and the shear strain in the xy plane (for a plate thickness z) during deformation are given by:

$$\varepsilon_x = -z \frac{\partial^2 w}{\partial x^2} + \frac{1}{2} \left(\frac{\partial w}{\partial x} \right)^2 \quad (5.2.1)$$

$$\varepsilon_y = -z \frac{\partial^2 w}{\partial y^2} + \frac{1}{2} \left(\frac{\partial w}{\partial y} \right)^2 \quad (5.2.2)$$

$$\gamma_{xy} = -2z \frac{\partial^2 w}{\partial x \partial y} + \frac{\partial w}{\partial x} \frac{\partial w}{\partial y} \quad (5.2.3)$$



 Bending Strain (Small deformation) Membrane Strain (Larger deformation)

The scaling factor between known energy parameters and the induced strain are found empirically by the measurement of the induced deflection for given energy parameters and desired final shape. In addition, if an incremental approach is used to form a surface rather than a single pass implementation, the data obtained from the first pass (providing the final shape has not been achieved) provides a strain scaling factor for the subsequent passes. This is based on the current plate being formed and so

should take account of residual stress history and material non-uniformity.

For calculating the speed the first step is to select a speed range. The maximum speed is chosen to be just under the forming threshold to allow for fine adjusting. A minimum speed is selected just above the point where damage will be done to the surface. This allows for maximum amount of possible forming with no damage to the work-piece. A minimum speed is then calculated before each pass, using strain equations. If this is less than the pre-selected minimum speed it is not used. An example of the speed range can be seen in figure 5.2.5.

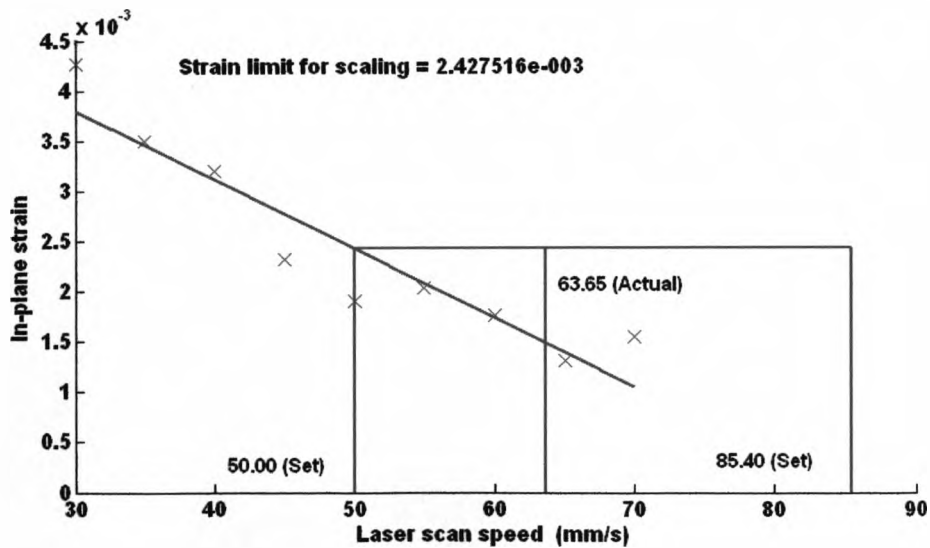


Figure 5.2.5: Example of speed range with calculated minimum speed (63.65mm/s) for the first model

5.2.2 Experiments for the Geometry Base Model

The experimental study was conducted on graphite coated 1.5mm mild steel using a 1.5kW ElectroX CW CO₂ laser employing a 3 axis Galil CNC beam delivery system with custom written control software. The mild steel sheet was laser cut into 400x200mm and 80x80mm coupons for a 2D and 3D LF study respectively. The smaller coupons were used to produce calibration data via simple 2D bends for the 3D study on the larger sheets. A diode laser range finder, mounted on the z-axis of the LF system, was used to verify/measure the bend angles in 2D LF and the surface shape in 3D LF, by using control software to create a co-ordinate measuring machine (CMM) set-up. The samples were held in place on the workstation table using a centre clamp; this required a hole to be drilled in the centre of the plates for a bolt to pass through. Although this may not be a desirable approach (introduction of additional residual stresses), very little forming was induced at the centre of the specimen (considered a reference point).

5.2.2.1 Closed Loop 3D Laser Forming of a Mild Steel Semi-Developable Shape

A potential method of scan strategy prediction has been developed based on lines of constant height. The energy distribution within the scan strategy can be given either by the gradient vector magnitude or the sum of the bending and membrane strains resolved in the direction of the

principle gradient. This gives a potential predictive capability to a system that takes into account material non-uniformity and residual stresses. The system developed here uses the predictive Matlab model to give an initial scan strategy based on a required geometry. When the geometry is not formed within one pass (or over formed), an incremental or iterative adaptive approach can then be used for subsequent passes, utilising the error between the current and desired geometry to give a new scan strategy. Thus any unwanted distortion due to material variability can be accounted for. The forming rate and distribution of the magnitude of forming across the surface can be controlled by the process speed, based on the factors above and the amount of forming required this avoiding any overshooting. A strategy of monitoring and controlling the process during a scan was also considered; however, this was not possible with the current monitoring hardware. In addition it was observed that the final formed surface was not realised until sometime after forming¹²⁰ making online monitoring ineffective. A strategy of per pass monitoring and control was therefore used.

The system was used to investigate the laser forming of the shape in figure 5.2.6 from graphite coated 400x200x1.5mm mild steel plate. For the first pass of the laser the system assumes it is forming from a flat sheet. It calculates the error between the contours and then uses this to calculate an irradiation pattern.

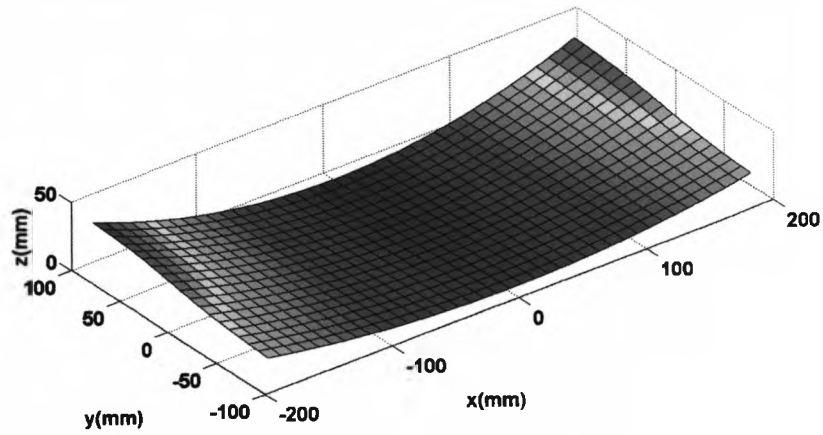


Figure 5.2.6: Desired shape, max forming 40mm

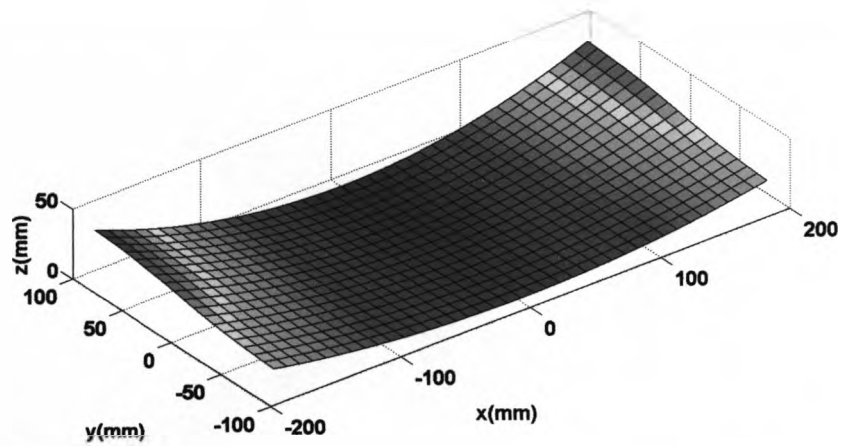


Figure 5.2.7: Surface of error between flat sheet and desired shape

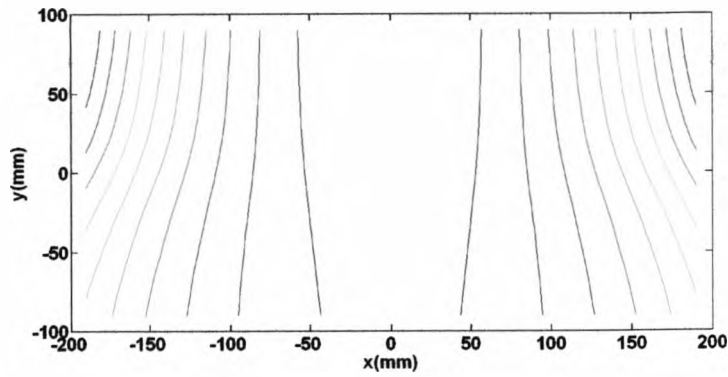


Figure 5.2.8: Contour of error between flat sheet and desired shape

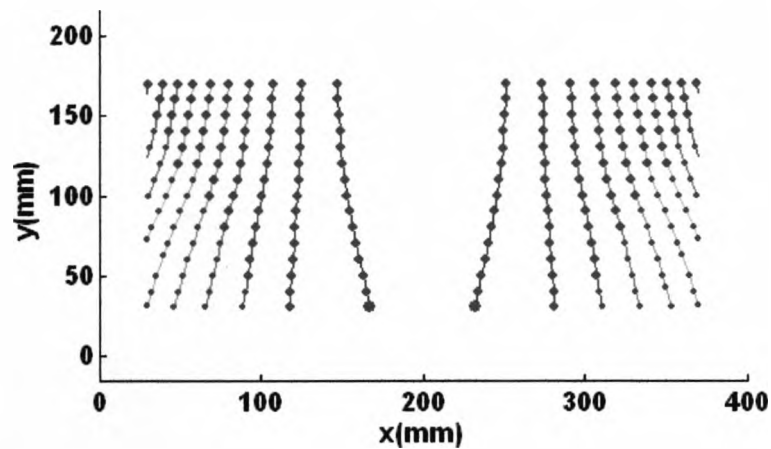


Figure 5.2.9: Irradiation pattern for pass 1, 760W CW CO₂, 5.5mm beam diameter, speed range 30-85mm/s

From the first pass (figure 5.2.10) it can be seen that the desired surface is already taking form at this shallow formed state.

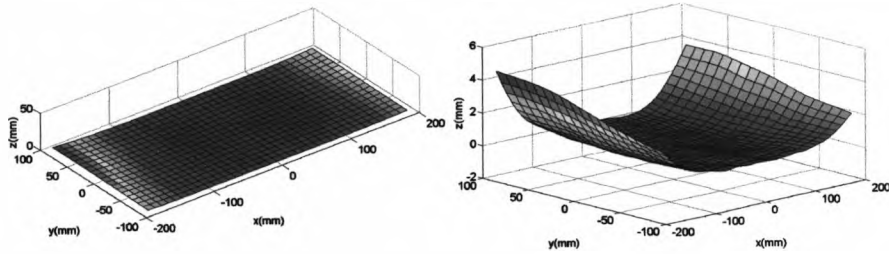


Figure 5.2.10: Result of first pass with normal scale and smaller scale of the z axis.

From the results of the first pass above, a strain scaling factor is calibrated. This allows the system to influence the amount of forming by controlling the laser traverse speed based on the amount of forming realised in the first pass.

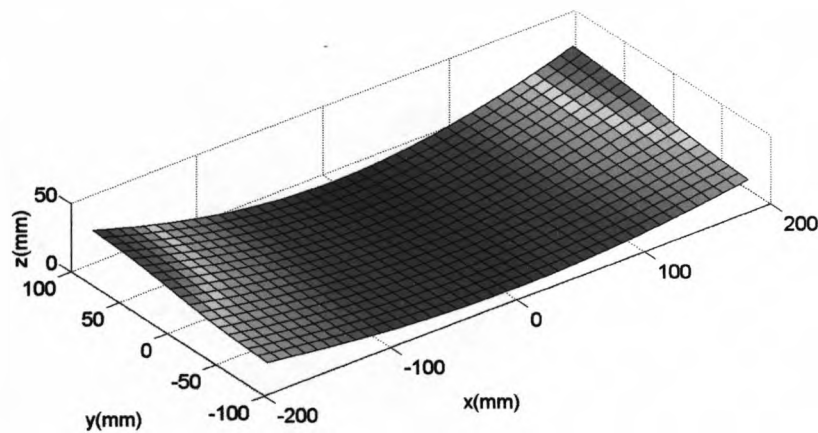


Figure 5.2.11: Error between measured shape and desired shape

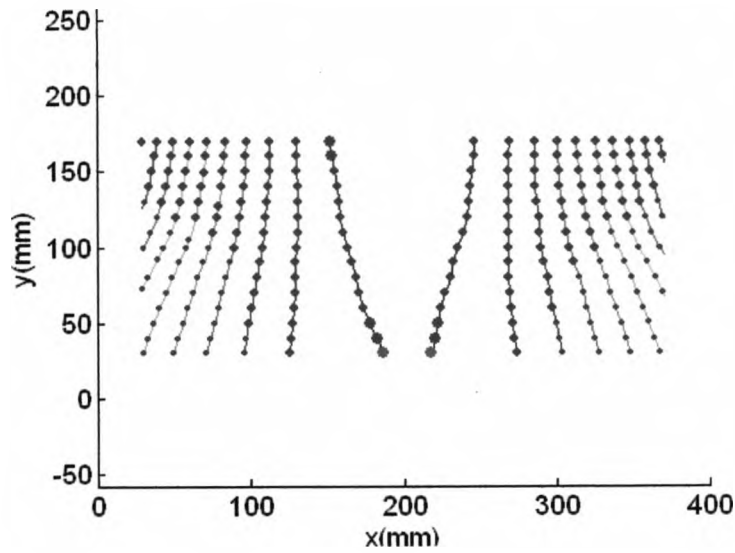


Figure 5.2.12: Irradiation pattern generated for the pass 2. Traverse speed range 30-85mm/s

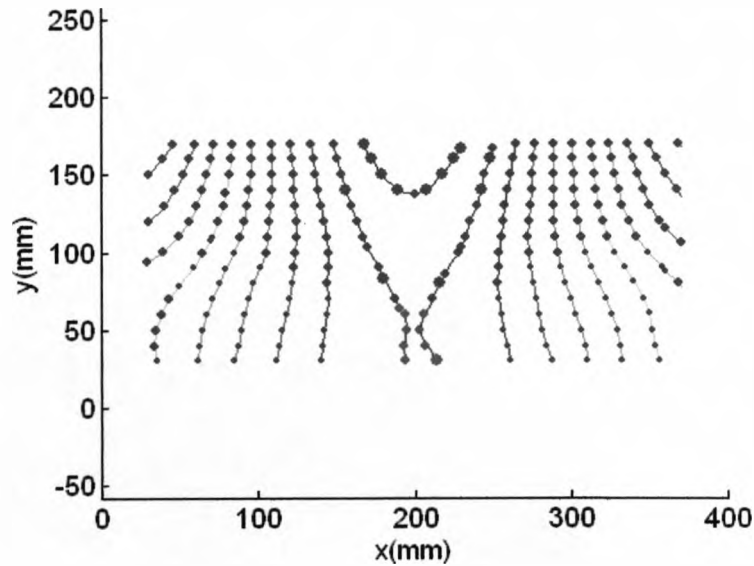


Figure 5.2.13: Irradiation path for pass 3. Traverse speed 40-85mm/s

After pass 3 the model tries to decrease the speed to 30mm/s even though the error between the surfaces has decreased. To avoid over forming from this point the speed is manually selected.

After pass 4 the work-piece became over-formed towards the edges. The system counteracts this by predicting forming on the reverse side. These lines are shown in figure 5.2.14 as red.

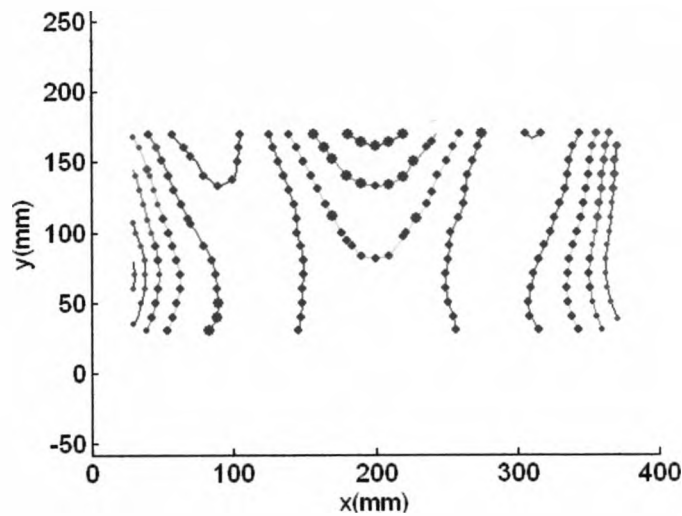


Figure 5.2.14: Irradiation path for pass 5. Traverse speed 50-85mm/s

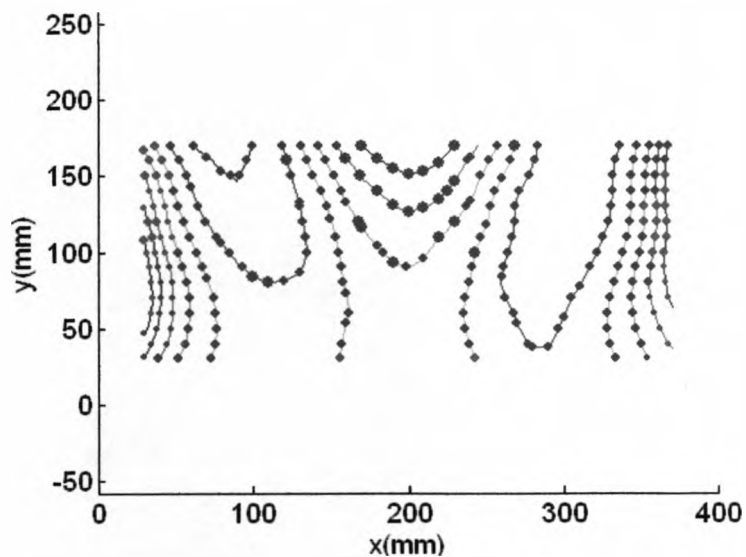


Figure 5.2.15: Irradiation path for pass 7. Traverse speed 65-85mm/s

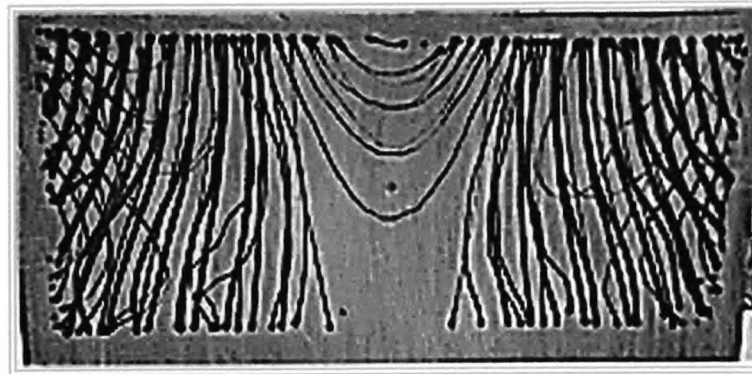


Figure 5.2.16: Final formed surface showing all irradiation paths

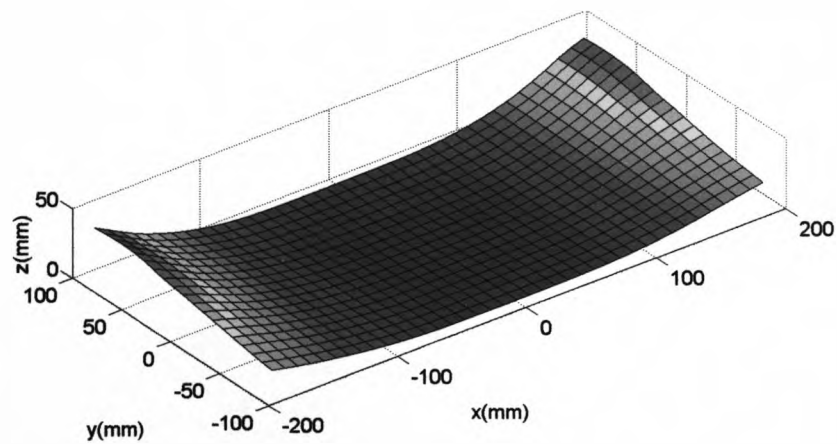


Figure 5.2.17: Final shape

The final pass, pass 7, forms completely on the front side of the work-piece subsequent to pass 4 and 5 forming the work-piece back into an

under-formed state. The surface measurement and irradiation path for every pass is contained in Appendix IV.

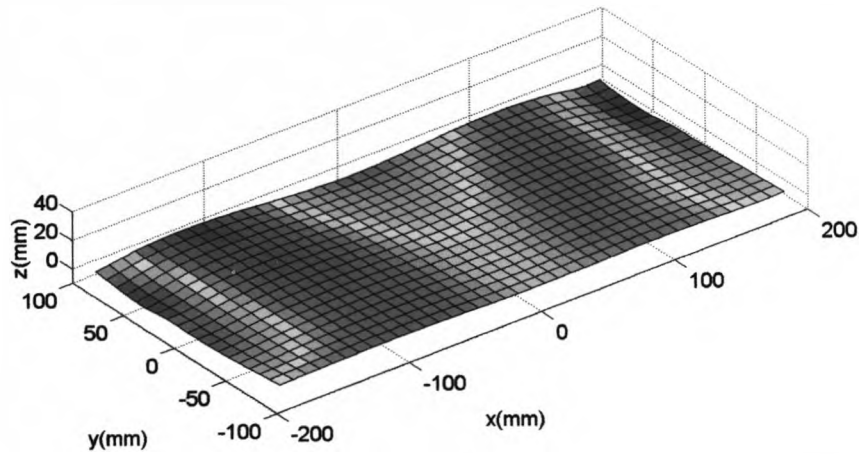


Figure 5.2.18: Error in the final shape

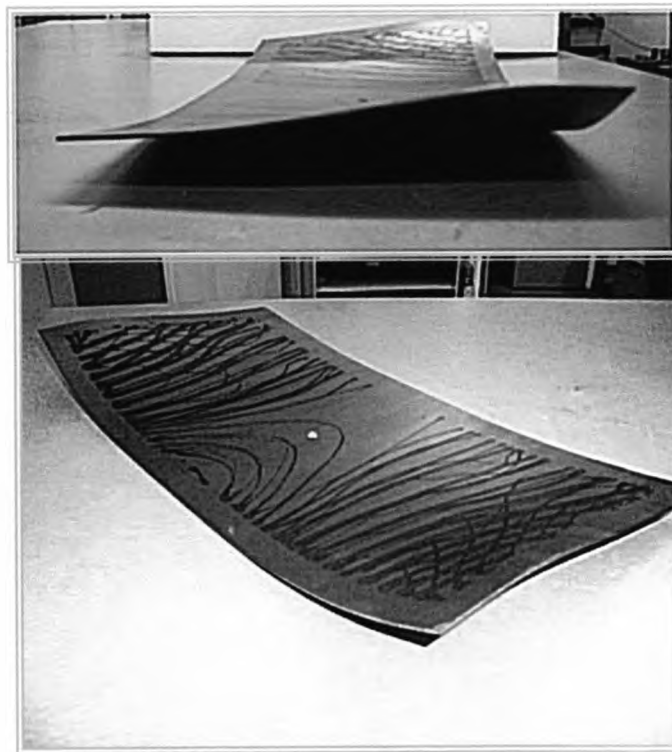


Figure 5.2.19: Views of the final component

Using an iterative approach, based on the error between the current and desired surfaces it has been possible to produce a component to within -1mm and $+5\text{mm}$ of the target shape. However this error may be exaggerated as the Bezier surface used to interpolate the measured data does not go through all measured points. Laser forming using scan patterns based initially on contours of constant height and then error difference plots has been shown to produce useful results.

Providing over-forming has not occurred on the first pass it has been possible to iterate towards the final shape, by increasing the traverse speed to reduce the bend angle rate and calibrating for the current plate's forming characteristics. It has the potential to produce a final component independent of residual stress history and material non-uniformity and to take account of unwanted distortion either brought about by these two factors or process variability.

The sum of bending and membrane strain for speed selection and the approximate calibration of the speed selection after pass 1 (this calibration is used because no accurate membrane calibration is available) is shown to have flaws in the laser forming of a semi-developable surface. One of the main reasons for this is that the strain calculations assume that most of the strain is membrane strain, which is true for a completely non-developable shape. However in the semi-developable shape this is not the case causing errors in the strain calculations.

A number of limitations of the laser forming system have been identified from the process trials for the developable shape. Firstly, it is currently possible to overshoot the target shape by a small degree. Refinements to

how the speed is scaled as the target shape is approached may avert this problem. It has been shown to be beneficial to over-form to some degree to reduce the error near the centre of the plate and then turn the plate over to bend the outer edges back to the required deformation, as shown in figure 5.2.20. Nevertheless this highlights another limitation of the system, as no account is taken of the influence on the rest of the plate of each forming line. The forming lines at the centre of the plate will cause a deflection of the outer edges and so the amount of forming required near the edges must be reduced.

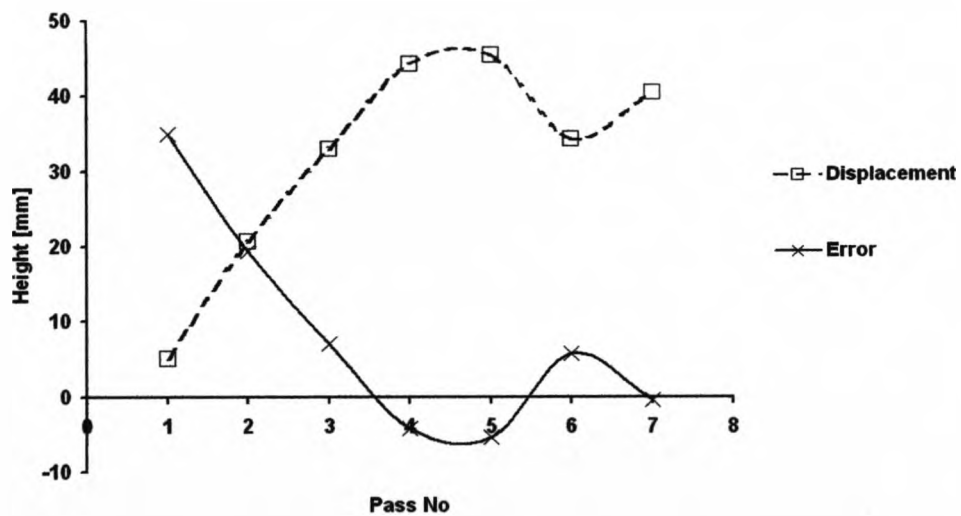


Figure 5.2.20: Displacement and error of a single point at the edge of the work-piece throughout the experiment

The system presented does demonstrate the potential of the laser forming process to produce accurate repeatable 3D surfaces in a controlled way. This suggests that laser forming could be utilised as a direct manufacturing tool or as a means of distortion removal in an industrial

environment. Providing the desired and the current surfaces can be realised in a virtual way (e.g. CMM data with a Bezier surface patch), a scan strategy can be predicted to give the final shape.

5.2.21 Feasibility of High Magnitude 3D Laser Forming of Mild Steel

The measurement system currently fails to measure components formed to a high degree as it does not take into account the viewable area decreasing as the amount of forming increases; this greatly reduces the amount of forming possible using the closed loop system. Another limitation is that the Matlab program also does not take into account this decrease in viewable area when calculating scan strategies. To show the feasibility of the process forming components to a higher degree, the component in figure 5.2.21 has been formed. This was produced using the original irradiation pattern created by the system for pass 1 of the desired semi-developable shape. The outer irradiation lines were then removed manually to take into account the decrease in viewable area.



Figure 5.2.21: Highly formed component using the original irradiation pattern from pass 1

5.3 Modified Geometry Based Model

For this investigation improvements are made to the original model and the resulting model is used in the fabrication of the 3D semi-developable shape and for the correction of distortion in struts. The material for these investigations has changed to aluminium 5251. As aluminium has greater heat transfer capabilities it inherently more difficult to laser form than mild steel because a temperature gradient is more difficult to achieve.

5.3.1 Irradiation Strategy

The basis of the original model is very strong and doesn't need to be modified. This includes the method of surface definition for the actual and desired shapes and the use of the error between these surfaces being used to calculate the irradiation strategy. In using the error between surfaces it is possible to use an iterative forming technique and also allows for any previous errors in forming or non-uniformity of a work-piece to be taken into account. This giving the model the ability to create irradiation strategies for laser forming as, both, a tool for the fabrication of 3D shapes and a method of removing distortion in already distorted components.

To modify the original model areas that require improvement are identified. The first improvement that needs to be made is that the decrease in viewable area of the work-piece as it forms is not taken into account. This causing the measured area to be larger than the work-piece and, more importantly, causes the irradiation pattern to be too large for the work-piece.

The irradiation pattern created by the original model is proven to be of use in 3D laser forming. However, this needs some subtle adjustment to take into account the over forming at the edges. This happens because the irradiation strategy does not take into account forming at the centre of the work-piece when irradiating the edges.

A weakness in the original model is the method of speed selection for the forming of a semi-developable surface. This is because the strain equations assume the whole plate is non-developable which encourages over forming. This was solved at the time by manually selecting the minimum speed.

5.3.1.1 Decrease in Viewable Area

To take account of the decrease in viewable area the reduction in length of each individual element in the x and y direction is calculated. The new length of the element is then added to the sum of the new length of every element before it from the centre line, as this is where the work-piece is clamped. The calculations to do this are as follows.

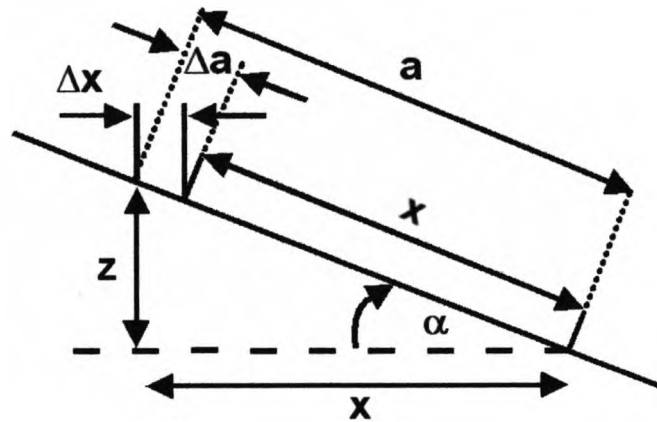


Figure 5.3.1: Calculation of Δa to find Δx .

To calculate Δx for each point the following calculations are made:

$$a = \sqrt{z^2 + x^2} \quad (5.3.1)$$

$$\Delta a = a - x \quad (5.3.2)$$

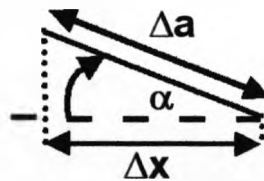


Figure 5.3.2: the calculation of Δx from Δa

$$\Delta x = \Delta a \cos \alpha \quad (5.3.3)$$

Δx is then subtracted from x to find the decreased value for x_d .

This is repeated for every point along in the x direction and then at every point in the y direction. This gives the decrease in view able area for the whole work-piece (figure 5.3.4).

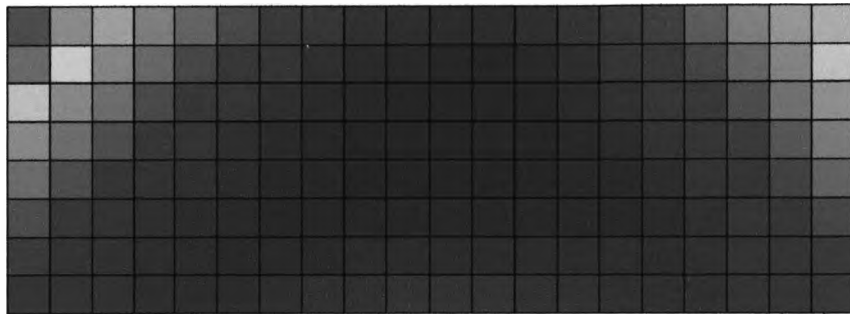


Figure 5.3.3: The measured points before the decrease in viewable area is calculated

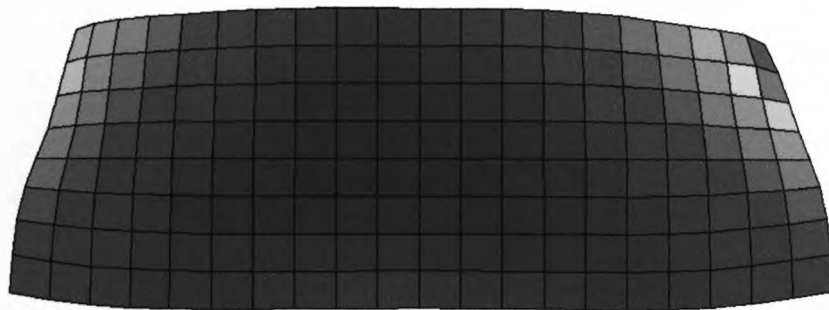


Figure 5.3.4: The measured points after the decrease in viewable area is calculated.

5.3.1.2 Irradiation Pattern

The original irradiation pattern uses lines of constant height. This produces lines that are perpendicular to the gradient direction. This follows conventional thinking on the laser forming process because in 2D laser forming the resultant gradient is always perpendicular to irradiation line.

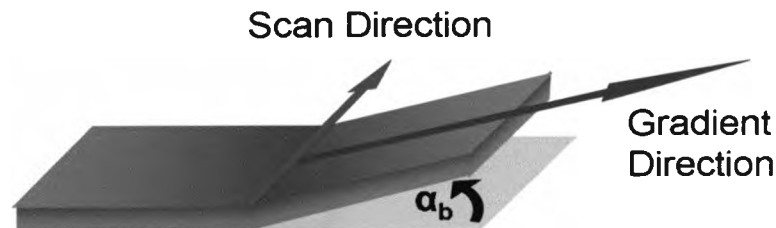


Figure 5.3.5: Illustration of required forming direction for a given bend direction

As the basic pattern is correct another method of creating an irradiation strategy for a mostly developable shape will have to have the same pattern but with a different distribution.

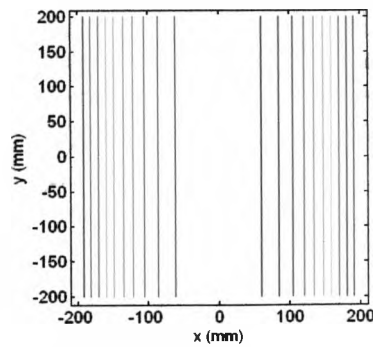


Figure 5.3.6: Lines of constant height for a part-cylinder

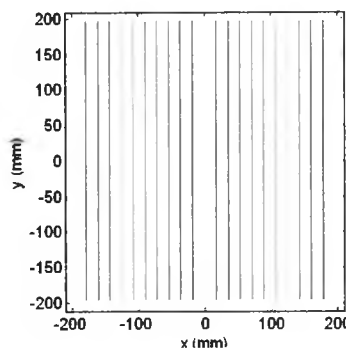


Figure 5.3.7: The lines of constant gradient magnitude for a part-cylinder

Let's take the simplest form of a 3D surface as an example. A part-cylinder is basically a series of many 2D bends. At each 2D bend the gradient changes. Using this to create lines of constant gradient it can be seen that the lines are spread equally (figure 5.3.7), unlike lines of constant height which produce a gathering of the irradiation lines at the edges. This is because in a part-cylinder the rate of change of gradient, the curvature, remains constant. To take into account forming at the centre of a work-piece and to prevent over forming it is necessary to laser form each region where the gradient changes as a single 2D bend. For example the gradient magnitude in a region, if looked at as a single 2D

bend, is considered to be the difference in the gradient on either side of the line where the gradient changes. In an irradiation pattern using lines of constant gradient this gradient is the increment between the lines. This means that a constant speed is required across the whole irradiation pattern based on the increment between the lines to achieve the same amount of bend at each point. This has the added advantage of a single speed across a whole work surface. By keeping the increment constant it is possible to keep the speed constant throughout processing. By doing this the optimum speed for a material can be chosen, this is especially useful in materials that may have a narrow operating window. Where the energy needed to form is close to the point where surface damage may occur.

To ensure this is correct the lines of constant gradient magnitude are compared to the lines of constant height for the saddle and pillow shape.

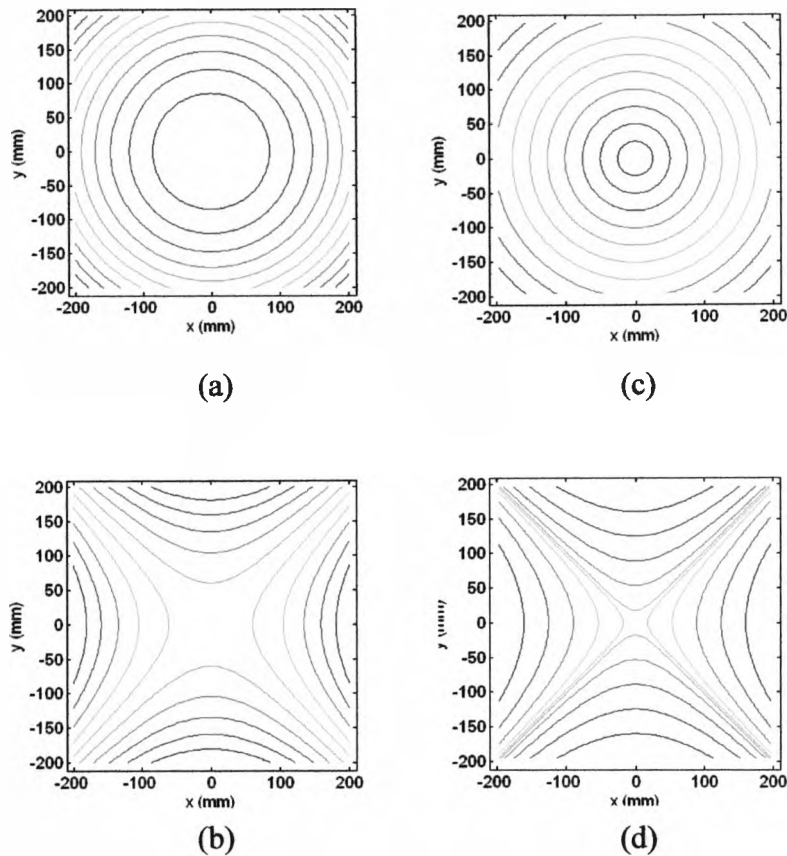


Figure 5.3.8: Lines of constant height for a bowl(a) and a saddle(b) and lines of constant gradient magnitude for a bowl (c) and a saddle (d)

The lines of constant gradient magnitude produce similar irradiation patterns as lines of constant height with a more even distribution (figure 5.3.8). This will solve the problem in the original model of over-forming at the edges.

An additional problem with the original was that during forming the focal position would remain static. This meant that as sections formed, especially at the side edges, the work-piece moved into focus. This would decrease the spot size affecting the amount of forming here, increasing the intensity and increasing the possibility of damage. This is solved here

by using the measured data to control the height of the z-axis keeping the focussing lens an equal distance away from the work-piece. Combined with an irradiation path that starts from the outside moving towards the centre the laser spot will have a consistent diameter throughout processing.

5.3.1.3 Speed selection

In the original model the gradient magnitude is used to distribute the speed so there is more forming in areas with a higher gradient. Here the speed is kept constant throughout the pass.

The speed is selected using experimental results from 2D forming of 80x80mm coupons of AA5251 in both 1mm and 2mm thickness. The traverse speed of the laser was altered keeping the power and beam diameter constant. The bend angle for each pass is measured. This is then used to produce a graph of gradient against speed. This relationship is then used to find a speed from the required gradient.

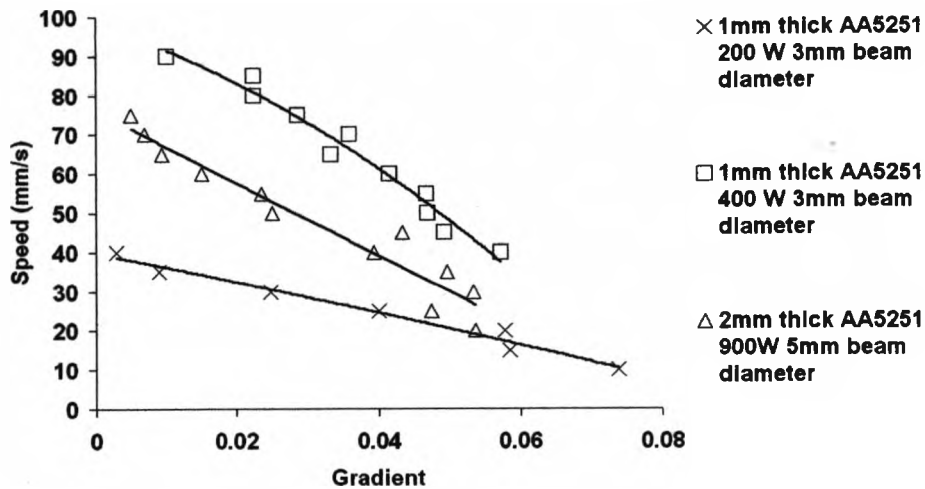


Figure 5.3.9: Results from operating window for laser forming of 1mm and 2mm AA5251

5.3.2 Experiments using the Modified Geometry Based Model

The fabrication 3D parts and the correction of distortion and design shape in manufactured components is increasingly in demand in industry, in particular for aluminium components, where the applications for aluminium and its alloys continue to expand. A process capable of achieving these actions in an automated, controlled and precise manner would be of significant benefit to industry. This Investigation uses the modified geometry based model to produce the required irradiation strategies.

5.3.2.1 3D Laser Forming Fabrication of Semi-Developable Shape in 1mm Thick 80x 200mm Aluminium at 400W

The experimental study was conducted on LF of graphite-coated 1mm thick AA 5251 using a 1.5kW ElectroX CW CO₂ laser with a 3-axis Galil CNC beam delivery system with custom written control software. The aluminium was cut into 400x200mm and 200x80mm coupons a 3D LF study and 80x80mm coupons for a 2D LF study. The coupons were used to produce calibration data via simple 2D bends for the 3D study. A diode laser range finder, mounted on the z-axis of the LF system, was used to verify/measure the bend angles in 2D LF and also the surface shape in 3D LF, by using control software to create a co-ordinate measuring machine (CMM) set-up. The samples were held in place on the workstation table using a centre clamp; this required a hole to be drilled in the centre of the plates for a bolt to pass through.

Using an iterative approach based on the error between the current and desired surfaces it was possible to produce a component within -6.5mm and 0.1mm maximum error in 200x80mm AA 5251 at 400W. This demonstrated both accurate 3D laser forming and a means of distortion correction as the system can create a new strategy based on the current shape.

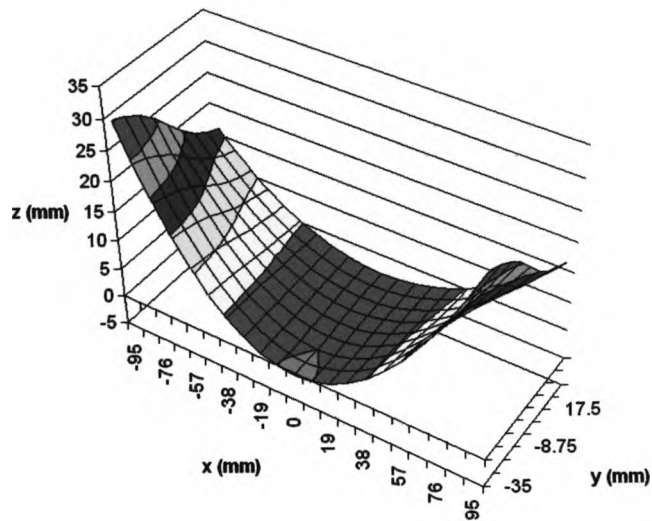


Figure 5.3.10: Desired shape for 80x200x1mm AA5251 being laser formed at a laser power of 400W

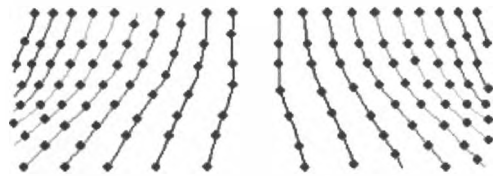


Figure 5.3.11: Irradiation strategy for first pass at 400W and 62mm/s

The irradiation pattern produced by the model has a more evenly spaced distribution than lines of constant height and a gradient increment of 73×10^{-3} . The minimum speed is set to 62mm/s to prevent damage to the surface. From the speed calibration this is expected to increase the gradient at each irradiation line by 40×10^{-3} .

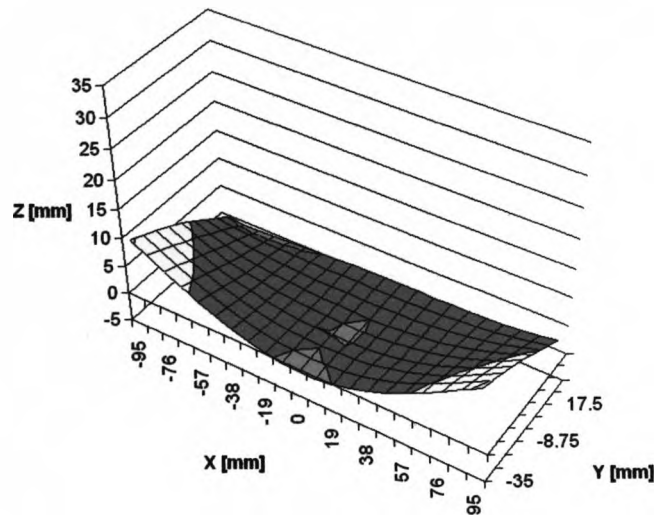


Figure 5.3.12: Height of measured points after pass 1 at 400W and 62mm/s

The irradiation successfully produces an evenly formed part that resembles the desired shape. However, much less forming than predicted by the model has occurred, with only approximately 16×10^{-3} increase in the gradient at each line. This is to be expected as the speed calibration is taken from the forming of a 2D samples which requires less strain to form than a 3D sample with curved lines. This reduces any risk of over forming and allows the piece to form in ever decreasing increments to its desired shape.



Figure 5.3.13: Irradiation strategy for pass 2 at 400W and 62mm/s

The irradiation pattern produced by the model for the second pass is similar to the first suggesting the initial pattern is correct. There are some subtle changes, especially around the centre; this is where the work-piece is clamped. The restriction of the clamp at this point is reducing the amount of forming and the model is trying to counteract this by producing an irradiation path in this area. The gradient increment between the irradiation lines for pass 2 is 57×10^{-3} . The speed is the same as pass 1, 62mm/s. This is because the speed to produce a 57×10^{-3} gradient is below the minimum speed.

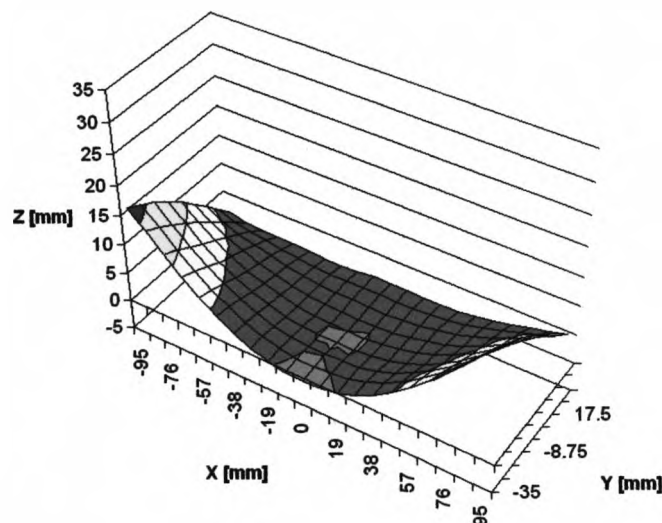


Figure 5.3.14: Height of measured points after pass 2 at 400W and 62mm/s

The change in gradient increment between the irradiation lines after the second pass is approximately 11×10^{-3} . This has decreased again for the same speed. This happens for two main reasons. The irradiation lines are becoming less linear requiring more strain to bend the work-piece and with approximately 20 passes from the first pass the piece may be

undergoing some of the effects of multiple irradiation passes such as strain hardening.

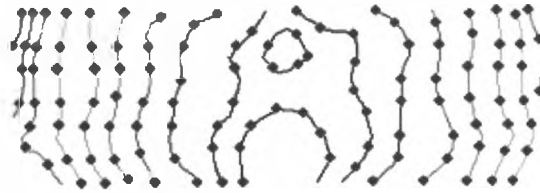


Figure 5.3.15: Irradiation strategy for pass 3 at 400W and 62mm/s

For the third pass the irradiation lines can be seen to become much less linear and the distribution is becoming more concentrated around the edges of the piece. As this is the non-developable area of the desired shape it is more difficult to form, as it requires some in-plane strains. The model recognises that this area isn't forming as much so therefore asks for more forming at this point. The same is happening at centre due to the clamp restricting forming. The increment between the lines here is a gradient of 46×10^{-3} .

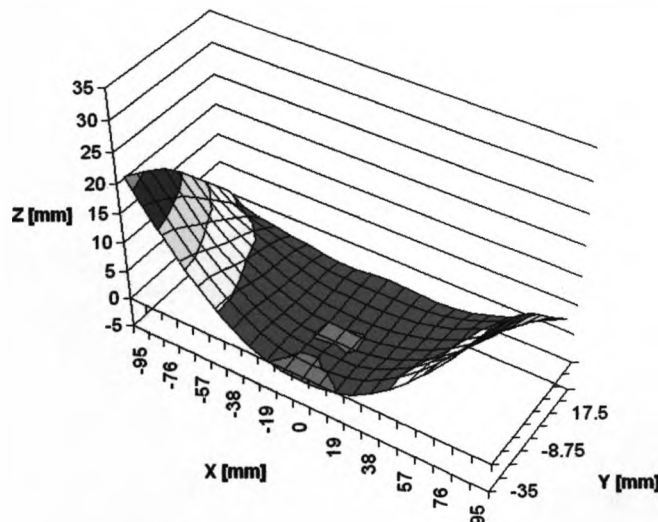


Figure 5.3.16: Height of measured points after pass 3 at 400W and 62mm/s

The change in increment of gradient between the lines after pass 3 is approximately 6×10^{-3} . This has reduced again showing that the factors responsible for this are cumulative increasing the number of passes required. The shape being generated is correct however.

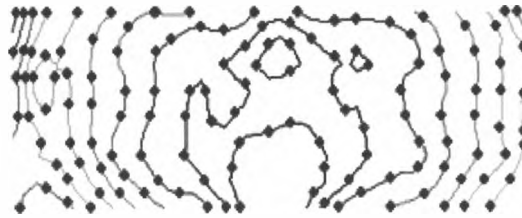


Figure 5.3.17: Irradiation strategy for pass 4 at 400W and 62mm/s

The fourth irradiation strategy performed has a gradient increment between the lines of 40×10^{-3} . Again the irradiation lines are becoming more erratic as the work-piece reaches its final shape. This is because as the gradient increment decrease so does the scale and the model attempts to correct smaller faults in the piece.

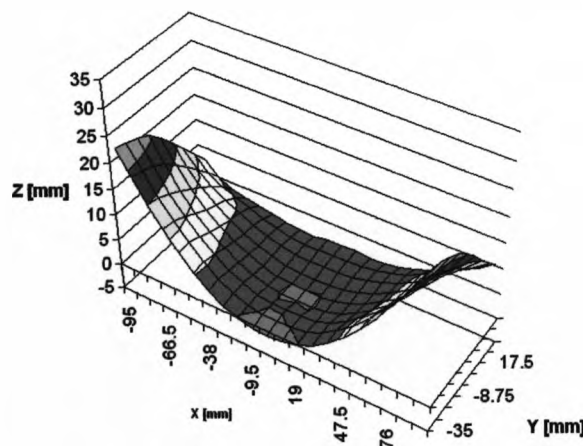


Figure 5.3.18: Measured points after pass 4 at 400W and 62mm/s

The final pass results in a change in gradient increment of approximately 0.2×10^{-3} . It may be possible to avoid the cumulative effects of multiple passes by increasing the number of irradiation lines and achieving the maximum amount of forming in the initial pass leaving the last few passes for fine adjustment taking advantage of these small increments that are now possible



Figure 5.3.19: Irradiation strategy for pass 5

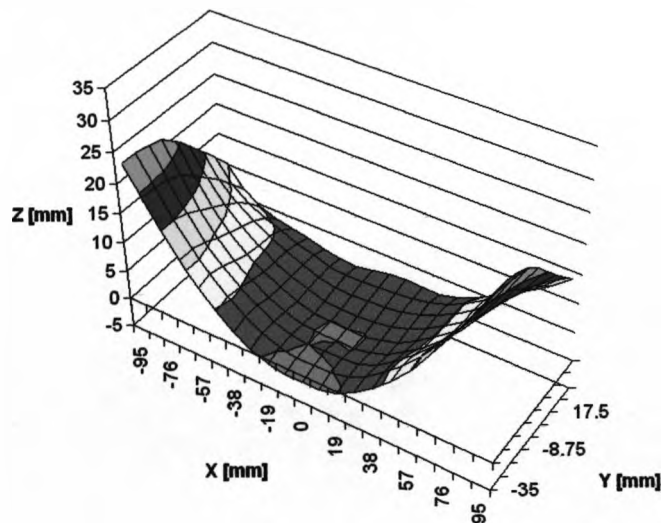


Figure 5.3.20: Final measured shape for 3D semi-developable forming of AA5251 at 400W

The error between the final shape (figure 5.3.20) and the desired shape shows a maximum error of 5 and -2mm (figure 5.3.21). This error is coming to the limits of the model as more in-plane strains are required.

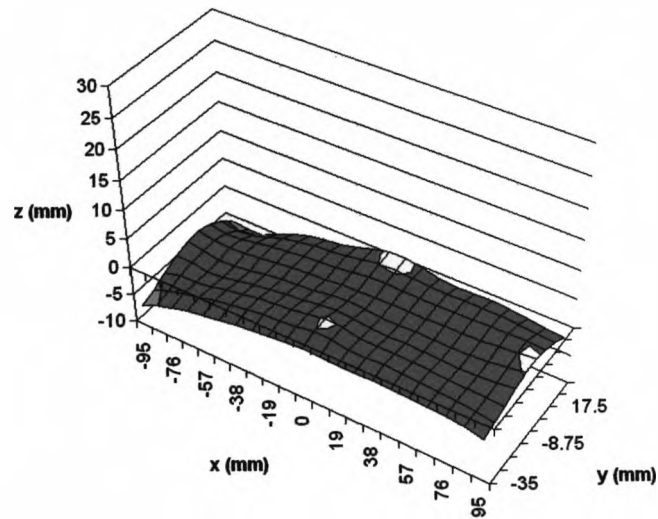


Figure 5.3.21: Error between desired shape and final shape of 200x80x1mm AA5251 at 400W, beam diameter of 3mm and a speed of 62mm/s



Figure 5.3.22: Heavily faceted component resulting from the initial strategy chosen

A drawback, to this strategy produces a heavily faceted piece with dwell marks, where the material has melted (figure 5.3.22). Areas at the end of the irradiation lines are viewed under a microscope to determine the affects of the dwell marks. The cuts for both samples are shown in figure 5.3.23.

In sample 1 it can be seen that melting has occurred (figure 5.3.24). This has caused some damage to the surface and altered the microstructure of the work piece. In sample 2 the heat input is more substantial. This is visible with a deeper penetration of the heat affected zone (HAZ) and a more distinct melt area (figure 5.3.25). This also shows a crack in the melt area.

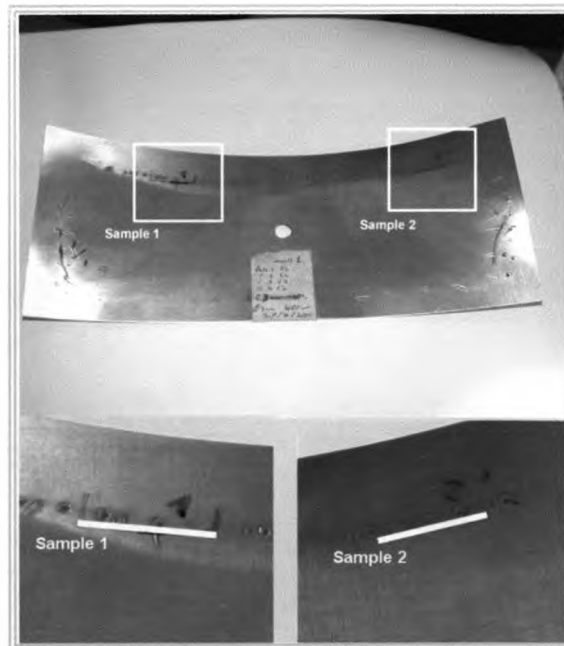


Figure 5.3.23: The selected area for analysis of sample 1 and 2

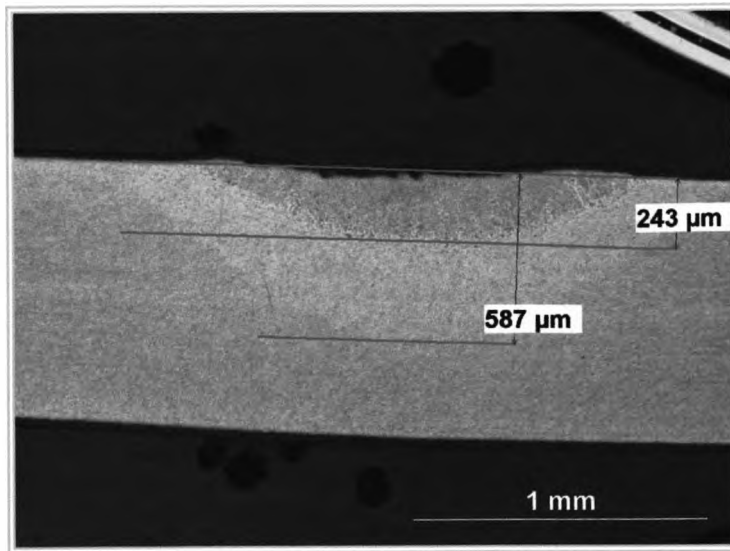


Figure 5.3.24: Magnified cross section of dwell point from sample 1.

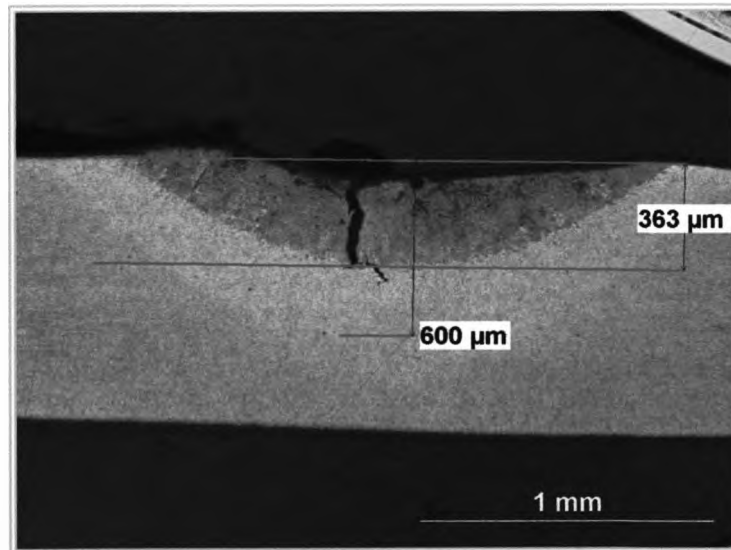


Figure 5.3.25: Magnified cross section of dwell point from sample 2.

Using the geometry based model it has been possible to form 200x80x1mm AA5251 at 400w with a 3mm beam diameter to within an error of 5 and -2mm. The piece became faceted and the dwell points caused areas to melt on the surface which in some cases also caused cracking. A solution to this is to decrease the power and increase the number of irradiation lines which reduces the energy required for each line and will create a smoother less faceted shape.

Another problem here is the decrease in the amount of forming in each pass with the same parameter. A reason for this is camber distortion from shrinkage in the traverse direction of the scan line^{33, 43}. This causes the irradiation lines to curve. As the curvature of the lines increases with each pass the work-piece appears to become more difficult to form. This is because a curved irradiation path is trying to bend the material in a traverse direction, to remove the distortion. This increase in the amount of strain the irradiation path is trying to produce decreases the amount of bend angle formed. To add to the effect this material is cold and more difficult to bend.

An associated problem with this is that as the actual shape reaches the desired shape the irradiation strategies become more erratic. This causes a further decrease in the amount of forming, which can be a benefit when very close to the final shape, but it begins at a point where there is a gradient of 39.2×10^{-3} to be formed at each point across the sheet. This is due to small defects in the forming process being seen by the model. These defects seem to be non-developable and therefore require the in-plane strain to be removed. Continuing with the process may have eventually removed these defects. This however would have increased processing time for minimal result.

An increase in the number of irradiation lines will help solve this as less forming is required per line increasing the processing speed. This develops a better temperature gradient and therefore decreases the amount of shrinkage in the traverse direction which is a cause of edge effects.

Here the work-piece formed less and less with each pass with a constant processing speed. A number of reasons for this can be attributed the same causes of fall off in multiple pass 2D laser forming, discussed earlier. Each pass has a series of 20 lines equating to about 100 passes in total. The effects of multiple pass 2D laser forming are:

- Section thickening
- Variation in absorption
- Strain hardening
- Thermal effects
- The change in the geometry of the beam

Although this is not the same condition as passing over the same line 100 times most of the factors involved are applicable. Because the same processing line isn't irradiated for every pass strain hardening, variation in absorption and section thickening will have an effect, though a smaller effect than in 2D laser forming. Thermal effects and the change in geometry of the beam will all have a significant effect and can go some way in explaining this drop off in forming.

Due to the nature of having many lines in a single pass of the work-piece the thermal effects can be vastly increased. Where normally a pause is normally experienced after each pass in 2D laser forming here it is almost continuous throughout the pass. This increases the temperature of the

whole work-piece potentially making it more difficult to initiate a temperature gradient^{47, 113, 116-118}. Because of this the number of irradiation lines and the spacing between them can have an effect on the amount of forming possible. However, this is not a cumulative effect, unlike the others, as the work-piece is allowed to cool after every pass.

5.3.2.2 3D Laser Forming Fabrication of Semi-Developable Shape in 1mm Thick 80x 200mm Aluminium at 200W

To prevent further faceting and melting the irradiation paths are expanded across the width to allow the paths to start and stop off the work-piece removing the dwell points.

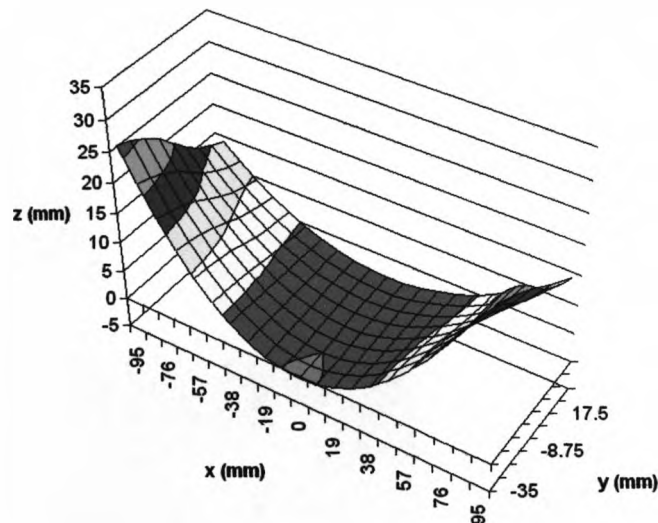


Figure 5.3.26: Desired shape for 200x80x1mm AA5251 being laser formed at a laser power of 200W

Also the power is reduced to 200W and the speeds are decreased to achieve the same amount of forming. This produces a component to within +/- 5mm of the desired shape and just about visible witness marks. The desired shape has been reduced in size to a maximum height of 30mm (figure 5.3.26) and the number of irradiation lines is doubled to 40 (figure 5.3.27) in an attempt to form the piece as much as possible in the first pass. This avoids the correction of edge effects which is a factor in the reduction in the amount of forming in subsequent passes. The speed has also been reduced to 10% less than the predicted. This is done to increase the amount of forming in an attempt to form the piece in as few passes as possible.

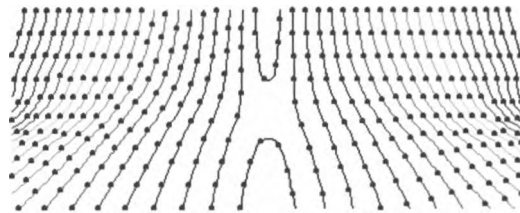


Figure 5.3.27: Pass 1 irradiation path at 200W and 25mm/s

The irradiation pattern produced by the model has a gradient increment of 27.4×10^{-3} . The process speed chosen by the model is 25mm/s.

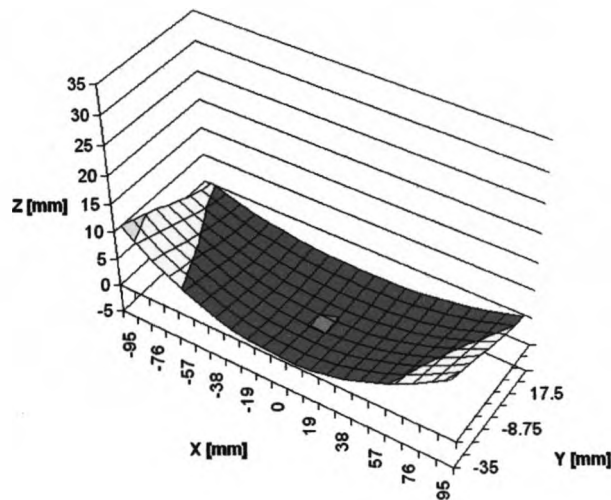


Figure 5.3.28: Height of measured points after first pass at 200W and 25mm/s

The first irradiation pass forms a shape resembling the desired shape. Each line has formed by a gradient magnitude of approximately 7.5×10^{-3} . Again this is much less than the 27.4×10^{-3} gradient magnitude that is predicted by the speed calibration, even with the decrease in speed.

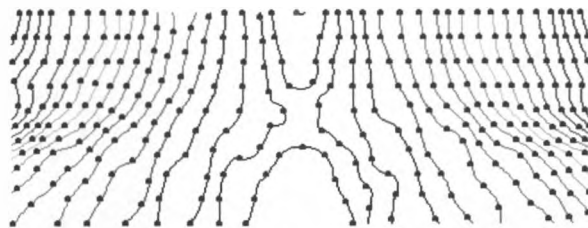


Figure 5.3.29: Pass 2 irradiation strategy at 200W and 28mm/s

The irradiation strategy for the second pass produced by the model has a gradient increment of 19.9×10^{-3} . The process speed chosen by the model is 28mm/s. The edge effects don't appear to be as much of a problem before. It can be seen here (figure 5.3.30) that the irradiation pattern has kept most of its shape when compared to the second pass in the previous experiment at 400W with 20 irradiation lines.

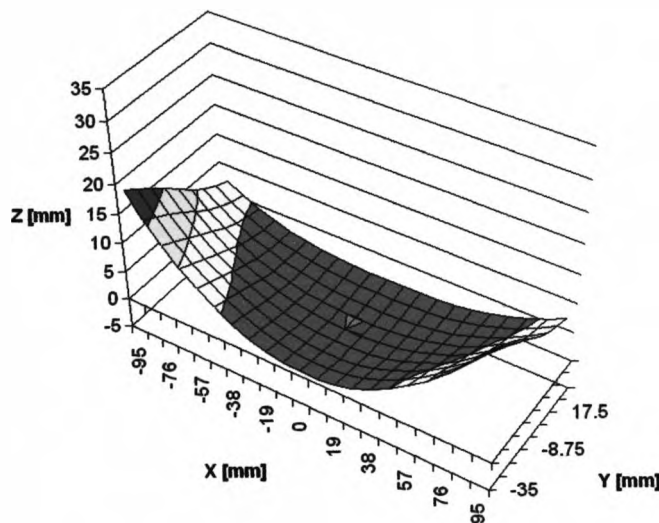


Figure 5.3.30: Height of measured points after pass 2 at 200W and 28mm/s

The change in the increment between the lines of constant gradient is approximately 7.7×10^{-3} after the second pass. Again this is not as much as the speed selection predicts but it is the same as the previous pass, unlike the previous experiment where the amount of forming reduced with the same speed. An explanation for this is that the irradiation pattern has kept most of its original shape. Factors in this are the increased number of lines decreasing the gradient increment between them requiring less energy. This therefore increasing the speed, together with the reduction in power this has produced more of a temperature gradient mechanism and

less of an upsetting mechanism than in the previous experiment reducing the amount of edge effects.

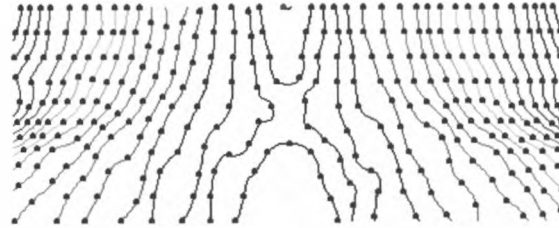


Figure 5.3.31: Pass 3 irradiation pass at 200W and 31mm/s

The irradiation strategy for pass 3 has an increment between the lines of constant gradient magnitude of 12.2×10^{-3} . Again most of the shape of the original pattern has been maintained. There is a small effect in the centre from the clamping beginning to restrict forming in the piece.

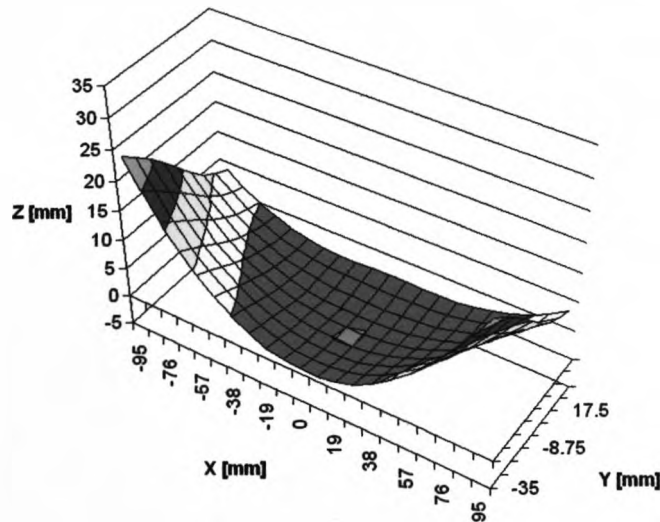


Figure 5.3.32: Height of measured points after pass 3 at 200W and 31mm/s

The change in gradient magnitude here is approximately 4.3×10^{-3} . Again lower than expected and a decrease in the amount of forming compared

to the previous pass which can be expected with a 3mm/s increase in speed.

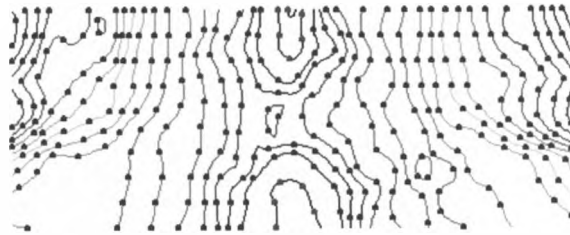


Figure 5.3.33: Pass 4 irradiation strategy at 200W and 32mm/s

The fourth irradiation strategy is starting to become erratic, though this appears to be more the effects of the clamp and the difficulty in forming the non-developable areas rather than the edge effect as experienced in the previous experiment. The gradient increment between the lines is 7.9×10^{-3} for this pass.

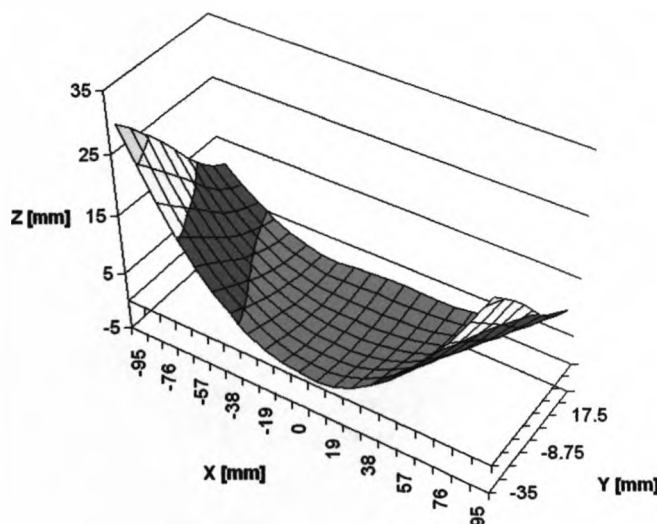


Figure 5.3.34: Final geometry produced. 200x80x1mm AA5251, 200W, 3mm beam diameter, speed range 25-32mm/s.

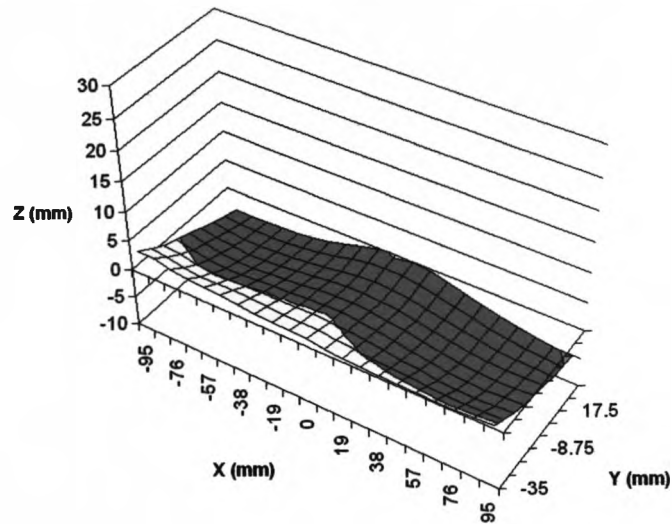


Figure 5.3.35: Error between desired and final shape in 200x80x1mm AA5251 at 200W 3mm beam diameter and speed range of 25-32mm/s

The error between the final shape and the desired shape is 3.8 and -5.2mm. This is similar to the error in the previous experiment. The main benefit of this method compared to the previous experiment is the improved consistency of the irradiation strategy due to the improved TGM with the greater number of irradiation lines.



Figure 5.3.36: Picture of final shape 200x80x1mm AA5251, 200W, 3mm beam diameter, speed range 25-32mm/s.



Figure 5.3.37: Marks from the 3D forming of 200x80x1mm AA5251 at 200W and a speed range of 25-32mm/s

The final piece has formed the required shape with minimal visible effects from the laser forming process. The part is smooth and isn't faceted, like the previous experiment at 400W. The witness lines are

barely visible and the dwell points have vanished with irradiation lines now starting and finishing off the work-piece (figure 5.3.37).

By increasing the number of irradiation lines and decreasing the power a more evenly formed shape is possible without any evidence of faceting. By increasing the size of the irradiation strategy it has been possible to remove any dwell. However the method of doing this isn't ideal as the irradiation strategy is stretched this may cause problems in the final pass where more subtle forming is required. A better method of increasing the length of the lines is needed.

By encouraging more of a temperature gradient less forming occurs at each line but the edge effects caused by traverse shrinkage of the line are reduced giving more consistent irradiation patterns than in forming at 400W with less irradiation lines.

5.3.2.3 3D Forming of Semi-Developable Shape in 1mm Thick 400x 200mm Aluminium 5251 at 200W

200W is used again with no reduction in speed from the speed section values. The irradiation strategy was increased in width to avoid dwell points but the irradiation paths in most cases still started and finished within the area of the work-piece. In this experiment there is a great deal more forming than expected with over forming occurring in 2 passes. The final shape has an error of 7.2mm and -11.6mm.

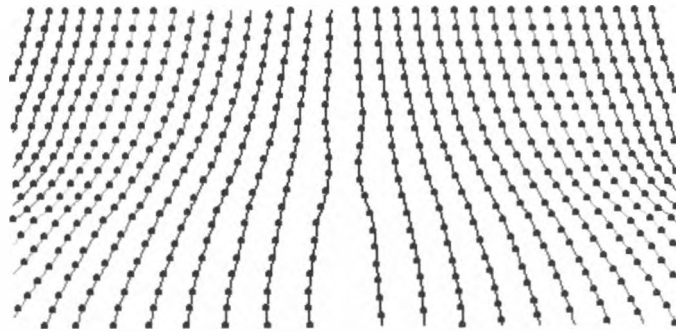


Figure 5.3.38: Pass 1 irradiation strategy for forming of 400x200x1mm AA5251 at 200W

The first irradiation strategy has an increment between the lines of constant gradient magnitude of 19×10^{-3} . This is much less than the previous two experiments due to the increase size of the sheet and the same height in desired shape as the previous experiment. The speed selected for this strategy is 31.4mm/s.

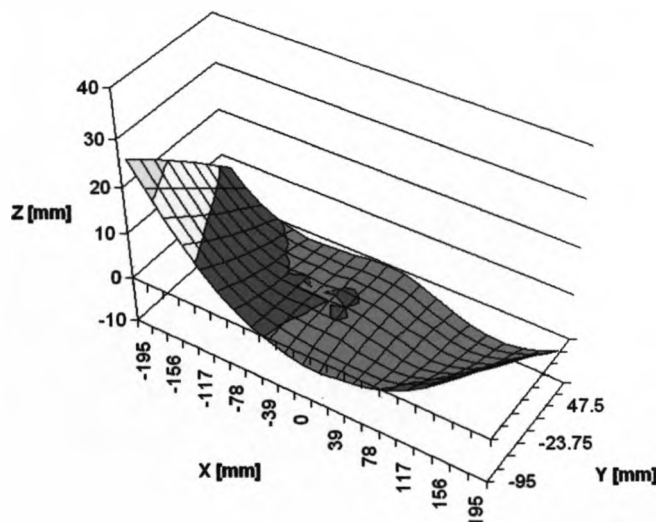


Figure 5.3.39: Measured point after pass 1 for forming of 400x200x1mm AA5251 at 200W

The beginnings of the desired shape is formed after the first pass but an uneven shape has been formed with 25mm in height on one side and

15mm in height on the other. The approximate decrease in gradient after the first pass is 8.81×10^{-3} . Even without the 10% reduction in speed used in the previous experiment at 200W this is much more forming than in previous experiments at this speed. This is due to the increased width of the work-piece giving a different temperature field due to the increased amount of material and also strain at the centre of the piece is different due to restraints caused by the increase in material⁶.

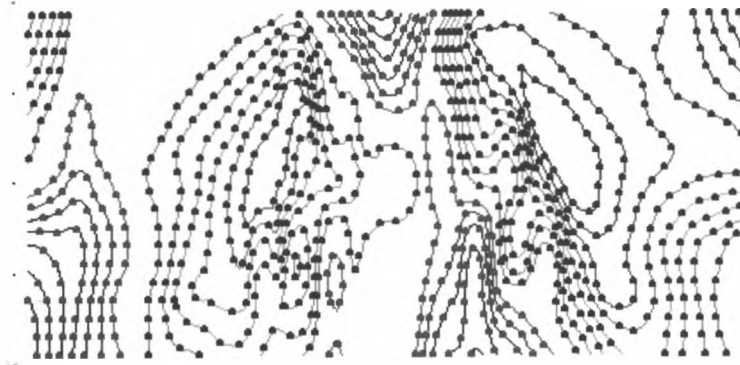


Figure 5.3.40: Pass 2 irradiation strategy for forming of 400x200x1mm AA5251 at 200W

The second and final irradiation strategy has an increment between the lines of constant gradient magnitude of 10.22×10^{-3} . This requires a speed of 35.9mm/s. We can see here that the model sees that the left side has over formed and areas at the centre as it wants to form on the reverse side of the work-piece, these are shown in red.

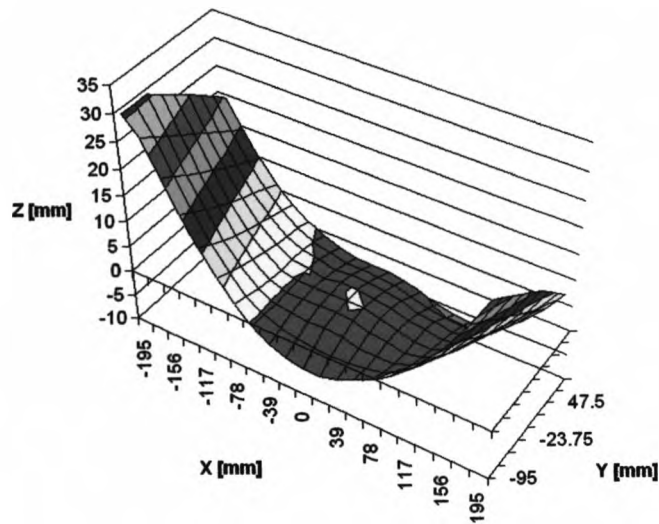


Figure 5.3.41: Final geometry produced after second pass.
400x200x1mm AA5251, 200W, 3mm beam diameter, speed 29mm/s.

As can be seen in figure 5.3.41 the part has formed the basic shape but is uneven and has over formed on one side. This distortion is difficult to remove as the centre requiring in-plane strains for this to be removed.

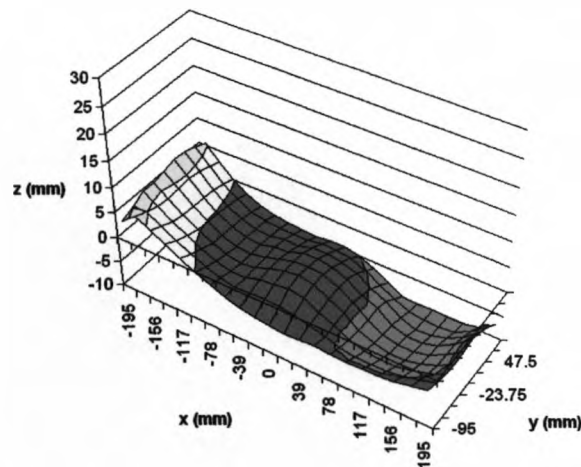


Figure 5.3.42: Error between the final and desired shape for
200x400x1mm component formed at 200W



Figure 5.3.43: Marks from the 3D forming of 400x200x1mm AA5251 at 200W and a speed range of 31.4-35.9mm/s. The marks on the left are where the piece comes into the focus of the laser beam.



Figure 5.3.44: Picture of final shape 400x200x1mm AA5251, 200W, 3mm beam diameter, speed 29mm/s.

The basic shape has been formed with a smooth surface and no faceting. There is some visible damage where the part has come into focus. The

dwell points can be seen as most of the irradiation paths started and finish on the work-piece. However at 200W these dwells, though visible appear to have caused a lot less damage than in the experiment using 400W.

Another reason for over forming was that the part moves into focus as it is formed, which reduced the spot size and increases the intensity on the outer paths, this also causes some melting (figure 5.3.43). A solution to this would be to start the scan path at the outside and working inwards, the laser then passes over sections that have not yet moved. This will reduce the increase in forming due too moving into focus. This doesn't happen in previous experiments as they are formed from the outside in to avoid this.

The reason this piece was formed in this direction is because in initial experiments on pieces this size resulted in stresses building towards the centre of the work piece. For these cases the piece would form normally initially and as the irradiation pass moved towards the centre a build up of stresses would cause it to begin to move downwards at the start of an irradiation line and popping up by the end of the line. This popping upwards eventually stopped resulting in the whole piece bending away from the laser. Forming from the centre out was a quick solution to this. A possible reason for this is that with longer irradiation lines the amount of traverse shrinkage will be increased. This effect will increase with each line passed. As this build up increase towards the centre a force is exerted onto the clamp eventually causing the piece to bend down. When forming from the inside out the strains caused by this effect though initially restricted by the clamp build up outwards and are free to move. Further work is needed to verify this.

To laser form larger components in this case isn't as simple as just increasing the size of the irradiation pattern. There are variations in the effects of laser forming of different dimensions. Vollertsen describes these influences of geometry of the work-piece⁶. For this case the thickness of the material is the same as the previous experiments but the width and length has altered. Vollertsen tells us that an increase in width can increase forming by a factor of 3. We do not see that here but we do see that the amount of forming per pass has certainly increased compared to the experiments on the smaller pieces. With the resultant forming being half of what is predicted by the speed calibration data which is double the amount of forming when compared to the previous experiment at 200W which formed approximately a quarter of the predicted amount in the first pass.

Overall for 3D forming of semi-developable shapes the predictive/adaptive model produced the desired shape using a pass by pass approach with lines of constant gradient magnitude as an irradiation path and using the increment between these lines to define the process speed. The model formed, in increments, towards the desired shape evenly across the whole surface without significant over forming at the edges. The adaptive nature of the model takes into account any residual stress of material non-uniformity as it increases the number of scan lines in problem areas, such as the more non-developable areas and the area restricted by the clamp.

5.3.3 Laser forming for the correction of distortion in aluminium structures

The need for correction of distortion in aluminium components arises from factors such as the accumulation of various process tolerances during production, unwanted distortion of the part shape that occur during or after processing (e.g. welding) with unpredictable and often irreversible effect, or deviation from design shape resulting from damage during operational service or storage (which may require remedial correction if its usefulness and value are to be maintained). Within this context, a process capable of achieving these actions in an automated, controlled and precise manner would be of significant benefit to industry. Remedial measures for distortion studied so far involve either increasing the rigidity of the structure during the stress-inducing process, through improved design and special clamping, or reducing the stresses through process modifications. However, there is currently no automated or controllable method for correction of the distortion either during or after processing of the structure. Although several techniques of stress reduction have been studied (including cold compression or stretching, thermal treatments and advanced ageing treatments), none have so far achieved full stress removal and all are limited in their flexibility of application. Because of this the following study has been conducted on the use of laser forming as a method of automated distortion correction.

In order to develop a corrective control strategy based on geometrical error it was necessary to investigate the capability of the laser forming process for the reversal or correction of negative deflections. These deflections were induced either mechanically (using a press tool) or by laser forming. It was discovered that, for 2mm AA5251, there was a limit to the amount of distortion that could be recovered by laser forming for a single bend location (figure 5.3.45). Research is ongoing to determine the reasons for this. Although this showed a potential limitation of the process, it was noted that for typical 3D distortion of a component due to say a welding operation the maximum bend angle at a given location is not likely to exceed 10 degrees. In addition, it was observed that the bend angle rate increased with increasing numbers of passes whilst the bend angle was negative (figure 5.3.45). This was, up till now, an unknown phenomenon in laser forming, where a decrease in bend angle rate with increasing scans was the norm. This was thought to be due to the additional moment required to be generated by the process for the geometry and also perhaps the angle of attack of the laser beam to the surface.

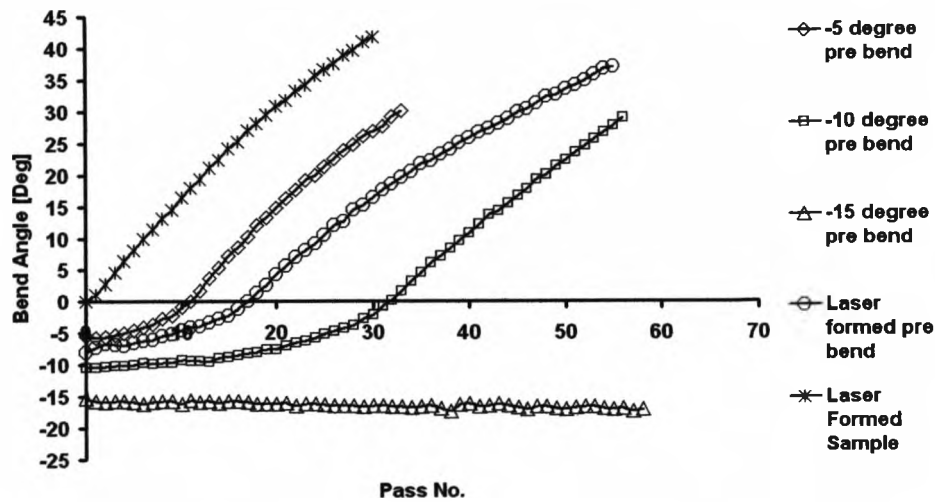


Figure 5.3.45: Reversal of process, laser formed and mechanically pre-bent samples (80x80x2mm AA5251; 900W; 45mm/s; 5mm beam diameter).

The geometry based model can be used in addressing the development of a laser forming system for automated correction of distortion and design shape. This also allows the presence of pre-existing residual stress in the parts to be taken into account, in that the internal stresses due to the previous processing history of the component material could not be guaranteed or closely predicted and it can be expected that much of the sheet material to be used will contain pre-existing residual stresses that influence the errors in a planned laser forming operation.

A strut component of 400x40x2mm AA5251 material was selected as being a generic part similar to chemically etched distorted components witnessed on the shop floor of aerospace partner companies visited during the investigation. A series of random non-uniform distortions were mechanically formed (by roller) on the struts (figure 5.3.46) and LF applied to try and 're-flatten' them in a controlled manner. Using the

iterative, corrective control method based on geometrical error and data calibration from previous tasks, it was possible to remove the distortion in these components and return them to the design shape (i.e. flat) to within a few millimetres of error.



Figure 5.3.46: Randomly mechanically distorted components (400x40x2mm AA5251).

5.3.3.1 Laser Forming for the Correction of Aluminium 5251 Strut Mechanically Deformed to 15mm

900W of laser power, a 5mm beam diameter and 20 irradiation lines with a speed 45mm/s for the first pass and 60mm/s for the second were used to flatten a 400x40x2mm AA5251 strut. The result produced a flat piece to within +/-0.5mm with melting at the dwell points. The speed was not adjusted from the predicted speed required, though a minimum speed of 45mm/s was selected.

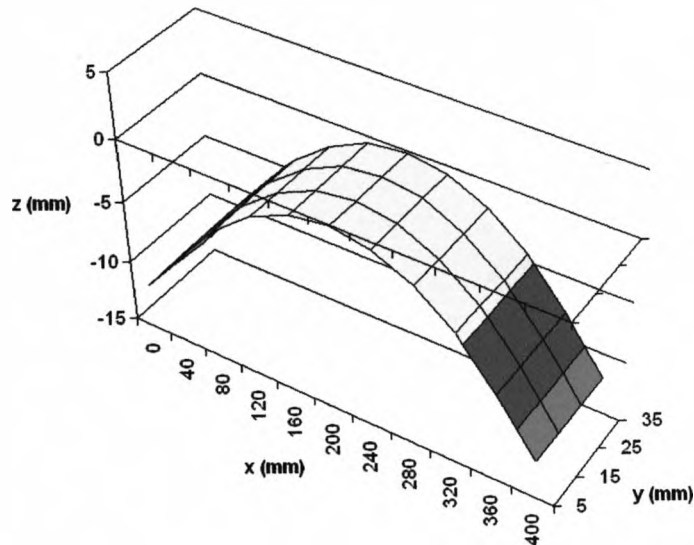


Figure 5.3.47: The starting shape to be flattened using the laser forming process

The initial shape was a reasonably even curve with a maximum magnitude of -15mm in height from the centre.



Figure 5.3.48: The irradiation strategy for the first pass

The first irradiation strategy calls for a process speed of 45mm/s, this is the selected minimum to try to avoid damaging the material, with a gradient increment of 42×10^{-3} between the irradiation lines. The slight irregularity at the edge of the irradiation may be down to the mechanical forming process.

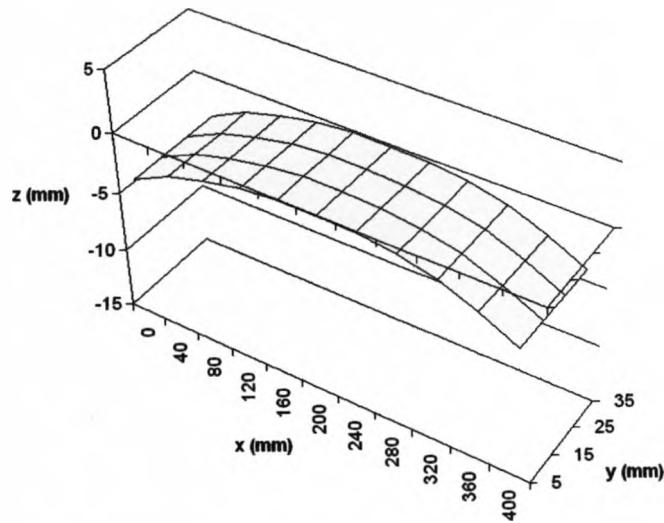


Figure 5.3.49: The measured shape after the first pass

After the first pass the strut can be seen to form evenly throughout reducing its maximum deformation to -4mm from the height at the centre. This has formed a gradient magnitude of approximately 26×10^{-3} . This value is much closer to the predicted amount from the speed calibration data than in any of the previous experiments. The combination of a much higher power on the thicker material will account for some of this. The main reason will be that this is very much developable forming.



Figure 5.3.50: Irradiation strategy for second pass

The second and final irradiation strategy has an increment between the lines of constant gradient magnitude of 16×10^{-3} . From this the model selects a speed of 60mm/s . This increase in speed can be seen on the irradiation strategy (figure 5.3.50) with the larger dots.

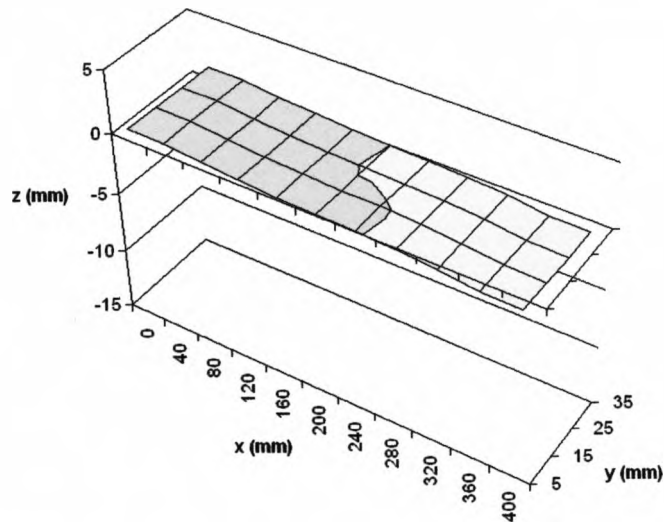


Figure 5.3.51: Final shape reached after second pass with approximately than $\pm 0.5\text{mm}$ error.



Figure 5.3.52: Dwell marks and irradiation lines left by the laser forming process

This strut reversal experiment successfully removed the distortion from the strut in 2 passes. However it did leave dwell marks (figure 5.3.52) which, as we know from previous experiments is undesirable, and the witness marks are more visible than in previous experiments. This is solved by increasing the width of the irradiation path to allow the start

and finish position to be off the work-piece and the minimum speed is increased to 62mm/s. The widening of the irradiation path is thought not to significantly affect the process as the struts are deformed in developable manner and therefore the irradiation is a series of straight lines across the work-piece. Also the higher speed will mean that more passes will be needed to correct the strut but with the advantage of minimising any material damage.

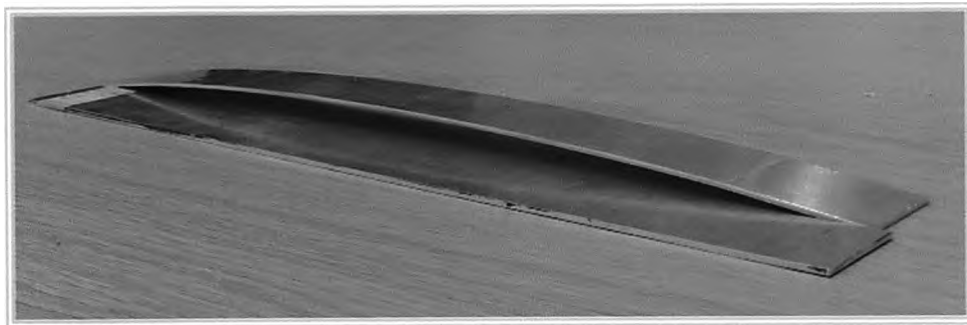


Figure 5.3.53: Flattened strut with an example of one of the pre laser formed struts with the same magnitude of mechanically forming

A significant result here is the amount of forming taking place in each pass. This is predicted by the speed calibration data a lot more accurately here than in the previous semi-developable experiments. This is because of the straight irradiation lines involved here. These don't require additional strains to create a bend, unlike a non-linear line. However the amount of forming is still lower than predicted. This can be accounted for by the same factors that influence multiple pass 2D forming as discussed earlier. With a multiple number of irradiation lines in a single pass the thermal effects of laser forming will have a greater effect than in 2D forming. This is because the dwell time between lines is smaller in comparison. This increases the temperature of the work-piece; this initially increases forming but at a certain point will increase the difficulty in producing a temperature gradient, which is essential for this

type of forming. This is however not a cumulative effect per pass as the work-piece is allowed to cool when it is measured, which takes a few minutes. It is difficult to tell how much the other influences on multi pass 2D laser forming are affecting the forming rate as the processing speed increases with each pass. The geometry of the beam will be changing across the work-piece more and more as it forms so there will be some influence from it here and also the work hardening of the work-piece will also be occurring though less than in 2D forming as the work hardening is spread across the piece unlike 2D forming. This also applies to the decrease in absorption due to the coating burning off and section thickening.

5.3.3.2 Laser Forming for the Correction of Aluminium 5251 Strut Mechanically Deformed to 45mm

Here the deformation is much greater than in the first experiment with a maximum deformation of approximately 45mm (figure 5.3.54). Again the desired surface is flat and the error between this and the actual deformed surface is used to create the irradiation strategy. A minimum speed of 62mm/s is selected to prevent any damage to the surface. The starting shape in this case is distorted unevenly with a maximum of -45mm on one side and -23mm on the other.

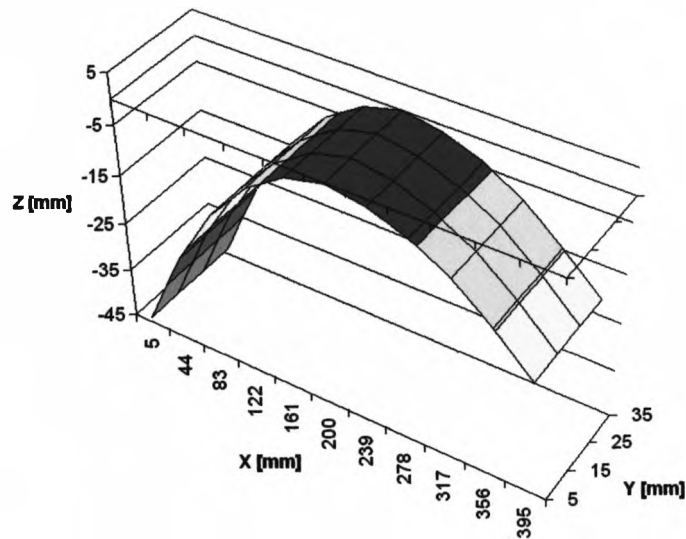


Figure 5.3.54: Aluminium strut deformed mechanically to a maximum deformation of -45mm from the height at the centre.

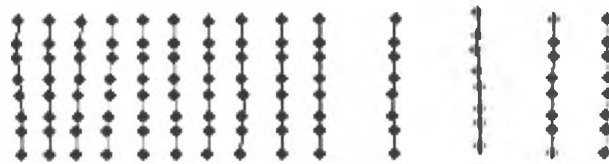


Figure 5.3.55: The irradiation strategy for the first pass.

As can be seen here the model recognises that the surface has an uneven distortion and calls for more irradiation lines at the end with the greater distortion. The increment between the irradiation lines here is 40×10^{-3} . The minimum selected speed, 62mm/s, used for this irradiation pass.

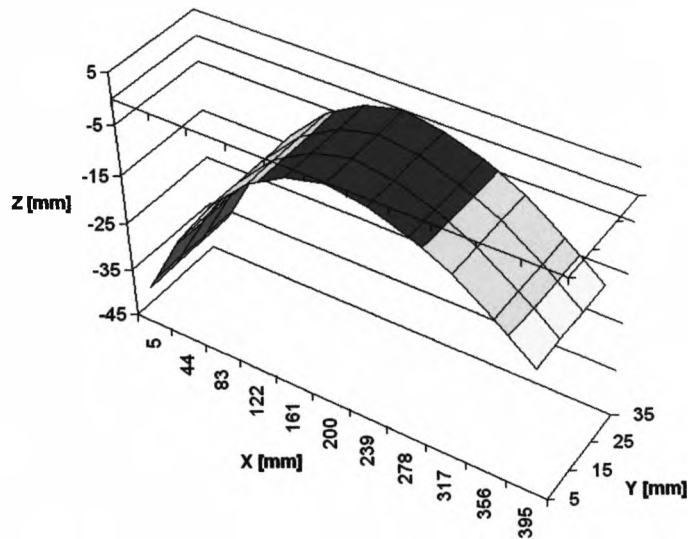


Figure 5.3.56: The result of the first pass

The resultant measurement shows a strut that has evenly formed with a change in gradient magnitude at each irradiation line of approximately 7×10^{-3} . This change is slightly lower than the speed calibration data would predict but is still closer than in the previous semi-developable forming experiments.

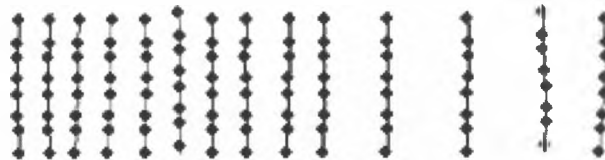


Figure 5.3.57: Irradiation strategy for the second pass

The irradiation strategy for the second pass is almost identical to the first with very subtle changes. This is a good sign as it shows the part is forming evenly throughout. The increment between the lines here is 33×10^{-3} with the speed at the selected minimum of 62mm/s.

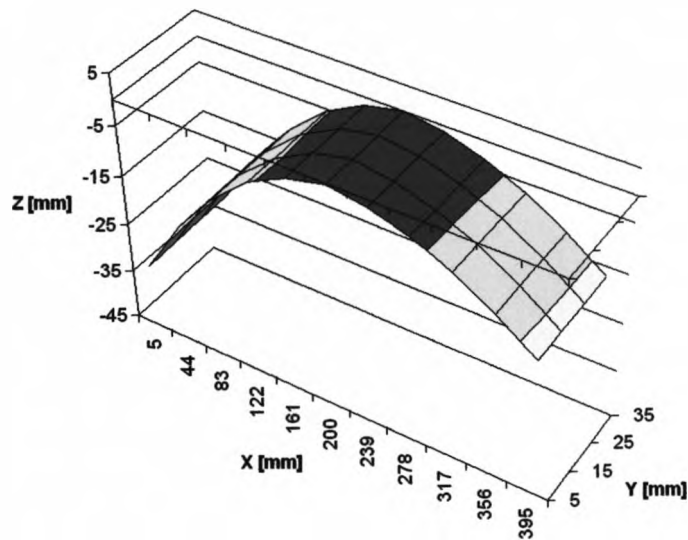


Figure 5.3.58: Resultant measurement from pass 2

Again the part as formed evenly here with an approximate decrease in gradient magnitude of 4×10^{-3} . This is similar to the change in the first pass.

This result remains constant until pass 6 where the first drop in speed occurs. As can be seen the irradiation pattern has change a minimal amount from the first irradiation pattern. A full pass by pass account is shown in appendix V. This shows a very even forming of the strut. The speed for this strategy is 62.2mm/s and the increment between the lines of constant gradient magnitude at this point is 18×10^{-3} .

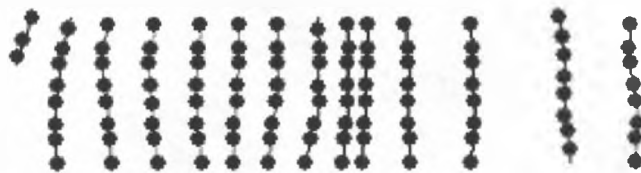


Figure 5.3.59: Irradiation strategy for pass 6

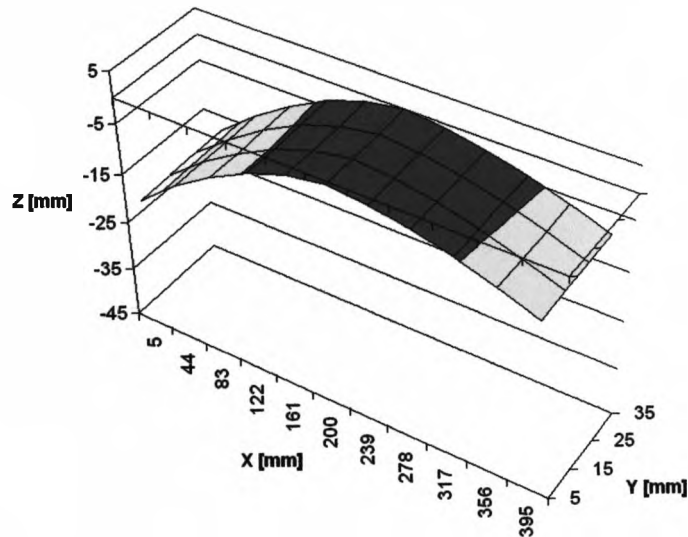


Figure 5.3.60: The resultant measurement from the sixth pass.

The strut at this point has a maximum deformation of -18.8mm one side and -9.9mm on the other. The change in gradient magnitude at each line form pass 5 is approximately 3×10^{-3} .

The irradiation pattern doesn't change much for the next few passes with the speed gradually increasing at each pass. For pass 10 the speed is 70.5mm/s with an increment between the lines of constant gradient of 10×10^{-3} .



Figure 5.3.61: Irradiation strategy for pass 10

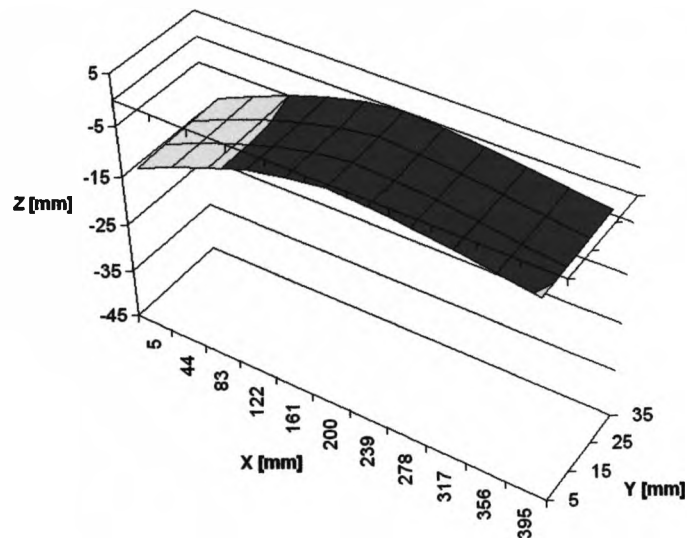


Figure 5.3.62: Resultant measurement from pass 10

A large drop in error from the starting shape can be seen here with a maximum deformation of 11.8mm and 5.3mm on either side of the strut. The change in the gradient magnitude at each line is approximately 2×10^{-3} .



Figure 5.3.63: The final irradiation strategy at pass 14

The final pass can be seen to start to be erratic, this is however after 13 passes and is to be expected as the piece has had about 260 irradiation lines passed over it and edge effects start occurring. This pass is

completed at 79.3mm/s with an increment between the lines of constant gradient magnitude of 4×10^{-3} .

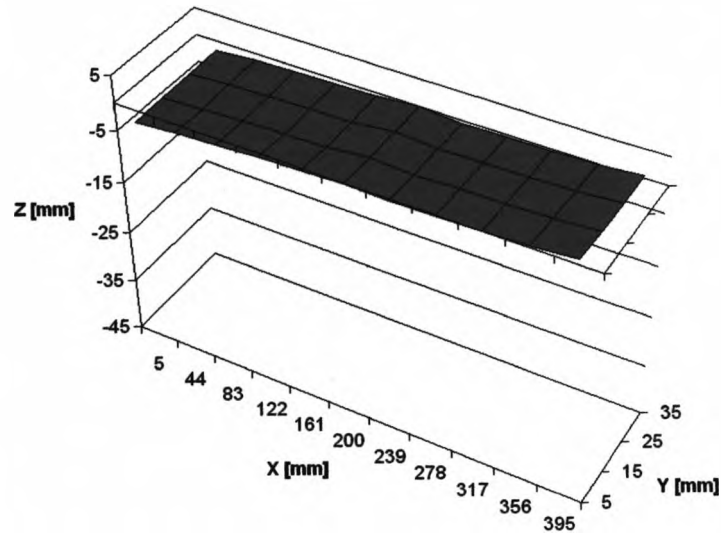


Figure 5.3.64: The resultant measurement of the final pass.

This is a strut that is now 2.1mm and 1mm away from flat at each end. The final pass changed the gradient increment at each line by approximately 2×10^{-3} .



Figure 5.3.65: Strut with maximum 45mm mechanical deformation



Figure 5.3.66: Strut after laser forming correction

The final piece has been corrected to within 2.1mm in 14 passes with 900W of laser power and a 5mm beam diameter with a processing speed range of 62mm/s – 79.3mm/s. The final piece has barely visible irradiation lines and no dwell marks. 14 passes may take too long to perform for it to be of use in industry. However this can be easily solved with an increase in irradiation lines.

Though the speed calibration data has not been accurate for these experiments it can be seen in figure 5.3.67 that it has been of use as the increase in process speed as the final shape approaches decreases the amount of forming to prevent over forming. An improvement in the speed calibration is needed to decrease the number of passes used to flatten a strut.

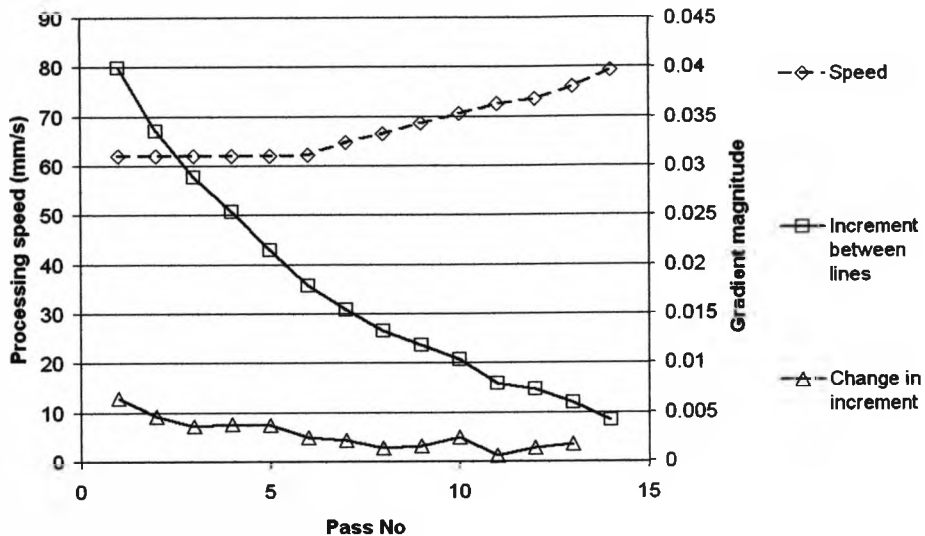


Figure 5.3.67: Increasing speed over 14 passes and resultant change in the increment between the lines of constant gradient for strut reversal experiment

Forming in the strut reversal experiments have been closer to the predicted amount of forming expected by the model than in semi-developable forming. The reasons behind this are that the majority of forming in strut reversal is developable and consists of easily formed straight bends, unlike semi-developable forming. Also for the strut reversal the material is thicker allowing for a temperature gradient to be initiated in a wider speed range.

Like semi-developable forming shrinkage in the irradiation lines in the traverse direction causing bending in this direction is a problem. This however was a greatly reduced problem in this case. The only obvious signs of this happening were after 10 passes. Because of the increased

thickness of the part in this case, 2mm instead of 1mm for semi-developable forming, shrinkage along the irradiation line is decreased because the irradiated material has to counteract a lot more cold material to bend in the traverse direction. This is also reduced because the strut is half the width of the 1mm aluminium parts and therefore the irradiation lines are shorter allowing for less shrinkage along the irradiation line in total.

5.3.4 Discussion on the Geometry Based Model

It is possible to produce parts in AA5251 using laser forming that have a good finish with minimal damage to the part. It is necessary to limit the heat input in localised areas removing the dwell on the work-piece and to increasing the speed. It is still possible to produce a significant amount of forming and not damage the surface by increasing the number of irradiation lines.

A geometry based model can produce semi-developable shapes and also correct distorted struts to within millimetres. Irradiation strategies can be produced in seconds using a simple height measurement across the work-piece and geometrical calculations. This is a versatile technique that has the potential for many applications. This model is useful for use in the correction and fabrication of developable or semi-developable shapes. More work is needed to be able to produce non-developable shapes to the accuracy.

The use of lines of constant gradient magnitude as a means of defining the irradiation path and the increment to determine speed worked well.

Any problem related to over forming in the original model has been solved using this method. All parts formed evenly, apart from areas of difficulty like non-developable areas or areas around the clamp. The speed selection is still a problem. Though the increase in speed had the desired effect in the final stages of reaching the desired shape by not causing any over forming, the predicted amount of forming was always much higher than the real amount of forming that took place.

The decrease in viewable area worked well for these experiments. The use of it was subtle for most of it and wasn't necessarily required for these applications as the size of the components or the amount of forming required would have meant that without it forming still would have been possible. Also with the increasing in size of the irradiation paths to prevent dwell points on the work-piece the decrease in viewable area calculation became less important.

In all the investigations a problem encountered is that a 2D forming produces a 3D result. Camber distortions are often found to cause problems, especially when approaching the final shape. These distortions often affect the irradiation strategy. A solution is to keep the increment constant decreasing the number of lines as the part forms. This allows for an ideal processing parameter for producing a temperature gradient to be used, as the speed will be constant for the whole process, and also allows for minor distortions which can often mask larger distortions, when close to the final shape, to be ignored.

The effects of heat build up in the part also have an effect on the forming. This is a factor in multiple pass 2D laser forming¹¹³. For a number of irradiation lines in close proximity and passed barely seconds apart this effect may be increased. More investigation is needed on this as the number of irradiation lines in a pass may be limited by this factor.

It is recommended that future work into further modification include work to improve the accuracy of the speed calibration data and also a method for larger magnitude non-developable forming, possibly using Gaussian curvature, which would not only improve non-developable capabilities of the model but also make it possible to produce developable shapes with increased accuracy. A combination of these would vastly increase the potential of a geometry based model.

Chapter 6

Conclusions

6.1 Geometrical Influences on Multi-Pass Laser Forming

This investigation looked at the variation in bend angle achieved per pass (or bend angle rate) during multi-pass laser forming along a single irradiation track (producing a positive bend), in particular the

decrease in bend angle per pass after many irradiations for a given set of process parameters consistent with the TGM⁶.

There are a number of conclusions from the work presented in here, these include:

- An additional influencing factor was proposed in this work. From the analytical and empirical data presented it was shown that the bend angle per pass, when laser forming employing a cantilever or edge clamp, is influenced by the formed bend angle.
- It was shown that as the bend angle increases the incident laser beam geometry is distorted, resulting in an effective increase in the beam area, a reduction in the incident energy fluence and hence a reduction in the resultant bend angle per pass.
- A prediction of the bend angle based on this phenomenon was shown to be reasonably close to experimental data in terms of the prediction of bend angle per pass fall off at higher number of passes. As a result this effect must be considered to be a highly influential factor in the fall off in bend angle per pass based on the presented data.
- The experimental V block data after an initial fall off up to 25 passes exhibited little or no fall off in the bend angle per pass for the remaining 35 passes. This appeared to confirm the significance of the geometrical effect of the component distortion influencing the process parameters i.e. energy fluence, in that by eliminating or reducing this effect by changing the clamping conditions it was possible to reduce the bend angle fall off per pass significantly.

6.2 Effects of Post Forming Heat Treatments on Laser Formed Components

Post forming heat treatments are often carried out in the aerospace industry to relieve any residual stresses that may have been induced into the part from the forming process. This may be a requirement for a laser formed component and any change in shape due to the method forming is investigated here.

The conclusions from this investigation are listed below:

- No significant changes in the geometry of the samples were observed in any of the heat treatments. The bend angle was maintained throughout with small changes in magnitude.
- In every case the changes in angle are attributed to the change in distortion in the samples. This distortion is caused by residual stresses in the samples initially from the laser forming process and in later measurement by the quenching process.
- Here the asymmetric nature of forming causes the sample to exert forces onto the clamp resulting in stresses in the work piece, resulting in distortion.
- After the effects of annealing no further effects of post forming heat treatments were observed that are linked to the laser forming process.

- In the annealing process it is observed that the residual stresses are relaxed and a removal of the distortion is observed. This is the reason for any changes in the geometry, and therefore bend angle, after the first heat treatment.
- Also observed here is the removal of distortion around the bend region in certain cases. This suggests that there are residual stresses in this region after the laser forming process that may not have been caused by the clamping arrangement. Further investigation with a less restrictive clamp is needed to confirm this.
- Another factor here is the dwell time. This allows the piece to cool fully. As the whole work-piece is cool the speed of cooling rate is increased. This increases the possibility of producing residual stresses and distortion.
- When tempering to T6 a similar effect to the annealing process is witnessed, with the relaxation of residual stresses obtained in quenching.
- Though the effects of post forming heat treatments on 2D laser formed parts are minimal this could be a cumulative effect in 3D laser forming with the increase of irradiation lines.
- The build up of residual stresses may be reduced due to the increasing temperature of the work-piece due to the increased number of irradiation lines.

6.3 3D Laser Forming of a Semi-Developable Shape using the Original Geometry Based Model

A potential method of scan strategy prediction has been developed based on lines of constant height. The energy distribution within the scan strategy is given by the gradient vector magnitude and the sum of the bending and membrane strains resolved in the direction of the principle gradient. This gives a potential predictive capability to a system that takes into account material non-uniformity and residual stresses. The investigation is carried out using the model to laser form a 3D semi developable shape the conclusions of which are presented here.

- The method for selection of the minimum speed needs improvement for the laser forming of semi-developable shapes.
- By using an iterative pass-by-pass approach, it has been possible to form a semi-developable 3D shape in a controlled manner to a reasonable degree of accuracy, taking account of unwanted deformations from program error or material non-uniformity.
- Through irradiating on the reverse side of the work-piece it has been possible to reduce the error due to over forming from the initial passes.
- The absence of adjustment in the measured area and area of the irradiation pattern as the viewable area decreases need to be addressed.
- Modifications are needed to form deeper shapes, as the

measurement system cannot cope with large oblique deflections.

- Improvements in the program to take into account the over forming of the edges also needs to be resolved, although irradiating on the reverse side does solve this to some degree.
- A limitation of the system is that there is an inability to take account of the fact that forming at the centre of a component also influences the edges.

6.4 3D Laser Forming of Semi-Developable Shape and the Correction of Distortion using the Modified Geometry Based Model

To modify the original model areas that require improvement are identified. This model uses lines of constant gradient magnitude as a means of defining the irradiation path and the increment between these lines to determine speed. This investigation included the forming of a 3D semi-developable shape and the correction of distortion in aluminium struts. The conclusions to this investigation are as follows:

- It is possible to use lines of constant gradient magnitude as a means of defining the irradiation path and the increment between these lines to determine speed, for the fabrication and correction of semi-developable and developable shapes.
- A geometry based model can produce semi-developable shapes and correct distorted developable struts to within millimetres.

- Irradiation strategies can be produced in seconds using height measurement across the work-piece and geometrical calculations.
- By using an iterative pass-by-pass approach, it has been possible to form a 3D shape in a controlled manner to a reasonable degree of accuracy, taking account of unwanted deformations from program error or material non-uniformity
- The system can be used for correction distortion with the ability to calculate a scan strategy to form a shape from just about any other shape
- It is possible to produce parts in AA5251 using laser forming that have a good finish with minimal damage to the part
- A significant amount of forming with reduced localised heating can be achieved with an increase in the number of irradiation lines.
- The problem of over forming in the original model has been addressed as all parts formed evenly.
- The model recognised areas that were difficult to form and increased the number of irradiation lines in this area.
- The speed selection allowed for the forming of shapes to approach the final shape in decreasing increments minimising the risk of over forming.
- The influence of the edge effect causes more non-linear irradiation lines which decrease the amount of forming possible
- Keeping the increment constant between the lines of constant gradient allowing the number of lines will allow for better

processing parameters and also prevent the problem of minor distortion masking area where more forming is required.

6.5 Future Work

Further work into the influences on forming rate is required to confirm the significance of each of the factors and at which point in a bend angle development during multi-pass 2D laser forming each factor is the more dominant.

Investigation in the way these factors influence multiple pass 3D laser forming is required. Strain hardening, section thickening and variation in absorption may have a minimal effect on 3D laser forming with few passes. These could become major factors in influencing the forming rate when many passes are taken. For the method of 3D forming in this thesis, with a long dwell time between passes, the thermal effect could influence the forming rate of every pass. Further work is needed to determine the amount the thermal effects influence 3D laser forming and what effect an increase in irradiation lines and the power has on this effect.

Further investigation is required to determine the effects of post forming of heat treatment on 3D laser formed components and therefore the amount of residual stress that occurs in a laser formed

part. Further investigation is also needed in the study of the effect clamping arrangement has on creating residual stresses

The effects of heat build up in the part have an effect on 3D laser forming. Investigation is needed to determine these effects and whether there is a limit to the proximity of adjacent irradiation lines. The size or ratio of a part effects how it reacts to laser forming, further 2D investigation is need to be able to increase the accuracy of the system to take this variation into account.

It is recommended that future work on the geometry based model include increasing the accuracy of the speed calibration data and to investigate a method for more non-developable laser forming capabilities. Gaussian curvature could hold a possible method for doing this.

References

1. A. Moshaiov, W. Vorus. The Mechanics of the Flame Bending Process, Theory and Applications, Journal of Ship Research, Vol. 31 No. 4: December, 1987: pp. 269-281.
2. R. E. Holt, "Flame Straightening Basics," Welding Engineer, 49-53 (June 1960).
3. T. Hashimoto, Y. Fujshiro. "An experiment of Line Heating Designed with the Table Orthogonal Array L32 (281)", Journal of The Society of Naval Architects of Japan, v.104, p.201, 1959.
4. M. Araki, N. Inoue, M. Horioka, M. Ando. "On Angular Distortion of Hull Steel Plates by Line Heating Methods", Journal of the Society of Naval Architects of Japan, v.133, p.343, 1973.
5. R.L. Rothman. "Flame Straightening Quenched-and-Tempered Steels in Ship Construction", SSC247, Ship Structure Committee, 1974.
6. F. Vollertsen. "Forming, Sintering and Rapid Prototyping." Handbook of the Eurolaser Academy, Vol. 2. Schuöcker, D (Editor), Chapman & Hall, 1998: pp. 357-453.
7. R.W. Hertzberg, "Deformation and Fracture Mechanics of Engineering Materials." John Wiley and Sons, New York (1983).
8. F. Vollertsen, "Laser forming, Mechanisms, Models, Applications" in LFT Erlangen monograph (1995).

9. G. Dearden, S. P. Edwardson 'Laser Assisted Forming for Shipbuilding' Proceeding of the SAIL Conference, 3rd - 5th June 2003, Williamsburg, Virginia.
10. F. Vollertson. "Mechanisms and Models for Laser Forming", Proceedings of Laser Assisted Net shape Engineering Conference (LANE 94), pp. 345-359, 1994.
11. F. Vollertsen, "An analytical model for laser bending," *Lasers Eng.* 2, 261- 276 (1994).
12. F. Vollertsen, M. Rodle, "Model for the Temperature Gradient Mechanism of laser Bending," in *Laser Assisted Net Shape Engineering, Proceedings of the LANE'94*, edited by M Geiger and F. Vollertsen, (Meisenbach Bamberg, Germany, 1994), Vol. I, pp. 371 - 378.
13. Z. Mucha, J. Hoffman, W. Kalita, and S. Mucha, "Laser Forming of Thick Free Plates". *Laser Assisted Net shape Engineering 2. Proceedings of the LANE'97*, edited by M. Geiger and F. Vollertsen, (Meisenbach Bamberg, Germany, 1997), Vol. 2, pp. 383-392.
14. M. Geiger, F. Vollertsen, "The Mechanisms of Laser Forming," *CIRP ANNALS* Vol. 42, 1, 301 - 304 (1993).
15. C. L. Yau, K. C Chan, W. B. Lee, "A New Analytical Model for Laser Bending," in *Laser Assisted Net Shape Engineering 2, Proceedings of the LANE'97*, edited by M. Geiger and F. Vollertsen, (Meisenbach Bamberg, Germany, 1997), Vol. 2, pp. 357-366.
16. K. Koloman, and P. Karol. "Formen durch locale Erwärmung." *Metal Forming - Theory and Practice: Proc. of 5th Int'l Conf. on Metal Forming*, M. Tisza and K. Kardos, eds., pp69-75 (1991).
17. J. Magee. "Laser Forming of Aerospace Alloys." PhD Thesis, University of Liverpool, 1999.

18. S. Yongjun, S. Hang, Y. Zhenqiang and H. Jun, "Temperature gradient mechanism in laser forming of thin plates." *Optics and Laser Technology*, Volume 39, Issue 4, (June 2007) pp858-863
19. F. Vollertsen, I. Komel, and R. Kals, "The laser bending of steel foils for microparts by the buckling mechanism - A model," *Model. Simul. Mater. Sci. Eng.* 3, 107 - 119 (1995).
20. J. Kraus, "Basic processes in laser bending of extrusions Using the Upsetting Mechanism," in *Laser Assisted Net Shape Engineering 2*, Proceedings of the LANE'97, edited by M. Geiger and F. Vollertsen, (Meisenbach Bamberg, Germany .1997) Vol. 2, pp.431
21. A. Moshaiov, J. G. Shin, "Modified Strip Model for Analysing the Line Heating Method (Part 2): Thermo-Elastic-Plastic Plates," *Journal of Ship Research*, Vol. 35, No. 3, 266-275 (Sept. 1991).
22. Y. Iwamura, E. F. Rybicki, "A transient Elastic -Plastic thermal Stress analysis of flame forming," *Transactions of ASME, Journal of Engineering for Industry*, 163-171 (February 1973).
23. T. Suhara, "Study on Thermo Plastic working: Bending of Beam of Rectangular Cross Section," *Journal of Zosen Kyokai*, Vol. 103, 233-243 (1958).
24. M. Araki, N. Inoue, M. Horioka, M. Ando, "On Angular Distortion of Hull Steel Plates by Line Heating Methods," *Journal of the Society of Naval Architects of Japan*, Vol. 133, 343-348 (1973).
25. F. Vollertsen, M. Geiger, W. M. Li, "FDM- and FEM- simulation of laser forming: a comparative study," *Advanced Technology of Plasticity*, edited by Z. R. Wang, Y. He, III, 1793-1798 (1993).
26. M. Geiger, S. Holzer, F. Vollertsen, "Laserstrahlbiegen - Simulation eines 3- dimensionalen, thermomechanischen Prozesses," in *Metal Forming Process Simulation in Industry*,

- edited by B. Kropli and, E. Luckey, Monchengladbach, Germany, 1994, pp. 335 - 352.
27. N. Alberti, L. Fratini, F. Micari, "Numerical simulation of the laser bending process by a coupled thermal mechanical analysis," in Laser Assisted Net Shape Engineering, Proceedings of the LANE'94, edited by M. Geiger and F. Vollertsen (Me Germany, 1994); Vol. I, pp.: 327 - 336.
 28. N. Alberti, L. Fratini, F. Micari, M. Cantello, G. Savant, "Computer Aided Engineering of a laser assisted bending processes," in Laser Assisted NetShape Engineering 2, Proceedings of the LANE'97, edited by M. Geiger and F. Vollertsen, (Meisenbach Bamberg, Germany, 1997), Vol. 2, pp.375-382
 29. Y-C. Hsiao, H. Shimizu, L. Firth, W. Maher, K. Masabuchi, "Finite Element Modelling Of Laser Forming," in Proceedings of the International Congress On Applications of Lasers and Electro-Optics, (ICALEO97), (San Diego, U.S.A, 1997), Section A. pp.31-40
 30. G. Yu, K. Masubuchi, T. Maekawa, N. M. Patrikalakis, "Thermomechanics of laser forming of metal plates" Massachusetts Institute of Technology (MIT) Fabrication Memorandum 99-1. November 1, 1999.
 31. W. Li, Y. L. Yao, " Effects of Strain Rate in Laser Forming" Proceedings of ICALEO'99, San Diego CA, Section F, 1998: pp. 107-116
 32. W. Li, Y. L. Yao, "Laser Forming with Constant Line Energy" International Journal of Advanced Manufacturing Technology, Vol. 17 (2001): pp 196-203

33. J. Bao & Y.L. Yao, 'Analysis and Prediction of Edge Effects in Laser Bending', *Journal of Manufacturing Science & Engineering*, Vol. 123, ASME, pp.53-61, 2001
34. C. Cosenza, L. Fratini, F. Micari, M. Cantello, M. Penasa, "Explicit Thermo- Mechanical Analysis of Laser Forming Processes" *Laser Assisted Net Shape Engineering 3*, Proceedings of the LANE'2001 Erlangen, Germany, 2001
35. K. C. Lee, J. Lin, "Transient Deformation of Thin Metal Sheets During Pulsed Laser Forming" *Optics & Laser Technology*, vol. 34 (2002): pp 639- 648.
36. H. Holzer, M. Arnet, M. Geiger, "Physical and Numerical modelling of the Buckling Mechanism," in *Laser Assisted Net Shape Engineering*, Proceedings of the LANE'94, edited by M. Geiger and F. Vollertsen, (Bamberg, Germany, 1994), Vol. I, pp. 379 - 386.
37. W. Li, Y. L. Yao, "Numerical and Experimental Investigation of Laser Induced Tube Bending" *Proceedings of ICALEO 2000*, Detroit, Section D, 2000: pp. 53-62
38. Y. Namba, "Laser Forming in Space". *Proceedings of the International Conference on Lasers'85*, edited by C. P. Wang, (STS Press, McLean 1986), pp.403-407.
39. K. Scully. "Laser Line Heating", *Journal of Ship Production*, v.3/4, p.237, 1987.
40. K. Masabuchi. "Studies at M.I.T related to Applications of Laser Technologies to Metal Fabrication," in *Proceedings of Laser Advanced Materials Processing (LAMP'92)* (Niigata, Japan, 1992), pp. 939 - 946.
41. A. Sprenger, F. Vollertsen, W. M. Steen, and K. G. Watkins, "Influence of strain hardening on laser bending" *Manuf Syst.* 24, 215-221 (1995).

42. J. Magee, K. G. Watkins, W. M. Steen, N. Calder, J. Sidhu, J. Kirby, "Laser Forming of Aerospace Alloys," Proceedings of ICALEO 97, Vol.83, Part 2, section e-156 (1997), pp.156-165.
43. J. Magee, K. G. Watkins, W. M. Steen, N. Calder, J. Sidhu, and J. Kirby, "Edge effects in laser forming," in Laser Assisted Net shape Engineering 2. Proceedings of the LANE'97, edited by M. Geiger and F. Vollertsen, (Meisenbach Bamberg, Germany, 1997), Vol. 2, pp.399-408.
44. J. Magee, K.G. Watkins, W.M. Steen, R.L. Cooke, J. Sidhu. "Development of an Integrated Laser Forming Demonstrator System for the Aerospace Industry." Proceedings of ICALEO'98, Section E, 1998; pp. 141-150.
45. J. Ramos, J. Magee, K.G. Watkins, W.M. Steen, F. Noble. "Microstructure of laser bent aluminium alloy Alclad 2024-T3." Proceedings of ICALEO'98, Section E, 1997: pp. 178-185.
46. J. Magee, K.G. Watkins, T. Hennige. "Symmetrical Laser Forming." Proceedings of ICALEO'99, San Diego CA, Section F, 1998: pp. 77-86
47. S. Edwardson. "A Study into the 2D and 3D Laser Forming of Metallic Components." PhD Thesis, University of Liverpool, March 2004.
48. G. Dearden, S. P. Edwardson "Some Recent Developments in Two- and Three-Dimensional Laser Forming for 'Macro' and 'Micro' Applications" Journal of Optics A: Pure and Applied Optics Vol. 5 No. 4: July 2003; pp. S8-S15
49. K. C. Chan, C. L. Yau, W. B. Lee, "Laser Bending of Thin Stainless Steel Sheets" Journal of Laser Applications, vol. 12, No. 6, 2000
50. Z. Mucha, M. Cabaj, R. Gradoń, M. Pawlowski, J. Widlaszewski, "Laser Forming of Plates by the use of Beam with Circular and

- Rectangular Crosssection” Laser Assisted Net Shape Engineering 3, Proceedings of the LANE’2001 Erlangen, Germany, 2001
51. X. F. Wang, J. Takacs, G. Krallics, A. Szilagyi, T Markovits, “Research on the Thermo-Physical Process of Laser Bending” *Journal of Materials Processing Technology*, vol. 127 (2002): pp 338-391
 52. L. Liqun, C. Yanbin, L. Shangyang, G. Dayong, “Characterization of Laser Bending under Different Cooling Conditions” Proceedings of ICALEO’2002, Scottsdale, Arizona, 2002.
 53. L. Lin, Y. Chen, S. Lin, “The Characteristics of Laser Forming of Aluminium Sheet Under Consecutive Irradiations” Proceedings of ICALEO’2003, Paper 109, Jacksonville, Florida, 2003
 54. K.C. Chan, Y. Harada, J. Liang & F. Yoshida, ‘Deformation Behaviour of Chromium Sheets in Mechanical and Laser Bending’, *Journal of Materials Processing Technology*, Vol.122, pp.272-277, 2002.
 55. N. Abe, N. Nakagawa, M. Tsukamoto, K. Nakacho, M. Sogabe, S. Miyake, “Laser Forming of Thick Steel Plates with a High Power Diode Laser” Proceedings of ICALEO’2001, Jacksonville FL, Section D, 2001
 56. J. Magee, L.J. De Vin, ‘Process planning for laser-assisted forming’, *Journal of Materials Processing Technology*, Vol.120 (2002), pp.322-326.
 57. J. Magee & L.J. De Vin, ‘Combining Forming Tools and Laser Beams’, *The Industrial Laser User*, Issue 21, pp.32-34, The UK Association of Industrial Laser Users (AILU), November 2000.
 58. G. Thompson & M. Pridham, ‘A Feedback Control System for Laser Forming’, *Mechatronics*, Vol.7, No.5, pp.429-441, 1997.

59. M. Pridham, G. Thompson, "Laser forming: a force for the future," *Materials World*, Vol. 2, (Nov 1994).
60. M. Pridhain, G. Thompson, "Laser forming," *Manufacturing Engineer*, p.24 (June 1995).
61. P. J. Cheng, S. C. Lin, "Using Neural Networks to Predict Bending Angle of Sheet Metal" *International Journal of Machine Tools & Manufacture* vol. 40 (2000): pp 1185-1197
62. D. E. Peck, G. Jones, "Line Induced Thermal Forming" *Proceedings of ICALEO'2002*, Scottsdale, Arizona, 2002.
63. P. O'Hara, "Lasershot Peening of Metals", *The Industrial Laser User*, Issue 19, pp.27-29, The UK Association of Industrial Laser Users (AILU), May 2000
64. J. Z. Zhou, J. C. Yang, Y. K. Zhang, M. Zhou, "A Study on Super-Speed Forming of Metal Sheet by Laser Induced Shockwaves" *Journal of Materials Processing Technology*, vol. 129 (2002): pp 241-244
65. W. Hoving, 'Accurate Manipulation Using Laser Technology', *Proc. Of SPIE*, 3097, pp.284-295, 1997.
66. W. Hoving, 'Accurate Manipulation Using Laser Technology', *Proc. of the 3rd International Conference on Laser Assisted Net-shape Engineering (LANE 2001)*, Erlangen, Germany, 28-31 August 2001, Eds. M. Geiger & A. Otto, Meisenbach, Bamberg, Germany, pp.113-124, 2001.
67. A.C. Tam, C.C. Poon & L. Crawforth, 'Laser Bending of Ceramics and Application to Manufacture Magnetic Head Sliders in Disk Drives', *Analytical Sciences*, Vol.17 (Special Issue), pp.419-421, The Japan Society for Analytical Chemistry, April 2001

68. J. Wildaszewski, "Micro Adjustment by Thermal Upsetting." Proceedings of the 1st International Workshop on Thermal Forming (IWOTE'05), pp.93-109, 2005.
69. X.R. Zhang, X. Xu, "Laser bending for adjusting curvatures of hard disk suspensions." Journal of Microsystems Technologies, Volume 11, Number 11, pp.1197-1203, October, 2005.
70. G. Dearden, C. Taylor, K. Bartkowiak, S.P. Edwardson, K.G. Watkins, "An experimental study of laser micro-forming using a pulsed Nd:YAG laser and scanning optics" Proceedings of ICALEO'2003, Paper M409, Jacksonville, Florida, 2003
71. T. Miyazaki, T. Misu, S. Yoshioka, T. Tokunaga, M. Saito, "Forming Characteristics of Thin Metal Plate with Diode Laser Beam" Proceedings of ICALEO'2002, Scottsdale, Arizona, 2002.
72. R. Oba, S. Yoshioka, T. Miyazaki, K. Nakamura, " Laser Forming of Metal Foil by the Upsetting Mechanism" Proceedings of ICALEO'2002, Scottsdale, Arizona, 2002.
73. S. Yoshioka, T. Miyazaki, T. Misu, R. Oba, M. Saito, " Laser Forming of Thin Foil by a Newly Developed Sample Holding Method" Journal of Laser Applications, Vol. 15, No. 2, 2003
74. Y. Okamoto, Y. Uno, T. Shibata & K-I. Ohta, 'Precision Laser Forming of Plastic with YAG Laser', Proc. 5th International Conference on Progress of Machine Technology, pp.221-226, 2000.
75. K. Bartkowiak, S.P. Edwardson, J. Borowski, G. Dearden, K.G. Watkins, "Laser Forming of Thin Metal Components for 2D and 3D Applications Using a High Beam Quality, Low Power Nd:YAG Laser and Rapid Scanning Optics." Proceedings of the 1st International Workshop on Thermal Forming (IWOTE'05), pp.111-129, 2005.

76. S.P. Edwardson, K.G. Watkins, G. Dearden, J. Magee. "Generation of 3D Shapes Using a Laser Forming Technique." Proceedings of ICALEO'2001, Section D, 2001.
77. S. Silve, B. Podschies, W.M. Steen & K.G. Watkins, 'Laser Forming – A New Vocabulary for Objects', Proceedings of the 18th Intl. Congress on Applications of Lasers & Electro-Optics (ICALEO'99), San Diego, Vol.87, Section F, pp.87-96, 1999.
78. T. Hennige, "Laser Forming of Spatially Curved Parts", Laser Assisted Net Shape Engineering 2, Proceedings of the LANE'97, edited by M. Geiger and F. Vollertsen, (Meisenbach Bamberg, Germany, 1997), Vol. 2
79. T. Hennige, "Development of irradiation strategies for 3D-laser forming" Journal of Materials Processing Technology, Vol. 103 n. 1 (2000): pp 102- 108.
80. M. Otsu, M. Fujii, K. Osakada, "Three-Dimensional Laser Bending of Sheet Metal" Advanced Technology of Plasticity Vol. II, Proceedings of the 6th ICTP Sept. 19-24, 1999.
81. G. Casalino, A. D. Ludovico, A. Ancona, P. M. Lugará, "Stainless Steel 3D Laser Forming for Rapid Prototyping" Proceedings of the 20th International Congress on Applications of Lasers & Electro-Optics (ICALEO 2001), Jacksonville, FL, October 2-5, 2001.
82. Vollertsen, F. and Holzer, S., "3D-Thermomechanical Simulation of Laser Forming", Simulation of Materials Processing: Theory, Methods and Applications, Balkema, Rotterdam, p.785, 1995.
83. M. Otsu, K. Osakada & M. Fujii, 'Controlled Laser Forming of Sheet Metal with Shape Measurement and Using Database', Proc. Metal Forming 2000, Balkema, pp.433-438, 2000.
84. J. Cheng, Y. L. Yao, "Process Synthesis of Laser Forming by Genetic Algorithm" Proceedings of the 20th International

- Congress on Applications of Lasers & Electro-Optics (ICALEO 2001), Jacksonville, FL, October 2-5, 2001.
85. C. Liu, Y. L. Yao, V. Srinivasan, "Optimal Process Planning for Laser Forming of Doubly Curved Shapes." *Journal of Manufacturing Science and Engineering*, Vol.126, n.1, pp.1-9, February 2004
 86. J. Kim, S.J. Na, "Feedback control for 2D free curve laser forming." *Journal of Optics and Laser Technology*, Vol.37, No.2, pp.139-146, March 2005.
 87. R. P. Martukanitz, E. W. Reutzel, R. W. Erskine, S. Nasla, "Adaptive and Heuristic Techniques for Laser Assisted Forming of Plate" *Proceedings of ICALEO 2000*, Detroit, Section D, 2000: pp. 47-52
 88. E.W. Reutzel, R.P. Martukanitz, P. Michaleris, L. Zhang, A.J. Savitz, J.P. Magnusen, J.U. Aburdene & K.J. Gombotz, 'Development of a System for the Laser Assisted Forming of Plate', *Proceedings of the 20th International Congress on Applications of Lasers & Electro-Optics (ICALEO 2001)*, Jacksonville, FL, October 2-5, 2001.
 89. E.W. Reutzel, J.U. Aburdene, K.J. Gombotz, , J. P. Magnusen, R.P. Martukanitz, P. Michaleris, L. Zhang, "Continuing Development of a Laser Line Forming System" *Proceedings of ICALEO'2002*, Scottsdale, Arizona, 2002.
 90. E.W. Reutzel, K.J. Gombotz, R.P. Martukanitz, P Michaleris, "Path Planning Strategies for Laser Line Forming" *Proceedings of ICALEO'2003*, Paper 106, Jacksonville, Florida, 2003
 91. E.W. Reutzel, L. Zhang, P. Michaleris, "A Differential Geometry Approach to Simulation of Thermal Forming" *Proceedings of the 1st International Workshop on Thermal Forming (IWOTE'05)*, pp.185-202, 2005.

92. J.E. Jones, V.L. Rhoades, J.C. Jones, A.C. Beck, P. Oberly, P. Sewell, D.D. Schwemmer, D. Stompro & T. Whipple, 'Use of the Flexible Laser Automated Intelligent Real-Time (FLAIR) System for Laser Thermal Forming', Proceedings of the International Conference on the Industrial Applications of Lasers in Manufacturing, Minneapolis, April 1998.
93. J. Cheng, Y.L. Yao, "Process Design of Laser Forming of Three-Dimensional Thin Plates." *Journal of Manufacturing Science and Engineering*, Vol. 126, n. 2, pp.217-225, May 2004.
94. W. Maher, K. Tong, C. Bampton, M. Bright, J. Wooten, C. Rhodes. Laser Forming of Titanium and Other Metals is Useable Within Metallurgical Constraints. Proceedings of ICALEO'98, Section E 1998; pp. 121-130.
95. J. Shackel, J. Sidhu, P.B. Prangnell, "The Metallurgical Implications of Laser Forming Ti-6Al-4V Sheet." Proceedings of ICALEO'2001, Section D, 2001
96. G. Thomson, M. Pridham, "Material Property Changes Associated with Laser Forming of Mild Steel Components" *Journal of Materials Processing Technology*, Vol. 118 (2001): pp 40-44.
97. M. Marya, G. R. Edwards, "A Study on the Laser Forming of Near-Alpha and Meta-stable Beta Titanium Alloy Sheets" *Journal of Materials Processing Technology*, Vol. 108 (2001): pp 376-383.
98. M. Marya & G.R. Edwards, 'Factors Affecting the Laser Bending of Ti- 6Al-2Sn-4Zr-2Mo', *Journal of Laser Applications*, Vol.12, Number 4, Laser Institute of America, pp.149-159, 2000.
99. M. Merklein & M. Geiger, 'A Comparative Study of Two Different Laser Forming Mechanisms Regarding the Mechanical Properties of Aluminium Alloys' *Laser Assisted Net Shape*

- Engineering 3, Proceedings of the LANE'2001 Erlangen, Germany, 2001
100. M. Merklein, T. Hennige, M. Geiger, "Laser Forming of Aluminium and Aluminium Alloys – Microstructural Investigation" *Journal of Materials Processing Technology*, Vol. 115 (2001): pp 159-165.
 101. K.C. Chan & J. Liang, 'Thermal Expansion and Deformation Behaviour of Aluminium-Matrix Composites in Laser Forming', *Composites Science & Technology*, Vol.61, pp.1265-1270, 2001.
 102. K.C. Chan, Y. Harada, J. Liang & F. Yoshida, 'Deformation Behaviour of Chromium Sheets in Mechanical and Laser Bending', *Journal of Materials Processing Technology*, Vol.122, pp.272-277, 2002.
 103. J. Zhang, D. Pirzada, L. V. Smith, C. Chin, J. G. Cheng, "Fatigue Life Prediction after Laser Forming" *Proceedings of ICALEO'2003*, Paper 105, Jacksonville, Florida, 2003
 104. J. Zhang, J. G. Cheng, "Experimental Study and Computer Simulation on Fracture Toughness of Sheet Metal after Laser Forming" *Proceedings of ICALEO'2003*, Paper 108, Jacksonville, Florida, 2003
 105. J. A. Ramos, "Creep Behaviour of Thin Metal Sheets during Laser Bending" *Proceedings of the 20th International Congress on Applications of Lasers & Electro-Optics (ICALEO 2001)*, Jacksonville, FL, October 2-5, 2001.
 106. P. Cheng, Y. L. Yao, "The Influence of Sheet Metal Anisotropy on Laser Forming Process" *Proceedings of ICALEO'2003*, Paper 101, Jacksonville, Florida, 2003
 107. D. Schuoker. "Mathematical modelling of laser-assisted deep drawing." *Journal of Materials Processing Technology*, Vol.115, n.1, pp.104-107, August 2001.

108. G. Dearden, S.P. Edwardson, E. Abed and K.G. Watkins, "Laser forming for the correction of distortion and design shape in aluminium structures," " Proceedings of the 25th International Congress on Applications of Lasers & Electro-Optics (ICALEO 2006), Paper No. 505, Laser Institute of America, Publication No.599, Vol 99, (2006)
109. J.R. Dydo, H.R. Castner & K. Koppenhoefer, 'Guidelines for Control of Distortion in Thin Ship Structures', EWI Project No. 42372-GDE, Edison Welding Institute, Columbus, Ohio, October 1999.
110. W.M. Steen, "Laser Materials Processing", 3rd Edition, Sprenger-Verlag, 2003.
111. H. Hügel and F. Dausinger, "Interaction Phenomena", Handbook of the euro laser academy, volume 2
112. Volume 1, "Properties and Selection: Irons, Steels, and High Performance Alloys," ASM Handbooks Online, Materials Park OH: ASM International, 2003
113. E.A. Brandes "Smithells Metals Reference Book," Sixth Edition, Butterworth & Co (Publishers), Ltd 1983
114. Volume 2, "Properties and Selection: Nonferrous Alloys and Special-Purpose Materials," ASM Handbooks Online, Materials Park OH: ASM International, 2003
115. Datasheet, "Aluminium Alloy 5251", Aalco Metals Limited
116. Volume 4, "Heat Treating," ASM Handbooks Online, Materials Park OH: ASM International, 2003 .
117. S. P. Edwardson, A. J. Moore, E. Abed, R. McBride, P. French. G. Dearden, D. P. Hand, K. G. Watkins, J. D.C. Jones. Iterative 3D Laser Forming of Continuous Surfaces Proceedings of ICALEO'2004, San Francisco, California, 2004

118. J. Cheng, Y.L. Yao, "Microstructure integrated modelling of multi-scan laser forming," *Journal of Manufacturing Science and Engineering*, vol.124, pp.379-388, 2002
119. S.P. Edwardson, K.G. Watkins, E. Abed, K. Bartkowiak and G. Dearden, "Geometrical Influences on the Bend Angle Rate per Pass during Multi-Pass 2D Laser Forming." *Proc. IWOTE'05 Conf. (Bremen, Germany)* pp.29-46, 2005
120. K. Bartkowiak, G. Dearden, S.P. Edwardson and K.G. Watkins, "Development of 2D and 3D Laser Forming Strategies for Thin Section Materials using Scanning Optics." *Proc. ICALEO Conf. (San Francisco, CA, USA)* 2004
121. K. Bartkowiak, S.P. Edwardson, G. Dearden and K.G. Watkins, "2-D Laser Forming Comparative Study using CW and Pulsed Nd:YAG lasers on titanium alloy Ti-6Al-4V in air and argon atmospheres." *Proc. ICALEO Conf. (San Francisco, CA, USA)*, 2004
122. S.P. Edwardson, K.G. Watkins, G. Dearden, P. French and J. Magee, "Strain Gauge Analysis of Laser Forming," *Journal of Laser Applications*, vol.15, pp.225-232, 2003
123. J. Cheng and Y.L. Yao, "Cooling effects in multi-scan laser forming," *Journal of Manufacturing Processes*, vol.3, pp.60-72, 2001
124. Z. Hu, M. Labudovic, H. Wang, R. Kovacevic, "Computer simulation and experimental investigation of sheet metal bending using laser beam scanning." *International Journal of Machine Tools & Manufacture*, vol. 41, pp.589-607, 2001
125. T. Hennige, S. Holzer, F. Vollertsen and M. Geiger, "On the working accuracy of laser bending." *Journal of Material. Processing Technology*. vol. 71, pp.422-32, 1997

126. M. Reeves, A.J. Moore, D.P. Hand, J.D.C. Jones, J.R. Cho, R C. Reed, S.P. Edwardson, G. Dearden, P. French and K.G. Watkins, "Dynamic distortion measurements during laser forming of Ti-6Al-4V and their comparison with a finite element model," Proceedings of the Institution of Mechanical Engineers, Part B: Journal of Engineering Manufacture, v 217, n 12, pp 1685-1696 2003
127. M.J. Mancewicz, W.H. Frey, "Developable surfaces: Properties, representations and methods of design." General Motors R&D Publication 7637,1992
128. K. Ueda, H. Murakawa, A.M. Rashwan, Y. Okumoto, R. Kamichika, "Development of computer-aided process planning system for plate bending by line heating (report 1) – relation between final form of plate and inherent strain." Journal of Ship Production, Vol.10 No.1, pp.59-67, 1994
129. I. R. Roberts. Geometric differentiation for the intelligence of curves and surfaces. Cambridge University Press 1994
130. D. McFarland, B. L. Smith, W. D. Bernhart, Analysis of plates Spartan Books, New York, 1972.

List of Publications to Date by the Author

**S.P. Edwardson, E. Abed, P. French, G. Dearden, K.G. Watkins,
A.J. Moore, R. McBride, D.P. Hand, J.D.C. Jones**

“Iterative 3D Laser Forming of Continuous Surfaces”

Proceedings of the 23rd International Congression on Applications of Lasers and Electro-Optics, 2004

**S.P. Edwardson, E. Abed, P.French, G. Dearden, K.G. Watkins
R. McBride, D. P. Hand, J.D.C. Jones, A.J. Moore**

“Developments Towards Controlled 3D Laser Forming of Continuous Surfaces”

Proceedings of the 23rd International Congression on Applications of Lasers and Electro-Optics, 2004

**S.P. Edwardson, E. Abed, P. French, G. Dearden, K.G. Watkins
R. McBride, D.P. Hand, J.D.C. Jones, A.J. Moore**

“Developments Towards Three-Dimensional Laser Forming of Continuous Surfaces”

Journal Of Laser Applications vol 17 issue 4 pp 247 – 255(2005)

S.P. Edwardson, K.G. Watkins, E. Abed, K.Bartkowiak, G.Dearden

“Geometrical Influences on the Bend Angle Rate per Pass during Multi-Pass 2D Laser Forming”

International Workshop on Thermal Forming, Bremen, April 13-14, 2005

**E. Abed, S. P. Edwardson, G. Dearden, K. G. Watkins, R. McBride,
D. P. Hand, J. D.C. Jones, A. J. Moore**

“Closed Loop 3-Dimensional Laser Forming of Developable Surfaces”

International Workshop on Thermal Forming, Bremen, April 13-14, 2005

E Abed, S Edwardson, G Dearden, K Watkins

*“Geometrical Technique for Closed Loop 3-Dimensional Laser
Forming”*

Photon06, September(2006)

G. Dearden, S. Edwardson, E. Abed, K. Watkins

*“Laser forming for the correction of distortion and design shape in
Aluminium structures”*

Photon06, September (2006)

**S.P. Edwardson, E. Abed, K. Bartkowiak, G. Dearden and
K. Watkins**

“Geometrical influences on multi-pass laser forming”

Journal of Physics D: Applied Physics vol 39 issue 2 pp 382-389
(2006)

E. Abed, S. P. Edwardson, G. Dearden, K. G. Watkins

“Geometrical Based control method for 3D Laser Forming”

Laser Assisted Net Shape Engineering (LANE 2007)

**S. P. Edwardson, E. Abed, C. Carey, K. R. Edwards, G. Dearden
K. G. Watkins**

“Factors Influencing the Bend per Pass in Multi-Pass Laser Forming”
Laser Assisted Net Shape Engineering (LANE 2007)

**S.P. Edwardson, E. Abed, C. Carey, K.R. Edwards, K. Bartkowiak,
G. Dearden, K.G. Watkins**

“Key Factors Influencing the Bend per Pass in Laser Forming”
Proceedings of the 26th International Congression on Applications of
Lasers and Electro-Optics, 2007

**E. Abed, S.P. Edwardson, K. Bartkowiak, G. Dearden,
K. G. Watkins**

“Control Method for 3D Laser Forming Based on Geometrical Data”
Proceedings of the 26th International Congression on Applications of
Lasers and Electro-Optics, 2007

Appendices

- Appendix I** Example of the Matlab Program that Produces The Irradiation Strategy
- Appendix II** Example of the Galil CNC Code produced by Matlab to Control Movement and the Laser Shutter for the Pass of an Irradiation Strategy
- Appendix III** Example of the Visual Basic Code produced by Matlab to Control the Movement of the CNC Tables for the CMM taking into Account the Decrease in Viewable Area
- Appendix IV** A Full Account of All the Irradiation Strategies and The Resulting Shape for the Closed Loop 3D Laser Forming of a Mild Steel Semi-Developable Shape
- Appendix V** A Full Account of All the Irradiation Strategies and The Resulting Shape for the Laser Forming for the Correction of Aluminium 5251 Strut Mechanically Deformed to 45mm

Appendix I

Example of the Matlab Program that Produces The Irradiation Strategy

```
% constant gradient magnitude

close all;
clear all;

%Experimental data range and increment (mm)
%x_min=10; x_max=390;      %M5,6,7 data
%y_min=10; y_max=190;
%x_step=10;
%y_step=10;
x_min=5; x_max=395;      %M11,12, 13 data
y_min=-20; y_max=60;
x_step=39;
y_step=8;
reverse_side_pass_number=0
front_side_pass_number=1
%pass_number=9; %First pass will calibrate strain...
%calibrate=0;      %...if calibrate=1
%Theoretical data
aspect=5;

element_width=4;      %Yields odd number of elements to simplify (Ox,Oy) calculation
element_length=4;
element_aspect=element_length/element_width;
width=80;      %Plate width in mm
number_of_points_in_x=3;      %number of columns in z3 matrix
number_of_points_in_y=3;      %number of rows in z3 matrix
x_axis=number_of_points_in_x-1;
y_axis=number_of_points_in_y-1;
num_contour=10;      %Number of contours to plot

%Given data points
[x3,y3]=meshgrid(-aspect*width/2:aspect*width/x_axis:aspect*width/2,width/2:-width/y_ax
is:-width/2);;
%z3=-[ 0.042, 0.017, -0.017, -0.042;
      % 0.017, 0.008, -0.008, -0.017;
      % -0.017, -0.008, 0.008, 0.017;
      % -0.042, -0.017, 0.017, 0.042; ]'; %Transpose here for consistency with pillow01.m

%[x3,y3]=meshgrid(0:aspect/4:aspect,0:1/4:1);
%z3=-[ 0, 0.042, 0.08, 0.042, 0;
      % 0.042, 0, 0, 0, 0.042;
      % 0.08, 0, 0, 0, 0.08;
      % 0.042, 0, 0, 0, 0.042;
      % 0, 0.042, 0.08, 0.042, 0; ];

%saddle
%z3=[0,-1,0;
     % 1,0,1;
     %0,-1,0;];

%asymmetrical
%z3=[ 0, 0, 0;
     %-1, 0, 1;
     %0, 0, 0; ];

%pillow
%z3=[ 1, 0.5, 1;
     %0.5, 0, 0.5;
     %1, 0.5, 1;];
```

```
%part-cylinder
    %z3=[ 1, 0, 1;
    %1, 0, 1;
    %1, 0, 1;];

%flat
z3=[0,0,0;
    0,0,0;
    0,0,0;];

%strut
%z3=[-11.3035   -7.5435  -4.1745  -1.831   -0.488   0   -0.531  -1.9775  -4.321  -7.8365  -11 ✓
    .865;
%-11.1815   -7.5435  -4.2235  -1.8735  -0.5125  -0.0485  -0.5125  -1.9895  -4.321  -7.8305  -11 ✓
    .8895;
%-11.2545   -7.5375  -4.199   -1.855   -0.488   -0.085   -0.5615  -1.9775  -4.3395  -7.8855  -11 ✓
    .914;
%-11.267    -7.5435  -4.205   -1.898   -0.537   -0.0975  -0.5855  -2.0015  -4.321  -7.8855  -11 ✓
    .938;
%-11.2545   -7.556   -4.199   -1.855   -0.5125  -0.073   -0.5795  -1.9895  -4.3515  -7.861   -11 ✓
    .9625;
%-11.4255   -7.5925  -4.248   -1.904   -0.5125  -0.1465  -0.6345  -2.0505  -4.4185  -7.922   -11 ✓
    .9625;
%-11.45    -7.5925  -4.2295  -1.904   -0.5125  -0.1465  -0.6345  -2.075   -4.3945  -7.9345  -11.962 ✓
    5;
%-11.45    -7.5925  -4.248   -1.904   -0.5615  -0.1525  -0.6345  -2.075   -4.4185  -7.9465  -11.962 ✓
    5;
%-11.444   -7.5985  -4.248   -1.904   -0.537   -0.1465  -0.659   -2.0565  -4.4185  -7.9345  -11 ✓
    .981;
%-11.45    -7.5985  -4.248   -1.9285  -0.5185  -0.1465  -0.6345  -2.069   -4.4185  -7.9345  -11.962 ✓
    5;
%-11.4745   -7.5925  -4.2965  -1.9285  -0.543   -0.1705  -0.6285  -2.075   -4.492   -7.959   -12 ✓
    .0115;];

%cowling
%z3=[ 1, 0.1, 0.1, 1;
    % 0.875, 0.1, 0.1, 0.875;
    % 0.625, 0.1, 0.1, 0.625;
    %0.5, 0.1, 0.1, 0.5; ];

%Interpolation
[x1,y1]=meshgrid(-20:element_length:width*aspect,-20:element_width:width);    %NB Now ✓
using square elements i.e. not aspect/num
Ox=round(size(x1,2)/2);
Oy=round(size(x1,1)/2);
x1(:,:)=x1(:,:)-x1(Oy,Ox);
y1(:,:)=y1(Oy,Ox)-y1(:,:);

z1=40*interp2(x3,y3,z3,x1,y1,'linear');    %Matlab interpolation.

%gcurvature(x1,y1,z1);
zg=gradient(z1);
G1=gradient_magnitude(x1,y1,z1,element_aspect);

%Experimental shape data (This is pillow03.m, but now interpolating to num points)
[x,y]=meshgrid(x_min:x_step:x_max,y_min:y_step:y_max);
Ox=round(size(x,2)/2);
Oy=round(size(x,1)/2);
x(:,:)=x(:,:)-x(Oy,Ox);
y(:,:)=y(Oy,Ox)-y(:,:);
```

```
pass((1:((y_max-y_min)/y_step)+1),1:((x_max-y_min)/x_step)+1),1)=0; %Start from fla  
t plate
```

```
[x4,y4]=meshgrid(-aspect*width/2:aspect*width/((x_max-x_min)/x_step):aspect*width/2,wid  
th/2:-width/((y_max-y_min)/y_step):-width/2);  
Ox=round(size(x4,2)/2);  
Oy=round(size(x4,1)/2);  
x4(:,:)=x4(:,:)-x4(Oy,Ox);  
y4(:,:)=y4(Oy,Ox)-y4(:,:);
```

%strut reversal

```
pass(:,:,1)=[ %Data min 30mm/s  
-22.0395 -13.7145 -7.9285 -4.1440 -1.7760 -0.8970 -1.0925 -0.4395 -0.189  
0 -0.3355 -0.6775  
-21.9516 -13.6779 -7.9247 -4.1367 -1.7687 -0.8330 -1.0559 -0.4321 -0.1  
964 -0.3319 -0.6628  
-21.8637 -13.6413 -7.9210 -4.1293 -1.7613 -0.7689 -1.0193 -0.4248 -0.2  
037 -0.3283 -0.6481  
-21.7758 -13.6047 -7.9173 -4.1220 -1.7540 -0.7049 -0.9827 -0.4174 -0.2  
111 -0.3247 -0.6334  
-21.6879 -13.5400 -7.8696 -4.0756 -1.7222 -0.6334 -0.9314 -0.3942 -0.2  
025 -0.3174 -0.6285  
-21.6000 -13.4613 -7.8000 -4.0098 -1.6783 -0.5583 -0.8728 -0.3630 -0.1  
860 -0.3083 -0.6285  
-21.5121 -13.3825 -7.7304 -3.9439 -1.6343 -0.4831 -0.8141 -0.3318 -0.1  
695 -0.2991 -0.6285  
-21.4193 -13.2952 -7.6401 -3.8682 -1.5788 -0.4086 -0.7555 -0.2958 -0.1  
427 -0.2924 -0.6273  
-21.3169 -13.1908 -7.5082 -3.7730 -1.5000 -0.3354 -0.6968 -0.2500 -0.0  
951 -0.2904 -0.6237  
-21.2144 -13.0864 -7.3764 -3.6777 -1.4213 -0.2622 -0.6382 -0.2042 -0.0  
475 -0.2884 -0.6201  
-21.1120 -12.9820 -7.2445 -3.5825 -1.3425 -0.1890 -0.5795 -0.1585  
0 -0.2865 -0.6165  
];
```

```
pass(:,:,2)=[ %Data min 30mm/s  
-2.0505 -1.4160 -1.0255 -0.7020 -0.4090 -0.2990 -0.4880 -0.8545 -1.1960  
-1.5625 -2.0200  
-2.0378 -1.4087 -1.0181 -0.6965 -0.3851 -0.2752 -0.4661 -0.8179 -1.1  
594 -1.5259 -1.9633  
-2.0250 -1.4013 -1.0108 -0.6909 -0.3613 -0.2513 -0.4442 -0.7813 -1.1  
228 -1.4893 -1.9066  
-2.0122 -1.3940 -1.0035 -0.6854 -0.3375 -0.2274 -0.4223 -0.7447 -1.0  
862 -1.4527 -1.8499  
-1.9982 -1.3866 -1.0034 -0.6737 -0.3222 -0.1976 -0.3955 -0.7044 -1.0  
496 -1.4112 -1.7968  
-1.9835 -1.3792 -1.0070 -0.6590 -0.3113 -0.1648 -0.3662 -0.6623 -1.0  
130 -1.3672 -1.7455  
-1.9688 -1.3719 -1.0106 -0.6443 -0.3003 -0.1319 -0.3370 -0.6201 -0.9  
764 -1.3233 -1.6942  
-1.9664 -1.3622 -1.0094 -0.6321 -0.2857 -0.0990 -0.3053 -0.5792 -0.9  
349 -1.2769 -1.6435  
-1.9884 -1.3476 -0.9984 -0.6249 -0.2636 -0.0660 -0.2685 -0.5408 -0.8  
836 -1.2256 -1.5942  
-2.0105 -1.3331 -0.9874 -0.6177 -0.2415 -0.0330 -0.2317 -0.5024 -0.8  
323 -1.1743 -1.5448  
-2.0325 -1.3185 -0.9765 -0.6105 -0.2195 0 -0.1950 -0.4640 -0.7  
810 -1.1230 -1.4955];
```

```
pass(:,:,3)=[ %Data min 30mm/s
```

```
1.2695    0.6835    0.3600    0.1710    0.0490         0    0.0060    0.2195    0.5430 ✓
  0.9340    1.2205
  1.3043    0.7056    0.3839    0.2003    0.0783    0.0293    0.0537    0.2708    0.6 ✓
108    0.9981    1.3084
  1.3391    0.7276    0.4077    0.2295    0.1075    0.0585    0.1014    0.3221    0.6 ✓
786    1.0621    1.3963
  1.3739    0.7496    0.4315    0.2588    0.1367    0.0877    0.1491    0.3734    0.7 ✓
464    1.1262    1.4842
  1.4111    0.7814    0.4688    0.2941    0.1807    0.1415    0.2150    0.4442    0.8 ✓
203    1.1963    1.5624
  1.4495    0.8180    0.5128    0.3325    0.2320    0.2075    0.2900    0.5248    0.8 ✓
973    1.2695    1.6358
  1.4879    0.8546    0.5567    0.3709    0.2833    0.2735    0.3650    0.6053    0.9 ✓
742    1.3427    1.7091
  1.5233    0.8992    0.6006    0.4179    0.3443    0.3443    0.4369    0.6858    1.0 ✓
560    1.4245    1.7867
  1.5527    0.9596    0.6446    0.4821    0.4249    0.4249    0.5028    0.7664    1.1 ✓
475    1.5233    1.8726
  1.5821    1.0200    0.6886    0.5463    0.5054    0.5054    0.5686    0.8469    1.2 ✓
390    1.6222    1.9586
  1.6115    1.0805    0.7325    0.6105    0.5860    0.5860    0.6345    0.9275    1.3 ✓
305    1.7210    2.0445];
[xld,yld]=decrease_in_viewable_area(x,y,pass(:,:,front_side_pass_number));
%All data!
if front_side_pass_number>=1
    pass(:,:,front_side_pass_number)=pass(:,:,front_side_pass_number)-pass(Oy,Ox,front_ ✓
side_pass_number);          %Zero at centre (Belt and braces)
elseif reverse_side_pass_number>=1
    reverse_pass(:,:,reverse_side_pass_number)=reverse_pass(:,:,reverse_side_pass_numbe ✓
r)-reverse_pass(Oy,Ox,reverse_side_pass_number);
end

%if front_side_pass_number>1
%    z_previous=interp2(x,y,pass(:,:,front_side_pass_number-1),x1,y1,'cubic');
%elseif front_side_pass_number==1
%    z_previous=0;
%elseif reverse_side_pass_number>1
%    z_previous=interp2(x,y,pass(:,:,front_side_pass_number-1),x1,y1,'cubic');
%elseif reverse_side_pass_number==1
%    z_previous=0;
%end

if front_side_pass_number>=1
    exp_original=interp2(x,y,pass(:,:,1),x1,y1,'cubic');
    exp=interp2(x,y,pass(:,:,front_side_pass_number),x1,y1,'cubic');%Data interpolated ✓
from pass1 on z1 x,y array
    expl=interp2(x4,y4,pass(:,:,front_side_pass_number),x1,y1,'cubic');
elseif reverse_side_pass_number>=1
    exp_original=interp2(x,y,reverse_pass(:,:,1),x1,y1,'cubic');
    exp=interp2(x,y,reverse_pass(:,:,reverse_side_pass_number),x1,y1,'cubic');%Data int ✓
erpolated from pass1 on z1 x,y array
    expl=interp2(x4,y4,reverse_pass(:,:,reverse_side_pass_number),x1,y1,'cubic');
end

figure
contour(x1,y1,exp);
title('height');
figure
surf(x1,y1,exp);
```

```
title('height');

G_original=gradient_magnitude(x1,y1,exp_original,element_aspect);
G2=gradient_magnitude(x1,y1,exp,aspect);

figure;
subplot (2,2,1);
[C,h] = contour(x1,y1,G1);
%clabel(C,h);
title('G1');

if front_side_pass_number>0
    subplot (2,2,2);
    [C,h] = contour(x1,y1,G2);
    clabel(C,h);
    title('G2');
elseif reverse_side_pass_number>0
    subplot (2,2,2);
    [C,h] = contour(x1,y1,G2);
    clabel(C,h);
    title('G2');
end

G3=G1-G2;
subplot (2,2,3);
[C,h] = contour(x1,y1,G3);
clabel(C,h);
title('G1-G2');

G_original=G1-G_original;
subplot(2,2,4);
[C,h]=contour(x1,y1,G_original,num_contour);
G_original_max=max(G_original(:));
G_original_min=min(G_original(:));
Gc_original=(G_original_max-G_original_min)/(num_contour+1);

clabel(C,h);
title('Original Gradient');

%Trim image edges to avoid exaggerated errors in gradient and cutvature
z1(1,:)=NaN; z1(end,:)=NaN; z1(:,1)=NaN; z1(:,end)=NaN;
%pass(1,:,pass_number)=NaN; pass(end,:,pass_number)=NaN; pass(:,1,pass_number)=NaN; pas
s(:,end,pass_number)=NaN;

%Trim bad data at edges and zero at centre
exp=z1-exp;
exp(1,:)=NaN; exp(end,:)=NaN; exp(:,1)=NaN; exp(:,end)=NaN; %In case experimental data
goes to edges
%exp=exp-exp(Oy,Ox); %Belt and braces

%x1(:,:)=(x1(:,:)-x1(1,1)); %Set origin back to bottom left hand corner for DMC p
lot
%y1(:,:)=(y1(:,:)-y1(end,1));

CGajm_LaserFormPlots03v1_2(x1,y1,G3,G3,exp1,G1,z1,G2,front_side_pass_number,reverse_sid
e_pass_number,xld,yld,Gc_original,num_contour); %exp has now become G3 for line of cons
tant gradient
```

Appendix II

**Example of the Galil CNC Code produced by
Matlab to Control Movement and the Laser
Shutter for the Pass of an Irradiation Strategy**

#Z1
SB1
SB3
SP16000,16000,30000
AC450000,450000,900000
DC450000,450000,900000
PA50000,36582,0
BG
AM
CB3
WT200
LM XY
VA100000
VD100000
LI-480,4085 <8000 >8000
LI918,4000 <8000 >8000
LI1921,3333 <8000 >8000
LI2974,3090 <8000 >8000
LI3164,2243 <8000 >8000
LI3503,1795 <8000 >8000
LI4000,1476 <8000 >8000
LI4000,1013 <8000 >8000
LI3333,558 <8000 >8000
LI4000,364 <8000 >8000
LI4000,52 <8000 >8000
LI4000,-260 <8000 >8000
LI4000,-583 <8000 >8000
LI4000,-947 <8000 >8000
LI4000,-1388 <8000 >8000
LI3333,-1600 <8000 >8000
LI3333,-2186 <8000 >8000
LI3110,-2961 <8000 >8000
LI2160,-3333 <8000 >8000
LI1154,-4000 <8000 >8000
LI-227,-4000 <8000 >8000
LI-1265,-3333 <8000 >8000
LI-2265,-3173 <8000 >8000
LI-3155,-2827 <8000 >8000
LI-3183,-2000 <8000 >8000
LI-3662,-1678 <8000 >8000
LI-4000,-1308 <8000 >8000
LI-4000,-885 <8000 >8000
LI-4000,-526 <8000 >8000
LI-4000,-208 <8000 >8000
LI-4000,104 <8000 >8000
LI-4000,417 <8000 >8000
LI-3971,751 <8000 >8000
LI-3363,942 <8000 >8000
LI-4000,1563 <8000 >8000
LI-3333,1804 <8000 >8000
LI-3161,2358 <8000 >8000
LI-2839,3163 <8000 >8000
LI-1814,3504 <8000 >8000
LE
BGS
AM
SB3
WT500
PA38000,33767,0
BG
AM

Appendix III

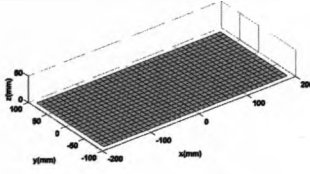
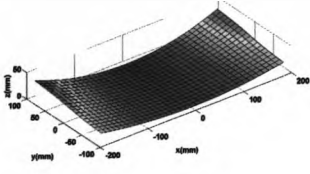
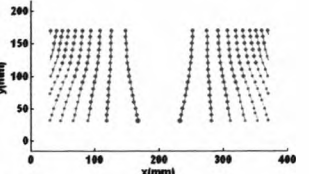
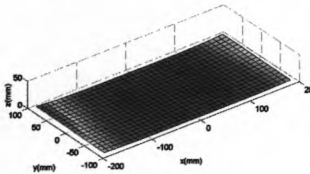
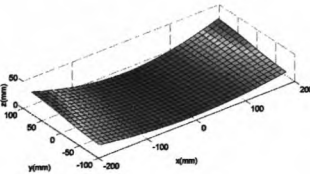
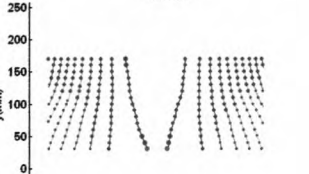
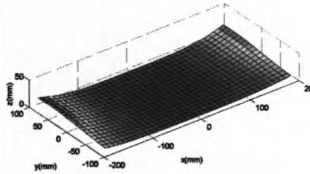
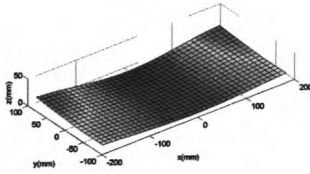
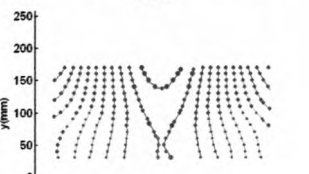
**Example of the Visual Basic Code produced by
Matlab to Control the Movement of the CNC
Tables for the CMM taking into Account the
Decrease in Viewable Area**

```
DMCSHELL11.DMCCOMMAND="SP16000,16000,3000"
DMCSHELL11.DMCCOMMAND="AC450000,450000,90000"
DMCSHELL11.DMCCOMMAND="DC450000,450000,90000"
FILE_N=TEXT1.TEXT
OPEN FILE_N FOR OUTPUT AS #16
DMCSHELL11.DMCCOMMAND = "PA-38000,14000,0"
DMCSHELL11.DMCCOMMAND = "BG"
DMCSHELL11.DMCCOMMAND = "AM"
DBLENDTIME = TIMER + 9#
DO WHILE DBLENDTIME > TIMER
DOEVENTS
LOOP
DMCSHELL11.DMCCOMMAND = "V1=@AN[1]"
DMCSHELL11.DMCCOMMAND = "V1="
ANALOG1 = 100 - (5 * (VAL(DMCSHELL11.DMCRESPONSE))) + 50
DBLENDTIME = TIMER + 1#
DO WHILE DBLENDTIME > TIMER
DOEVENTS
LOOP
WRITE #16, ANALOG1,
DMCSHELL11.DMCCOMMAND = "PA-30400,14000,0"
DMCSHELL11.DMCCOMMAND = "BG"
DMCSHELL11.DMCCOMMAND = "AM"
DBLENDTIME = TIMER + 3#
DO WHILE DBLENDTIME > TIMER
DOEVENTS
LOOP
DMCSHELL11.DMCCOMMAND = "V1=@AN[1]"
DMCSHELL11.DMCCOMMAND = "V1="
ANALOG1 = 100 - (5 * (VAL(DMCSHELL11.DMCRESPONSE))) + 50
DBLENDTIME = TIMER + 1#
DO WHILE DBLENDTIME > TIMER
DOEVENTS
LOOP
WRITE #16, ANALOG1,
DMCSHELL11.DMCCOMMAND = "PA-22800,14000,0"
DMCSHELL11.DMCCOMMAND = "BG"
DMCSHELL11.DMCCOMMAND = "AM"
DBLENDTIME = TIMER + 3#
DO WHILE DBLENDTIME > TIMER
DOEVENTS
LOOP
DMCSHELL11.DMCCOMMAND = "V1=@AN[1]"
DMCSHELL11.DMCCOMMAND = "V1="
ANALOG1 = 100 - (5 * (VAL(DMCSHELL11.DMCRESPONSE))) + 50
DBLENDTIME = TIMER + 1#
DO WHILE DBLENDTIME > TIMER
DOEVENTS
LOOP
WRITE #16, ANALOG1,
DMCSHELL11.DMCCOMMAND = "PA-15200,14000,0"
DMCSHELL11.DMCCOMMAND = "BG"
DMCSHELL11.DMCCOMMAND = "AM"
DBLENDTIME = TIMER + 3#
DO WHILE DBLENDTIME > TIMER
DOEVENTS
LOOP
DMCSHELL11.DMCCOMMAND = "V1=@AN[1]"
DMCSHELL11.DMCCOMMAND = "V1="
ANALOG1 = 100 - (5 * (VAL(DMCSHELL11.DMCRESPONSE))) + 50
DBLENDTIME = TIMER + 1#
```

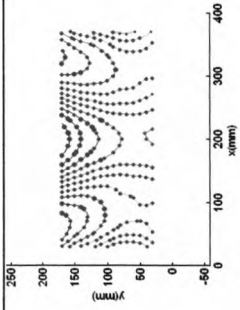
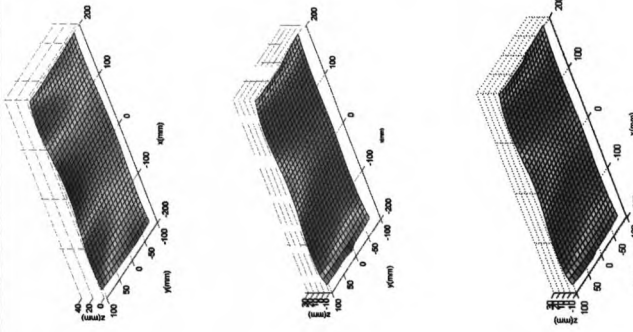
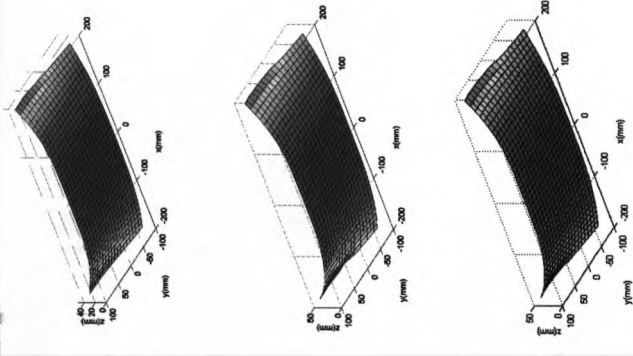
Appendix IV

**A Full Account of All the Irradiation Strategies
and the Resulting Shape for the Closed Loop 3D
Laser Forming of a Mild Steel Semi-
Developable Shape**

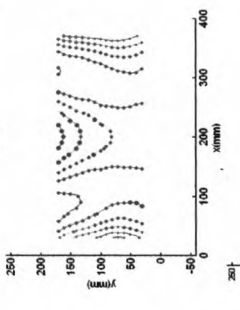
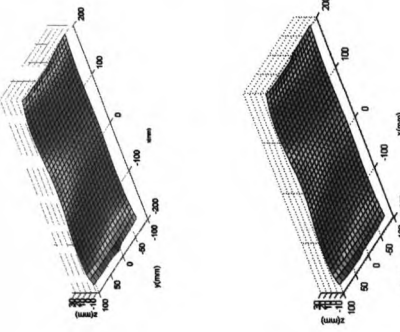
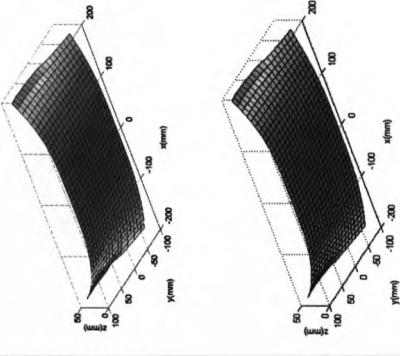
Appendix IV

Calculation of irradiation strategy for pass number	Measured surface	Error between desired and current surface	Irradiation strategy
1			
2			
3			

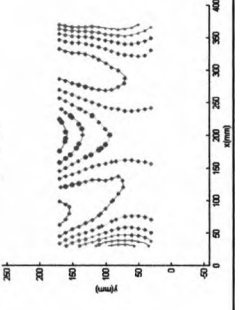
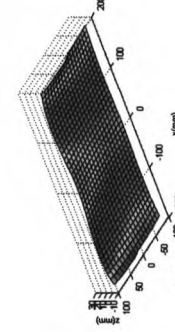
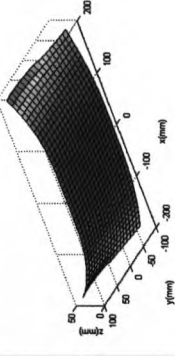
4



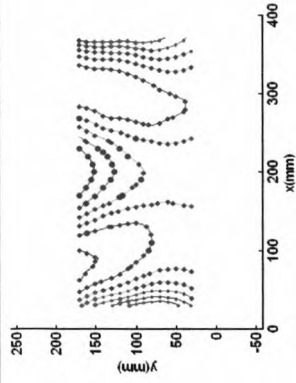
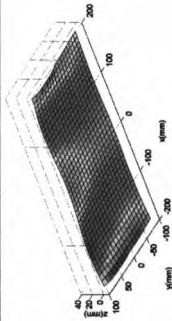
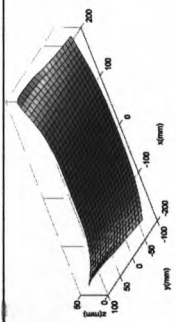
5



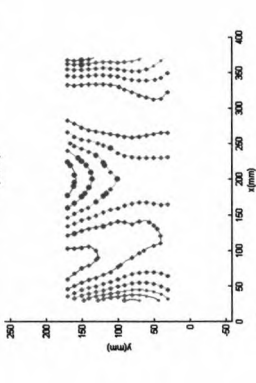
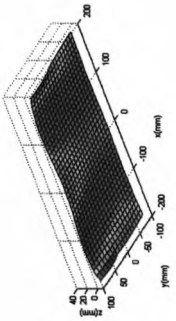
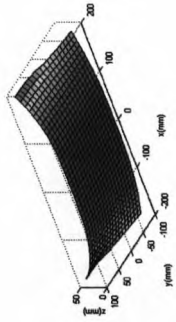
6



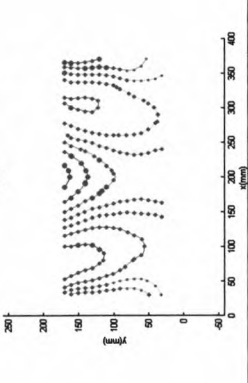
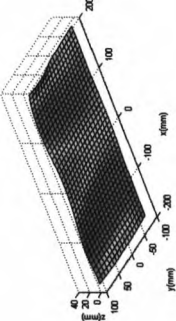
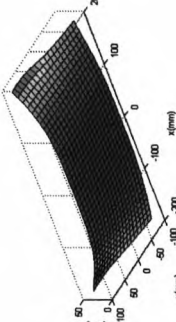
7



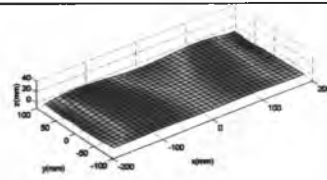
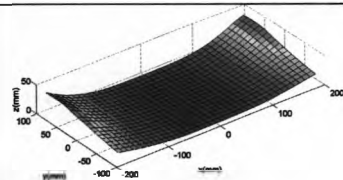
8



9



Final Shape



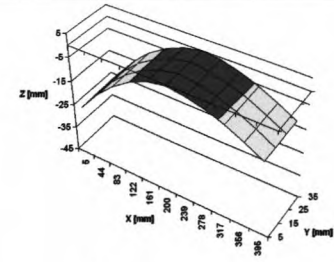
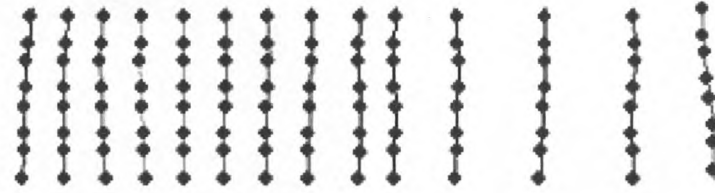
Appendix V

**A Full Account of All the Irradiation Strategies
and the Resulting Shape for the Closed Loop 3D
Laser Forming for the Correction of Aluminium
5251 Strut Mechanically Deformed to 45mm**

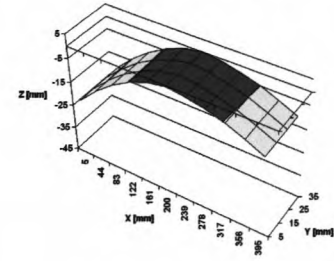
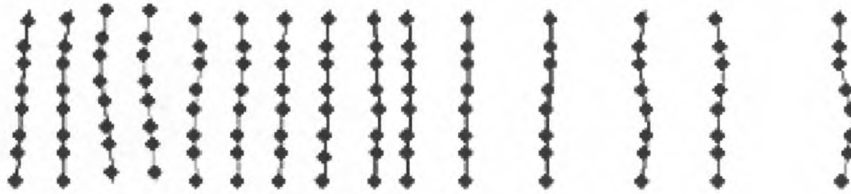
Appendix V

Pass No.	Process Speed (mm/s)	Irradiation Strategy	Measured points
1	61.9		
2	61.9		
3	61.9		

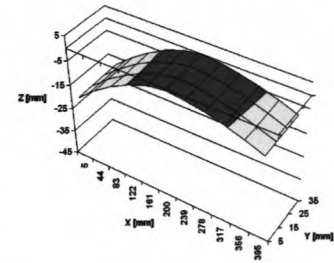
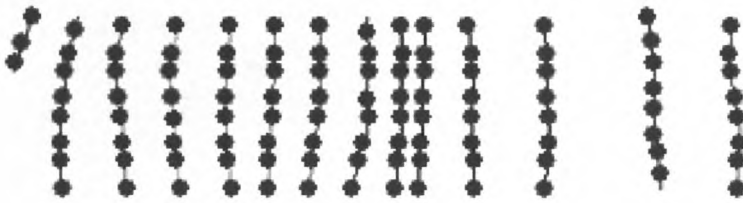
4 61.9



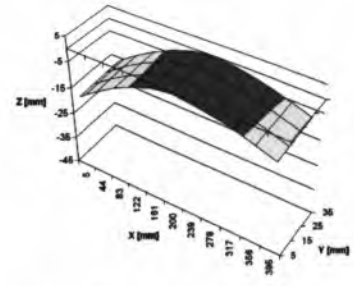
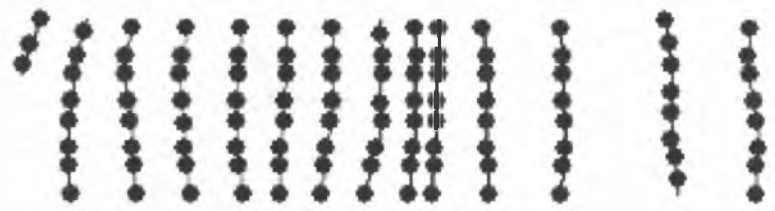
5 61.9



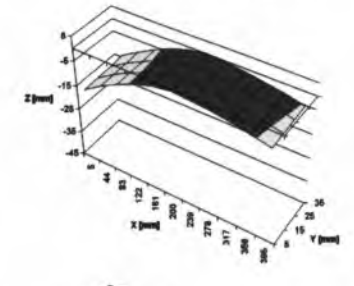
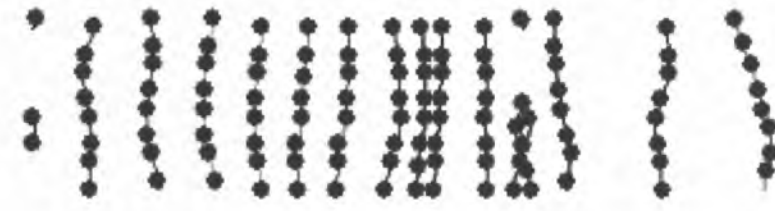
6 62.2



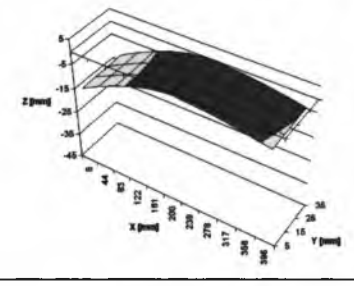
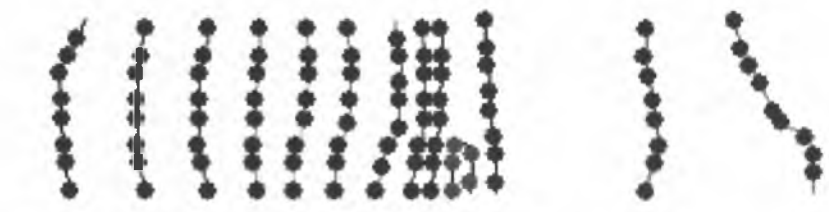
7 64.7



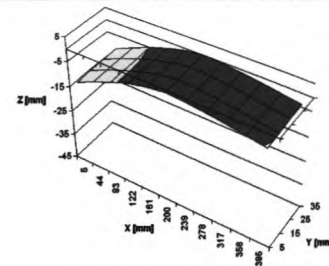
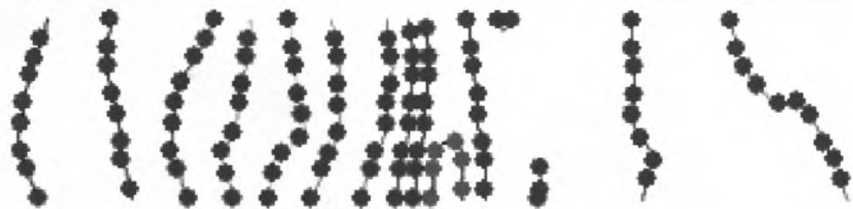
8 66.5



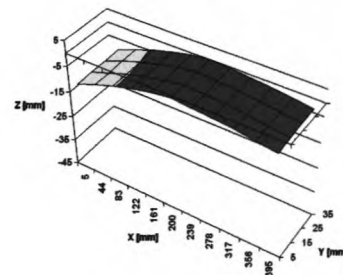
9 68.5



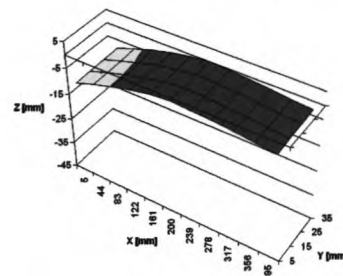
10 70.5



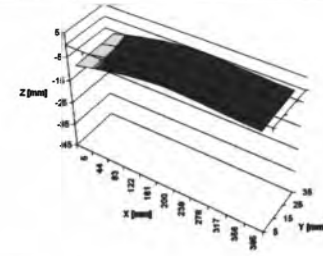
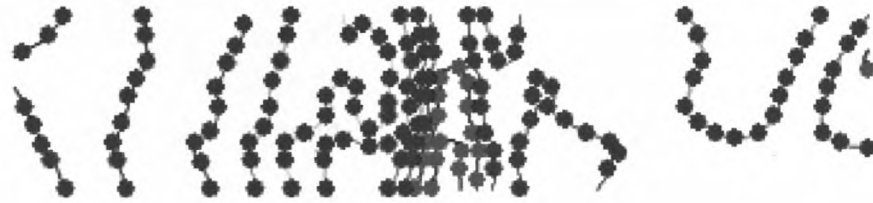
11 72.4



12 73.5



13 75.9



14 75.9

